

SINGLE PARTICLE STUDIES OF BINARY A TERNARY CATION-EXCHANGE KINETIC

**A Thesis Submitted
In Partial Fulfilment of the Requirements
for the Degree of
DOCTOR OF PHILOSOPHY**

**By
ASHOK KUMAR GUPTA**

to the

**DEPARTMENT OF CHEMICAL ENGINEERING
INDIAN INSTITUTE OF TECHNOLOGY KANPUR
JUNE 1973**

TO

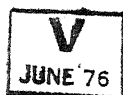
MY FATHER

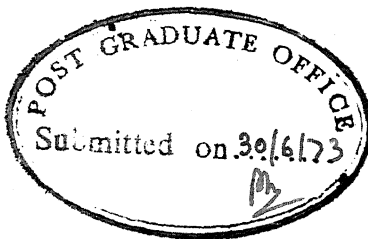
AND

THE MEMORY OF MY LATE MOTHER

4 26720

4E-1973-D-GUP-SIN





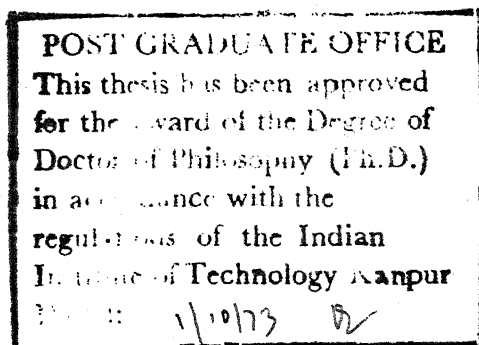
(11)

CERTIFICATE

This is to certify that the work on "Single Particle Studies of Binary and Ternary Cation Exchange Kinetics" has been carried out under my supervision and that the work has not been submitted elsewhere for a degree.

Date

M. Gopala Rao
Associate Professor
Department of Chemical Engineering
Indian Institute of Technology
Kanpur-208016, India



ACKNOWLEDGEMENTS

The author takes this opportunity to express his deep sense of gratitude to Professor M. Gopala Rao, for suggesting the problem, providing constant guidance and encouragement throughout the course of the work, and for invaluable criticism inducing the author to a sense of preciseness.

Professor P.S. Goel (Nuclear Chemistry) and Professor G.K. Mehta (Nuclear Physics) have been very helpful in commissioning some of the Nuclear Instruments. Thanks are also due to Professor G.H. Shroff, Head of Chemical Engineering Department, and other colleagues of the author at H.B. Technological Institute, Kanpur for encouragement during the writing stage of the thesis.

The author appreciates the help of Mr. S.Y. Kekre in learning the experimental technique and Mr. R.K. Bajpai in performing some of the computations. Help rendered by Mr. V.N.R. Sarma (Met. Engg.), Mr. S. Bhatia and Mr. S.B. Rath at various stages of work is gratefully acknowledged.

The author is also thankful to Shri B.S. Pandey for typing the dissertation with utmost care and to Shri D.S. Panesar for his excellent drawing work.

Author

CONTENTS

			Page
	List of Tables	...	vi
	List of Figures	...	ix
	Synopsis		xii
	Nomenclature		xvii
CHAPTER			
1	INTRODUCTION	...	1
	Aim of the Work	...	4
2	LITERATURE REVIEW	...	8
	Ion-Exchange Kinetics	...	8
	Self Exchange	...	10
	Binary Exchange	...	15
	Ternary Exchange	...	21
	Ion-Exchange Equilibria	...	26
	Binary Exchange	...	27
	Ternary Ionic Equilibria	...	35
3	THEORY	...	38
	Ion-Exchange Kinetics	...	38
	Diffusion in Ion-Exchange Resin	...	39
	Film-Phase Control	...	44
	Both Resistances Controlling Mass Transfer		46
	Ion-Exchange Equilibria	...	48
	Phase Equilibrium Approach	...	49
	Ternary Ionic Equilibria	...	53
4	EXPERIMENTAL	...	55
	Single Particle Radioactive Tracer (SPRT)		
	Technique	...	55
	Materials	...	59

	Preparation of the Resin for Experimental Studies	61
	Experimental Procedure	66
	Systems Studied in the Present Investigation			76
	Sources of Error	77
5	RESULTS AND DISCUSSION	81
	Ion-Exchange Equilibria		...	81
	Capacity Measurements		...	81
	Binary Equilibria	84
	Ternary Equilibria	104
	Ion-Exchange Kinetics			112
	Self Exchange	112
	Binary Exchange	118
	Ternary Rate Studies	129
6	CONCLUSIONS AND RECOMMENDATIONS	...		155
	Conclusions	155
	Equilibrium	155
	Kinetics	156
	Recommendations for Further Work	...		158
	BIBLIOGRAPHY	160

APPENDICES

A	Exchange Characteristics of ^{137}Cs	...	166
B	Theory	...	179
C	Experimental	...	215
D	Ion-Exchange Equilibria: Data Correlation		225
E	Ion-Exchange Kinetics	...	232

LIST OF TABLES

TABLE		PAGE
1	Ion-Exchange Equilibrium Studies	28
2	Capacities of Dowex 50W-X8 Resin Beads (in Micro-Equivalents) ...	82
3	Ion-Exchange Equilibria: Cs-Na-Dowex 50W-X8 System ...	85
4	Ion-Exchange Equilibria: Mn-Na-Dowex 50W-X8 System ...	85
5	Ion-Exchange Equilibria: Mn-Cs-Dowex 50W-X8 System ...	88
6	Ion-Exchange Equilibria: Ba-Mn-Dowex 50W-X8 System ...	91
7	Rational Equilibrium Constants of Binary Systems ...	94
8	Resin-Phase Activity Coefficients: Cs-Na-Dowex 50W-X8 System ...	95
9	Resin-Phase Activity Coefficients: Mn-Na- Dowex-50W-X8 System ...	97
10	Resin-Phase Activity Coefficients: Mn-Cs- Dowex 50W-X8 System ...	99
11	Ternary Ion-Exchange Equilibria: Mn-Cs-Na- Dowex 50W-X8 System ...	105
12	Comparison of Experimental and Computed Ternary Equilibrium Data: Ba-Cu-Na-Dowex 50W-X8 System ...	111
13	Self Exchange of Cs^+ Ions	172
14	Binary Exchange Rate Data: $\bar{\text{Cs}}^*$ -Na System	173
15	Binary Exchange Rate Data: $\bar{\text{Cs}}^*$ -Mn System	174
16	Binary Exchange Rate Data: $\bar{\text{Cs}}^*$ -Sr System	175
17	Ternary Exchange Rate Data: $\bar{\text{Cs}}^*$ -(Mn-Na) System	176

18	Ternary Exchange Rate Data: $\bar{\text{Cs}}^*-(\text{Mn}-\text{Na})$ System	176
19	Ternary Exchange Rate Data: $(\bar{\text{Cs}}^*-\bar{\text{Na}})-\text{Mn}$ System	177
20	Ternary Exchange Rate Data: $(\bar{\text{Cs}}^*-\bar{\text{Na}})-\text{Mn}$ System	177
21	Ternary Exchange Rate Data: $(\bar{\text{Cs}}^*-\bar{\text{Mn}})-\text{Na}$ System	178
22	Ternary Exchange Rate Data: $(\bar{\text{Cs}}^*-\bar{\text{Mn}})-\text{Na}$ System	178
23	Capacity Measurements ...	215
24	Binary Equilibrium Data: Experimental Resin-Phase Composition (Non-Normalized)	221
25	Ternary Equilibrium Data: Experimental Resin Phase Composition (Non-Normalized)	222
26	Experimental Kinetic Run	224
27	Rational Equilibrium Constant: Ba-Mn-Dowex 50W-X8 System ...	225
28	Ion-Exchange Equilibria: Ba-Na-Dowex 50W-X8 System ...	226
29	Empirical Constants for Various Pairs of Ions	226
30	Solution-Phase Activity Coefficients in Ternary Mixtures ...	231
31	Limiting Ionic Conductances and Diffusivities of Ions Employed in the Present Study	233
32	Computed Film-Diffusion Controlled Exchange Rate Data: Mn-Na System	236
33	Self Exchange of Sodium Ions (0.1N NaCl Solution) ...	238
34	Self Exchange of Sodium Ions (0.001938N NaCl Solution) ...	240
35	Self-Exchange of Manganese Ions	241
36	Self-Exchange of Barium Ions	242
37	Self Exchange of Strontium Ions	243

38	Binary Exchange Rate Data: $\bar{\text{Na}}^*-\text{Mn}$ System	244
39	Binary Exchange Rate Data: $\bar{\text{Mn}}^*-\text{Na}$ System	245
40	Binary Exchange Rate Data: $\bar{\text{Na}}^*-\text{Ba}$ System	246
41	Binary Exchange Rate Data: $\bar{\text{Ba}}^*-\text{Na}$ System	247
42	Binary Exchange Rate Data: $\bar{\text{Na}}^*-\text{Cs}$ System	248
43	Binary Exchange Rate Data: $\bar{\text{Mn}}^*-\text{Sr}$ System	249
44	Binary Exchange Rate Data: $\bar{\text{Sr}}^*-\text{Mn}$ System	250
45	Binary Exchange Rate Data: $\bar{\text{Mn}}^*-\text{Cs}$ System	252
46	Binary Exchange Rate Data: $\bar{\text{Sr}}^*-\text{Cs}$ System	253
47	Binary Exchange Rate Data: $\bar{\text{Mn}}^*-\text{Ba}$ System	254
48	Ternary Exchange Rate Data: $\bar{\text{Na}}^*-(\text{Mn}-\text{Cs})$ System	255
49	Ternary Exchange Rate Data: $(\bar{\text{Na}}-\bar{\text{Cs}})^*-\text{Mn}$ System	257
50	Ternary Exchange Rate Data: $(\bar{\text{Na}}^*-\bar{\text{Mn}})-\text{Cs}$ System	259
51	Ternary Exchange Rate Data: $\bar{\text{Mn}}^*-(\text{Cs}-\text{Na})$ System	262
52	Ternary Exchange Rate Data: $(\bar{\text{Mn}}^*-\bar{\text{Na}})-\text{Cs}$ System	264
53	Ternary Exchange Rate Data: $(\bar{\text{Mn}}^*-\bar{\text{Cs}})-\text{Na}$ System	267
54	Ternary Exchange Rate Data: $\bar{\text{Na}}^*-(\text{Ba}-\text{Mn})$ System	270
55	Ternary Exchange Rate Data: $(\bar{\text{Na}}^*-\bar{\text{Mn}})-\text{Ba}$ System	273
56	Ternary Exchange Rate Data: $(\bar{\text{Na}}^*-\bar{\text{Ba}})-\text{Mn}$ System	275
57	Ternary Exchange Rate Data: $\bar{\text{Mn}}^*-(\text{Ba}-\text{Na})$ System	277
58	Ternary Exchange Rate Data: $(\bar{\text{Mn}}^*-\bar{\text{Ba}})-\text{Na}$ System	279
59	Ternary Exchange Rate Data: $(\bar{\text{Mn}}^*-\bar{\text{Na}})-\text{Ba}$ System	281
60	Ternary Exchange Rate Data: $(\bar{\text{Mn}}^*-\bar{\text{Cs}})-\text{Sr}$ System	283
61	Ternary Exchange Rate Data: $(\bar{\text{Mn}}^*-\bar{\text{Sr}})-\text{Cs}$ System	285
62	Ternary Exchange Rate Data: $\bar{\text{Sr}}^*-(\text{Mn}-\text{Cs})$ System	287
63	Ternary Exchange Rate Data: $(\bar{\text{Sr}}^*-\bar{\text{Mn}})-\text{Cs}$ System	289
64	Ternary Exchange Rate Data: $(\bar{\text{Sr}}^*-\bar{\text{Cs}})-\text{Mn}$ System	291

LIST OF FIGURES

FIGURE		PAGE
1	Experimental Set-up for Obtaining Rate Data ...	70
2.	Binary Ion-Exchange Equilibria: Cs-Na-Dowex 50W-X8 System ...	86
3	Binary Ion-Exchange Equilibria: Mn-Na-Dowex 50W-X8 System ...	87
4	Binary Ion-Exchange Equilibria: Mn-Cs-Dowex 50W-X8 System ...	89
5	Binary Ion-Exchange Equilibria: Ba-Mn-Dowex 50W-X8 System ...	92
6	Resin-Phase Activity Coefficients: Cs-Na-Dowex 50W-X8 System ...	96
7	Resin-Phase Activity Coefficients: Mn-Na-Dowex 50W-X8 System ...	98
8	Resin-Phase Activity Coefficients: Mn-Cs-Dowex 50W-X8 System ...	100
9	Resin-Phase Activity Coefficients: Ba-Mn-Dowex 50W-X8 System ...	101
10	Ternary Ion-Exchange Equilibria: Mn-Cs-Na-Dowex 50W-X8 System ...	106
11	Experimental Self Exchange Curves	114
12	Binary Exchange Curves for the System: Mn-Na-Dowex 50W-X8 ...	119
13	Binary Exchange Curves for the System: Ba-Na-Dowex 50W-X8 ...	120
14	Binary Exchange Curves for the System: Sr-Mn-Dowex 50W-X8 ...	121
15	Binary Exchange Curves with Cs in the Bulk	122
16	Film-Diffusion Controlled Self Exchange Curve ...	125

29	Ternary Exchange Rate Data for the System: ($\bar{\text{Sr}}^*$ - $\bar{\text{Mn}}$)-Cs-Dowex 50W-X8	149
30	Self and Binary Exchange Curves with Cs in the Resin ...	157
31	Tracing of an Original Recorder Graph of an Experimental Kinetic Run	223

+++

SYNOPSIS

Ashok Kumar Gupta, Ph.D.
Department of Chemical Engineering
Indian Institute of Technology, Kanpur

JUNE 1973

SINGLE PARTICLE STUDIES OF BINARY AND TERNARY CATION-EXCHANGE KINETICS

In the present investigation, particle-diffusion controlled kinetic data for self, binary and ternary exchanges of Mn-Cs-Na-Dowex 50W-X8 system were obtained with 0.1N chloride solutions. Ternary exchange kinetics of the Ba-Mn-Na-Dowex 50W-X8 system were also studied. Equilibrium data for the following systems were obtained with 0.1N chloride solutions and Dowex 50W-X8 resin: ternary system Mn-Cs-Na and the component binaries Mn-Cs, Mn-Na and Cs-Na; and binary system Ba-Mn. For both equilibrium and rate measurements, single particle radioactive tracer techniques developed earlier by Gopala Rao and David (G.4) for their study of binary exchanges, were used in the present investigation.

Equilibrium Studies

From the experimental data, the order of resin-phase selectivity was found to be $Ba^{2+} > Mn^{2+} > Cs^+ > Na^+$. The ternary equilibrium data could be conveniently presented on a triangular diagram with the resin-phase composition given by the regular grid and the solution-phase composition along the constant parameter curves.

Binary data were deduced from the ternary data neglecting the presence of the third ion. While the equilibrium data for Mn-Na and Mn-Cs binaries deduced from the ternary system Mn-Cs-Na, agreed satisfactorily with the respective experimental data, the deduced data for Cs-Na binary did not show such an agreement.

The equilibrium data were correlated by a phase-equilibrium approach. For the binary systems, rational equilibrium constants and resin-phase activity coefficients of the ions were calculated. The resin-phase activity coefficient of an ion in a binary pair varied with its fraction in the resin phase, and also with the nature of the second ion.

The triangle rule failed when expressed in terms of the rational equilibrium constants of the three component pairs of the ternary system Mn-Cs-Na. Ternary equilibrium data for this system were successfully predicted from the experimental data of the two binary pairs each containing the most favoured ion in the resin phase (viz. Mn-Cs and Mn-Na binaries, and the Mn^{2+} ion is the most favoured ion). Ternary equilibrium data obtained by S.E. Smith (S.5) for the system Ba-Cu-Na-Dowex 50W-X8 were also successfully predicted by the above approach.

Kinetic Studies

The resin-phase ionic self diffusivities determined in the present investigation are:

$$\bar{D}_{\text{Na}} = 20.5 \times 10^{-7} \text{ cm}^2/\text{sec} \quad (\text{experimental})$$

$$\bar{D}_{\text{Mn}} = 2.22 \times 10^{-7} \text{ cm}^2/\text{sec} \quad (\text{experimental})$$

$$\bar{D}_{\text{Cs}} = 30.0 \times 10^{-7} \text{ cm}^2/\text{sec} \quad (\text{estimated})$$

For a binary system A-B, particle-diffusion controlled rate data for self exchanges as well as binary exchanges for both forward and reverse directions were obtained. In general,

the binary exchange curves fall between the two self-exchange curves.

For the ternary exchange, two types of studies were made: (i) ion A (tagged) initially present in the resin phase, exchanging with ions B and C present in the desired proportions in the solution, $\bar{A}^*-(B-C)$; (ii) a bead in the ionic form A and tagged with its radioactive isotope was partially eluted with a cation B, and ions A and B were then exchanged with ion C present in the solution, $(\bar{A}^*-\bar{B})-C$. The depletion history of only the tagged ion was measured. Depletion curves for various initial and boundary conditions of the two ternary systems were obtained. In general, ternary rate curves for the system $\bar{A}^*-(B-C)$ fall within an envelope composed by the two binaries \bar{A}^*-B and \bar{A}^*-C . For the case of $(\bar{A}^*-\bar{B})-C$ exchange, and with the mobility of ion B in the resin phase being greater than that of ion A, the depletion rate of A decreases as the initial fraction of B in the resin is increased, and the ternary depletion curves fall above the binary curve, \bar{A}^*-C . However, if ion B is slower than ion A, the depletion rate of A increases and ternary rate curves fall below the binary curve for \bar{A}^*-C .

A rigorous mathematical model in which the coupling of ionic fluxes other than by electric-potential gradient is neglected, was derived from principles of irreversible thermodynamics to describe the ternary ion-exchange kinetics. In the proposed model, the effect of both fluid-film and resin-phase resistances to mass transfer was considered. Resin-phase diffusion coefficients \bar{D}_{11} , \bar{D}_{12} , \bar{D}_{21} and \bar{D}_{22} in the ternary system were expressed in terms of the self-diffusion coefficients, \bar{D}_1 , \bar{D}_2 and \bar{D}_3 which were obtained independently. Equations employed in the present model can also be derived using the Nernst-Planck equations for the three ions.

The equations of continuity in the resin phase and the momentary flux equations in the film phase were solved simultaneously along with the equilibrium relationships at film-resin interface, with the help of IBM 7044 computer. The computations were made to determine ionic composition in the resin phase as a function of time. The same computer programme with appropriate additional conditions was also used for binary and self exchanges.

The proposed model describes particle-diffusion controlled ion-exchange kinetic data adequately for both the ternary systems (Mn-Cs-Na and Ba-Mn-Na) and the component binaries in both the directions. Rate data for the ternary system Sr-Mn-Cs-Dowex 50W-X8 (B.1) were also correlated.

Computed results of the rate curves were also obtained neglecting the effect of film diffusion and with the assumption that the resin surface is instantaneously saturated with incoming ions. The binary and ternary rate data under favourable equilibrium conditions were correlated well by this method. But for unfavourable cases, the agreement between the computed and the experimental rate curves was rather poor.

Resin-surface compositions for the exchanges were also computed with the help of the proposed model. In the case of binary and ternary exchanges under favourable equilibrium conditions, the computed values of the resin-surface compositions quickly approximated the equilibrium values corresponding to the bulk-fluid composition. For unfavourable equilibrium exchange, the computations showed that the resin surface was not appreciably saturated with the incoming ions for a considerable extent of exchange. Thus, the computed results indicate that film resistance is relatively significant for the unfavourable exchange, and a consideration of it is necessary to predict the rate of mass transfer for the so called particle-diffusion

controlled ion-exchange kinetics.

Families of binary and ternary exchange curves for an ionic system can be predicted with the help of the proposed model using relatively small amount of information which is either readily accessible or can be obtained with ease from a simple experiment, such as limiting ionic conductances in aqueous solution, fluid-film thickness, equilibrium ionic distributions and the resin-phase self diffusivities.

* * *

NOMENCLATURE

a_i	Thermodynamic activity of species i
a, b, c	Empirical constants, Equation 27
C_i	Concentration of species i in a phase in the context m moles/ml
\bar{C}_i	Resin phase equivalent fraction of species i
C_o	Capacity of resin m eqvt/ml
ΔC_i	$C_{i, \text{interface}} - C_{i, \text{bulk}}$ m moles/ml
\bar{C}_{io}	Initial equivalent fraction of species i in the resin phase
\bar{C}_{is}	Resin-surface equivalent fraction of species i after exchange has started taking place
CPM	Counts per minute
d_o	Diameter of resin bead
D_i	Diffusion coefficient of species i cm^2/sec
D_{kj}	Diffusion coefficient in ternary system, Equations 10, 11 and 13a
\bar{D}_{kj}	Diffusion coefficient in ternary system, Equations 13b, 14 and 15
D_{kk}	Diffusion coefficient in ternary system, Equations 11 and 13a
E_{Don}	Donnan potential
F	Faraday constant
J_i	Flux of species i m moles $\text{cm}^{-2} \text{sec}^{-1}$
K_j^i	Rational thermodynamic equilibrium constant for exchange of i and j, Equation 33
$K_{c_j}^i$	Molar selectivity coefficient for exchange of ions i and j, Equation 34

$K_{c_j}^i$	Modified selectivity coefficient for exchange of ions i and j, Equation 35
l_{o_i}	Limiting ionic conductance of species i in the aqueous phase $\text{cm}^2 \text{ phm}^{-1} \text{ equivalent}^{-1}$
L_{kj}	Phenomenological coefficient, Equation 1
L_{k5}	Phenomenological coefficient, Equation 3
P	Pressure
q_o	Resin-phase initial equivalent fraction of species i in the context**
q_t	Resin-phase equivalent fraction of species i in the context at time t**
r	Radial position cm
r_o	Radius of the resin bead cm
R	Gas law constant
t	Time
T	Temperature
v_i	Partial molar volume of species i $\text{cm}^3 \text{ mole}^{-1}$
X_i	Mole fraction of species i
y	Equivalent fraction at interface
$Y_{A,R} \big _{AB}$	Resin surface equivalent fraction of species A in a pair A-B, neglecting the presence of third ion, Equation 28
Z_i	Valency of species i
α_j^i	Separation factor for exchange of species i and j
β_i	Equilibrium equivalent fraction of species i
γ_i	Molal activity coefficient of species i
δ	Film thickness cm

**Numerical values of (q_t/q_o) for tagged species have been presented in the thesis.

- n_j Electrochemical potential of species j, Equations 1 and 31
- λ_i Distribution coefficient of species i, Equation 26
- μ_j Chemical potential of species j
- Π Swelling pressure
- Φ Electric-potential

Subscripts and Superscripts

Subscripts Na, Mn, Cl, A, B, i, j etc. refer to the species named; ij are arbitrary species

Quantities and symbols with overbars refer to the resin phase, unless mentioned otherwise

- (*) Refers to tagged ion in the resin phase
- i,f Refer to species i in the film at the interface
- i,R Refer to species i at the resin surface
- ij Refer to the binary pair ij (in a ternary system i-j-k) neglecting the presence of third ion k, Equations 28,29 and 42
- bg Refer to background
- eb Refer to equilibrated bead
- tb Refer to tagged bead

Abbreviations

eqvt.fr Equivalent fraction

m.eqvt. Milli equivalents

N.P. Nernst-Planck Model

Mathematical Operator

∇ $\frac{\partial}{\partial r}$ (gradient along the radius)

Explanations

tagged bead	Resin bead containing radioactive ionic species (before equilibration or before elution)
tagged ion, \bar{A}^*	Species A along with its radioactive iosotope in the resin phase
equilibrated bead	Tagged bead after equilibration
$\bar{A}^*-(B-C)$ 1 0.4 0.6	This is a ternary exchange, ion A (tagged) initially in the resin phase exchanging with a solution containing a mixture of ions B and C, the equivalent fractions of which are 0.4 and 0.6 respectively.
1 0 1	This is a binary exchange, ion A(tagged) initially in the resin phase exchanging with ion C in the solution
$(\bar{A}^*-\bar{B})-C$ 0.4 0.6 1	This is a ternary exchange, a mixture of ions A and B initially in the resin phase, A being tagged and its equivalent fraction 0.4, exchanging with ion C in the solution.

CHAPTER 1

INTRODUCTION

During the past three decades, remarkable advances in ion-exchange technology have taken place. Availability of synthetic ion-exchange resins possessing a wide range of properties such as structure, functional groups, capacity, porosity etc., has resulted in widespread use of these materials in commercial processes. Current applications of ion-exchange resins extend from demineralization of water, separation and purification of rare-earths, biochemical and pharmaceutical products to catalysis of chemical reactions.

In most of the industrial applications, ion-exchange fixed-bed systems are employed although continuous counter-current flow systems are also finding increasing use in recent years. In what is known as 'exhaustion period', solute ions are removed continuously from the feed stream and are accumulated in the resin phase. Initially, the effluent stream contains very little of the ions being adsorbed. As the resin bed gets saturated with the entering ions, the concentration of the ions in the effluent stream increases and finally equals its value in the feed stream. The concentration history of the entering ion in the effluent stream is called the 'breakthrough curve', and its prediction is important for the design of fixed-bed systems. If the resin is to be

reused after the exhaustion period, as is normally the case, the bed is regenerated under conditions favourable to the desorption of the solute ions.

Thomas (T.5) was one of the first research workers to develop the basic mathematical theory for the description of a fixed-bed ion-exchange process. He solved simultaneously a material-balance partial differential equation, a rate equation written in terms of chemical reaction kinetics, and an equilibrium relationship between the two phases in order to obtain an equation for breakthrough curve for a given set of initial and boundary conditions. A number of investigators presented equations for breakthrough curve for certain limiting cases such as proportionate-pattern and constant-pattern breakthroughs, and for simple equilibrium relationships and rate models. A discussion on such equations is given in Perry's Handbook (P.2). For complex rate and equilibrium conditions, solutions of the equations may be obtained using high-speed digital computers. However, a realistic and theoretically sound rate model should be incorporated in the set of equations to make the effort worthwhile.

Although ion exchange is a metathetical process, rates of ion exchange are determined by mass transfer steps, namely, ionic transport between the bulk fluid and external surface of the resin, and the ionic diffusion within the resin itself. Boyd and coworkers (B.8) were the earliest investigators to

establish the diffusional nature of ion-exchange mass transfer. In equations for the design of ion-exchange systems, the rate of mass transfer through the liquid film is usually represented as a product of the mass-transfer coefficient incorporating the interfacial area and the concentration driving force, and the particle-diffusion process by the Fick's law model. However, when ions of dissimilar mobilities diffuse, an electric-potential gradient is set up which tends to slow down the faster ions and speed up the slower ones. The effect of electric-potential gradient on ion exchange kinetics was first considered by Helfferich and coworkers (H.6, S.1).

It is now well established that the electric-potential gradient produced by diffusion of ions of dissimilar mobilities affects the rate of mass transfer both in the fluid film and in the resin phase, and that the Nernst-Planck model describes ion-exchange kinetics more realistically than the Fick's law model. However, prediction of experimental rate data obtained under unfavourable equilibrium conditions, with the Nernst-Planck model is not satisfactory (M.4, V.3). Also, the Nernst-Planck model has not been generally extended to multicomponent systems which are frequently encountered in industrial processes. While the present investigation was in final stages of completion, the author came to know about the work of Lupa (L.3) who

attempted the extension of Nernst-Planck model to ternary ionic systems. However, his experimental results were not conclusive.

Due to experimental difficulties and also mathematical complications, research work in ion-exchange kinetics has largely been restricted to binary ionic systems. There is no comprehensive experimental rate study for ternary systems, particularly for the exchange rates controlled by the resin-phase diffusion. Prediction or interpretation of the limited amount of ternary data that is available in literature has not been completely satisfactory. Therefore, it is necessary to formulate adequate, theoretically-sound mathematical model to describe the exchange kinetics in ternary systems (as a first step in tackling a multicomponent system), and to obtain sufficient experimental data to evaluate the correctness of the model proposed. Also, the data should be obtained at a fundamental level.

Aim of the Work

The objective of the present study was to obtain comprehensive, particle-diffusion controlled rate data for a ternary ionic system, and to develop theoretically-sound generalized mathematical model to interpret the data. In the present investigation, single-particle radioactive-tracer method was used to obtain the rate data under conditions of particle-diffusion control. An important feature of this

method is that the concentration history of the resin bead can be measured directly and with a reasonable accuracy. Earlier workers (B.1, G.3, V.3) have shown that equilibrium and rate data obtained with a single-resin bead method agreed well with the corresponding measurements made using other methods.

In an ion-exchange process, it is necessary to know the equilibrium relationship between the ions in the solution phase and in the resin phase. Hitherto, some methods have been proposed by earlier research workers (D.5, P.3) to predict binary equilibria from ternary equilibria. Actually, it is easier to obtain experimentally binary-equilibrium data. Another objective of the present work was to obtain experimentally binary and ternary equilibrium data, and to propose a method to predict the ternary data from the binary ones.

The following criteria were considered in selecting the system:

- i. durable and homogeneous cation-exchange resin which is commonly used in industry;
- ii. a heterovalent system to provide generality to study;
- iii. an ionic system which does not form complexes in the solution or resin phase under experimental conditions; and
- iv. isotopes of ions which are readily available in carrier-free form and which have long half-lives

and strong gamma-emitting properties.

After a careful analysis, the ternary system Mn-Cs-Na-Dowex 50W-X8 was selected for the present study.

The aim, therefore was to obtain comprehensive experimental data of the particle-diffusion controlled ion-exchange kinetics for the ternary system Mn-Cs-Na-Dowex 50W-X8 including self exchange, binary exchanges in both the directions, and the ternary exchanges. The total anion concentration for the present study was kept at 0.1N, as the concentration is high enough to give particle-diffusion controlled rates at reasonable superficial fluid velocities, and at the same time low enough to minimise the effect of pore solution in the resin phase. It was also the aim of the present work to obtain binary and ternary equilibrium data for the above system at 0.1N anion concentration. It is intended to propose a theoretically-based mathematical model for the exchange rate process and to correlate the experimental data.

During the period of present investigation, equilibrium and rate data on the Sr-Mn-Cs-Dowex 50W-X8 system were obtained by a colleague of the author (B.1). Correlations performed by the author for the above system, have also been included in the present dissertation. Also, rate studies of the system Ba-Mn-Na-Dowex 50W-X8 are included. Rate and equilibrium data for the binary system Ba-Na-Dowex 50W-X8 were already

available (K.2, V.3) and the additional experimental data for the ternary system were obtained by the author.

* * *

CHAPTER 2

LITERATURE REVIEW

As mentioned earlier, the present work was undertaken to study the particle-diffusion controlled kinetics of ion exchange in ternary systems. It was also found necessary to measure ternary exchange equilibria. In view of the above, a survey of salient literature on both ion-exchange kinetics and equilibria has been presented in this chapter. Naturally, emphasis has been placed on literature of ternary systems. Literature review on important developments in binary exchange has also been presented.

The survey was confined to the systems comprising of strongly acidic resins, and aqueous solutions of strong electrolytes, with no chemical reaction accompanying the exchange. The emphasis in the presentation is considerably more on modelling of ion-exchange kinetics than on performance of ion-exchange columns.

ION-EXCHANGE KINETICS

Simplified rate equations which describe the ion-exchange kinetics are commonly used in the design of ion-exchange columns, and these equations have been very well summarized by Helfferich (H.2(g)). In some of these rate models, ion exchange is treated as a chemical reaction,

and the rate equations are represented in terms of forward and reverse reaction rate constants. The concept of mass transfer coefficients has also been used in some other rate models. The advantage of simplified rate models is mainly in that they can be integrated under complex boundary conditions to give a quantitative picture of the performance of ion-exchange columns. However, these equations would only be valid under limited range of exchange conditions. Also, the flux equations in these models are written without taking into account the electric-field effect.

In view of the ambiguities that crept in the usage of simplified rate models, efforts were made towards a better understanding of the rate controlling mechanism of ion exchange. A number of attempts have been made during the past two and a half decades to obtain the basic rate data of ion exchange, starting from isotopic exchange to a limited extent multi-component exchange, over a wide range of ionic parameters such as size, valency, mobility, as well as resin parameters such as functional group, cross-linkage and bead size.

Now it has been well established that rate of ion exchange is a diffusion-controlled process. In view of the objectives of the present study, emphasis was placed on mathematical models, particularly diffusion models that were employed to represent ion-exchange kinetics. No attempt has been made to review exhaustively the vast body of literature on kinetics of ion exchange.

Self Exchange

Self exchange which is also called isotopic exchange is the exchange of two isotopic counterions between the two phases (namely, resin phase and solution phase), in a system which is in equilibrium except for the isotopic distribution. Mathematical modelling of self exchange is relatively simple. Boyd and coworkers established in 1947 that the rate of ion-exchange is determined by diffusion process (B.8). They showed that the mass transfer rate would either be controlled by diffusion through the film adhering to resin beads, or by the diffusion of ions within the ion exchanger itself, or by both. Rate laws of self exchange are usually described by Fick's first law, and the self-diffusion coefficient is constant throughout any phase of the system. The literature presented below is for particle-diffusion controlled self-exchange processes unless mentioned otherwise.

Boyd and Soldano (B.9) measured particle-diffusion controlled self-exchange rates at two temperatures (0.3°C and 25°C) in Dowex 50 resins of different cross linkages (upto 24%). From a correlation of their rate data using the Fick's law model, they reported self-diffusivities for the following ions: Ag^+ , Na^+ , K^+ , Rb^+ , Cs^+ , Zn^{2+} , Y^{3+} , Th^{4+} . It was observed that the resin-phase self-diffusivities strongly decreased with an increase in ionic valency; the diffusivity values were lower in resins of higher cross-linkage, and increased

with an increase in temperature. They also studied the effect of heteroionic environment on self exchange in the resin phase (S.7). It was concluded that the diffusion coefficient of a cation decreased in the presence of a slower ion and increased in the presence of a faster one.

Spiegler and Coryell (S.10) determined self-diffusion coefficients of Na^+ , Zn^{2+} and Ca^{2+} ions in phenolsulphonic cation-exchange membrane "Nepton CR-51" by observing the spread of radiotracers and also by measuring the electrical conductances. Nernst-Einstein relationship was used to calculate the self-diffusion coefficients in the latter case. The agreement was reported to be fairly good except for Ca^{2+} ions. They concluded that mechanisms of diffusion and conductance in the membrane were similar.

Tetenbaum and Gregor reported in 1954 (T.3) isotopic exchange data of K^+ ion in 12% cross-linked polystyrene sulphonate acid cation-exchange resin. They used two experimental methods to obtain rate data, viz. shallow-bed technique and limited bath method. External fluid concentration and the superficial fluid velocity were the variables in their study. The data were interpreted with the Fick's law model describing the mass transfer in both the film and resin phases. They calculated film thickness from the exchange rate data obtained with dilute solutions. Different values of film thickness, 1.2 microns at high flow rates of solution in

the shallow bed technique, and 11 microns at high rates of stirring in the limited bath method were reported by them.

Self-exchange rates for the ions Cs^+ , Ag^+ and Ca^{2+} in ion exchange membranes were reported by Lagos and Kitchner (L.1). In their experimental study, they varied the moisture content in the membrane strips and thereby swelling characteristics. It was observed that ionic self diffusivities decreased appreciably with a decrease in the moisture content, and that the variation was more pronounced with Ca^{2+} (bivalent) ion than with Cs^+ or Ag^+ (monovalent) ions.

Gopala Rao, Kuo and David (G.4, K.4) developed a Single-Particle Radioactive Tracer (hereafter referred as SPRT) Technique for the measurements of ionic self-diffusivities in the resin phase. In addition to their binary-exchange rate studies (referred to later in this chapter), they measured resin-phase diffusivities for Ba^{2+} and Na^+ ions in Dowex 50W-X8 resins.

In 1968, Kunitaro et al. (K.3) used the above technique to study the self-exchange of Na^+ ions in a porous ion-exchange resin. The experimental data were compared with theoretical results to obtain the intraparticle diffusivity and fluid-phase mass transfer coefficient. The intraparticle diffusivity was dependent upon the concentration of solution and was expressed as the sum of solid-diffusivity and effective pore-diffusivity.

Huang et al. (H.9) studied self exchange of Fe^{3+} ions in Dowex 50W-X8 resin in the temperature range of 15-55°C. Measurements were made with resin beads in the diameter range 0.0210 cm to 0.05 cm and with different solution concentrations (0.03N to 0.984N). Self-diffusion coefficient values were obtained using Fick's law model. The diffusion-coefficient values were reported to decrease with an increase in the concentration of the solution, decrease with an increase in particle size and increase with an increase in temperature.

Bodashkova et al. (B.6) studied the sorption characteristics of Y^{3+} ion present in a trace form in the solution phase. They used several cations such as Li^+ , Na^+ , K^+ , Cs^+ , NH_4^+ and Ca^{2+} as macrocomponents. Self-diffusion coefficients were calculated with Fick's law model. In dilute solutions, external film diffusion was found to be the main resistance to sorption, whereas internal diffusion was the main resistance in concentrated solutions. The self-diffusion coefficient of the microcomponent ion was reported to approach the value of self diffusion coefficient of the macrocomponent ion in the resin.

Diffusion of Cs^+ , Ca^{2+} , La^{3+} , Tb^{3+} and Lu^{3+} ions in Dowex 50W-X8 resin, was studied in the presence of a large excess of another counterion by Sharma et al (S.3). The agreement between the theory using diffusion models, and

experimental data was reported to be very good when the contributions due to both film and particle-diffusion processes were taken into account. Their data of self-diffusion coefficients for Tb^{3+} , La^{3+} and Lu^{3+} ions in HCl solutions indicate that large hydrated ions having the same charge have higher mobility inside the resin matrix, contrary to the earlier concepts. It was also found that self-diffusivity value of a trace component in the presence of a less mobile macrocomponent was less than that obtained in the presence of a more mobile macrocomponent. This confirms the observation of earlier research workers about the strong heteroionic effect on the magnitude of self diffusivity.

From the preceding discussion, the current status of understanding about self-exchange kinetics in strongly acidic resins may be summarized as follows:

1. Ion exchange is a diffusion controlled process, and the overall rate of exchange is controlled either by diffusion in the film adhering to the resin beads or by the particle diffusion or by both.
2. In resins of heteroionic form, self diffusion coefficient of an ion is different from its value obtained in the respective homoionic form of the resin.

Binary Exchange

Ion exchange in a binary system is more complex than self or isotopic exchange. Earlier research workers did not take into account the diffusion-induced electric forces in their consideration of binary exchange, and they used a simple rate law such as Fick's law model to describe the ionic fluxes. Many research workers in the past reported a constant internal diffusion coefficient for binary systems. However, as discussed later in this section, the inter-diffusion coefficient depends upon the relative concentrations of diffusing species. In this section some of the significant contributions of research workers in the area of binary exchange are presented.

Helfferich and coworkers in late fifties indicated that the effect of electric-potential gradient produced by the diffusion of ions of dissimilar mobilities must also be considered in the analysis of mass transfer rates in fluid film (S.1) and diffusion inside ion exchangers (H.6). They used the Nernst-Planck equations to describe the flux of each counterion. According to this theory, when two ions of dissimilar mobilities diffuse, an electric-potential gradient is set-up which tends to slow down the faster ion and speed up the slower one. Taking into account the contribution of electric-potential gradient to ionic fluxes, an expression for the interdiffusion coefficient was obtained in terms of self diffusivities and ionic composition (H.6). In a

binary system, the magnitude of interdiffusion coefficient varies as a function of ionic composition between the values of the two self-diffusion coefficients.

This theory has been experimentally verified for both the film-diffusion controlled and particle-diffusion controlled exchange rates by many research workers (G.2, G.4, H.3, H.4, H.7, K.1, K.4, M.4, S.6, T.1, T.4, T.9, T.10). In many cases self diffusion coefficients in the resin phase were obtained from isotopic exchange data in the absence of data on self-diffusion coefficients in heteroionic systems.

Film-Diffusion Controlled Exchange: Glaski and Dranoff (G.2) studied forward exchange rates in the exchange of H-Na and H-Cs systems using Dowex 50W-X8 resin. The Nernst-Planck model very well interpreted their rate data. However, their data could also be correlated by the chemical reaction model and the film-diffusion model. Smith and Dranoff (S.6) studied the film-diffusion controlled kinetics of forward and reverse exchange for the system Na-H-Dowex 50W-X8. The experimental data were very well interpreted by the Nernst-Planck model.

Turner and Snowdon (T.10) reported the liquid-phase mass-transfer coefficients for the exchange of H^+ and Na^+ ions between dilute aqueous chloride solutions and Zeo-Kerb 225 resin. Equations incorporating the effect of electric-potential gradient were written to describe ionic fluxes. An expression for mass transfer coefficient in terms of

parameters such as ionic diffusivities, film thickness and solution concentration in the film, was obtained. The computed results showed a satisfactory agreement with the experimental results.

Film-diffusion controlled exchange rate data were also obtained by Talasek and Eliasek (T.1) with Dowex 50W-X16 resin in H^+ ionic form with $5 \times 10^{-3} M$ chloride (or nitrate) solutions of 17 cations. According to the authors, their integral kinetic data could be interpreted by means of the Nernst-Planck model. Their kinetic data in the film-diffusion region was primarily dependent upon the valency of ion, and its mobility, hydration and steric arrangements. The integral diffusion coefficient values were reported to decrease with the valency of ion and increase with its mobility.

Kataoka et al. (K.1) studied the film-diffusion controlled rates of ion exchange of H-Zn and H-Ca systems with Diaion Skib resin with coions of different valencies. Their results showed that the experimental data agreed with the theoretical ones based upon the Nernst-Planck model, and also showed the existence of the effect of valency of the coion on the exchange.

Particle-Diffusion Controlled Exchange: Helfferich (H.3, H.4) showed the validity of Nernst-Planck model to describe the flux equations in terms of independently determined resin-phase

self-diffusivities and electric-potential gradient. H-Na exchange rates and concentration profiles were measured in a stack of five phenol-sulphonicacid resin discs with a solution-phase concentration of 0.1N chloride (H.3). One end of the stack (of discs in monoionic form) was exposed to a jet of solution containing only the second counterion. The concentration profiles were measured by analysing the composition in each of the five discs. The experimentally observed rates and concentration profiles for forward and reverse exchanges for the two ions were different, and agreed with the results predicted by the Nernst-Planck model.

Hering and Bliss (H.7) who studied rates of ion-exchange in Dowex 50W resins for six pairs of ions viz., Na-Zn, Na-Ag, Ag-Al, Zn-Ca, Zn-Al and Al-Ca, found that the rate data could be correlated by the Fick's law model. Different values of inter-diffusivities for forward and reverse exchanges for each ionic pair were obtained. They also found that their data could as well be represented with the help of Nernst-Planck model. They observed that the self-diffusivity values obtained from a correlation of their data with the Nernst-Planck model were greatly influenced by the nature of the second ion. In view of the simplicity of the Fick's law model, the authors recommended it for design purposes.

Kuo and David (K.4) who reported the exchange kinetics of the Ba-Na-Dowex 50W-X8 system, employed the SPRT technique

with anion concentrations of N/100 and 2N. The data obtained with N/100 solutions were correlated by fluid-phase mass-transfer coefficient approach. The numerical values of the mass transfer coefficient for Ba^{2+} ion sorption was greater than that for the Na^+ ion sorption. The data with 2N solutions were correlated by the Fick's law model with different invariant diffusivities in the two directions of exchange. Their data for Ba^{2+} ion sorption could also be correlated with the Nernst-Planck model incorporating the effect of electrical potential gradient. But the agreement between the experimental and computed results for Na^+ ion sorption was not good.

Gopala Rao and David (G.4) made single-particle studies of ion exchange in packed beds for the system Cu-Na-Dowex 50W-X8. They measured sorption rates of Cu^{2+} ions employing cupric chloride solutions of 0.01N, 0.1N, 1.0N, 2.0N and 4.0N concentrations. For dilute solutions, they represented the rate of mass transfer from the bulk solution to the particle surface by a model in which a fluid-phase mass-transfer coefficient was used. They correlated particle-diffusion controlled rate data by the use of Fick's law model with a constant interdiffusivity. Their constant interdiffusivity values for the sorption of Cu^{2+} ions were found to vary with the bulk fluid concentration. The authors also correlated their particle-diffusion controlled data by the use of

theoretically more correct Nernst-Planck equations. Although their experimental results could be fitted both by the Fick's law model (constant diffusivity) and the Nernst-Planck model, the authors concluded that the use of the former model was unrealistic as it would be invalidated by any change in geometry or boundary conditions. The authors showed that for those cases in which a constant inter-diffusivity model was satisfactory, its value could be computed from the internal self-diffusivities of the exchanging ions.

Morig and Gopala Rao (M.4) reported particle-diffusion controlled ion-exchange rate data for both forward and reverse exchanges of the Sr-Na-Dowex 50W-X8 system. Resin-phase self diffusivities for Na^+ and Sr^{2+} ions were independently measured. They interpreted their rate data with both Fick's law and Nernst-Planck models. Their experimental rate curve for the reverse exchange was slower than the curve predicted by the Nernst-Planck model. This could be due to partial control of film-diffusion on the reverse exchange. The authors proposed a modification of the Nernst-Planck model using different resin-phase self diffusivities for the forward and reverse exchange.

Turner et al. (T.9) measured binary inter-diffusion coefficients in Zeo-Kerb 225 resin for the exchange of H^+ and Na^+ ions at different resin-phase compositions, using a differential bed technique. Their results showed a good

agreement with the values predicted by Nernst-Planck model.

Thibodeaux (T.4) studied particle-diffusion controlled anion-exchange kinetics in a binary system. He defined an integral diffusion coefficient and found that the rate model in which the integral diffusion coefficient was incorporated, interpreted the ion-exchange rates quite well. It was claimed by him that the model proposed by him retained the linearity and simplicity of the Fick's law model, and the precision of the Nernst-Planck model.

From the preceding review of literature on the binary exchange, it can be concluded that (i) for the film-diffusion controlled exchange, Nernst-Planck equations for the ionic fluxes adequately describe the exchange behaviour; (ii) for particle-diffusion controlled exchange, Nernst-Planck equations adequately describe the exchange behaviour for the favourable exchange.

Ternary Exchange

Chemical Reaction Model: Dranoff and Lapidus (D.6) used the chemical reaction model to predict the breakthrough curves for the system Na-Ag-H-Dowex 50. They used fixed beds of 0.42 to 5.52 cm depth in their studies. Concentration history of the effluent stream was determined by chemical analysis. The kinetics of ternary exchange were described by equations corresponding to second order reversible chemical reactions.

The reaction rate constants were calculated from the exchange rate data obtained with shallow beds (0.25 cm) and from equilibrium data. Though the model is quite simple for design purposes, it does not describe realistically the physical phenomena of the exchange process.

Linear Driving Force Model: Clazie (C.1) studied the pore diffusion controlled ion-exchange kinetics in packed beds (about 2 ft. and 4 ft deep) for the system Ag-Na-H-Duolite C-25. Composition history of the effluent stream was determined by chemical analysis. A linear driving force model (mass-transfer coefficient approach) was used to analyse the experimental data. Mass-transfer coefficients for the binary systems were obtained by matching slopes of experimental breakthrough curves with those of computed ones available in literature. The numerical values of mass-transfer coefficients were analysed with the help of Fick's law model and Nernst-Planck model. Using an analogy of the relationships between binary and ternary diffusivities mass-transfer coefficients for the ternary systems were calculated from the binary ones. It was reported that the experimental data matched satisfactorily with the computed values.

Tan and Spinner (T.2) simulated the cyclic-exchange operation of a shallow bed using a linear driving force model. The system studied was Na-Mg-Ca-Dowex 50W-X12 and the bed

height was varied from 7.6 cm to 20.3 cm. The anion concentration of the feed solution was 0.6N chloride, and the regenerant was 2.4N sodium chloride. Experiments were also carried out for the binary system Na-Ca-Dowex-50W-X12. The concentration history of the effluent stream was determined by chemical analysis. In the ternary studies, calcium and magnesium ions were assumed to have similar exchange properties and the ternary system was considered as pseudobinary, sodium being one component and calcium-magnesium being the other component (termed as the 'hardness component'). They defined an effective resin phase diffusivity which was evaluated at the average resin composition using Nernst-Planck model. This value of the diffusivity was then used in the calculation of resin phase mass-transfer coefficient. The agreement between the computed and experimental results was reported to be satisfactory.

Nernst-Planck Models for Ternary Systems: Lupa (L.3) analyzed the film-diffusion controlled binary rate data of the system Na-H-Dowex 50W-X8 studied earlier by Smith and Dranoff (S.6) and of the systems Na-H-Dowex 50W-X8 and Cs-H-Dowex 50W-X8 reported by Glaski and Dranoff (G.2). For analysis, resin-phase resistance was also incorporated. Nernst-Planck equations were used to describe ionic fluxes in the film as well as in the resin phase. It was reported that there was a significant improvement in the prediction of experimental

results. Film-diffusion controlled rate data obtained (by Dranoff and Lapidus (D.6)) for the ternary system H-Na-Ag-Dowex 50 and the data obtained (by Glaski at Northwestern University) for the system H-Na-Cs-Dowex 50W-X8 were also correlated by Lupa. He expressed the ionic fluxes in the film phase by the Nernst-Planck equations. The resin phase ionic fluxes were expressed in terms of Stefan-Maxwell equations in which electric potential gradient was also incorporated. It was reported that there was a significant improvement in the prediction of experimental results as compared to the case when only film resistance was considered.

Viswanathan (V.3) studied the solid-diffusion controlled binary and ternary ion-exchange kinetics for the system Ba-Sr-Na Dowex 50W-X8 using the SPRT technique. The anion concentration of the fluid phase in his studies, was 0.1N (chloride). For Na-Ba and Na-Sr binaries, he found that the experimental depletion rate of Na^+ ions initially in the resin phase, exchanging with Ba^{2+} or Sr^{2+} ions in the solution, was faster than that predicted by the Nernst-Planck model, whereas for the reverse exchange, the experimental rates were much slower than the predicted values. In his ternary studies, he assumed that diffusion of ions in the exchanger was analogous in terms of mathematical relationships to ternary diffusion of species in liquids or gases. The ternary diffusion coefficients were expressed in terms of inter-

diffusivities for the binary pairs and the resin-phase composition. The rate equations were solved numerically. However, the agreement between the experimental and computed results was not good.

Irreversible Thermodynamics Model: An irreversible thermodynamics model for the solid-diffusion controlled ion-exchange rates was developed by the research group with which the author of this dissertation was also associated (V.4). For a single component, the model reduces to Fick's law model and for a binary system, it reduces to Nernst-Planck model. This model was used to correlate Viswanathan's rate data. The equations were solved numerically using IBM 7044 computer. It was found that the computed rate curves agreed well with the small amount of experimental data then available.

Bajpai (B.1) who was also associated with this research group, studied the binary and ternary solid-diffusion controlled exchange rates for the system Sr-Mn-Cs-Dowex 50W-X8. He also employed SPRT technique using 0.1N chloride solutions. It was found that for favourable exchange, the experimental rate data could be predicted very well by the above model. However, the agreement for the unfavourable exchange was not equally good.

The following conclusions can be drawn from the preceding discussion. There are no exhaustive studies on ternary ion-exchange kinetics, and particularly particle-

diffusion controlled ion-exchange kinetic data are scarce. There is also a need for development of theoretically based mathematical model to describe ion-exchange kinetics in a multicomponent system.

ION-EXCHANGE EQUILIBRIA

In a multicomponent system, the selectivity of the resin phase for a particular ionic species will be influenced by the presence of the other ionic species. Even in a binary system, ionic selectivity of the resin phase will be effected by the presence of other ion. In a ternary system, preference for a particular ion over another by the resin phase can be predicted quantitatively from the selectivity behaviour of the resin for the ionic pair containing the two ions in question, provided the third ion has no influence. An understanding of the equilibrium behaviour of a binary ionic system will thus be necessary before a quantitative treatment of ternary ionic behaviour is possible.

In this section, important literature on both binary and ternary ion-exchange equilibria is presented. Correlations of experimental binary equilibrium data available in literature are also presented. No attempt has been made to refer to any work on thermodynamic properties other than the ionic distribution. At the end of the section, literature on ternary cationic equilibria has been discussed with the emphasis on correlation of ternary data in terms of more easily accessible

binary data.

Binary Exchange

For various binary systems, a number of research workers have reported data on ionic distribution between the resin phase and solution phase. In many cases, data were obtained with solutions of different ionic concentrations. In general, for a heterovalent cationic system, ions of a higher valency are preferred by the resin and the preference increases with a decrease in anionic strength of the solution. For the case of homovalent cationic systems, the ionic species with a smaller hydrated volume is preferred in the resin phase. Temperature is reported to have an insignificant effect on the distribution. It has also been observed that exchangers sorb less water when they are saturated with a more favourable ion in a homovalent series. The selectivity of an ion exchanger is enhanced with an increase in cross-linkage.

Selectivity of ionic species in resin phase follows the commutative principle. For example, if in two binary pairs A-B and B-C, A is preferred over B and B is preferred over C, then, A will be preferred over C in a binary pair A-C, and also in a ternary system A-B-C, the order of preference will be $A > B > C$. Some significant studies of ion exchange equilibria are summarized in Table 1.

TABLE 1: ION-EXCHANGE EQUILIBRIUM STUDIES

No.	Authors	System	Remarks on correlation	Ref.
<u>Binary Studies</u>				
1.	Bauman and Eichorn (1947)	Na-H, Ca-H-Dowex 50, 0.1N chloride solution	Resin phase assumed to be equivalent to strong chloride solution; Donnan membrane theory used for correlation	B.5
2.	Ekedahl and coworkers (1950)	H-Ag-Wofatit KS and Dowex 50 resins	Resin phase activity coefficient data from experimental selectivity data	E.1
3.	Argersinger and coworkers (1950, 52)	H-NH ₄ -Dowex 50, 1.0M chloride solution; H-Ag-Dowex 50, 1.0M nitrate solution; H-Na-Dowex 50, 1.0 and 0.3M chloride solutions	Resin phase activity coefficient data calculated from the experimental selectivity data	A.1
4.	Davies and Yeoman (1953)	K-H-polystyrene sulphonated resin, 0.004N and 0.1N chloride solutions	Donnan membrane theory; activity coefficients in the resin phase shown to be equal to those in strong chloride solutions	D.1
5.	Bonner and coworkers (1957, 58)	Cu ²⁺ , Zn ²⁺ , Co ²⁺ , Ni ²⁺ , Hg ²⁺ Cd ²⁺ , UO ₂ ²⁺ , Pb ²⁺ , NH ₃ OH ⁺ Mn ²⁺ , Ba ²⁺ , Cr ³⁺ , Ce ³⁺ , La ³⁺ Dowex 50 (4, 8, 16% DVB)	Equilibrium quotient with respect to Li ⁺ ; selectivity scale related to water uptake	B.7

No.	Authors	System	Remarks on correlation	Ref.
6.	Djurfeldt and Samuelson (1957)	Na-Zn, Na-Cu, Na-Mn-Wofatit KS resin, 0.05-0.2N nitrate solutions	Used Rothmund-Kornfield equation; the constants in the equation are found to be independent of solution concentration	D.4
7.	Subbarao and David (1957)	Cu-Na-Dowex 50, 0.01 to 4N chloride solutions	Used Donnan membrane theory; activity coefficients in the resin phase obtained from the corresponding data in the concentrated solutions	S.11
8.	Vasishth and David (1959)	Fe-H-Dowex 50, 0.05-2N nitrate and perchlorate solutions	Ratio of activity coefficients in resin phase assumed to be unity; law of mass action used to correlate the data	V.1
9.	Hogfeldt (1966)	Ag-H-Dowex 50(2-24% DVB crosslinkage), 0.1N solution	At low concentrations in the bulk fluid phase, the equilibrium quotient, decreased markedly, and in a few cases showed a selectivity reversal	H.8
10.	Mears and Thain (1968)	Na-H, Na-Cs, Na-Sr-Zeo Karb 315, 0.01M to 0.4M chloride and bromide solutions	Studied the effect of coion sorption and water uptake on ion-exchange equilibria	M.2
11.	Gorshkov and Kustova (1970)	H-Sr, H-Ba, K-Ba-Dowex 50 (4, 10, 16% DVB crosslinkage), 0.1N chloride solutions	Obtained activity coefficients in the resin phase from water vapour sorption data; used thermodynamic equilibrium constant	G.5

No.	Authors	System	Remarks on correlation	Ref.
12.	Reddy and Marinsky (1970, 71)	Ca ²⁺ , Sr ²⁺ , Co ²⁺ , Ni ²⁺ , Zn ²⁺ , Cd ²⁺ (trace components), H ⁺ (macrocomponent)-Dowex 50 AGW, perchlorate and poly- styrene sulphonate solutions	In perchlorate solutions, bivalent ions preferred by the resin; in polystyrene sulphonate solutions, H ⁺ ions preferred by the resin	R.1
13.	Fricke (1971)	H-Na, H-Cs, Na-Cs-partially sulphonated (25 to 100%) styrene resins	Relative affinity of the of the resin for different ions affected by the extent of sulphonation	F.1
<u>Ternary Studies</u>				
1.	Dranoff and Lapidus (1957)	H-Cu-Ag, H-Na-Ag-Dowex 50, 0.1N nitrate solutions	For a binary pair in a ternary system used adsorption isotherm model; binary data independent of the presence of the third ion.	D.5
2.	Jangg (1958)	Ni-Cu-Ca ions	Experimental ternary data found to differ from the predicted values obtained by using binary separation factors	J.1
3.	Jasz and coworkers (1961-63)	Cs ⁺ , H ⁺ , Na ⁺ , Ag ⁺ , K ⁺ , Tl ⁺ , Rb ⁺ -Dowex 50W-X8	Equilibrium distribution for component binary pairs found to be independent of the presence of the third ion; data for a quaternary system also presented	J.2

No.	Authors	System	Remarks on correlation	Ref.
4.	Pieroni and Dranoff (1963)	H-Na-Cu-Dowex 50W-X8, 0.01, 0.05 and 0.1N nitrate solutions	Selectivity coefficient for each ionic pair calculated; binary data not affected by the presence of third ion	P.3
5.	Walter Meyer (1964)	H^+ , Cs^+ , Sr^{2+} , Ce^{3+} -Dowex 50W-X8, 0.1 to 3.0N chloride solutions	Used phase-equilibria theory; binary data independent of the presence of the third ion	M.3
6.	Davydov and Radushinskaya (1966)	Ca-Mg-K, Ag-K-Ca-KU-1 0.05 to 0.1M solutions	Could use an empirical equation for correlation of the data obtained only with dilute solutions	D.2
7.	Smith (1968)	Na-Cu-Ba-Dowex 50W-X8, 0.01 and 2N chloride solutions	Used Rothmund-Kornfeld equation to correlate binary data deduced from ternary data; such binary data compared well with the individual binary data obtained experimentally	S.5
8.	Soldatov and Kharevich (1968)	NH_4 -H-K-Dowex 50-X10, 0.1N chloride solutions	Used an empirical equation to correlate ternary data	S.9
9.	Cloete et al. (1969)	Na-K-H-Zeo Karb 225, 0.1N chloride solutions	Ternary data plotted on a triangular diagram	C.2
10.	Soldatov and Bychkova (1970)	NH_4 -K-H-Dowex 50-X10, 0.1N chloride solutions	Resin-phase activity coefficients in the ternary system calculated from the binary activity coefficient data by the same method as used for calculating the corresponding data of liquid equilibria in ternary systems using data on binary systems; nearly a constant value of equilibrium constant for ternary system	S.8

No.	Authors	System	Remarks on correlation	Ref.
11.	Bajpai (1972)	Sr-Mn-Cs-Dowex 50W-X8, 0.1N chloride solutions	Generalized phase equilibria approach; data for pairs Sr-Mn and Sr-Cs could be deduced from the ternary data.	B.1

In general, the objectives of ion-exchange equilibrium studies have been two-fold: (i) to use the information for design purposes, (ii) to understand the ion-exchange selectivity phenomenon. Research workers have tried to predict ion-exchange equilibria with the help of mechanistic models as well as from purely thermodynamic considerations. When the object is to develop equations for design purposes semi-theoretical or empirical equations have been used to correlate the distribution data obtained experimentally.

Similar or slightly different expressions for equilibrium coefficient may be obtained for different theories interpreting the equilibrium data. No one approach can be considered theoretically more sound though the data could be correlated better by a particular equation. For example, Walter Meyer (M.3) correlated his binary equilibrium data using phase-equilibrium theory, law of mass action and Donnan membrane theory, and found that the data were correlated the best by the phase-equilibrium approach. It does not necessarily follow that the phase-equilibrium approach is more sound theoretically.

In many correlations, the effect of resin-phase activity coefficients was neglected (for example, D.5, P.3, V.1). A rigorous method for predicting activity coefficients in the resin phase is yet to be developed. Some other research workers (for example B.5, S.11) assumed that the

resin phase was equivalent to a concentrated solution, the composition of which could be obtained from the ionic composition in the resin phase and its moisture content. The activity coefficients in the resin phase were thus obtained from concentrated solution values of activity coefficients. According to the above authors, selectivity coefficients calculated from such data on activity coefficients, compared well with the values obtained from the experimental ionic distribution. Davies and Yeoman (D.1) showed the concentrated electrolyte nature of the resin from their experimental study of the uptake of water and electrolyte by sulphonated-polystyrene ion exchangers of varying degrees of crosslinkage. The resin phase activity coefficients were calculated with the help of Donnan equations. The authors claimed that the activity coefficients in the heteroionic forms could be satisfactorily predicted from the sorption data of the monoionic forms of the exchanger.

However, Schubert (S.2) has noted for several electrolytes that if the activity coefficient for the resin phase is plotted as a function of the equivalent solution strength computed from the water content and the ionic composition of the resin phase, the curve has the same shape, but lies below the corresponding curve for aqueous solutions of the same electrolyte.

Some research workers made attempts to calculate the resin-phase activity coefficients from the experimental equilibrium data. Argersinger et al.(A.1) and Ekedahl et al.(E.1) calculated activity coefficients in this manner. Once relationship between activity coefficient and the resin-phase composition is known, the selectivity of the resin for any solution composition can be obtained. This will be further discussed in the next chapter.

In the present investigation, the author of this dissertation was interested in the equilibrium measurements to the extent of knowing the boundary conditions for the binary and ternary rate studies. After going through the literature, it was concluded that it was more practical to obtain the experimental equilibrium data directly rather than make an attempt to predict the same. Therefore, no mention has been made of prediction methods of ion-exchange equilibria in the present report. An excellent discussion on earlier research work on prediction methods is given in Helfferich's book (H.2(a)). Diamond and Whitney (D.3) and Reichenberg(R.1) have also reviewed ion-exchange selectivity behaviour.

Ternary Ionic Equilibria

When there are three competing counterions present in a system, ionic distribution would be influenced by the relative affinity of the resin phase for the ions. Speaking qualitatively, the selectivity sequence in a ternary system

would be the same as obtained from the component binaries.

Data on equilibrium studies of ternary systems are relatively scarce*. Attempts were made to correlate the ternary data with the component binary data by Dranoff and Lapidus (D.5), Jangg (J.1), Jasz et al. (J.2), Pieroni and Dranoff (P.3), Walter Meyer (M.3), Smith (S.5) and Bajpai (B. In most cases, the reported work suffered from two main limitations: (i) empirical methods were used in some of the correlations; (ii) comparisons were made between experimental observed binary equilibrium data and those deduced from the ternary equilibrium data. There is no significant effort in predicting ternary equilibria from the binary data. Lack of information regarding resin-phase activity coefficients of ions in ternary systems and an inadequate treatment of binary data have often hampered further progress in this area.

In general, it has been reported that distribution of any two of the three cations in a ternary system between the two phases compared well with corresponding experimental binary data (obtained in the absence of the third ion). However, upon closer scrutiny, it can be seen that the agreement is not good in some cases (for example B.1, M.3).

Soldatov and Kharevich (S.9) gave an empirical equation for correlating the compositions in the two phases. Cloete et al. (C.2) plotted the ternary data on a triangular diagram with resin-phase composition given by the regular grid

*A list of references on ternary systems was presented in Table 1.

and the solution-phase composition along constant parameter curves. The method was applied for the K-Na-H-Zeo Karb 225 system. The data were also presented as a combination of two rectangular diagrams.

Though it was claimed in the literature that the ternary ion-exchange equilibrium data could be predicted from a knowledge of ionic distribution of two component binaries, the author of this dissertation measured experimentally both the ternary equilibrium data and the data on the component binaries. Certainly the interesting results that were obtained in the present study justified the additional measurements.

* * *

CHAPTER 3

THEORY

Theoretical developments on ion exchange kinetics and equilibria have been presented in this chapter. Naturally, greater emphasis has been placed on ion-exchange kinetics and particularly on ternary systems. No attempt has been made to present theoretical developments made by other research workers. Excellent reviews are available on theory of ion-exchange kinetics and equilibria in Helfferich's book (H.2(a,c)) as well as in the book edited by Marinsky (H.5, R.2). This chapter is mainly devoted to theoretical developments in the ion-exchange kinetics and equilibria made by the author of the present dissertation and the research group with which he has been associated at the Indian Institute of Technology, Kanpur.

ION-EXCHANGE KINETICS

It is now well established that the rate of ion exchange is determined by the diffusion processes. It may be controlled either by particle diffusion, or by film diffusion, or by both. Particle-diffusion control is favoured by large resin particles, concentrated fluid solutions, and a high degree of agitation or high superficial fluid velocities. On the other hand, film-diffusion control on ion-exchange rates is enhanced by dilute fluid solutions, smaller sizes of resin beads and reduced stirring speeds, or smaller superficial fluid velocities.

The fixed ionic groups have no effect on the ion-exchange rates as long as they do not associate with counterions. The particle diffusion coefficients are reduced in higher crosslinked resins. Helfferich (H.2(d)) has described a criterion to determine a priori, relative dependence of ion-exchange rates on particle diffusion and film diffusion.

Diffusion in Ion-Exchange Resin

The Fick's law model can be used to describe isotopic-exchange or self-exchange rates. Nernst-Planck equations, which take into account the effect of electric-potential gradients induced by unequal mobilities of diffusing ions were used by Helfferich to describe binary-exchange kinetics in ion-exchange resins (H.6). Barrer and coworkers (B.3) studied binary exchange in chabazites and described ionic fluxes in terms of equations derived from principles of irreversible thermodynamics.

A similar approach has been followed in the treatment given below for a ternary ion-exchange system under isothermal and isobaric conditions. The effect of swelling pressure on ion-exchange kinetics is neglected. The whole resin is treated as quasi-homogeneous. The resin beads are assumed completely spherical in shape. Coupling of ionic fluxes other than by electric-potential field is neglected.

Considering ternary cationic diffusion inside ion-exchange resin, one can write an expression for the molar

flux of kth species, J_k :

$$J_k = - C_k \sum_{j=1}^4 L_{kj} \nabla \bar{\eta}_j \quad (1)$$

where water is the fourth component. The gradient of the electro-chemical potential of species j , $\nabla \bar{\eta}_j$ is obtained by

$$\nabla \bar{\eta}_j = \nabla \bar{\mu}_j + Z_j F \nabla \bar{\phi} \quad (2)$$

where $\bar{\mu}_j$ is the chemical potential. F is Faraday constant and $\bar{\phi}$ is electrical potential. Substituting Equation 2 in Equation 1

$$J_k = -C_k \sum_{j=1}^4 L_{kj} \nabla \bar{\mu}_j - C_k L_{k5} \nabla \bar{\phi} \quad (3)$$

where $L_{k5} = \sum_{j=1}^4 L_{kj} Z_j F$

(Note: Z_4 = Valency of water is zero)

The principle of electroneutrality requires that the total concentration of counterions in equivalents, is constant throughout the bead. Hence

$$\sum_{i=1}^4 Z_i \nabla C_i = 0 \quad (4)$$

The absence of electric current inside ion-exchanger gives the condition

$$\sum_{i=1}^3 Z_i J_i = 0 \quad (5)$$

From a manipulation of Equations 3 and 5, one obtains an

expression for $\nabla \bar{\Phi}$,

$$\nabla \bar{\Phi} = - \frac{\sum_{k=1}^3 Z_k C_k \sum_{i=1}^4 L_{ki} \bar{\mu}_i}{\sum_{i=1}^3 C_i Z_i L_{i5}} \quad (6)$$

Substituting for $\nabla \bar{\Phi}$ in Equation 3, one obtains flux of ion k,

$$J_k = - \sum_{j=1}^4 D_{kj} \nabla C_j \quad (7)$$

where,

$$D_{kj} = C_k \left(L_{kj} \frac{d \bar{\mu}_j}{dC_j} - L_{k5} \frac{\sum_{i=1}^3 C_i Z_i L_{ij} \frac{d \bar{\mu}_j}{dC_j}}{\sum_{i=1}^3 C_i Z_i L_{i5}} \right) \quad (8)$$

Assuming that cross phenomenological coefficients are zero, one can make further simplifications,

$$L_{k5} = L_{kk} Z_k F \quad (9)$$

$$D_{kj} = - \frac{C_k C_j Z_k Z_j L_{kk} L_{jj}}{\sum_{i=1}^3 C_i Z_i^2 L_{ii}} \frac{d \bar{\mu}_j}{dC_j} \quad (10)$$

$$D_{kk} = C_k \left(L_{kk} - \frac{L_{kk}^2 C_k Z_k}{\sum_{i=1}^3 C_i Z_i^2 L_{ii}} \right) \frac{d \bar{\mu}_k}{dC_k} \quad (11)$$

$j, k = 1, 2, 3, 4$

It can be shown that

$$C_j \frac{d \bar{\mu}_j}{d C_j} = \frac{d \bar{\mu}_j}{d \ln C_j} = RT \left(1 + \frac{d \ln \bar{\gamma}_j}{d \ln C_j} \right) \quad (12)$$

where $\bar{\gamma}_j$ is the resin-phase activity coefficient of ionic species j . Assuming flux of water is negligible, one can rewrite Equation 7

$$J_k = - \sum_{j=1}^2 \left(D_{kj} - D_{k3} \frac{Z_j}{Z_3} \right) \nabla C_j \quad (13a)$$

$$\text{or} \quad J_k = - \sum_{j=1}^2 \bar{D}_{kj} \nabla C_j \quad (13b)$$

where,

$$\bar{D}_{kj} = \frac{\bar{D}_k C_k Z_k Z_j \left(\bar{D}_3 \left(1 + \frac{d \ln \bar{\gamma}_3}{d \ln C_3} \right) - \bar{D}_j \left(1 + \frac{d \ln \bar{\gamma}_j}{d \ln C_j} \right) \right)}{\sum_{i=1}^3 C_i Z_i^2 \bar{D}_i} \quad (14)$$

and

$$\bar{D}_{kk} = \left(\bar{D}_k \left(1 + \frac{d \ln \bar{\gamma}_k}{d \ln C_k} \right) - \frac{C_k Z_k^2 \left(\bar{D}_k \left(1 + \frac{d \ln \bar{\gamma}_k}{d \ln C_k} \right) - \bar{D}_3 \left(1 + \frac{d \ln \bar{\gamma}_3}{d \ln C_3} \right) \right)}{\sum_{i=1}^3 C_i Z_i^2 \bar{D}_i} \right) \quad (15)$$

In the above expressions $RT L_{kk}$ is taken to be \bar{D}_k , the self-diffusion coefficient of k th ion in the resin.

Special Cases: Assume

$$\frac{d \ln \bar{\gamma}_i}{d \ln C_i} = 0 \quad i = 1, 2, 3$$

Self Exchange: In Equation 13, $C_3 = 0$, $Z_1 = Z_2$, $L_{11} = L_{22}$, the flux equations reduce to Ficks law equations. (See Appendix B).

Binary Exchange: For this case $C_3 = 0$, Equations 13a and 13b reduce to the Nernst-Planck equations (See Appendix B).

Ternary Exchange: These equations reduce to equations which can be derived from a set of three Nernst-Planck equations written for three cationic species. (See Appendix B).

It was indicated by Helfferich (H.2(h)) that for multicomponent ion exchange, Nernst-Planck equations could describe the ionic fluxes for all the ionic species.

Continuing with the developments of Equation 13, one can combine flux equations with the equations of continuity to calculate the concentration profiles in the resin phase.

$$\frac{\partial C_1}{\partial t} = - \frac{1}{r^2} \frac{\partial}{\partial r} (r^2 J_1) \quad (16a)$$

$$\frac{\partial C_2}{\partial t} = - \frac{1}{r^2} \frac{\partial}{\partial r} (r^2 J_2) \quad (16b)$$

in which J_1 and J_2 are obtained from

$$J_1 = -(\bar{D}_{11} \nabla C_1 + \bar{D}_{12} \nabla C_2) \quad (17a)$$

$$J_2 = -(\bar{D}_{21} \nabla C_1 + \bar{D}_{22} \nabla C_2) \quad (17b)$$

where \bar{D}_{11} , \bar{D}_{12} , \bar{D}_{21} and \bar{D}_{22} are given by Equations 14 and 15.

While performing computations, equivalent fractions instead of molar concentrations were considered. Equivalent fractions are defined as

$$\bar{C}_k = \frac{C_k Z_k}{C_o} \quad k = 1, 2, 3$$

where C_o is the capacity in equivalents per unit volume of

the resin, $\sum_{i=1}^3 C_i Z_i \cdot \dots$

The rate equations then become

$$\frac{\partial \bar{C}_1}{\partial t} = \frac{1}{r^2} \frac{\partial}{\partial r} \left(r^2 (\bar{D}_{11} \nabla \bar{C}_1 + \bar{D}_{12} \frac{Z_1}{Z_2} \nabla \bar{C}_2) \right) \quad (18a)$$

$$\frac{\partial \bar{C}_2}{\partial t} = \frac{1}{r^2} \frac{\partial}{\partial r} \left(r^2 (\bar{D}_{21} \frac{Z_2}{Z_1} \nabla \bar{C}_1 + \bar{D}_{22} \nabla \bar{C}_2) \right) \quad (18b)$$

The initial and boundary conditions for the case of particle-diffusion controlled rates are given by

$$\bar{C}_1 = \bar{C}_{10}, \quad \bar{C}_2 = \bar{C}_{20} \quad \text{at } t = 0 \quad 0 \leq r \leq r_0$$

$$\bar{C}_1 = \bar{C}_{1s}, \quad \bar{C}_2 = \bar{C}_{2s} \quad \text{for } t \geq 0 \quad r = r_0$$

The total fraction of any ion present in the resin bead at time t can be obtained by the following expression:

$$q_t = \frac{3}{r_0^3} \int_0^{r_0} \bar{C}_i(r, t) r^2 dr$$

Equations 18a and 18b along with boundary conditions were solved by numerical methods using IBM 7044 digital computer. A finite difference approximation with the forward difference technique was employed.

Film-Phase Control

Consideration of film-diffusion control on exchange rates is important even for the so called "particle-diffusion controlled" ion-exchange kinetics. The assumption of instantaneous saturation of the resin surface at time, t equals

zero, as one of the boundary conditions may not be realistic. In the initial exchange period, when the gradients are not completely set-up in the resin phase, film diffusion does control the exchange kinetics. The following development takes into consideration film-diffusion control of ion-exchange kinetics.

Consider diffusion of three counterions 1,2 and 3 with a common coion (chloride) in the liquid film adhering to the resin bead. Assuming quasi-steady state, ionic fluxes of counter-ions and the coion can be obtained for dilute solutions from the Nernst-Planck equations

$$J_i = - D_i \left(\frac{\partial C_i}{\partial r} + \frac{C_i Z_i F}{RT} \cdot \frac{\partial \Phi}{\partial r} \right) \quad (19)$$

$$i = 1, 2, 3$$

$$J_{Cl} = - D_{Cl} \left(\frac{\partial C_{Cl}}{\partial r} - \frac{C_{Cl} F}{RT} \frac{\partial \Phi}{\partial r} \right) = 0 \quad (20)$$

From the electroneutrality conditions,

$$\sum_{i=1}^3 C_i Z_i = C_{Cl} \quad (21)$$

As there is no flow of current

$$\sum_{i=1}^3 J_i Z_i = 0 \quad (22)$$

The term $\frac{F}{RT} \frac{\partial \Phi}{\partial r}$ can be eliminated from the expressions for J_1, J_2, J_3 after suitable manipulations, to obtain

$$J_1 = - \left((D_1 D_2 C_2 Z_2^2 + D_1 D_3 C_3 Z_3^2) \frac{\partial C_1}{\partial r} + D_1 C_1 Z_1 D_2 Z_2 \frac{\partial C_2}{\partial r} + D_1 Z_1 C_1 D_3 Z_3 \frac{\partial C_3}{\partial r} \right) / \sum_{i=1}^3 D_i C_i Z_i^2 \quad (23)$$

$$J_2 = - \left((D_1 Z_1 D_2 C_2 Z_2 \frac{\partial C_1}{\partial r} + (D_1 C_1 Z_1^2 D_2 + D_3 C_3 Z_3^2 D_2) \frac{\partial C_2}{\partial r} + D_2 C_2 Z_2 D_3 Z_3 \frac{\partial C_3}{\partial r} \right) / \sum_{i=1}^3 D_i C_i Z_i^2 \quad (24)$$

J_3 can be obtained from Equation 22, if J_1 and J_2 are known.

As $\frac{\delta}{r_0} \ll 1$ (where δ is film thickness) concentration gradient $\frac{\partial C_i}{\partial r}$ in the film may be assumed to be equal to $\Delta C_i / \delta$
 $\Delta C_i = C_{i,\text{interface}} - C_{i,\text{bulk}}$.

Total anionic concentration in the film was assumed to be constant for computations. The validity of this assumption will be discussed later in this dissertation.

Both Resistances Controlling Mass Transfer

At the film-resin interface

$$J_{i,R} = J_{i,f} \quad i = 1, 2, 3 \quad (25)$$

$$y_{i,R} = \lambda_i y_{i,f} \quad i = 1, 2, 3 \quad (26)$$

where y_i refers to equivalent fraction of ionic species i at the interface, subscripts R and f refer to resin and film phases respectively, and λ_i is the distribution coefficient

$$y_{i,R} = \bar{C}_i(r_0, t) \quad \text{and} \quad y_{i,f} = \frac{Z_i C_{i,\text{interface}}}{\sum_{j=1}^3 Z_j C_{j,\text{interface}}}$$

$$\bar{C}_i(r_0, t) = \bar{C}_{is}$$

The value of λ_i depends upon the composition, and for binary exchange, it can be obtained from binary distribution data. Such data for the ionic pair A-B (selectivity of the resin for the ions in the order of A>B) may be correlated in terms of an empirical equation of the type

$$\frac{\bar{\beta}_A}{\beta_A} = a + b \bar{\beta}_A + c \bar{\beta}_A^2 = \lambda_A \quad (27)$$

where $\bar{\beta}_A$ and β_A refer to the equilibrium equivalent fractions of the ion A in the resin phase, and in the solution phase respectively.

Assuming that equilibrium exists at the interface of the resin and fluid film, one can write for a binary system

$$\lambda_A = a + b y_{A,R} + c y_{A,R}^2 \quad (27a)$$

$$\text{and } \lambda_B = (1 - y_{A,R}) / (1 - y_{A,f}) \quad (27b)$$

For ternary exchange, λ_i may be calculated as follows. Consider a system A-B-C where selectivity of the resin for the ions A, B and C is in the order A > B > C, and the binary equilibrium data for pairs A-B and A-C are available. Given the ionic fractions at the resin surface, $y_{A,R}$, $y_{B,R}$ and $y_{C,R}$, one can write

$$\frac{y_{A,f}}{y_{A,f} + y_{B,f}} \times \lambda_A \Big|_{AB} = \frac{y_{A,R}}{y_{A,R} + y_{B,R}} = y_{A,R} \Big|_{AB} \quad (28)$$

$$\frac{y_{A,f}}{y_{A,f} + y_{C,f}} \times \lambda_A \Big|_{AC} = \frac{y_{A,R}}{y_{A,R} + y_{C,R}} = y_{A,R} \Big|_{AC} \quad (29)$$

$$y_{A,f} + y_{B,f} + y_{C,f} = 1$$

Solving for $y_{A,f}$, $y_{B,f}$ and $y_{C,f}$, one can write

$$\lambda_A = \frac{y_{A,R}}{y_{A,f}}, \quad \lambda_B = \frac{y_{B,R}}{y_{B,f}}, \quad \lambda_C = \frac{(1-y_{A,R} - y_{B,R})}{(1-y_{A,f} - y_{B,f})} \quad (30)$$

$\lambda_A \Big|_{AB}$ and $\lambda_A \Big|_{AC}$ which are the distribution coefficients for the ion A in the binary systems A-B and A-C respectively can be obtained from Equation 27a with appropriate values of a, b and c, in which $y_{A,R}$ is replaced by $Y_{A,R} \Big|_{AB}$ and $Y_{A,R} \Big|_{AC}$ respectively.

The equations presented above were incorporated in the ternary kinetics. The validity of the above procedure will be justified later in the dissertation. Sample calculations are shown in the Appendix E.

ION-EXCHANGE EQUILIBRIA

As mentioned earlier, different theories leading to similar expressions for equilibrium constant, have been used by research workers to correlate their equilibrium data, e.g. law of mass action, theory of competitive sorption, Donnan membrane theory, phase equilibrium theory. However, no one theory is theoretically more sound than the other.

In phase equilibrium approach, resin phase activity coefficients and rational thermodynamic equilibrium constant can be calculated from experimentally determined selectivity

data for a binary pair. From a knowledge of resin-phase activity coefficients of an ion in two binary pairs, one can estimate activity coefficients of the ion in the corresponding ternary system. In view of this, phase equilibrium approach has been preferred in the present study, and the relevant developments of the theory are presented below.

Phase Equilibrium Approach

When an ion exchange resin is in equilibrium with an external solution, electrochemical potential of any counterion in the two phases must be same.

$$\bar{n}_i = n_i \quad (31)$$

where n_i is the electrochemical potential of the i th species in the solution phase,

Equating electrochemical potentials of a counterion in both the phases

$$\begin{aligned} \bar{\mu}_i + Z_i F \bar{\phi} &= \mu_i + Z_i F \phi \\ \therefore \bar{\phi} - \phi &= \frac{\mu_i - \bar{\mu}_i}{Z_i F} = \frac{1}{Z_i F} (RT \ln a_i + P v_i - (RT \ln \bar{a}_i + \bar{P} v_i)) \end{aligned}$$

where P is the atmospheric pressure, \bar{P} is the pressure in the resin phase, v_i is the partial molal volume of i th ionic species, and a_i is the activity of the ion

$$\therefore \bar{\phi} - \phi = \frac{1}{Z_i F} \left(RT \ln \frac{a_i}{\bar{a}_i} - (\bar{P} v_i - P v_i) \right)$$

Swelling pressure, Π , is given by, $\Pi = \bar{P} - P$

$$\text{Therefore, } E_{\text{Don}} = \bar{\phi} - \phi = \frac{1}{Z_i F} (RT \ln \frac{a_i}{\bar{a}_i} - H v_i)$$

E_{Don} is termed as Donnan potential. Donnan potential acts equally on all ions present in the system. Application of the above principle to counterions i and j leads to

$$\ln \left(\frac{\bar{a}_i}{a_i} \right)^{Z_j} \left(\frac{a_j}{\bar{a}_j} \right)^{Z_i} = \frac{H}{RT} (Z_i v_j - Z_j v_i)$$

However, the contribution of the right-hand side term is generally small and one may write

$$\left(\frac{\bar{a}_i}{a_i} \right)^{Z_j} \left(\frac{a_j}{\bar{a}_j} \right)^{Z_i} = 1 \quad (32)$$

Standard state for the solution phase is defined as hypothetical one molal solution of the solute in which the activity coefficient of the solute is unity. For all practical purposes, extremely dilute solutions approach the ideal state.

However, resin-phase activity coefficients cannot be defined in an analogous manner. Some research workers (A.1, E.1, G.1) have adopted the convention that the resin-phase activity coefficient for ion A $\bar{\gamma}_A$, is unity when the exchanger is entirely in the homoionic form (A form). In the present study also, the same convention to define resin-phase activity coefficients has been adopted.

However, it may not be out of place to mention that the standard states for the activity coefficients in the resin and solution phases are different in character. For

modified selectivity coefficient respectively.

Activity Coefficients from Experimental Selectivity Coefficient

Data: Application of Gibbs-Duhem equation to the exchanger phase gives

$$\bar{X}_A d \ln \bar{\gamma}_A + \bar{X}_B d \ln \bar{\gamma}_B = 0 \quad (36)$$

Expressing rational equilibrium constant and resin-phase activity coefficients in terms of modified selectivity coefficients, one may write

$$K_B^A \left(\frac{\bar{\gamma}_B^{Z_A}}{\bar{\gamma}_A^{Z_B}} \right) = K_{c_B}^A \quad (33a)$$

With the help of Equations 36 and 33a, and expressions

$$\bar{\beta}_A = \frac{\bar{X}_A Z_A}{\bar{X}_A Z_A + \bar{X}_B X_B}$$

$$\bar{\beta}_A + \bar{\beta}_B = \bar{X}_A + \bar{X}_B = 1 \quad \text{we get}$$

$$- \frac{Z_B}{(1 - \bar{\beta}_A)} d \ln \bar{\gamma}_A = d \ln K_{c_B}^A \quad (37)$$

Integrating Equation 37 by parts with respect to $\bar{\beta}_A$, we get

$$Z_B \ln \bar{\gamma}_A = -(1 - \bar{\beta}_A) \ln K_{c_B}^A + \int_0^1 \ln K_{c_B}^A d \bar{\beta}_A \quad (38), \text{ similarly}$$

$$Z_A \ln \bar{\gamma}_B = \bar{\beta}_A \ln K_{c_B}^A - \int_0^{\bar{\beta}_A} \ln K_{c_B}^A d \bar{\beta}_A \quad (39)$$

and, from Equations 33a, 38 and 39

$$\ln K_B^A = \int_0^1 \ln K_{c_B}^A d \bar{\beta}_A \quad (40)$$

From a knowledge of ionic distribution and solution-phase activity coefficients, modified selectivity coefficient can be calculated as a function of solution-phase (and also resin-phase) composition (Equation 35). With the help of Equations 38 to 40, resin-phase activity coefficients and the equilibrium constant K_B^A , can be obtained.

Ternary Ionic Equilibria

For a system containing three counterions A, B and C, it can be shown that

$$(K_B^A)^{Z_C} (K_C^B)^{Z_A} (K_A^C)^{Z_B} = 1 \quad (41)$$

The above relationship is called triangle rule (B.4).

Equation 33 is applicable to any ionic pair (i,j) in a multicomponent system. Since a binary equilibrium constant is characteristic of the pair, it may be used to predict ternary ion exchange equilibria provided that resin-phase activity coefficients of ions in such a system are known. Activity coefficients of component ions of a binary system cannot be used as such because activity coefficient of an ion (say A) in one binary pair (A-B) and in another binary pair (A-C) having the same fraction of A, need not be the same, particularly due to the strong influence of the other ion. However assuming that counterion present in a ternary system makes only its own contribution of the binary pair towards the resin-phase activity coefficients of other counterions,

one can define weighted average activity coefficients for ions in the resin phase as follows:

$$\bar{\gamma}_1 = \frac{\bar{\beta}_2}{\bar{\beta}_2 + \bar{\beta}_3} \bar{\gamma}_1 \Big|_{1-2} + \frac{\bar{\beta}_3}{\bar{\beta}_2 + \bar{\beta}_3} \bar{\gamma}_1 \Big|_{1-3} \quad (42a)$$

$$\bar{\gamma}_2 = \frac{\bar{\beta}_3}{\bar{\beta}_3 + \bar{\beta}_1} \bar{\gamma}_2 \Big|_{2-3} + \frac{\bar{\beta}_1}{\bar{\beta}_3 + \bar{\beta}_1} \bar{\gamma}_2 \Big|_{1-2} \quad (42b)$$

$$\bar{\gamma}_3 = \frac{\bar{\beta}_1}{\bar{\beta}_1 + \bar{\beta}_2} \bar{\gamma}_3 \Big|_{1-3} + \frac{\bar{\beta}_2}{\bar{\beta}_1 + \bar{\beta}_2} \bar{\gamma}_3 \Big|_{3-2} \quad (42c)$$

where $\bar{\beta}_i$ is equivalent fraction of i th ion in the resin phase and $\bar{\gamma}_i \Big|_{i-j}$ is the resin-phase activity coefficient of species i in a binary system $i-j$. In a ternary system when

$$\bar{\beta}_k \approx 0, \quad \bar{\gamma}_i = \bar{\gamma}_i \Big|_{i-j} \quad (i \neq j \neq k)$$

Equations 33 and 42 written for two of the three binary pairs in a ternary system, were used to predict the resin-phase composition in a ternary system in equilibrium with the solution of a given composition.

* * *

CHAPTER 4

EXPERIMENTAL

In the present study, single particle radioactive tracer (SPRT) technique was employed for ion-exchange measurements. In this chapter, scope of this experimental technique for the measurements of kinetic and equilibrium data has been discussed. A list of materials employed in the study, and a description of the experimental set-up have been presented. Experimental procedures for the measurement of resin-capacity, equilibrium and kinetic data have also been given. Systems studied in the present investigation, possible sources of error, and accuracy of measurements have also been discussed.

SINGLE PARTICLE RADIOACTIVE TRACER (SPRT) TECHNIQUE

Gopala Rao (G.3) discussed in detail the suitability, relative advantages and limitations of the deep-bed, shallow-bed and limited-bath techniques for the measurements of ion-exchange kinetics. All the above techniques have some inherent limitations not only in the measurement but also in the analysis of data. To overcome these difficulties, Gopala Rao and David (G.4) developed the SPRT technique for the studies of ion-exchange kinetics in binary systems. The effectiveness of this technique was further established by Kuo and David (K.4), and Morig and Gopala Rao (M.4). Recently,

Kunitaro et al. at the University of Tokyo, Japan (K.3) have measured the self-exchange rates using the single particle technique. Viswanathan (V.3) and Bajpai (B.1) have also used the SPRT technique in their studies of ion-exchange kinetics of ternary systems. A single particle radioactive tracer method was also developed by Gopala Rao (G.3), and Kuo and David (K.5) for measuring ion-exchange equilibria. Smith at the University of Washington, Seattle also used this technique for the measurement of ternary equilibrium data (S.5).

In the SPRT technique, the amount of exchange occurring is so small that the solution composition remains essentially constant during the exchange. This particular characteristic of the method facilitates the elimination of the material balance equation which is usually described by a partial-differential equation (for deep beds) from the mathematical model. The rate of ion-exchange from the resin phase can be directly and continuously measured by monitoring the radioactivity of the tracer present in the bead. High superficial fluid velocities can be employed to obtain particle-diffusion controlled ion-exchange kinetics. As the amount of ion-exchange is small, solution once passed past the bead can be recirculated because its radioactivity will be insignificant as compared to that of the tagged bead itself. Thus large volumes of solution are not necessary for the studies. The

SPRT technique is easy to employ and will give reliable kinetic data. Kinetic data even with concentrated bulk solutions can be obtained with ease by means of the SPRT technique.

The advantages of the SPRT technique are considerable for the case of ternary studies. Cumbersome chemical analysis of component ions in the fluid phase and in the resin phase, is not necessary. Rate data can be obtained with solutions of pre-determined compositions in the bulk fluid phase. (For example, fluid composition varies along the length of the column in the deep-bed method). Again mathematical complications are considerably reduced due to the elimination of material balance equation. Because of this, it is possible to consider a sophisticated model for describing ternary kinetics. One can also obtain kinetic data with pre-determined resin phase compositions using this technique.

The research group at the Indian Institute of Technology, Kanpur was the first to employ this technique for ternary kinetic studies. Though no distinct advantage can be accrued by using the SPRT method for the measurement of equilibrium data, the above group extended the SPRT method for obtaining the ternary equilibrium data. Incidentally, in the SPRT method used by Smith (S.5) for obtaining ternary equilibrium data, ions in the solution were tagged. In the present study ions in the resin bead were tagged.

Though the SPRT technique facilitates the use of a considerably more sophisticated rate model (such as the Nernst-Planck equations), it is not without disadvantages. The ionic systems that can be studied are limited because carrier-free, strong gamma-emitting, radioactive isotopes with long half-lives of ionic components of the system must be available. Homogeneity of each batch of the resin will have to be established by obtaining the data with several single beads. In view of this limitation, only certain well-developed resins (such as Dowex 50W) can be employed for the study. A careful selection of the bead will have to be made under a microscope to eliminate the beads with cleavages or surface blemishes. A resin bead should be of reasonably large size (about one mm). Tagging of the bead with radioisotope and handling of the tagged bead pose certain problems which of course, can be overcome.

Another practical difficulty in the SPRT technique is that the resin beads do get lost occasionally. The loss of a resin bead usually occurs during the washing of the bead or in its transfer from one container to another. It was only after the loss of many a resin particle that the author of the present dissertation could master the technique. Loss of a bead used in taking the data does not mean discarding the data already obtained for kinetic and equilibrium measurements for these measurements are independent of a particular

resin bead. However, particle size and capacity measurements of the lost bead would no longer be useful for subsequent runs. The data reported in the present dissertation were obtained with 5 beads for equilibrium and 12 beads for kinetic studies.

MATERIALS

Chemicals, instruments, and apparatus used in the present study are listed below:

Chemicals

As mentioned earlier, Mn-Cs-Na-Dowex 50W-X8 and Ba-Mn-Na-Dowex 50W-X8 systems were investigated in this study. Barium chloride, manganese chloride and sodium chloride of analytical grade were supplied by the British Drug House (India) Private Limited. Sodium chloride was also supplied by Sarabhai Merck Limited of India. Cesium chloride of laboratory grade was supplied by the BDH Chemicals Limited (England) and Merck and Co., West Germany. Cesium chloride was relatively more expensive, and was also difficult to obtain in India. In view of these difficulties, concentrated solution of cesium chloride (for example, 1N solution) could not be employed when required. All the chemicals were used as such without further purification.

Carrier-free, gamma-emitting ^{137}Cs , ^{54}Mn and ^{22}Na isotopes were obtained from the Chemical and Radioisotope

Division of the International Chemical and Nuclear Corporation of U.S.A. ^{54}Mn was also supplied by the Bhabha Atomic Research Centre of India. The isotopes were supplied in concentrated (about 0.5N) hydrochloric acid solutions. The half-lives of these isotopes are 30 years for ^{137}Cs , 313.5 days for ^{54}Mn and 2.58 years for ^{22}Na .

Instruments and Apparatus

Instruments employed in the equilibrium studies consisted of a scaler (Tracerlab model 132 MA) and a scintillation well shield (Tracerlab model WS-1) containing a photomultiplier tube (RCA 6342A) with a thallium-activated sodium iodide crystal.

For the kinetic studies, a scintillation detector assembly consisting of scintillation head (type SH 635), a low voltage unit (model LV230 A) and a high voltage unit (model HV 200A), was used. These instruments were supplied by the Trombay Electronic Instruments, Bombay (India). The signal from the scintillation head is picked up by the Universal Spectrometer (Tracerlab model 401A) from where it is fed to the Universal Ratemeter (Tracerlab model 231). A Bausch and Lomb voltage recorder (model Vom 7) was used to record the signal from the ratemeter. The scintillation-detector assembly along with the spectrometer, ratemeter and the recorder was mounted on a trolley.

For equilibrium studies, a graduated pipette of 2 ml (with a least count of 0.02 ml) was used to add the solution to a polythene vial (1.7 cm diameter and 5.5 cm long) with a snap-in-cap. Standard glassware such as measuring flasks and pipettes etc. were used to prepare the solutions.

In the kinetic studies, a glass column of 1 cm internal diameter and 15 cm long, with standard ground-glass joints at both ends was used. The column was made by fusing together female parts of two B10 standard joints. A centrifugal pump (0.025 H.P.) was used for circulating the solution. Tygon tubing was used for connections in the flow system.

PREPARATION OF THE RESIN FOR EXPERIMENTAL STUDIES

About 10 grams of resin from a lot of Dowex 50W-X8 were taken in a glass column for conditioning purposes. The resin was converted to sodium form by passing ten bed volumes of 1N sodium chloride solution through the bed at a rate of 0.5 ml per minute per ml of the resin. The bed was then backwashed with distilled water. The resin in sodium form was converted to hydrogen form by passing ten bed volumes of 1N hydrochloric acid solutions at the same flow rate as mentioned earlier. The resin bed was again backwashed. Once again, the resin was converted to the sodium form according to the procedure stated above. This cycle was repeated thrice for proper conditioning of the resin. The conditioned resin in hydrogen

form was placed in a glass bottle and stored under distilled water.

Selection of the Bead

Many conditioned resin particles were examined under a microscope. Only large spherical beads (0.8 - 1.2 mm diameter) without cracks or surface blemishes were selected. Each selected bead was transferred to a different polythene vial with the help of a piece of tissue paper. Each vial was labelled. A bead could be converted into a desired ionic form by equilibrating it with 5 ml of 1N chloride solution of the ion. After about 4 hours the solution was replaced by another 5 ml of the solution used earlier. Usually, the bead was kept in this solution for about 20 hours. After this equilibration period, the bead was washed thoroughly with double-distilled water, and stored under double distilled water in a clean vial.

Bead Diameter Measurement

The diameter of the washed bead in the desired ionic form was measured with the help of a microscope of magnification 50X (10X objective and 5X eye piece). The eyepiece had an ocular micrometer attached to it. The least count of the measurements was 0.02 mm. Diameter of the swollen bead in the desired form was measured at four or five places. The mean value was taken as the actual diameter.

Preparation of Radioactive Tracer Solution

The amount of each isotope solution supplied was only 2-3 drops. It was first diluted to about 5 ml with double-distilled water. The container of the isotope solution was kept in a glass beaker and the solution was evaporated to dryness by means of a low-wattage space heater. The container was cooled, and to it were added 5 ml of double-distilled water and the solution was again evaporated. This procedure was repeated three times. All the hydrochloric acid was thus evaporated away. The final solution was made up to 10 ml and was used as stock solution. Two ml each of this solution were transferred by means of a special pipette to two well-stoppered glass containers. The solution in these containers was used for tagging purposes.

Surgical gloves were used while handling the radioactive solutions. As a safety measure against radiation, film badges supplied by the Directorate of Radiation Protection, Bhabha Atomic Research Centre, Bombay (India) were used.

Tagging of the Resin Bead

The bead in the desired ionic form was transferred to a small basket made of a stainless-steel wire-mesh and fitted with a S.S. wire handle. The basket was washed with double-distilled water before use. The basket was gently immersed (to avoid floating of the bead) in the radioactive

isotope solution of the same cation. After about 24 hours (which was found to be adequate for picking up the radioactive isotope ions), the basket was taken out. The basket and the bead were washed with a thin jet of double-distilled water. The bead was removed from the basket and transferred to a clean vial. The basket was stored under distilled water.

The resin bead in a cationic form (say A) containing radioactive isotope, of $A(A^*)$ is termed as 'tagged bead' and ionic species A, is termed as the tagged ion.

Washing of the Tagged Bead: The author found it necessary to standardize the washing procedure of the tagged bead because all pore solution in the bead, containing radioactive isotope ions, will have to be washed out completely.

To the vial containing the tagged bead, a few milliliters of double distilled water were added and shaken vigorously for a minute. The wash water was removed. This washing procedure was repeated 5 times. The bead was then removed and dried between the folds of tissue paper and again placed in a clean vial and its count rate was taken. The above procedure was repeated till a constant count rate was obtained. Normally 3 sets of washings (5 times in each set) and countings were found to be adequate.

Count-Rate Measurements: The vial containing the tagged bead was placed in the well of the splash-guard (a thin circular aluminium plate fitted with a well at its centre) kept on the scintillation probe. The well of the splash guard fitted into the well of the scintillation probe. The dimensions of the vials used matched with the dimensions of the well. The scintillation detector assembly was covered on all sides by a lead shield (Tracerlab Well Shield WS-1).

Standard procedure given in the operation manual (T.6) of the scaler was employed in determining the various settings (such as gain, discriminator and high voltage) of the scaler for count rate measurements.

In the count rate measurements of a radioactive source of long half-life, the standard deviation is \sqrt{n} , where n is the total number of counts (E.2). Therefore higher the number of the counts, less will be the percentage standard deviation. In the present measurements, the count rate of the tagged bead was about 50 times greater than that of the bead after equilibration (hereafter referred as equilibrated bead), which was in turn atleast 20 times greater than the back-ground count rate. In general, the counts of the tagged bead were measured for 30 minutes, and of the equilibrated bead and back ground each for 60 minutes. The count rate of the vial without the bead was taken as back-ground count rate.

EXPERIMENTAL PROCEDURE

Capacity Measurements

A tagged bead was placed in a vial containing one ml of the double-distilled water and its count rate was measured. The water was removed from the vial, and the vial and the bead were dried with a tissue paper. To the dry vial containing the bead, one ml of 0.1N chloride solution of the same cation was added with the help of a graduated pipette. Sufficient care was taken in adding the solution so that all of it remained at the bottom of the vial in contact with the bead. The equilibration time was around 24 hours. It was found by Gopala Rao (G.3) and Viswanathan (V.3) that the period was sufficient for equilibration. Though shaking of the vial containing the bead might have drastically reduced the equilibration time, it could not be employed lest some solution should stick to the cap or walls of the vial and thereby not contribute to the exchange.

After the equilibration period, the total count rate of the resin bead together with the solution in the vial was measured. The bead was removed from the solution and was thoroughly washed (as per the procedure given earlier). The washed bead was transferred to the cleaned vial (used previously) containing one ml of distilled water, and the count rate of the bead in the vial was again measured. Special precautions for cleaning the used vials to free them from

adhering radioactive materials were taken.

The capacity of the bead in milli-equivalents is given by

$$\text{Bead Capacity (m.eqvts.)} = \frac{\text{CPM}_{eb} - \text{CPM}_{bg}}{\text{CPM}_{tb} - \text{CPM}_{eb}} \times (\text{m.eqvts. of the cation in the solution})$$

where CPM refers to counts per minute and the subscripts eb, tb and bg refer to equilibrated bead, tagged bead and back ground respectively.

In the early stages of investigation, capacity of a bead in a cationic form had to be determined 4-6 times to get atleast two consistent values in succession. Later, the first two capacity determinations were enough for the purpose. Capacity of each experimental bead was determined in each cationic form.

Equilibrium Measurements

Binary Data: Experimental procedure for the measurement of binary equilibrium data is the same as that of capacity measurements except for the composition of the equilibrating solution. When the equilibrating solution contains two species of counterions, the count rates of the tagged and the equilibrated bead, and its capacity determine the ionic fraction in the resin phase.

The equivalent fraction of the tagged ion in the resin phase is given by

$$\text{Fraction} = \frac{\frac{\text{CPM}_{\text{eb}} - \text{CPM}_{\text{bg}}}{\text{CPM}_{\text{tb}} - \text{CPM}_{\text{bg}}}}{\text{Capacity (in m. eqvts)}} \times \begin{matrix} \text{(m. eqvts. of the tagged ion} \\ \text{in the solution + capacity} \\ \text{of the bead)} \end{matrix}$$

It may be noted that the composition in the solution phase after equilibration will be slightly different from the composition of the solution added to the tagged bead because of the exchange between the bead and solution.

Experiments were performed with different proportions of cations in the solution phase. Total anion (chloride) concentration of the solution was kept at 0.1N. Each experiment yields one ionic fraction in the resin phase.

Though only one ionic fraction in a binary system completely defines the resin phase composition, in the present study both the fractions were determined individually and the sum total was found to be nearly equal to unity.

Experiments may either be performed with one bead at a time, or two beads separately at the same time. In case only one bead is used, the bead will have to be tagged successively with the two isotopes and equilibrated with the solution of the same composition in two different runs. When two beads are used at a time, beads in respective ionic forms are equilibrated individually with solution of the same composition in different vials. The later procedure saves time. Both the methods when used on a test run produced nearly identical results.

The data were reproducible within the experimental error. All the data were taken at a room temperature of about 23°C. The procedure for regeneration of the bead to different ionic forms was given earlier.

Ternary Data: In the ternary equilibrium studies, a tagged bead was equilibrated with one ml of 0.1N chloride solution containing three cations in definite proportions. The equivalent fraction of the tagged ion in the resin phase was determined from the count rates of the tagged bead and of equilibrated bead as in binary studies. The other two ionic fractions were obtained by equilibrating the tagged single beads in appropriate ionic forms with one ml of the solution of the same composition as used earlier. Although determination of only two (instead of three) ionic fractions was necessary to define the resin-phase composition, all the three fractions were determined individually and their sum total was found to be nearly equal to unity. A wide range of solution compositions was used to obtain the equilibrium data.

Kinetic Measurements

A tagged bead was washed thoroughly and stored under double distilled water for about 24 hours to remove the concentration profiles, if any, in the resin bead before employing it for a kinetic run.

The schematic diagram of the experimental set-up is shown in Figure 1. It consisted of a glass reservoir of one

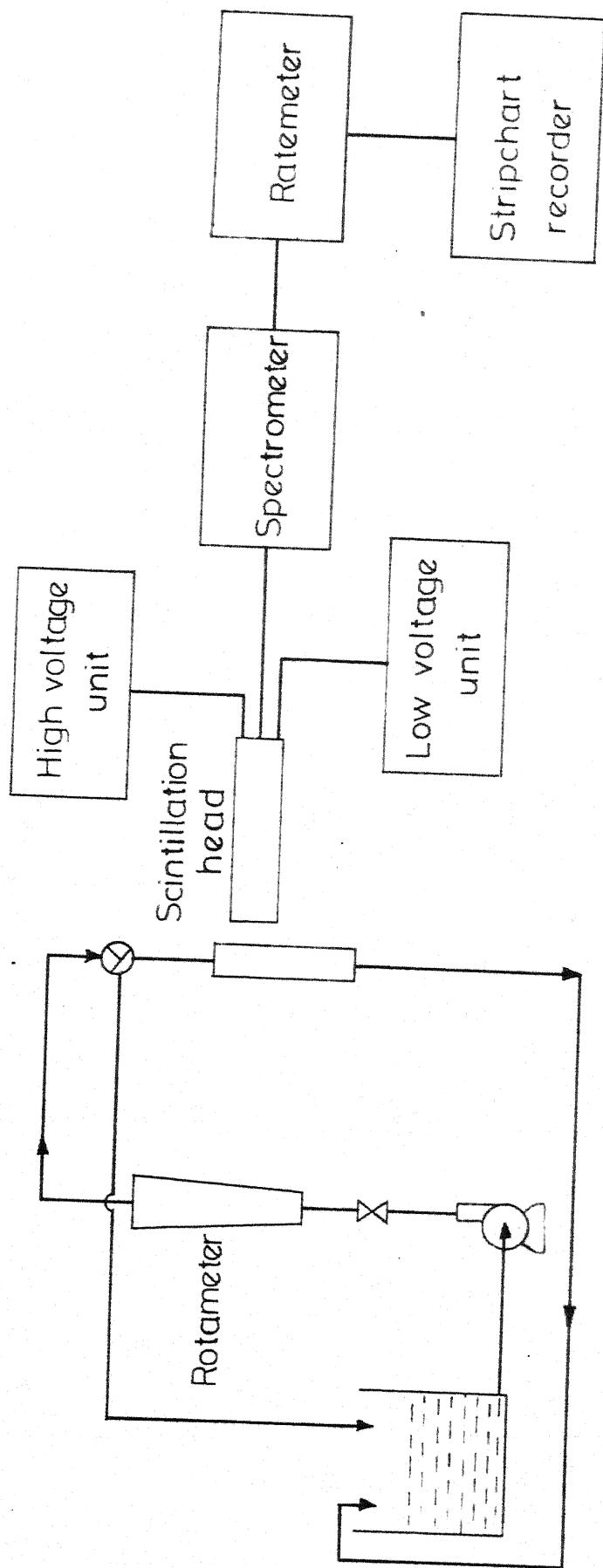


Fig. 1 - Experimental setup for obtaining rate data.

litre capacity for the solution, a centrifugal pump for circulating it, a rotameter for measurement of flow rate and a glass column containing a bed of glass beads into which a tagged resin bead was imbedded. The reservoir was kept in a constant temperature bath maintained at a room temperature of about 28°C.*

The bed of glass beads in the column was prepared in the following manner. The column was first packed with glass beads upto 3 cm above the support of glass wool and was filled with water to remove air bubbles. The tagged resin bead was then transferred to the column and was centered in it on the top of glass beads. More glass beads were carefully added without disturbing the resin bead upto a further height of about 2 cm. A thin glass-wool plug was placed on the top of the glass beads to ensure uniform flow distribution. Again precautions were taken to eliminate the air bubbles. In order to avoid drying up of the bed, it was kept immersed in distilled water until it was hooked to the flow set-up for a kinetic run.

Before the start of a kinetic run, an auxiliary glass column (empty) was placed in the flow assembly and the entire flow set-up was thoroughly cleaned by circulating distilled water, and the water was drained. The auxiliary column was

*Equilibrium and kinetic measurements were made in different parts of a year, hence the variation in room temperature.

replaced by the experimental column containing the resin bead imbedded in the bed. The scintillation head was placed sufficiently close to the column in order to get a strong signal. The voltage signal from the ratemeter was recorded for about 5 minutes.

Standard procedure for determining the settings of the spectrometer and the ratemeter units was employed (T.7, T.8).

The signal showed fluctuations indicating the statistical nature of gamma radiation from the radioactive source. The fluctuations could be reduced by setting the time constant of the ratemeter at a higher value (out of 0.5, 1.5, 5, 15 and 50 seconds). But higher the value of the time constant, greater is the time lag introduced in recording a step change in the signal. A time constant of 1.5 seconds was found quite satisfactory. In general, the fluctuations increased with a weaker signal (of a lesser count rate).

Solution of the desired composition was poured in the reservoir and the experimental column was isolated from the flow loop by a three way stop cock located at the top of the column. The total anion concentration of the solution was 0.1N, unless mentioned otherwise. The solution was circulated through the flow loop by means of the pump to purge out air from the system. As mentioned earlier, the initial count rate of the bead was recorded for about 5 minutes. At the start of the run, stop cock was opened to the column and the solution

was passed through it and the instantaneous signal from the ratemeter was recorded continuously.

The author could not notice any time lag between the starting of the flow down the column and beginning of the decrease in the signal. This could be due to very high fluid velocities, sufficiently high counterion concentration in the fluid (0.1N), and very small distance between stop cock and top of the bed.

Flow through the column was stopped after sufficient elution from the tagged bead had taken place. The column was removed and emptied in a clean petri dish, and the resin bead was sorted out. The auxiliary glass column was inserted in the flow set-up and the back ground signal from the solution passing through the column was recorded. Care was taken to ensure the same geometry.

The eluted bead was converted into the desired ionic form and was tagged for further runs as per the procedure mentioned earlier.

Fluid Velocity Used in the Kinetic Studies: Gopala Rao and David (G.4) used a superficial fluid velocity of 0.6 - 0.7 cm/sec in their rate studies. Morig and Gopala Rao (M.4) used velocities of about 6 cm/sec and Viswanathan (V.3) employed fluid velocities of nearly 20 cm/sec. In all the studies, the above workers obtained particle-diffusion controlled exchange rates with 0.1N chloride solutions.

In the present investigation, the flow set-up was similar to the ones used by the above research workers. Superficial fluid velocities of about 25 cm/sec were employed in the present investigation to ensure particle-diffusion control of ion-exchange kinetics.

Self and Binary Exchanges: For self-exchange rate studies, the tagged bead was eluted with a solution containing the same counterion as in the resin phase. In the binary-exchange rate studies, the tagged bead was eluted with a solution containing only the other counterion in the binary system. Both forward and reverse exchange rates were measured. Particle-diffusion controlled kinetic runs for various self and binary exchange rates were taken and the results have been presented in the next chapter.

Ternary Exchange: Rate data for ternary exchanges were taken for different initial and boundary conditions of the resin phase. The studies were restricted to the following two cases: (i) one ion, say A, initially in the resin phase exchanging with a mixture of ions B and C in the solution phase, $\bar{A}^*-(B-C)$; (ii) two ions, say A and B, initially in the resin phase, with one ion, say A, tagged with its radioactive isotope exchanging with the third ion, C in the solution phase, $(\bar{A}^*-\bar{B})-C$.

$\bar{A}^*-(B-C)$: Exchange rate data were obtained with

different fractions of the two ions B and C in the solution phase. In a given ternary system, there are three such combinations.

$(\bar{A}^*-\bar{B})-C$: The two ions were introduced in the resin phase in the following manner. A resin bead in an ionic form A was tagged with its isotope and its count rate was measured. The bead was brought in contact with about 5 ml of 1N chloride solution of the counterion B for some time (from a few seconds to two minutes depending upon the selectivity of the resin for the ions and their ionic mobilities in the resin phase). The bead was removed and washed free of adhering ions including those in pores. The count rate of the partially eluted bead was measured. The ratio of this count rate to the previous one gives the fraction of A in the resin phase. The bead was stored under double distilled water for about 24 hours before a kinetic run was taken.

Rate data were obtained with ion C in the solution phase and different initial fractions of ions A and B in the resin phase. There are six such combinations of ions in a given ternary system. It may be noted that the concentration history of only one ion (i.e. the tagged ion) can be obtained for each run.

SYSTEMS STUDIED IN THE PRESENT INVESTIGATION

As indicated in the Introduction Chapter the ternary system Mn-Cs-Na-Dowex 50W-X8 was chosen for the present investigation. Equilibrium and rate data for the above system were obtained. A considerable amount of difficulty was faced by the author in interpreting the kinetic data obtained with ^{137}Cs tagged beads. Rate data obtained with such beads could not be employed to test the validity of the proposed rate model. Therefore, the necessity of obtaining more ternary rate data was felt during the course of the investigation. For this purpose, Ba-Mn-Na-Dowex 50W-X8 system was chosen.

Ba^{2+} ion was chosen as the third component in the second ternary system even though the author failed to procure carrier-free, gamma-emitting ^{133}Ba isotope both from B.A.R.C. of India and the International Chemical and Nuclear Corporation of U.S.A. Some of the considerations that went into the decision are as follows. Ba^{2+} ion is bivalent, and is highly preferred in the resin phase. Viswanathan (V.3) studied Ba-Na binary exchange rates in Dowex 50W-X8 resin. The self-diffusion coefficient of Ba^{2+} ions was also available from his study. Also, Ba-Na equilibrium data were available (K.2).

In the Mn-Cs-Na ternary system, binary and ternary equilibria, self, binary and ternary exchange rates were

measured by the author of the present dissertation. For the Ba-Mn-Na system, the author obtained the following equilibrium and rate data:

- (i) Ba-Mn equilibria;
- (ii) $\bar{\text{Mn}}^*-\text{Ba}$, $\bar{\text{Mn}}^*-(\text{Ba}-\text{Na})$, $\bar{\text{Na}}^*-(\text{Ba}-\text{Mn})$ ($\bar{\text{Mn}}^*-\bar{\text{Na}}$)-Ba, ($\bar{\text{Mn}}^*-\bar{\text{Ba}}$)-Na, ($\bar{\text{Na}}^*-\bar{\text{Mn}}$)-Ba, and ($\bar{\text{Na}}^*-\bar{\text{Ba}}$)-Mn rate exchanges.

Results of the experimental measurements for all the above cases have been presented in the next chapter. Rate data obtained with cesium tagged beads are given in the Appendix A. In addition to the above two ternary systems, the author correlated the rate data of the Sr-Mn-Cs system studied by Bajpai (B.1).

SOURCES OF ERROR

Equilibrium Measurements

Geometry of the Radioactive Source: The count rate measured by a scaler-scintillation detector-well shield assembly depends upon the geometry of the radioactive source. Therefore, for reproducible results, geometry of the source must remain constant.

The polythene vials used were not exactly identical to each other. Therefore, same vial was used for measuring the count rates of the tagged bead as well as of the equilibrated bead to minimize the error due to this factor.

Although the total radioactivity of the equilibrated bead together with the solution is the same as that of the original tagged bead itself, it was observed that the count rate of the equilibrated bead together with the solution was 5 to 10% less than that for the tagged bead. This is because of the fact that a major fraction of the radioactive isotope initially in the bead (point source) is leached out into the solution (volume source). Therefore, all the calculations were done with count rate of the tagged bead (point source) and not with the count rate of tagged bead together with the solution after equilibration (volume source).

Small Volume of the Equilibrating Solution: Each time 1.0 ml of solution was used for capacity and equilibrium measurements. The least count of the graduated pipette was 0.02 ml. A maximum of 2 percent error might be introduced due to this factor. A larger volume of solution was not used lest the residual radioactivity of the resin bead should reduce to a very great extent. This is of more significance for a weaker radioactive source.

Variation of the Voltage from the Mains: The count rate of a radioactive source as indicated on the scaler, depends upon the high voltage applied to the scintillation detector. A voltage stabilizer was used to minimize the fluctuations in the voltage. However, the average voltage supplied from the

mains and thereby the voltage output from the voltage stabilizer, varied sometimes from day to day. This could result in variation of the count rate measurements by as much as 5 percent. Since the experimental work involved measurements of count rates on two consecutive days, this variation had to be taken care of. For this purpose, standard sources of the radioisotopes under study were used. The count rates of the standard sources were of the same order of magnitude as that of the tagged bead. The count rate of the standard source was measured before and after each measurement of the count rate in the experimental work. Count rates of the equilibrated bead and of the tagged bead were normalized with the help of count rates of the standard source. A sample calculation is shown in the Appendix C.

As mentioned earlier, in the initial stages of the investigation, 4-6 capacity measurements were carried out to get atleast two consistent values within the experimental error (± 2.0 percent). After the technique was perfected, the first two measurements were enough to give consistent data and the mean value of capacity in a cationic form was used for all calculations. Some times, equilibrium measurements were repeated to check the consistency of the equilibrium data.

Kinetic Studies

Smoothing of the Monitored Rate Curve: A possible source

of error in the kinetic studies could be the smoothening of the experimental curve monitored by the recorder. Since the fluctuations in the curve are inherent in the radioactive tracer method, their magnitude (in relation to the mean value of the signal) could be reduced by employing a tagged bead with a greater radioactivity.

It is relatively easy to draw a straight line to indicate the mean value of the signal when no exchange was taking place. A smooth curve was drawn through the recorded rate plot, making sure that nearly equal number of peaks appear on both sides of the curve. A photoreduced tracing of a typical recording is shown in the Appendix C (Figure 31).

In general, the maximum error in estimating the average value of the initial count rate is around ± 1 percent. Errors in estimation of instantaneous values of count rate could be higher particularly at the tail end. Self-exchange rate data were repeatedly taken to check the consistency of the data obtained by smoothening the recorded graph, and the procedure was found to be satisfactory.

* * *

CHAPTER 5

RESULTS AND DISCUSSION

This chapter has been divided into two main sections: (i) ion-exchange equilibria and (ii) ion-exchange kinetics. In the first section, results of capacity and equilibrium measurements have been presented and discussed. In the second section, experimental rate data have been presented and compared with the computed data.

ION-EXCHANGE EQUILIBRIA

This section has been further divided into three sub-sections namely, capacity measurements, binary equilibria, and ternary equilibria. In each section, the corresponding results have been presented and discussed.

Capacity Measurements

Table 2 shows capacity data for five resin beads in three different cationic forms. These five beads were used for equilibrium measurements. As mentioned in the Experimental Chapter, the capacity value reported for a bead is the mean value. Variation of individual measurements from the mean value was within 1.5 per cent. Bead capacities in sodium and manganese forms of the resin as shown in the Table 2, are comparable. Except for one bead, capacities in the

TABLE 2: CAPACITIES OF DOWEX 50W-X8 RESIN BEADS
(IN MICRO-EQUIVALENTS)

Ionic Form Bead No.	Na	Cs	Mn
20B/11	1.694	1.502	1.675
32C	0.970	0.788*	1.040
34B/8	1.620	1.590*	1.750
34C/10	1.790	1.720	1.857
32D/9	1.750	1.546	1.810

*Calculated from the total count rates
obtained from a measurement of the
equilibrated bead together with the
solution.

manganese form are generally higher (in two cases, as much as 8 percent higher); capacities of the beads in cesium form are uniformly lower than the corresponding values in sodium and manganese forms.

Reasons for higher values of bead capacities in manganese form could be the following: (i) possible impurities in the chemicals used in the study; (ii) hygroscopic nature of manganese chloride, and of course, (iii) experimental error. Standard manganese chloride solution of 0.1N strength was prepared with $\text{MnCl}_2 \cdot 4\text{H}_2\text{O}$ crystals. It is known that manganese chloride is hygroscopic. The actual quantity of manganese chloride (MnCl_2) in the standard solution was not measured by chemical analysis. The concentration of manganese chloride (in milliequivalents per ml) occurs in the formula for the bead capacity, and if a higher value is substituted for the concentration, one gets a higher value of bead capacity in manganese form. This error will be cancelled out in equilibrium measurements if the same standard solution is used for preparing the equilibrating solutions.

The capacity values of the beads in cesium form are significantly less than the values in the sodium form except for two beads namely 34B/8 and 34C/10. The author experienced difficulty in regenerating cesium tagged beads with 0.1N cesium chloride solutions. Though the equilibrium data obtained with cesium tagged beads did not give rise to

difficulties in interpretation, the author experienced difficulties in correlating kinetic data obtained with such beads. An attempt has been made to explain this behaviour of cesium tagged beads in the Appendix A.

Binary Equilibria

Most of the equilibrium data were obtained using three resin beads namely, 20B/11, 34C/10 and 32D/9. Binary equilibrium data of ionic pairs Cs-Na, Mn-Na and Mn-Cs obtained with 0.1N chloride solutions have been presented in Tables 3 to 5 and Figures 2 to 4 respectively.

Equivalent percent ($= \text{equivalent fraction} \times 100$) of one of the ions in the resin phase in equilibrium with a solution containing a binary mixture was obtained by the method mentioned earlier. Sample observations and calculations have been given in the Appendix C. For a particular equilibrating solution, sum total of the two individual resin phase ionic fractions may not be exactly equal to unity. For example, the sum total of the fractions for the sample case mentioned in the Appendix is 1.0375. This may be attributed to: (i) slight variation in the composition of the solution for the two cases due to the exchange between the tagged beads and the equilibrating solution, and (ii) experimental error (already discussed in the Experimental Chapter).

Even though the same stock solution was used for getting both the resin-phase fractions, there would be a

TABLE 3: ION-EXCHANGE EQUILIBRIA: Cs-Na-
DOWEX 50W-X8 SYSTEM

A = Cs

B = Na

No.	Solution-Phase Equivalents %		Resin-Phase Equivalents %	
	β_A	β_B	$\bar{\beta}_A$	$\bar{\beta}_B$
1.	19.5	80.5	33.8	66.2
2.	29.9	70.1	41.4	58.6
3.	37.4	62.6	47.4	52.6
4.	59.3	40.7	70.2	29.8
5.	79.9	20.1	84.8	15.2

TABLE 4: ION-EXCHANGE EQUILIBRIA; Mn-Na-
DOWEX 50W-X8 SYSTEM

A = Mn

B = Na

No.	Solution-Phase Equivalents %		Resin-Phase Equivalents %	
	β_A	β_B	$\bar{\beta}_A$	$\bar{\beta}_B$
1.	9.9	90.1	63.7	36.3
2.	18.2	81.8	78.0	22.0
3.	29.7	70.3	82.4	17.6
4.	39.7	60.3	86.5	13.5
5.	59.7	40.3	95.5	4.5

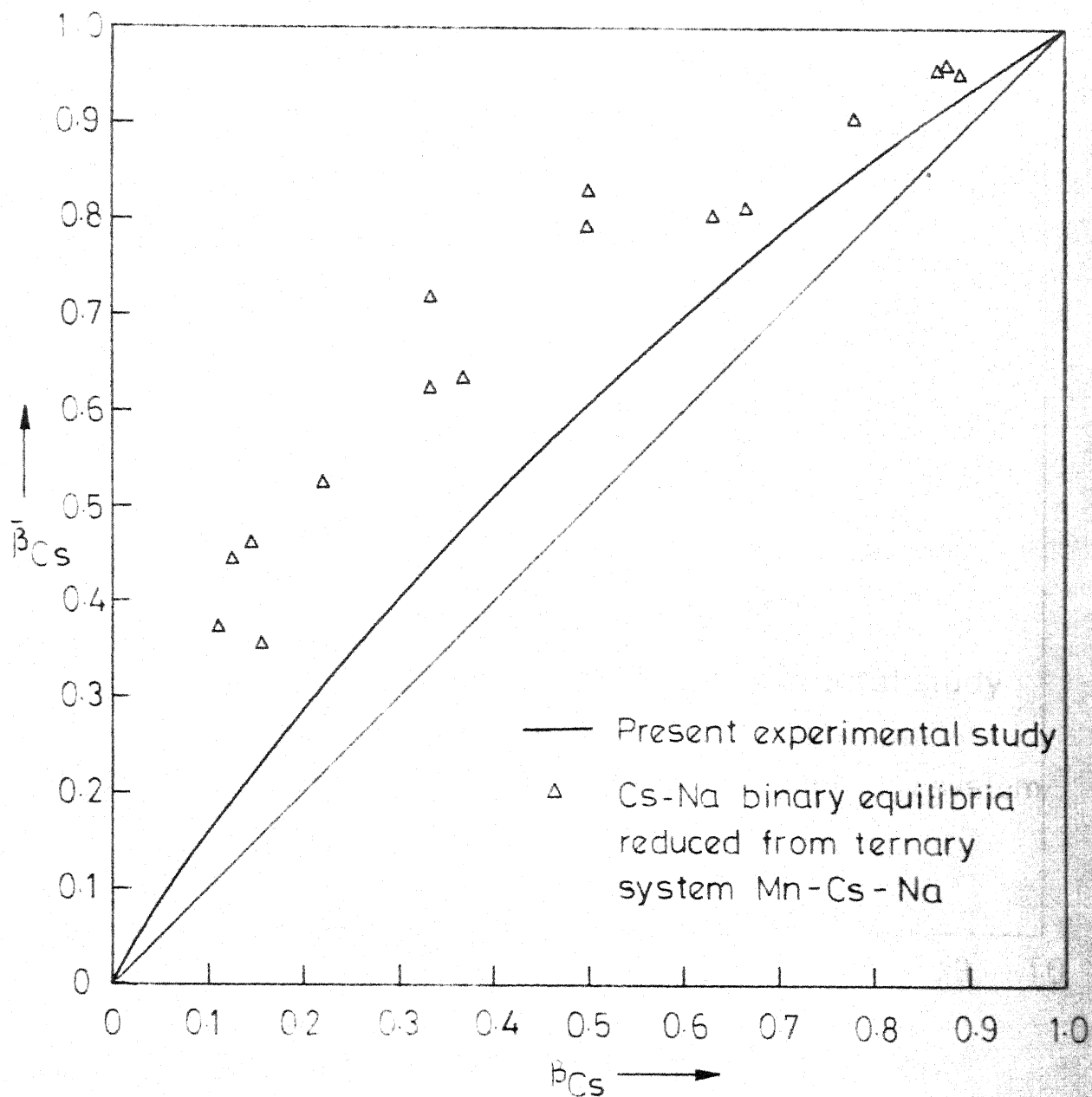


Fig. 2 - Binary Ion-Exchange Equilibria:
Cs - Na - Dowex 50 W-X8 System.

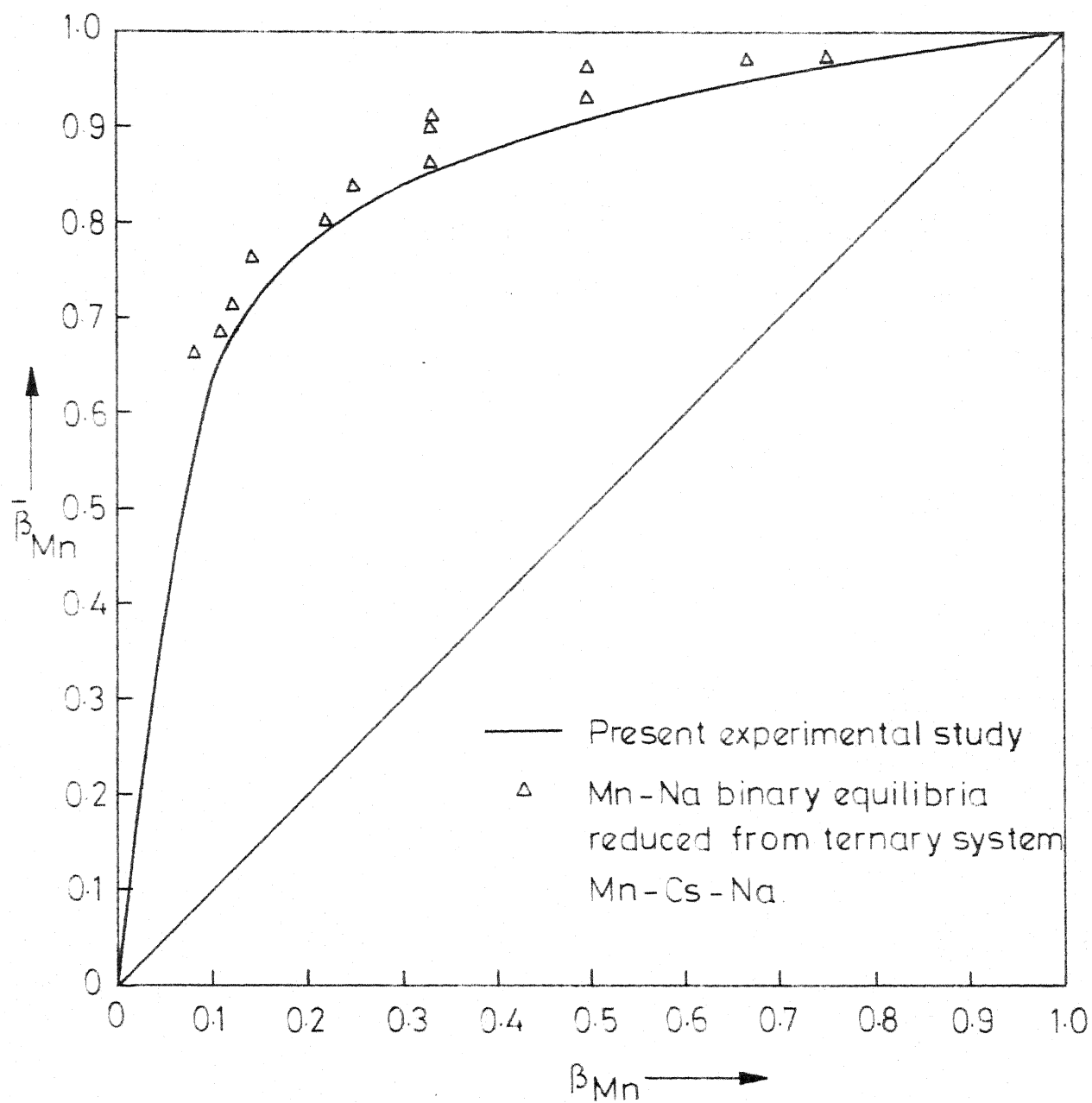


Fig. 3 - Binary Ion-Exchange Equilibria: Mn-Na-Dowex 50W-X8 System.

TABLE 5: ION-EXCHANGE EQUILIBRIA: Mn-Cs-
DOWEX 50W-X8 SYSTEM

A = Mn

B = Cs

No.	Solution-Phase Equivalents %		Resin-Phase Equivalents %	
	$\bar{\beta}_A$	$\bar{\beta}_B$	$\bar{\beta}_A$	$\bar{\beta}_B$
1.	9.9	90.1	50.2	49.8
2.	19.9	80.1	57.9	42.1
3.	40.0	60.0	63.2	36.8
4.	60.0	40.0	78.2	21.8

slight difference after equilibration in actual solution compositions for the two cases due to the beads being initially in different ionic forms. The percentage variation will increase with a smaller value of fraction of one of the two components in the equilibrating solution.

Also ionic fractions of species A and B for a given solution-phase composition were not necessarily obtained with the same resin bead. In the calculations, this aspect was taken care by substituting the value of corresponding ionic capacity of the bead used. Because of the slight variation after equilibration in the composition of the solution, there are eight experimental points for a set of four equilibrating solutions. A smooth curve was drawn through all such points (though actually not shown in the figures) to obtain the experimental equilibrium plot.

In the tables, normalized values of resin-phase ionic equivalents percent are given. A normalized value was obtained by dividing the value of individual ionic fraction by the sum of the two such ionic fractions in the binary system. Again a reference can be made to the sample calculations mentioned earlier. In the tables, only the initial compositions of the equilibrating solutions are given.

Equilibrium data for the binary pair, Ba-Mn, have been presented in Table 6 and Figure 5. Since the carrier-free, gamma-emitting radioisotope of barium ^{133}Ba could not

be procured, all the data were obtained with beads initially in the manganese form and tagged with ^{54}Mn isotope. The resin-phase equivalents percent of manganese, $\bar{\beta}_{\text{Mn}}$ determined experimentally have been tabulated. Resin phase barium percents could not be obtained experimentally, and were determined by subtracting $\bar{\beta}_{\text{Mn}}$ from hundred.

TABLE 6: ION-EXCHANGE EQUILIBRIA: Ba-Mn-DOWEX 50W-X8 SYSTEM

A = Ba

B = Mn

No.	Solution-phase Equivalents %		Resin-phase Equivalents %	
	β_A	β_B	$\bar{\beta}_A$	$\bar{\beta}_B$
1.	10.1	89.9	44.8	55.2
2.	18.5	81.5	63.1	36.9
3.	38.3	61.7	77.9	22.1
4.	58.1	41.9	90.4	9.6
5.	78.0	22.0	95.7	4.3

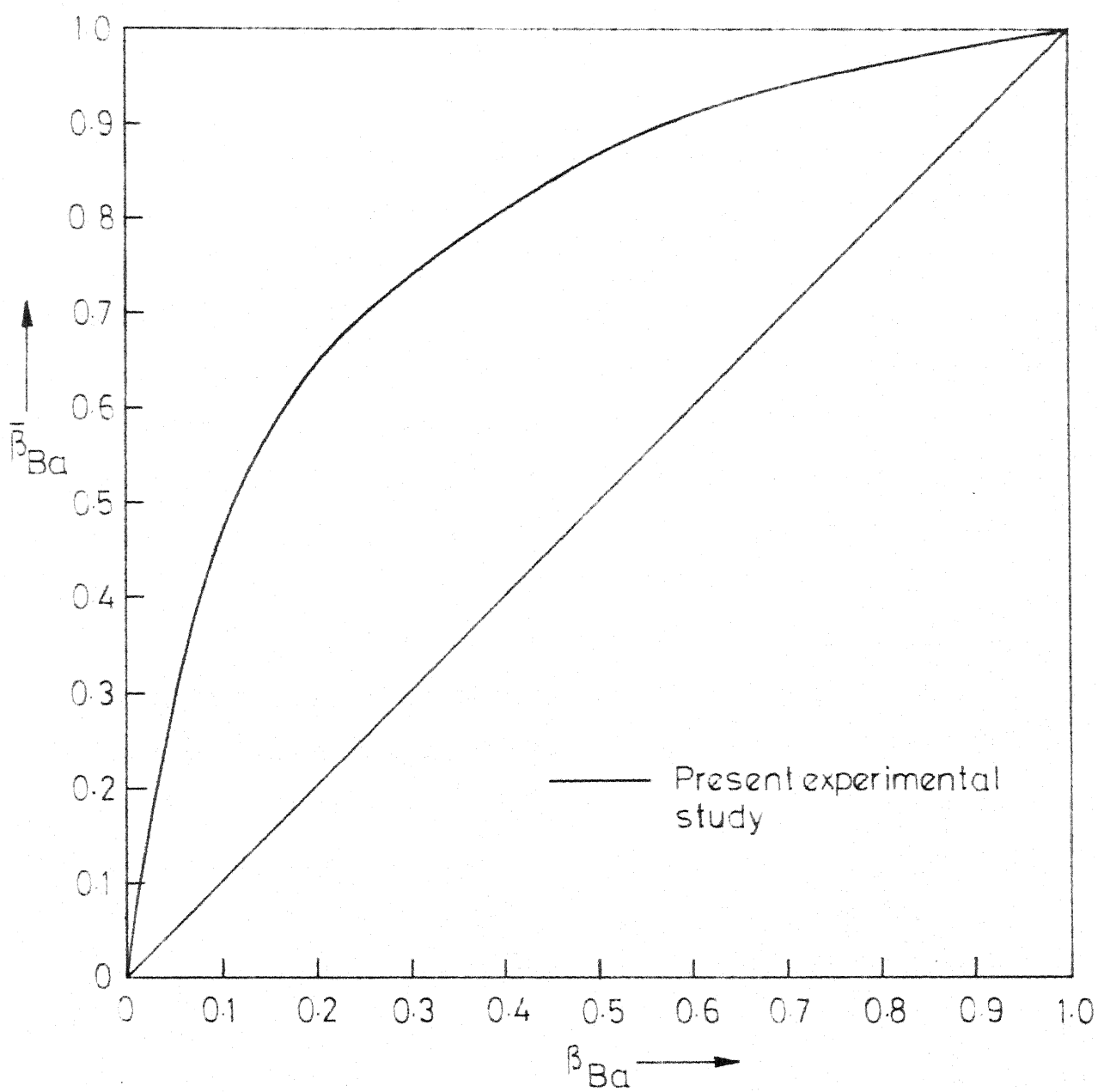


Fig. 5 - Binary Ion-Exchange Equilibria: Ba - Mn - Dowex 50W-X8 System.

From the experimental results, it can be observed that the preference of the resin Dowex 50W-X8, is in the order of $Ba > Mn > Cs > Na$. Preference of the resin for Ba^{2+} and Mn^{2+} ions over Cs^+ and Na^+ ions is because both Ba^{2+} and Mn^{2+} are bivalent ions where as Cs^+ and Na^+ are monovalent ones. Selectivity of the resin for Cs^+ over Na^+ is to be expected because the hydrated volume of Cs^+ ion is smaller than that of Na^+ ion. It was indicated by Bonner and coworkers (B.7) that Dowex 50 resins would take up Ba^{2+} ions preferentially as compared to Mn^{2+} ions.

In the SPRT method as mentioned earlier, the experimental data are obtained with only a few beads taken from a batch of ion-exchange resins. It was shown by Gopala Rao (G.3) and Kuo and David (K.4) that experimental equilibrium data obtained by their method compared very well with the data obtained using other methods. Equilibrium data for the system Sr-Cs-Dowex 50W-X8 obtained using the SPRT method by Bajpai (B.1) of the present research group at IIT-Kanpur agreed very well with the data obtained by Walter Meyer (M.3) who used a liquid-scintillation technique.

In view of the discussion above, the following conclusions can be drawn regarding the SPRT method: (i) the method is reliable and reproducible; (ii) a single bead with which the data is obtained is representative of the entire batch of the resin.

In Table 7 rational equilibrium constants as defined by Equation 33, for various binary pairs have been tabulated.

TABLE 7: RATIONAL EQUILIBRIUM CONSTANTS OF BINARY SYSTEMS

System		K_B^A
A	B	
Cs	Na	1.69
Mn	Na	37.02
Mn	Cs	8.53
Ba	Mn	49.42

Tables 8 to 10 and Figures 6 to 8 show the resin-phase activity coefficients for the component ions in the binary pairs of the ternary system Mn-Cs-Na. Figure 9 presents the activity coefficient data for the binary pair Ba-Mn. The data are also presented in a tabular form in the Appendix D.

The equilibrium constant K_B^A (for a binary pair A-B, A being preferred by the resin as compared to B), was calculated as shown below. From the experimental equilibrium data modified selectivity coefficients K_{cB}^A were calculated at different values of resin-phase equivalent fractions of A, $\bar{\beta}_A$.

$$K_{cB}^A = \left(\frac{\bar{X}_A}{\bar{X}_B} \right)^{Z_B} \left(\frac{X_B}{X_A} \right)^{Z_A} \frac{\gamma_B^{Z_A}}{\gamma_A^{Z_B}} \quad (35a)$$

$$\bar{\beta}_A = \frac{\bar{X}_A^{Z_A}}{\bar{X}_A^{Z_A} + \bar{X}_B^{Z_B}}$$

TABLE 8: RESIN-PHASE ACTIVITY COEFFICIENTS:
Cs-Na-DOWEX 50W-X8 SYSTEM

A = Cs

B = Na

β_A	$\bar{\gamma}_A$	$\bar{\gamma}_B$
0.085	0.896	0.994
0.150	0.978	0.981
0.283	0.983	0.980
0.407	0.974	0.986
0.518	0.971	0.990
0.606	0.992	0.964
0.690	1.003	0.941
0.771	1.010	0.921
0.858	1.003	0.957
0.931	1.005	0.952

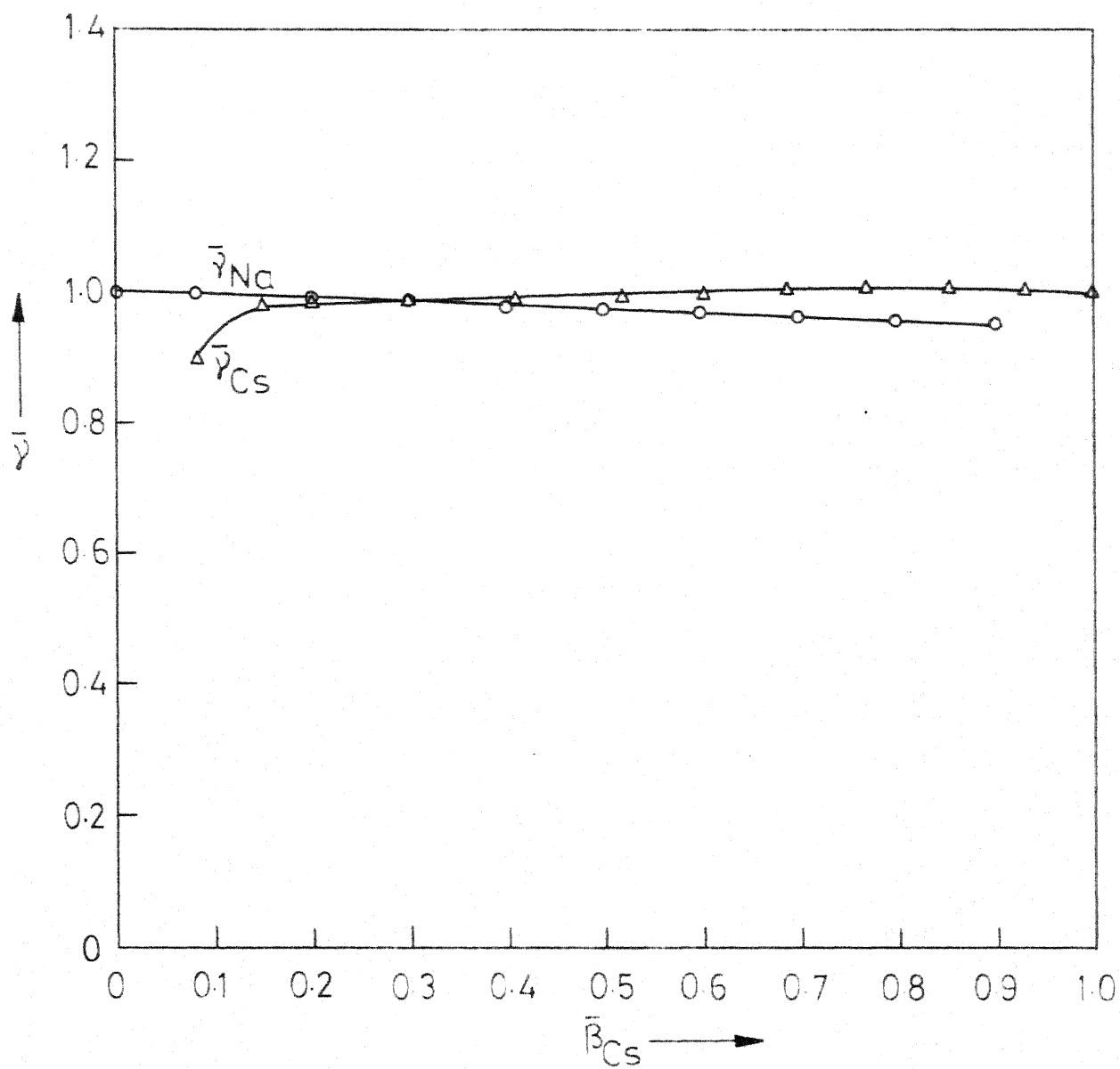


Fig.6 - Resin - Phase Activity Coefficients:
Cs - Na - Dowex 50W -X8
System.

TABLE 9: RESIN-PHASE ACTIVITY COEFFICIENTS:
Mn-Na-DOWEX 50W-X8 SYSTEM

A = Mn		B = Na
\bar{B}_A	\bar{Y}_A	\bar{Y}_B
0.100	1.953	0.991
0.200	1.705	1.001
0.300	1.508	1.037
0.400	1.408	1.053
0.485	1.339	1.063
0.575	1.246	1.094
0.662	1.186	1.148
0.725	1.173	1.172
0.700	1.152	1.234
0.860	1.113	1.372
0.900	1.089	1.478
0.932	1.058	1.671
0.960	1.023	2.133
0.975	1.010	2.463
0.995	0.998	3.946

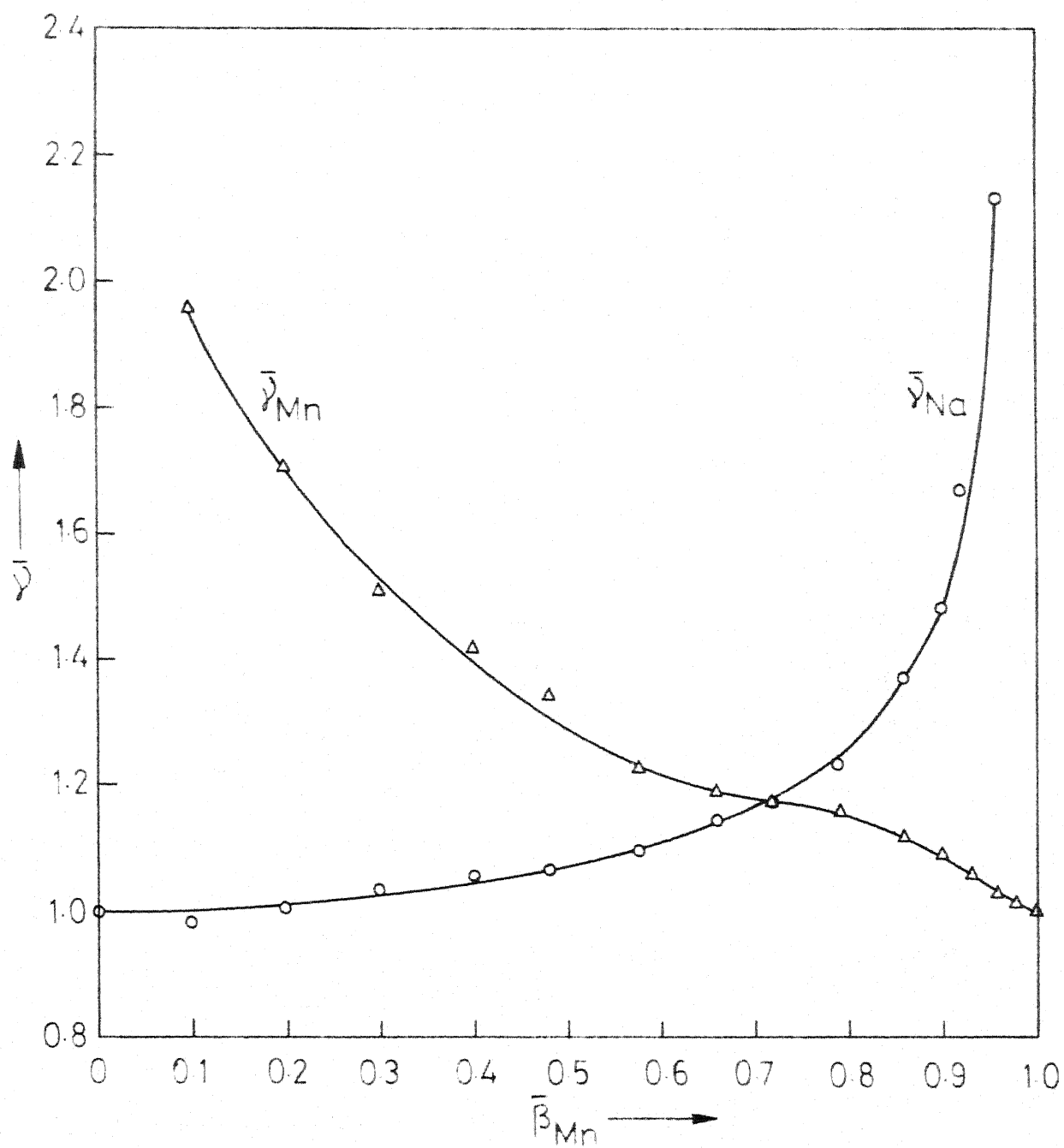


Fig. 7 - Resin - Phase Activity Coefficients Mn-Na-
Dowex 50W-X8.

TABLE 10: RESIN-PHASE ACTIVITY COEFFICIENTS:
Mn-Cs-DOWEX 50 W-X8 SYSTEM

A = Mn

B = Cs

\bar{S}_A	\bar{Y}_A	\bar{Y}_B
0.080	0.442	0.999
0.150	0.433	1.003
0.225	0.494	0.988
0.280	0.526	0.976
0.360	0.563	0.958
0.415	0.592	0.943
0.472	0.632	0.921
0.525	0.706	0.874
0.572	0.749	0.844
0.632	0.837	0.775
0.688	0.892	0.725
0.742	0.930	0.685
0.797	0.954	0.657
0.850	0.973	0.630
0.900	0.992	0.596
0.950	1.001	0.561

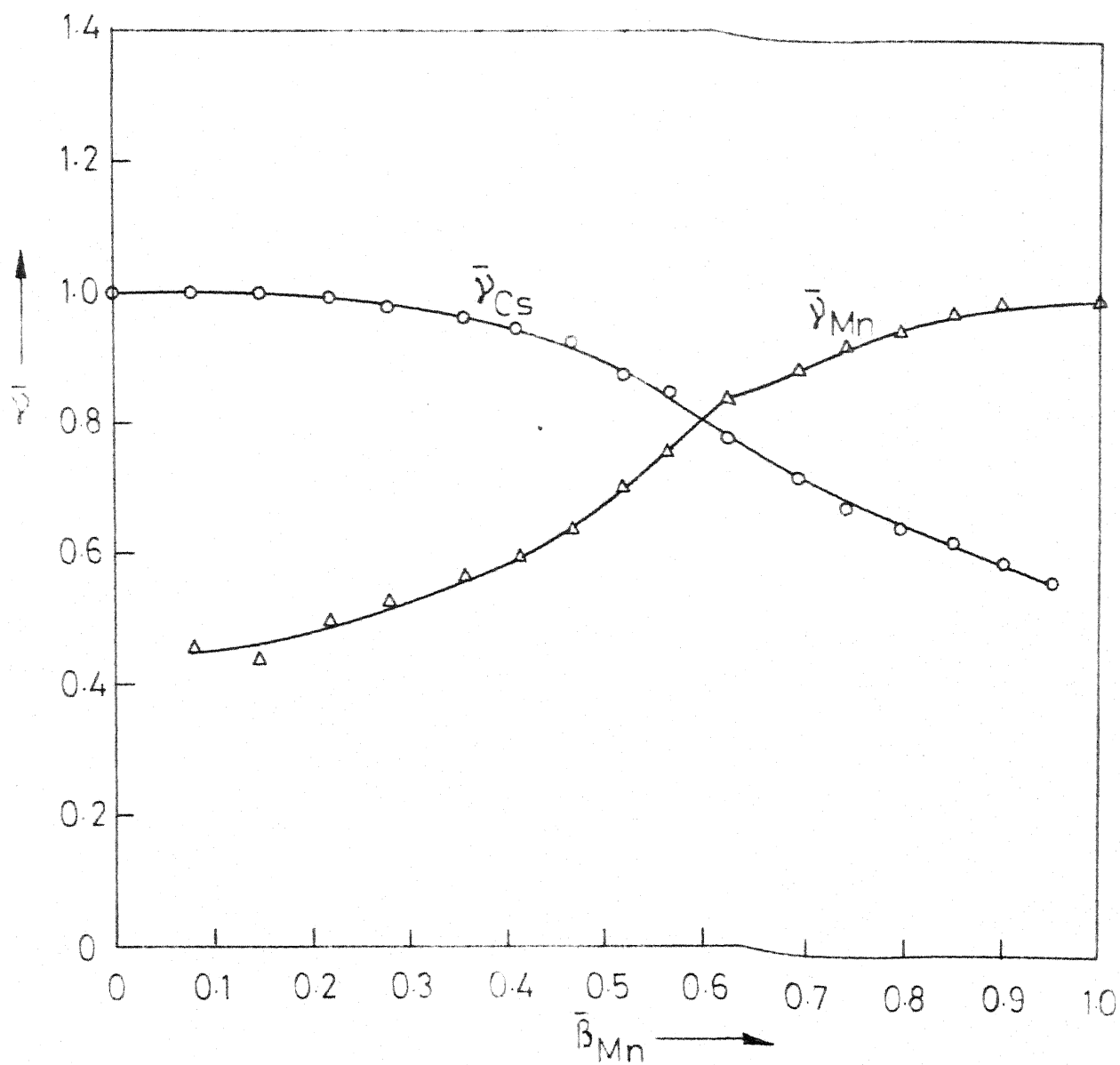


Fig.8 - Resin - Phase Activity Coefficients: Mn - Cs -
Dowex 50W-X8 System.

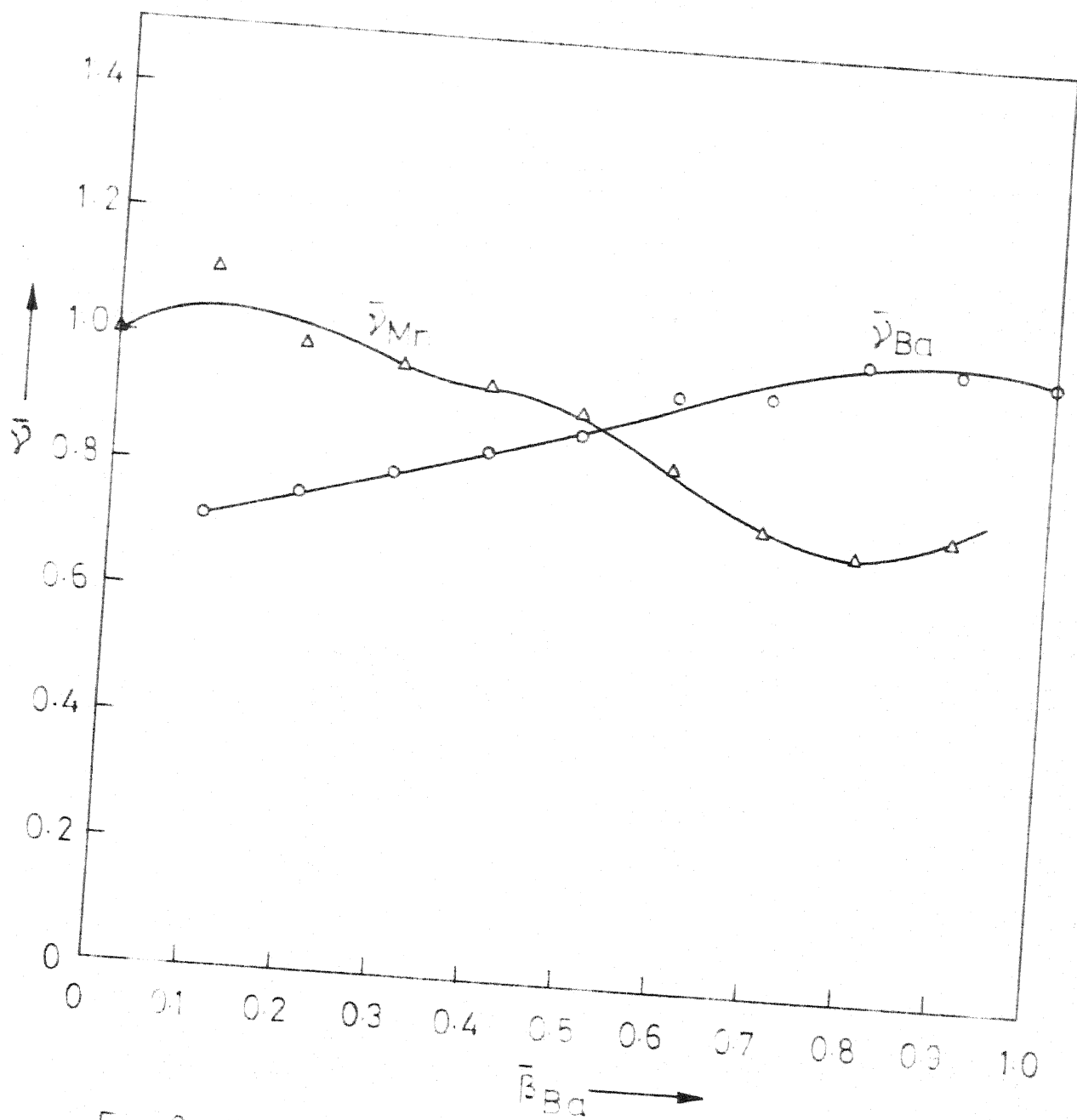


Fig 9 - Resin - Phase Activity Coefficients Ba-Mr -
Dowex 50W-X8 System.

Values of K_{cB}^A were substituted in Equations 38 and 39 to obtain $\ln \bar{\gamma}_A$ and $\ln \bar{\gamma}_B$.

$$Z_B \ln \bar{\gamma}_A = -(1 - \bar{\beta}_A) \ln K_{cB}^A - \int_{\bar{\beta}_A}^1 \ln K_{cB}^A d\bar{\beta}_A \quad (38)$$

$$Z_A \ln \bar{\gamma}_B = \bar{\beta}_A \ln K_{cB}^A - \int_0^{\bar{\beta}_A} \ln K_{cB}^A d\bar{\beta}_A \quad (39)$$

Substituting the values of resin-phase activity coefficients and modified selectivity coefficient in Equation 33a, one can calculate the rational equilibrium constant, K_B^A .

$$K_B^A = \frac{\bar{\gamma}_A^{Z_B}}{\bar{\gamma}_B^{Z_A}} K_{cB}^A$$

The computer programme and its flow chart for the entire calculations have been given in the Appendix B. The value of K_B^A was found to be independent of the values of $\bar{\beta}_A$. A typical table for Ba-Mn pair is given in Appendix D.

Incidentally, K_B^A could also have been evaluated with the help of Equation 40,

$$\ln K_B^A = \int_0^1 \ln K_{cB}^A d\bar{\beta}_A \quad (40)$$

However, this procedure was not adopted because of possible errors of extrapolation near extreme values of $\bar{\beta}_A$ in the numerical integration.

It is evident that the resin-phase activity coefficient for each ionic species varies with its fraction in the resin-

phase as well as with the nature of the second component in the binary pair. It may be recalled that the numerical value of $(\bar{\gamma}_A^{Z_B} / \bar{\gamma}_B^{Z_A})$ is an index of the deviation of K_{CB}^A (modified selectivity coefficient) from K_B^A (rational equilibrium constant). The individual activity coefficients of the component ions, A and B are related by Gibbs-Duhem equation mentioned earlier.

For the Cs-Na pair, the resin phase activity coefficients are close to unity thereby indicating that modified selectivity coefficients are very nearly equal to the rational equilibrium constant. In other words, the experimental data at one point are sufficient to predict the entire isotherm. For Mn-Na pair, $(\bar{\gamma}_{Mn} / \bar{\gamma}_{Na}^2)$ is considerably greater than unity for small values of $\bar{\beta}_{Mn}$. The value goes on reducing with the increasing fraction of Mn^{2+} ion in the resin phase. However, the trend shown by Mn-Cs and Ba-Mn pairs is quite opposite.

The binary equilibrium data could be very well correlated by an empirical equation of type given below:

$$\frac{\bar{\beta}_A}{\bar{\beta}_A} = a + b \bar{\beta}_A + c \bar{\beta}_A^2 \quad (27)$$

where a, b and c are constants and are evaluated from a correlation of the experimental binary distribution data. This equation is quite helpful while performing computations in ternary kinetic studies (to be discussed later in this

chapter). Constants a , b and c for different binary pairs are tabulated in Appendix D.

Ternary Equilibria

In Table 11 and Figure 10, ternary equilibrium data for the system Mn-Cs-Na-Dowex 50W-X8 are presented. In the triangular diagram, the method proposed by Cloete et al. (C.2) was used to present the data. The normalized resin-phase fractions are presented on the regular grid. Solution phase equivalent fractions of any two (of the three) component ions define the solution-phase composition completely. Therefore, constant values of solution-phase equivalent fractions of the component ions were used as parameters. A smooth curve was drawn through all the points (representing the resin-phase compositions) in equilibrium with solutions having a constant equivalent fraction of one of the components. Intersection of two such parameter curves gives the resin phase composition for which solution phase composition is automatically fixed. In this method of plotting the experimental data, a considerable extent of information can be obtained from a small number of experimental results. The data interpolation is also facilitated.

Earlier research workers made a comparison between experimentally observed binary equilibrium data and those deduced from the ternary experimental data. In the present

TABLE 11: TERNARY ION-EXCHANGE EQUILIBRIA: Mn-Cs-Na-DOWEX 50W-X8 SYSTEM

No.	Solution-Phase Equivalents %			Resin-Phase Equivalents %									
				Experimental			Computed						
	β_{Mn}	β_{Cs}	β_{Na}	$\bar{\beta}_{\text{Mn}}$	$\bar{\beta}_{\text{Cs}}$	$\bar{\beta}_{\text{Na}}$	Equations 33 & 42			Empirical			
							β_{Mn}	$\bar{\beta}_{\text{Cs}}$	$\bar{\beta}_{\text{Na}}$	$\bar{\beta}_{\text{Mn}}$	$\bar{\beta}_{\text{Cs}}$	$\bar{\beta}_{\text{Na}}$	
1.	4.9	14.7	80.4	49.7	18.5	31.8	35.5	20.2	44.3	33.6	22.4	44.0	
2.	4.9	34.4	60.6	45.4	34.2	20.4	30.6	34.7	34.7	35.7	35.7	28.6	
3.	4.9	59.5	35.6	45.5	43.5	11.0	29.4	49.5	21.1	36.0	47.3	16.3	
4.	10.1	10.1	79.8	58.8	15.6	25.6	57.8	11.1	31.1	53.5	19.5	27.0	
5.	9.8	19.6	70.6	55.0	24.1	20.9	53.3	18.1	28.6	49.7	26.9	23.4	
6.	10.0	30.4	59.6	55.5	27.9	16.6	50.2	24.1	25.7	47.8	31.8	20.4	
7.	10.0	60.4	29.6	52.7	37.3	10.0	45.1	40.7	14.2	46.3	43.0	10.7	
8.	10.0	69.5	20.5	50.9	44.0	5.1	44.1	46.2	9.7	46.0	46.0	8.0	
9.	10.0	79.7	10.3	56.9	46.5	2.6	43.1	52.0	4.9	45.8	49.7	4.5	
10.	20.0	10.2	69.8	70.1	12.5	17.4	Not computed						18.0
11.	20.3	39.6	40.1	63.5	28.6	7.9	65.7	22.2	12.1	58.0	32.0	10.0	
12.	19.9	69.8	10.3	55.7	42.6	1.7	60.8	36.3	2.9	54.6	38.0	7.4	
13.	29.5	9.9	60.6	75.7	11.9	12.4	83.1	5.6	11.3	74.0	12.0	13.8	
14.	29.9	59.8	10.3	67.7	30.6	1.7	72.8	25.4	1.8	63.3	34.0	2.7	
15.	40.3	19.8	39.9	78.6	15.3	6.1	86.4	7.9	5.7	77.0	15.6	7.4	
16.	40.4	39.6	20.0	72.4	24.9	2.7	Not computed						2.4
17.	59.7	19.9	20.4	82.3	14.8	2.7	95.4	3.7	0.9	83.0	13.6	3.4	

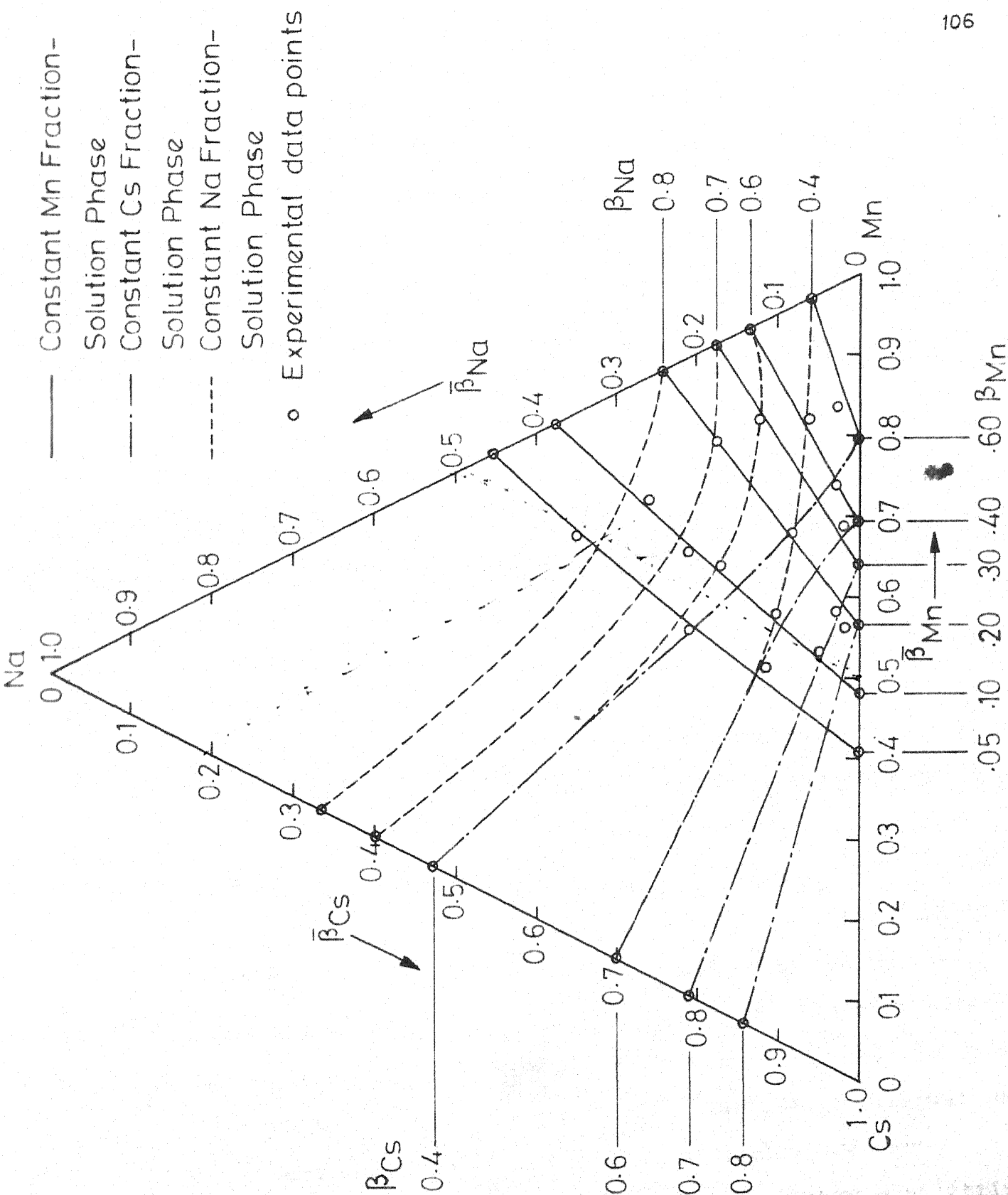


Fig.10 - Ternary Ion-Exchange Equilibria : Mn-Cs-Na -Dowex 50W-X8 System.

investigation also a similar attempt has been made. A sample calculation to evaluate the binary data from the ternary ones, neglecting the presence of the third ion, is shown in the Appendix D. The data thus deduced are presented in Figures 2,3 and 4. While the data for Mn-Na and Mn-Cs binaries deduced from the ternary system Mn-Cs-Na are fairly close to those experimentally observed, the deduced data for Cs-Na binary did not agree with the experimental data. It should be noted that Mn^{2+} is the most preferred ion in the system.

Figure 4 shows an interesting result of the correlation. Data for Mn-Cs binary pair were deduced from the experimental data for two ternary systems, namely Sr-Mn-Cs (B.1) and Mn-Cs-Na. For the case of Sr-Mn-Cs system the binary pair Mn-Cs does not contain the most favourable ion of the ternary system (i.e. Sr^{2+}) and the correlation between the deduced data and the experimental data is not satisfactory. On the other hand, for the case of Mn-Cs-Na ternary system, the deduced data for Mn-Cs do correlate the experimental data satisfactorily. (In this case, the binary pair Mn-Cs contains the most favourable ion Mn^{2+}). This particular observation is in variance with the hypothesis of earlier research workers (D.5, J.2, M.3, P.3 S.5) that the binary equilibrium data can be predicted in all cases from the ternary equilibrium data by neglecting the presence of the third ion.

As the introduction of each additional component in the system increases the experimental work many times, there is actually more need and justification for predicting such data from somewhat more easily accessible binary data. Such a prediction has been attempted in the present investigation. Equation 33 presented in the Theory Chapter is applicable to any ionic pair i, j in a multicomponent system. Since binary equilibrium constants are characteristic of the pairs, they may be used to predict the ternary ion-exchange equilibria.

For a system containing three counter ions A, B and C, the equilibrium constants of the three pairs A-B, B-C, and C-A are related by the triangle rule (B.4).

$$(K_B^A)^{Z_C} (K_C^B)^{Z_A} (K_A^C)^{Z_B} = 1$$

In other words, equilibrium constants of two binary pairs in a ternary mixture are sufficient to evaluate the equilibrium constant of the third pair. Substituting the values of K_{Cs}^{Mn} , K_{Na}^{Cs} and K_{Mn}^{Na} (obtained from binary equilibrium data) in the above equation, one gets

$$(K_{Cs}^{Mn})(K_{Na}^{Cs})^2(K_{Mn}^{Na}) = 8.53 \times 1.69^2 \times 37.02^{-1} = 0.655$$

which is far from unity. It is clear from this result that one or more of the binary equilibrium constants in the ternary system and the equilibrium constants for the corresponding binary systems are not the same. This behaviour was also

observed while comparing the deduced binary data (from the ternary experimental data) with the experimental binary equilibrium data obtained independently. Smith (S.5) has reported the failure of the triangle rule by a factor of six when he applied it to the ternary data of the system, Ba-Cu-Na-Dowex 50W-X8.

Earlier, the need for prediction of ternary equilibrium data from the more easily accessible binary data has been emphasized. In the present study binary equilibrium constants were utilized for predicting the ternary equilibrium data* of the system Mn-Cs-Na-Dowex 50W-X8. Solution phase activity coefficients were calculated with the help of the law of constant ionic strength (L.2), and the results have been presented in the Appendix D. Resin-phase activity coefficients of ions in a ternary system were calculated from their corresponding values in the component binary pairs (Tables 9 to 11 and Figures 6 to 8) using Equations 42a, 42b and 42c (Presented in Theory Chapter).

It is to be noted that an iterative procedure would be required to calculate resin-phase activity coefficients in a ternary system as the resin-phase composition is not initially known. As an approximation for the first trial, one can ignore the effects of activity coefficients in calculating the resin-phase composition. A knowledge of ionic distribution for any two binary pairs (say A-B, B-C) of the

*In spite of the failure of the triangle rule.

ternary system A-B-C should normally be sufficient to predict the ternary equilibria. Even then calculations were made with all the three combinations of two binary pairs in the system. The detailed procedure is given in the Appendix B.

However, prediction from all the three combinations did not give the same result. If the two binary pairs were so chosen as to contain the most favoured ion in each of them (Mn-Cs, Mn-Na, Mn^{2+} is the most favoured ion), the computed ternary data agreed reasonably well with the experimental data. This is an important finding of the present study. The results of the computations (using the most favourable ion approach) are shown in Table 11. For an ease in computations a solution-phase equivalent percent was rounded off to the nearest whole number divisible by five. The same method was used by Bajpai (B.1) to predict successfully the ternary equilibrium data for the system Sr-Mn-Cs-Dowex 50W-X8. The above procedure was also used (B.2) to predict the ternary equilibrium data for the system. Ba-Cu-Na-Dowex 50W- X8 studied by Smith (S.5), from the component binary data for the pairs Ba-Cu. and Ba-Na (Table 12). Ba^{2+} is the most preferred ion in this ternary system.

Ternary data for the system Mn-Cs-Na were also predicted from the data on two binary pairs namely, Mn-Na and Mn-Cs with

TABLE 12: COMPARISON OF EXPERIMENTAL AND COMPUTED TERNARY
EQUILIBRIUM DATA: Ba-Cu-Na-DOWEX 50W-X8 SYSTEM

Solution-Phase Equivalents%			Resin-Phase Composition Equivalents %					
β Ba	β Cu	β Na	Experimental (Smith S.5))			Computed		
			β Ba	β Cu	β Na	β Ba	β Cu	β Na
15.0	5.0	80.0	94.0	3.4	2.6	95.3	2.2	2.5
15.0	15.0	70.0	89.3	8.0	2.7	89.4	7.7	2.9
5.0	5.0	90.0	81.7	11.8	6.5	83.2	6.9	9.9
5.0	15.0	80.0	66.4	33.0	0.0	72.1	18.8	9.1
30.0	10.0	60.0	92.7	7.3	0.0	94.4	3.7	1.9
20.0	20.0	60.0	89.7	10.3	0.0	88.3	9.1	2.6
10.0	30.0	60.0	70.9	28.0	1.1	80.0	15.9	4.1
25.0	5.0	70.0	89.9	10.1	0.0	95.8	2.1	2.1
10.0	20.0	70.0	82.8	17.2	0.0	84.3	11.5	4.2
20.0	10.0	70.0	92.7	7.3	0.0	92.8	4.8	2.4
25.0	15.0	60.0	93.8	6.2	0.0	91.6	6.2	2.2
5.0	10.0	85.0	73.8	19.7	6.5	76.6	13.8	9.6
10.0	5.0	85.0	93.0	0.4	6.6	93.7	2.7	3.6
2.5	2.5	95.0	75.6	8.4	16.0	68.1	7.5	24.4
2.5	30.0	67.5	36.6	63.4	0.0	39.9	47.4	12.7

the help of an empirical method. The method is the reverse of the one used for deduction of binary data from the ternary ones. The results have been presented in Table 11 and the sample calculations have been shown in Appendix D.

To sum up, ternary equilibrium data can be predicted with the help of the data on two binary pairs each containing the ion most favoured by the resin phase.

ION-EXCHANGE KINETICS

In this section, results of experimental and computed rate studies of self (isotopic), binary and ternary exchanges for the systems Mn-Cs-Na-Dowex 50W-X8 and Ba-Mn-Na-Dowex 50W-X8 have been presented. The isotpic exchange rate data of Ba^{2+} ions and the binary rate data for the system Ba-Na were those obtained earlier by Viswanathan (V.3). A run number with suffix 'V' indicates such a run. The experimental rate data for the system Sr-Mn-Cs-Dowex 50W-X8, taken by Bajpai (B.1) in the present research group at IIT-Kanpur, have also been analyzed by the theoretical approach proposed by the author of this dissertation. A run number with the suffix 'B' indicates the experimental rate data taken by Bajpai. All experimental rate data in tabular form are given in the Appendixes A and E.

Self Exchange

In the preliminary part of the present study, different fluid velocities upto 25 cm/sec were tried to study self-exchange

kinetics of Na^+ ions. When 0.1N solutions were employed, even a velocity of 6 to 7 cm/sec was found to be high enough to obtain particle-diffusion controlled exchange data. In the present experimental set-up, a maximum velocity of approximately 25 cm/sec was obtained, and all the rate studies were carried out at this fluid-velocity.

The experimental results of the self-exchange rate studies are given in Figure 11 and Tables 33,35,36 and 37. The Fick's law model works very well for correlating particle-diffusion controlled rates of isotopic exchange, and the Equation 44 (discussed later) for the fractional attainment of equilibrium as a function of the dimensionless group, $\bar{D}t/r_0^2$ was available (H.2(e)). Self-diffusion-coefficients obtained with an interpretation of the experimental data by the above model (except for Cs^+ ions) are given below:

$$\bar{D}_{\text{Na}} = 20.5 \times 10^{-7} \text{ cm}^2/\text{sec} \quad (\text{experimental})$$

$$\bar{D}_{\text{Mn}} = 2.22 \times 10^{-7} \text{ cm}^2/\text{sec} \quad (\text{experimental})$$

$$\bar{D}_{\text{Sr}} = 1.95 \times 10^{-7} \text{ cm}^2/\text{sec} \quad (\text{experimental})$$

Bajpai's work (B.1)

$$\bar{D}_{\text{Ba}} = 1.16 \times 10^{-7} \text{ cm}^2/\text{sec} \quad (\text{experimental})$$

Viswanathan's work (V.3)

$$\bar{D}_{\text{Cs}} = 30.0 \times 10^{-7} \text{ cm}^2/\text{sec} \quad (\text{estimated})$$

The following procedure was adopted to evaluate the self-diffusion coefficients from the self-exchange data. The self-diffusivity value was calculated at different extents of exchange using Vermeulen's approximation (V.2).

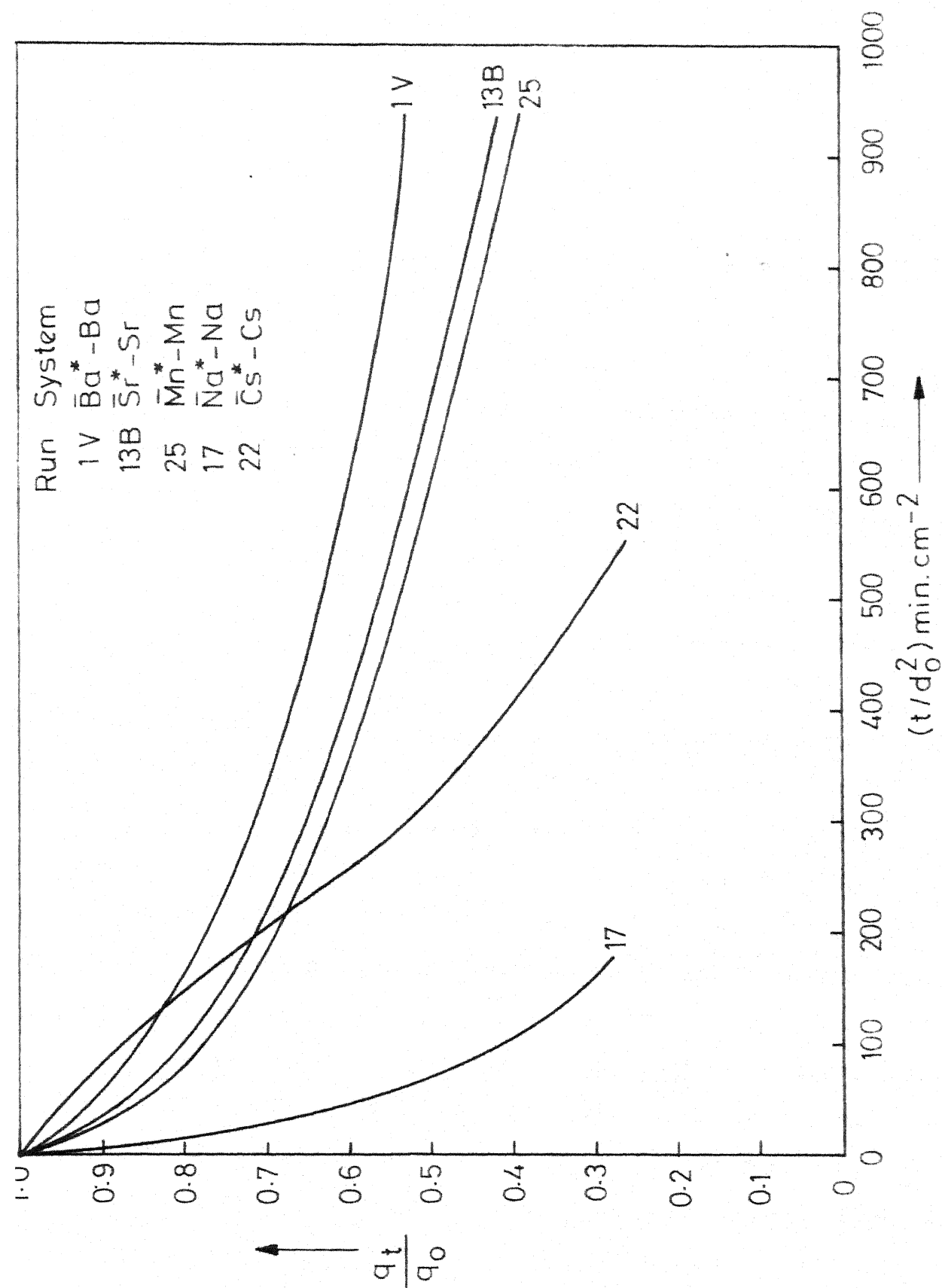


Fig. 11 - Experimental Self Exchange Curves.

$$1 - \frac{q_t}{q_c} = \left(1 - \exp \left(- \frac{\bar{D}t \pi^2}{r_o^2} \right) \right)^{1/2} \quad (43)$$

A constant value of diffusivity was obtained for higher extents of exchange. This value was used as a trial value for substituting in the infinite series expression for the depletion history (given below) and the depletion history curves were computed (using IBM 1620 computer, and first five terms of the series were used) and matched with the experimental curve.

$$1 - \frac{q_t}{q_c} = 1 - \frac{6}{\pi^2} \sum_{n=1}^{\infty} \frac{1}{n^2} \exp \left(- \frac{\bar{D}t \pi^2 n^2}{r_o^2} \right) \quad (44)$$

The diffusivity value was adjusted to get the best fit. Computed and experimental self-exchange rate data for Na^+ and Mn^{2+} ions are given in the Appendix E. The computed rate data agreed very well with the experimental data except for brief initial period of exchange. To establish further the control of particle diffusion on the exchange, Helfferich's criterion (H.2(d)) was applied. (See Appendix E).

In the present study, rate data obtained by tagging a resin bead with ^{137}Cs isotope gave rise to a considerable amount of difficulties in terms of data interpretation. All such rate data (self, binary and ternary exchanges) obtained by tagging Cs^+ ions were completely dissimilar to the rate

behaviour of the other ions. ^{137}Cs -tagged rate data did not look like the other particle-diffusion controlled exchanges (see Figures 11 and 30), and could not be interpreted by the present approach. As mentioned earlier in the equilibrium section, beads tagged with ^{137}Cs did pose problems in capacity measurements as well as in the regeneration of the bead. However, the presence of non-radioactive cesium ions either in the solution or in the resin phase, for both binary and ternary exchanges created no problems for data interpretation. The behaviour of cesium tagged beads in the rate studies has been discussed in detail in Appendix A.

The self-diffusivity of Cs^+ ion in the resin phase was estimated by an interpretation of the rate data of $\bar{\text{Na}}^*-\text{Cs}$ exchange (depletion of Na^+ ions initially in the resin phase with Cs^+ ions in the bulk fluid phase, Run 23) with the Nernst-Planck model. It has been well established that the above model works very well for binary exchange under favourable equilibrium conditions. The ratio of Na^+ to Cs^+ ionic self diffusivities in the present study is comparable to the various values reported in the literature (B.9, M.1).

Comparison of the experimental self-diffusivity values of Na^+ ions in Dowex 50W-X8 resin with literature values is given below. Hering and Bliss (H.7) calculated the self-diffusivity value of Na^+ ions from their binary exchange rate data for the systems Na-Zn-Dowex-50W-X8 and Na-Ag-Dowex 50W-X8

obtained with 1N solutions. The values reported are 20.3×10^{-7} and $20.5 \times 10^{-7} \text{ cm}^2/\text{sec}$ respectively. Gopala Rao and David (G.4) have reported a value of $16.0 \times 10^{-7} \text{ cm}^2/\text{sec}$ for the sodium diffusivity, and they obtained their rate data with 0.1N chloride solution. A possible explanation for the lower value reported by them could be a higher value of the time constant (5 seconds) of the ratemeter used in their studies. As discussed in the Experimental Chapter, the instantaneous value of the recorded signal will be different for higher and lower values of the time constants used in the ratemeter settings. With a higher value of the time constant, the recorded depletion history tends to be slower. Another possible reason could be smaller superficial fluid-velocities (0.6 to 0.7 cm/sec) used by the above authors.

Morig and Gopala Rao (M.4) have reported values of $15.8 \times 10^{-7} \text{ cm}^2/\text{sec}$ and $18.0 \times 10^{-7} \text{ cm}^2/\text{sec}$ for the sodium self diffusivity and they obtained their rate data with 0.1N and 0.5N chloride solutions respectively. The value of the time constant used for their set-up was 10 seconds.

Viswanathan (V.3) reported a value of $20.3 \times 10^{-7} \text{ cm}^2/\text{sec}$ for self-diffusivity of Na^+ ions in the Dowex 50W-X8 resin. From the value of $t_{1/2}$ (time needed for 50% depletion of the ions initially in the resin phase) reported by Hamish Small (S.4) for Na^+ self exchange, the present author calculated the self-diffusivity of Na^+ , and obtained a value of $5.9 \times 10^{-7} \text{ cm}^2/\text{sec}$.

Hamish Small used 0.1N chloride solutions and a volume flow rate of 12 ml/min. The fluid velocity was quite small as compared to the velocities used in the present investigations.

Binary Exchange

Binary exchange rate data for Mn-Na, Ba-Na, Sr-Mn pairs in both forward and reverse directions, are presented in the Figures 12, 13 and 14 and Tables 38 to 41, 43, 44. Rate data for the Ba-Na system were obtained from Viswanathan's work (V.3). A consolidated plot of Cs^+ ions replacing Sr^{2+} , Mn^{2+} and Na^+ ions individually in the resin phase is shown in Figure 15. Only one rate curve in the Ba-Mn exchange was available, and the rate data for Ba^{2+} ions in the solution phase replacing Mn^{2+} ions in the resin phase, are shown in Figure 19 along with the ternary exchange curves.

In binary exchange, the rate curve in both the directions usually fall between the two self-exchange curves. Sr-Mn and (possibly) Ba-Mn system are exceptions to the above statement. The Sr-Mn system is unique in that the self diffusivities of the two ions are very close to each other, but Sr^{2+} ions are preferentially taken up by the resin phase. In the Ba-Mn system, both the diffusivities and selectivities for the two ions are quite different.

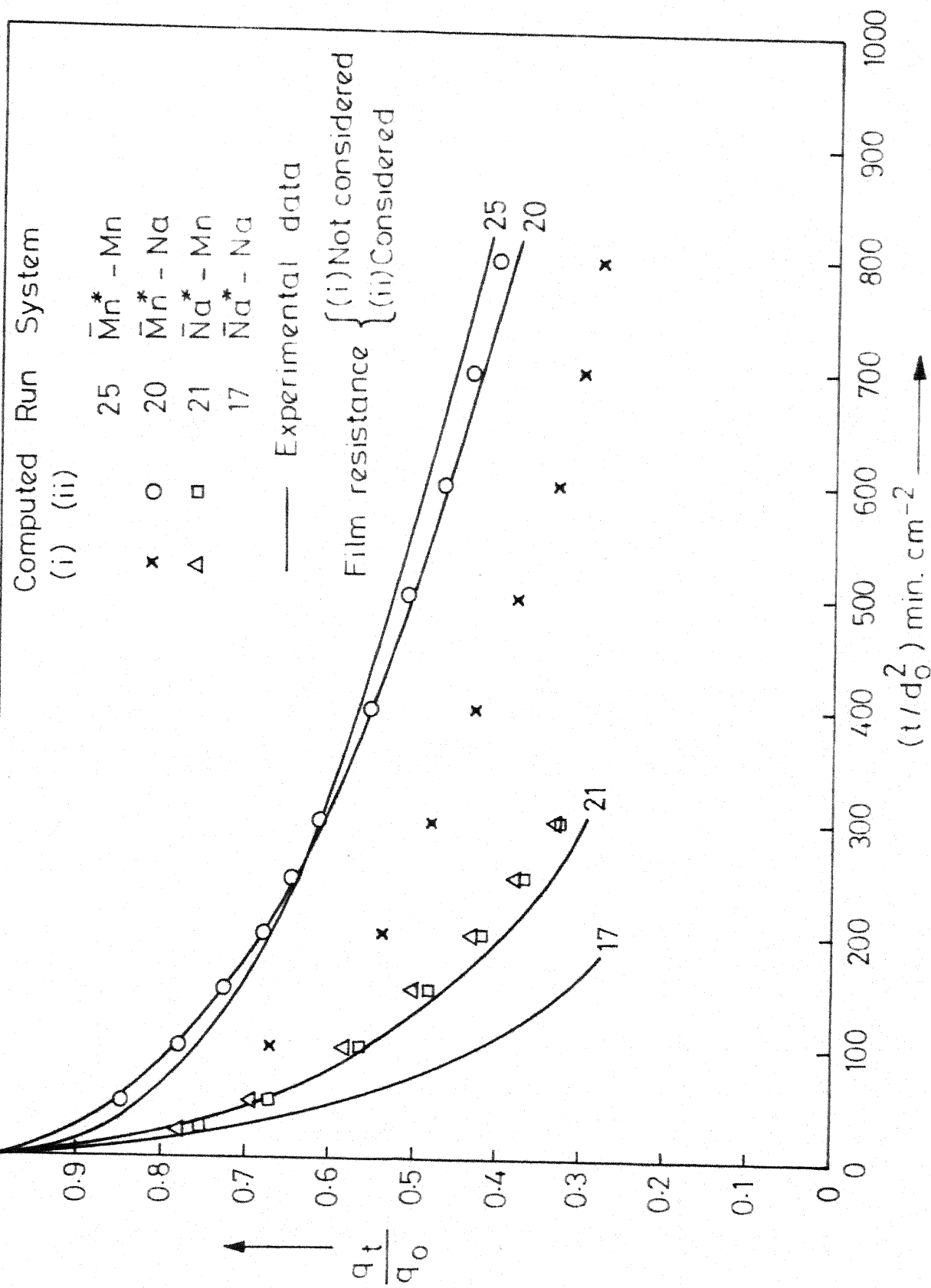


Fig.12 - Binary Exchange Curves for the System: Mn - Na - Dowex 50W-X8.

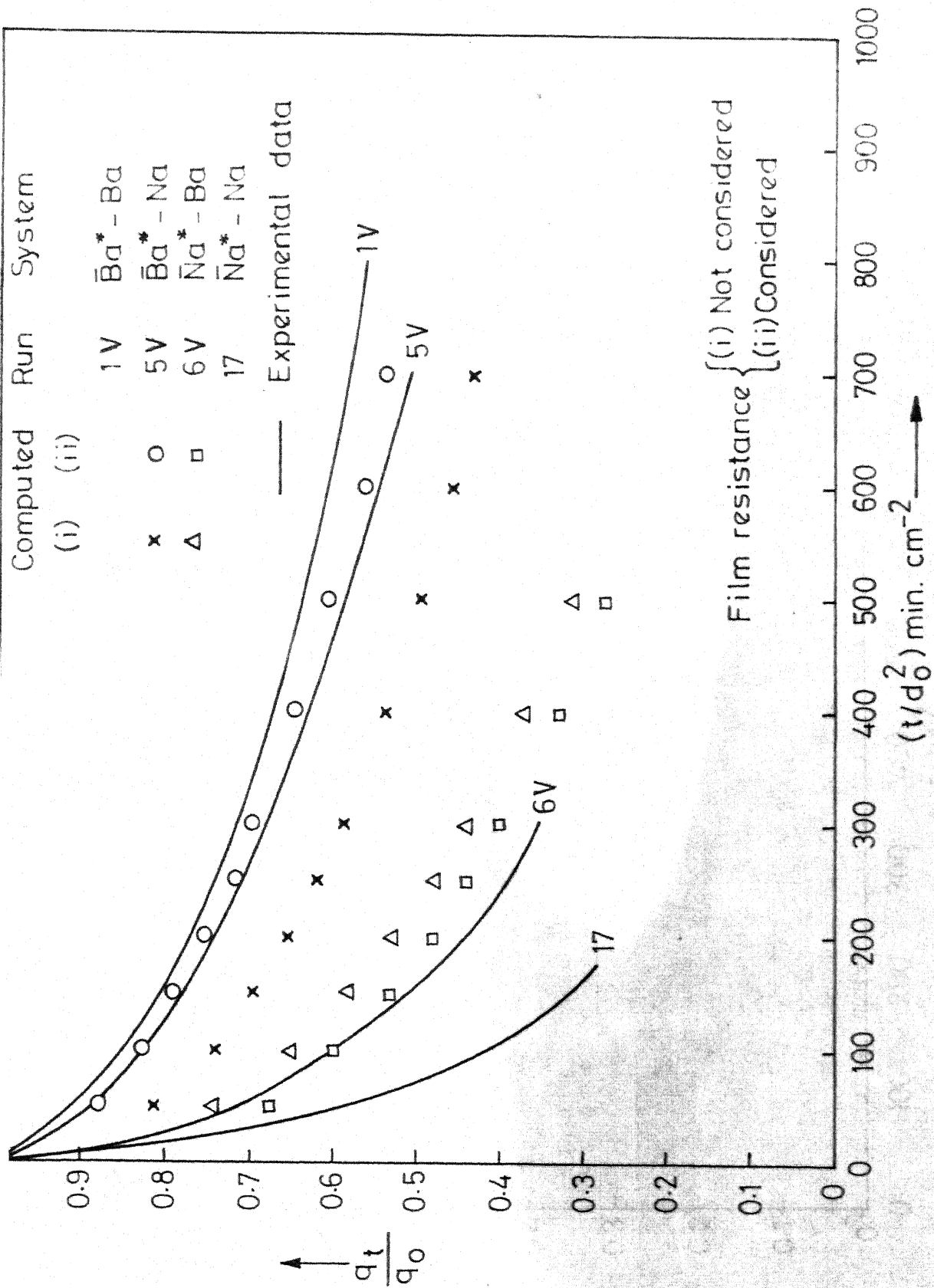


Fig. 13 - Binary Exchange Curves for the System Ba-Na-Dowex 50W-X8

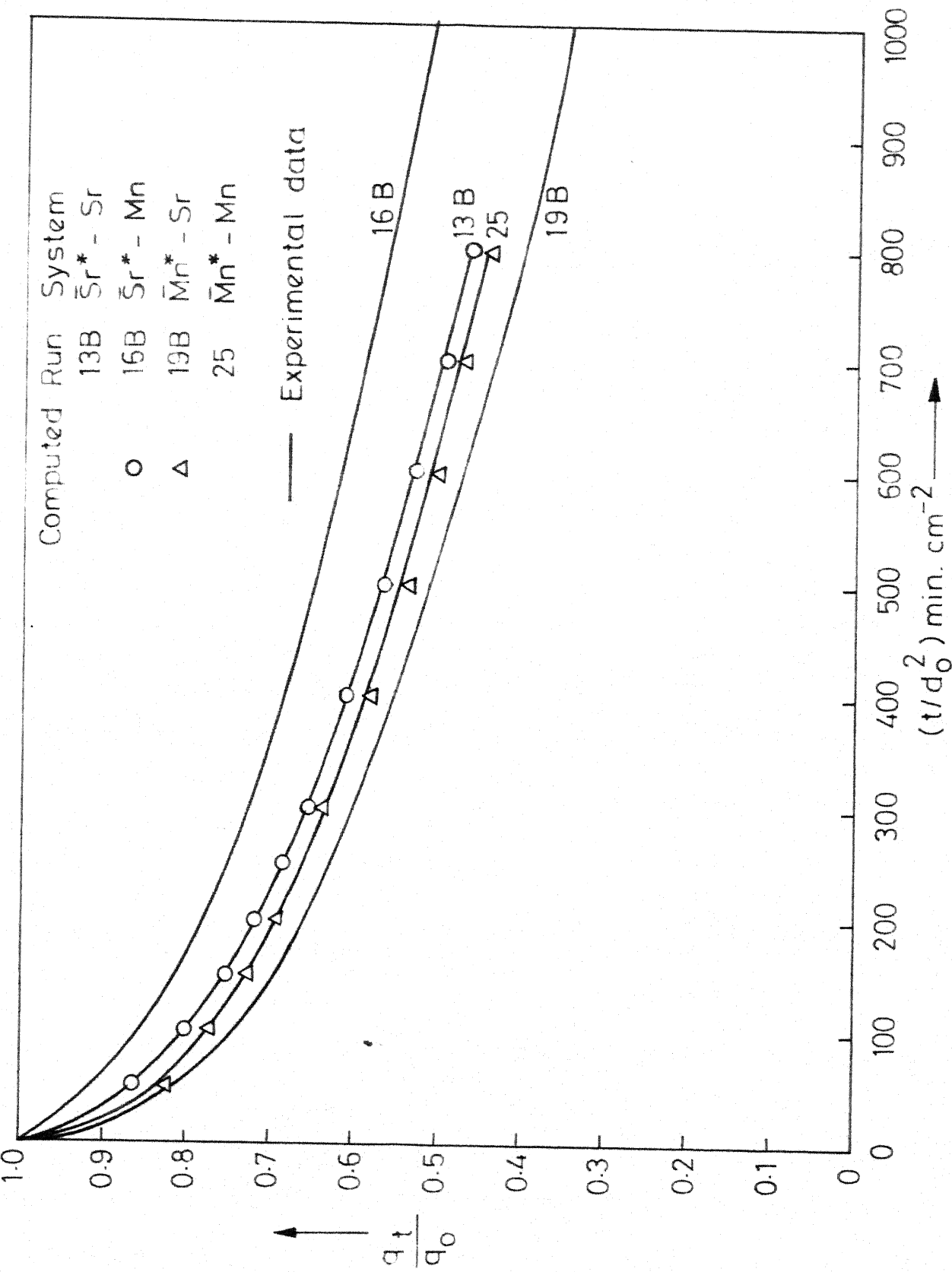


Fig 14 - Binary Exchange Curves for the System: Sr - Mn - Dowex 50W-X8.

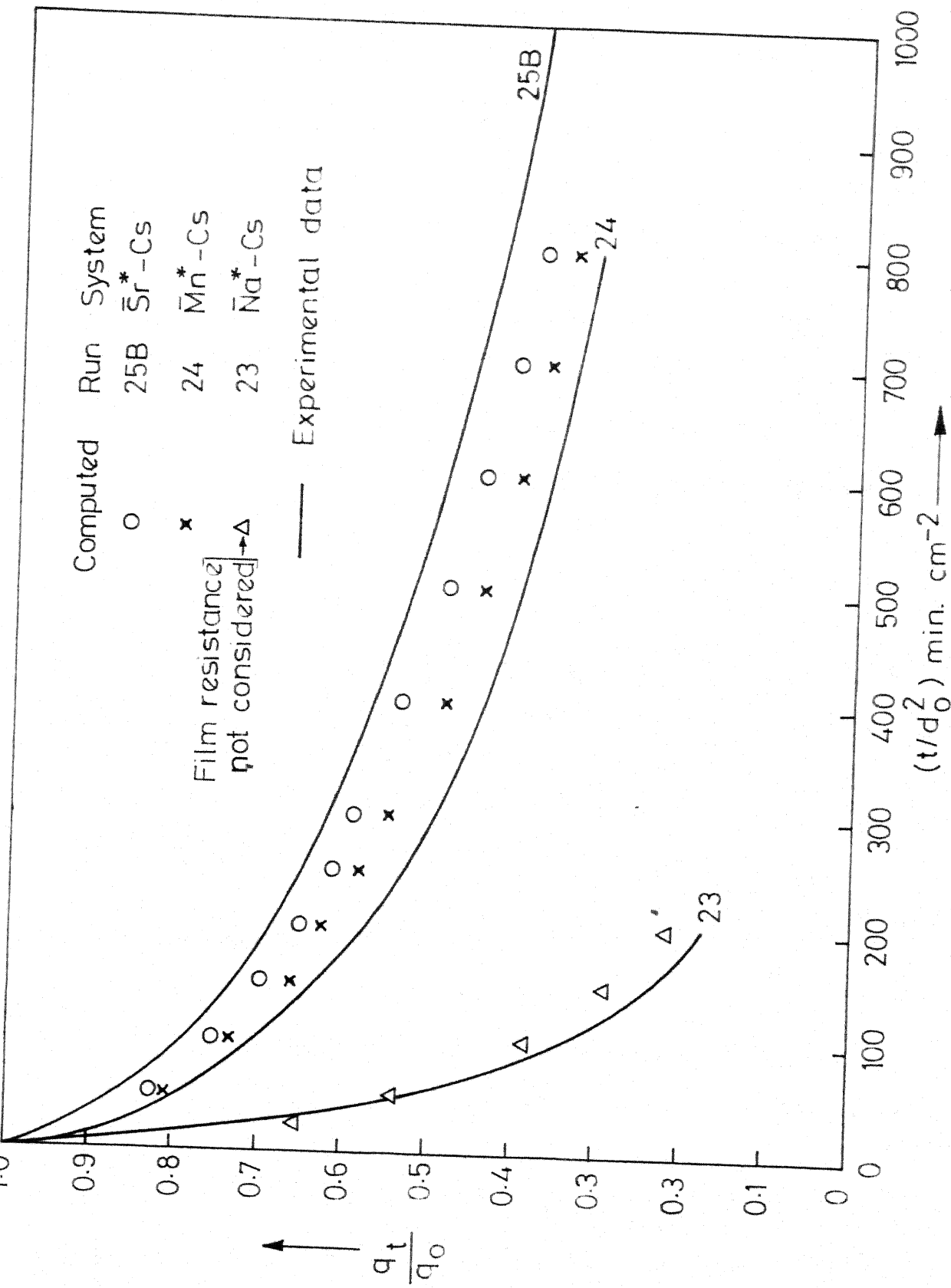


Fig.15 - Binary Exchange Curves with Cs in the Bulk.

As pointed out earlier, the Nernst-Planck model works well in predicting the binary exchange under favourable equilibrium conditions. This was confirmed in the present study also (see $\bar{\text{Na}}^*$ -Mn and $\bar{\text{Na}}^*$ -Ba curves, and Figures 12 and 13). However, the Nernst-Planck model does not work satisfactorily for the case of unfavourable equilibrium exchange; the experimental rates are very much slower than the computed ones. Morig and Gopala Rao (M.4) and Viswanathan (V.3) have reported similar observations. In the Nernst-Planck model for the particle-diffusion controlled rates, the resin surface is assumed to be saturated with the in-coming ions instantaneously at time $t \geq 0$. As discussed earlier in the Theory Chapter, this may be an unrealistic assumption particularly for the case of unfavourable exchange. There is always a finite film thickness even at high fluid velocities and the driving force for mass transfer through the film will be considerably smaller for the case of unfavourable exchange, particularly during the initial period of exchange, and thus the resistance to mass transfer in the film would be significant. In the present study, the effect of film resistance was also taken into account in the correlation of exchange rate data. In order to do that, the value of the fluid-film thickness was necessary.

The film thickness, δ at fluid-velocities used in the present study (superficial velocities of about 25 cm/sec) was

obtained from a correlation of fluid-film controlled rate data of self-exchange of sodium ions using a solution of about 0.00194N (chloride anion) concentration (see Figure 16). Film thickness was calculated from the expression given below (H.2(f)).

$$1 - \frac{q_t}{q_0} = 1 - \exp \left(- \frac{3 Z_1 D_1 C_1 t}{r_0 \delta C_0} \right) \quad (45)$$

where D_1 is diffusivity of the counterion in the aqueous phase, C_1 is its concentration in the aqueous phase, and C_0 in the resin phase. Self-diffusion coefficient D in the aqueous phase was calculated for Na^+ ions using the Nernst-Einstein relation. The fluid phase was assumed to be an ideal solution, and the limiting ionic conductance of Na^+ ions was used in the calculation of self-diffusion coefficient in the aqueous phase. Details are shown in the Appendix E. The value of film thickness was found to be 0.000354 cm. For comparison, the following literature values are worth noting. Tetenbaum and Gregor (T.3) and Sharma et al (S.3) reported the values of film thickness of 0.00012 cm and 0.001 cm respectively in their experimental fixed-bed studies.

For binary exchange (and also for ternary exchange), the effect of electric field on the diffusion of ions in the film was considered. For relative ease in computations the total anion concentration in the film was assumed to be constant. This assumption was checked by computing the

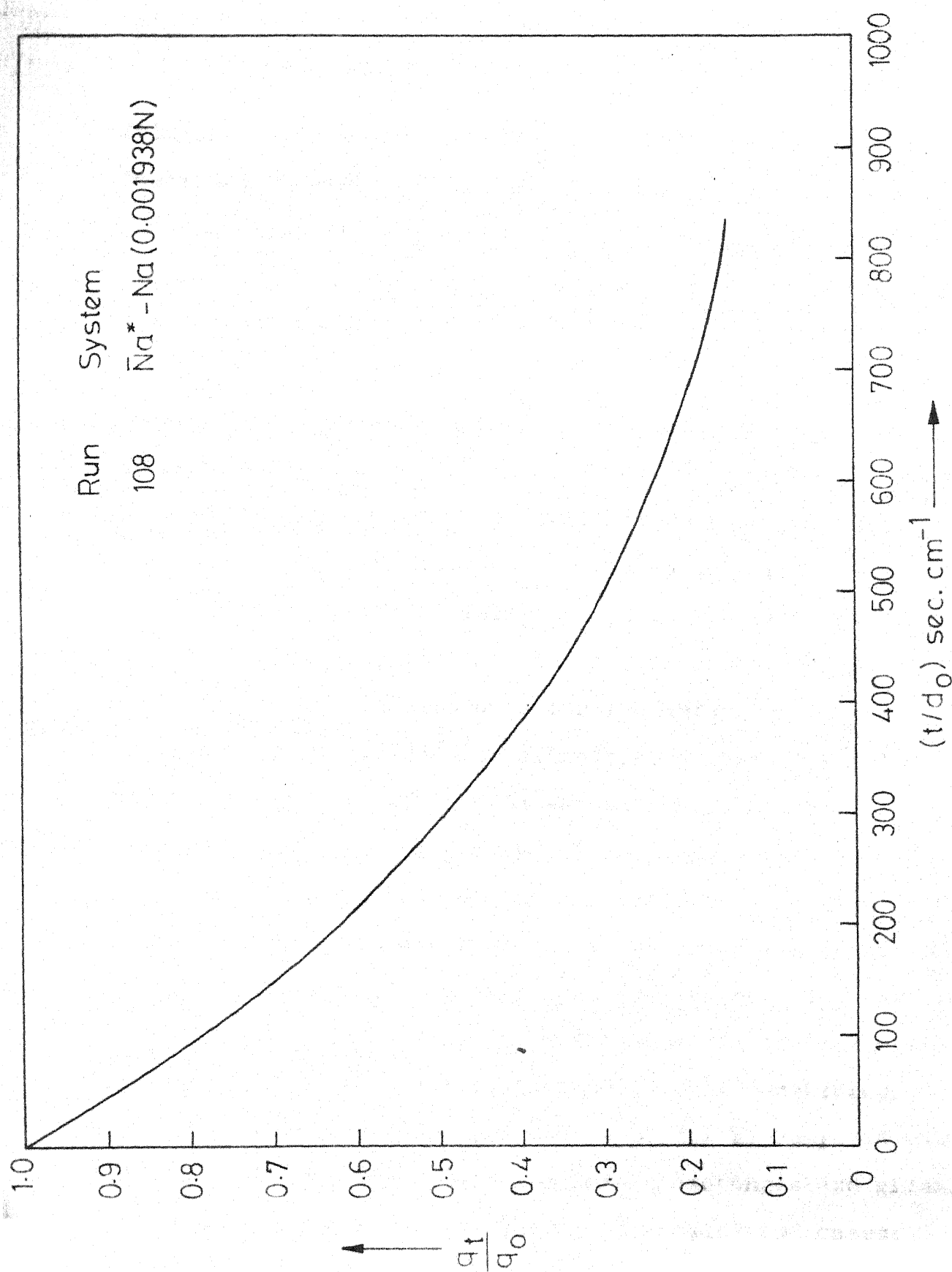


Fig.16-Film - Diffusion Controlled Self Exchange Curve.

film-diffusion controlled exchange-rate curves for the $\bar{\text{Mn}}^*\text{-Na}$ -Dowex 50W-X8 system under both the conditions viz. variant and invariant anion concentrations. The computation results are given in the Appendix E. There was less than one percent difference in the values of the fractional attainment of equilibrium for the two cases. This difference will be further reduced when both the resistances to mass transfer control the exchange rate.

To incorporate the fluid-film resistance, film-phase composition at the interface was evaluated using Equations 27a and 27b. When the fluid-film resistance was also taken into account in the computations, the matching between the experimental and computed rate data for the unfavourable cases significantly improved. For example, the improvement in the correlation for $\bar{\text{Mn}}^*\text{-Na}$ and $\bar{\text{Ba}}^*\text{-Na}$ exchanges can be seen in Figures 12 and 13. Similarly for the case of cesium in solution phase exchanging with manganese or strontium in the resin phase, the matching of the rate curves was better when the fluid-film resistance also was considered. For favourable cases, there is no significant difference in the correlations with or without fluid film resistance being considered.

In Tables 38 and 39 (see the Appendix E) computed values of the rate data for $\bar{\text{Mn}}^*\text{-Na}$ and $\bar{\text{Na}}^*\text{-Mn}$ exchanges are given. The computations were done for the following two cases:

(i) only particle diffusion controlling the exchange rate, and

(ii) both film and particle-diffusion controlling the exchange. In the above tables, computed values of the resin surface composition have also been given. It is evident that for $\bar{\text{Na}}^+ \text{-Mn}$ exchange (favourable case) resin surface is almost saturated with Mn^{2+} ions even when the film diffusion also is considered. However, for $\bar{\text{Mn}}^+ \text{-Na}$ exchange (unfavourable case), the resin surface is far from saturation with the incoming Na^+ ions for a considerable extent of the exchange when the film resistance is also considered. Similar are the observations with the Ba-Na system also. Therefore, it can be concluded that atleast for the unfavourable exchange, film resistance must also be considered in the computations of the exchange, and that the assumption of the instantaneous saturation of the resin surface with the incoming ions is not correct for that case.

In an experimental study of particle-diffusion controlled rates for the unfavourable case, there could be significant fluid-film resistance. In a recent report Sharma et al (S.3) who studied the exchange of trace components, observed that film resistance should also be considered in the correlation of particle-diffusion controlled exchange rates.

In all the computations in the present study, film-diffusion resistance was also considered unless otherwise, mentioned. When the term 'present or ~~proposed~~ model' is used in dissertation, it means that film-diffusion is also incorporated

in the model along with particle diffusion. Of course, incorporation of this effect would take more computer time (about 50% more) for computations.

The effect of variation of resin-phase activity coefficients was not incorporated in the present model. To find out this effect, computations were performed for the same Mn-Na binary exchange with and without the relevant activity coefficient terms in the rate equations. In these computations, the resin surface was assumed to be instantaneously saturated with the in-coming ions. The resin-phase activity coefficients were calculated from the equilibrium data. The depletion rates for both directions of exchange obtained with the incorporation of activity coefficient terms were slower than those obtained without the incorporation of the same. The computed data for both the cases are given in the Appendix E. Although with the incorporation of activity coefficient data the results for the case of unfavourable exchange ($\bar{Mn}^* - Na$) improved, the matching of the rate curve for the favourable exchange was not satisfactory. It may be recalled that activity coefficients in the resin phase and in the solution phase are different in character. Also an incorporation of activity coefficients in the resin-phase would make the computations complicated and lengthy without necessarily yielding additional benefits in terms of correlation. In view of the above, the activity coefficient

terms were neglected in all the computations.

For the binary system Sr-Mn-Dowex 50W-X8, the computed rate curves obtained by incorporating the film diffusion did not show any significant difference with the ones obtained by not considering the film diffusion. The computed results are presented in Tables 43 and 44. The agreement between the experimental and computed values for the unfavourable case $\bar{\text{Sr}}^*-\text{Mn}$ is poor (Figure 14). The computed rate curves for the cases of $\bar{\text{Mn}}^*-\text{Sr}$ and $\bar{\text{Sr}}^*-\text{Mn}$ almost coincide with the self-exchange rate curves of Mn^{2+} and Sr^{2+} ions respectively. A qualitative explanation is presented later in this section.

Ternary Rate Studies

Both experimental and computed ternary rate curves are shown in Figures 17 to 29. Experimental ternary exchange data in tabular form are given in Appendix E. In all the computations for the above, film-resistance to mass transfer was also considered. In the figures, numerical values associated with a system refer to the initial and boundary conditions, a value below a symbol with an overbar refers to the equivalent fraction of the species initially in the resin phase (initial condition) and that below a symbol with also a star (*) refers to the equivalent fraction of tagged species; a value below a symbol without an overbar refers to the equivalent fraction of the species in the bulk-fluid phase (boundary condition.).

In the ternary exchanges (equally applicable for binary exchanges also), the equilibrium value of the resin-surface composition has a significant effect in determining the mass transfer rates. Any variation in these values tended to shift the computed exchange curves significantly. As one can expect the difference is more significant for the unfavourable cases. In the computations, the equilibrium value of the film-phase composition at the interface was calculated from a value of the resin surface composition with the help of Equations 25 to 30.

Two types of initial and boundary conditions were considered for the ternary exchange: (i) one ion (A) initially present inside the resin exchanging with a mixture of the other two ions (B and C) in the bulk solution, $\bar{A}^*-(B-C)$; (ii) two ions (A and B) initially inside the resin phase A being tagged, exchanging with ion C in the bulk solution, $(\bar{A}^*-\bar{B})-C$. In both the cases, experimentally obtained depletion-history of the tagged ion has been compared with the computed values.

Case $\bar{A}^*-(B-C)$: In Figure 17, the exchange of Na^+ ions from the resin phase with Mn^{2+} and Cs^+ ions in one case, and Ba^{2+} and Mn^{2+} ions in the other case, in the bulk solution is shown. It may be noted that the solid lines in all the rate curves represent the experimental curves and the symbols represent the computed values. In the figures, computed points

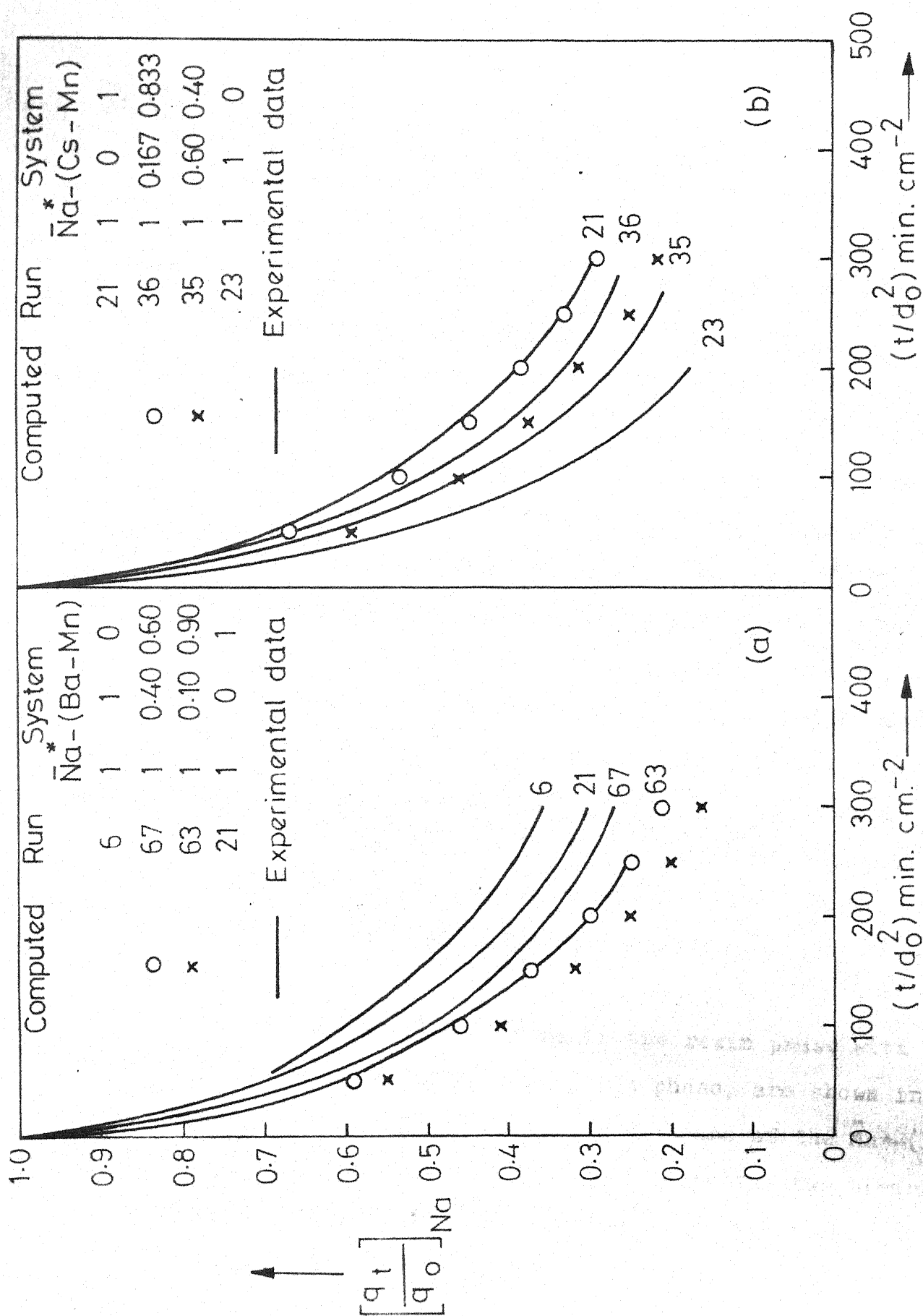


Fig.17 - Ternary Exchange Rate Data for the Systems (a) \bar{Na}^* -(Ba-Mn) - Dowex 50W-X8, (b) \bar{Na}^* -(Mn-Cs) - Dowex 50 W-X8.

for only ternaries, not for the binary ones are shown. For the $\bar{\text{Na}}^{\ast}-(\text{Mn}-\text{Cs})$ system, the ternary data fall within the envelope composed by the two binaries $\bar{\text{Na}}^{\ast}-\text{Mn}$ and $\bar{\text{Na}}^{\ast}-\text{Cs}$. The proposed model also predicts the same thing. For the $\bar{\text{Na}}^{\ast}-(\text{Ba}-\text{Mn})$ system, the ternary curves fall outside the envelope and show greater rate of depletion than the two binaries, $\bar{\text{Na}}^{\ast}-\text{Ba}$ and $\bar{\text{Na}}^{\ast}-\text{Mn}$. It is interesting to note that the model also shows the same result. However, if the film resistance to mass transfer is ignored and only the particle diffusion is considered, the ternary curves fall within the binary envelope. To substantiate the above statement, computed values are given in the Appendix E. The above result again emphasizes the necessity to consider film-diffusion also in the so-called particle-diffusion controlled exchange rates. It is also to be noted that Ba^{2+} ion is the most favourable ion amongst the four ionic species mentioned above. Ba^{2+} ion is also the slowest ion in the resin phase (amongst the above four).

The exchanges of Mn^{2+} ions in the resin phase with $(\text{Cs}-\text{Na})$ and $(\text{Ba}-\text{Na})$ ions in the bulk solution phase, are shown in Figures 18 and 19 respectively. In the case of the $\bar{\text{Mn}}^{\ast}-(\text{Ba}-\text{Na})$ exchange the ternary rate curves fall below the two binaries. It is interesting to note that the results are similar to those of the $\bar{\text{Na}}^{\ast}-(\text{Ba}-\text{Mn})$ system. The extent to which the ternary rate curves for the $\bar{\text{Mn}}^{\ast}-(\text{Ba}-\text{Na})$ system are shifted

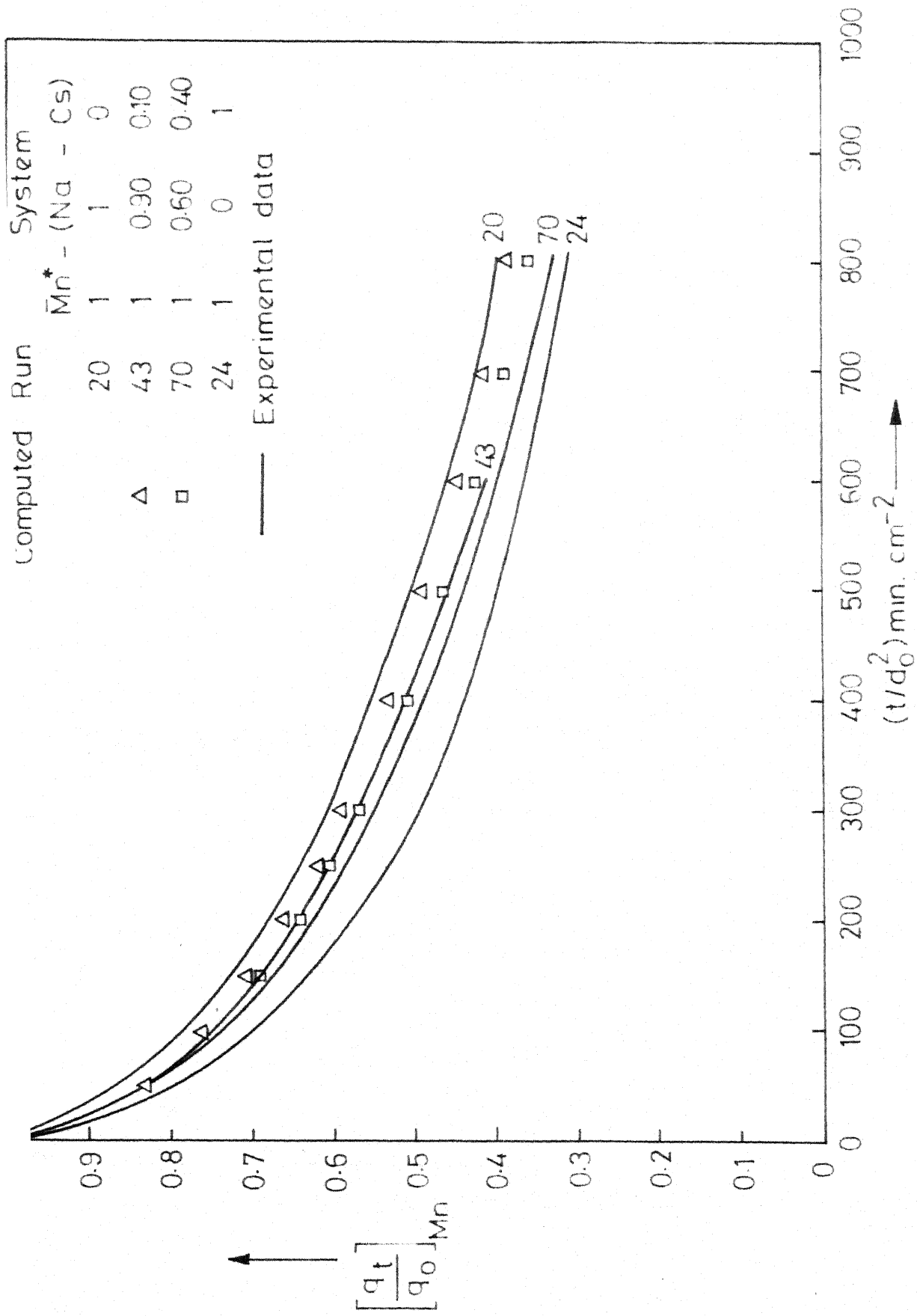
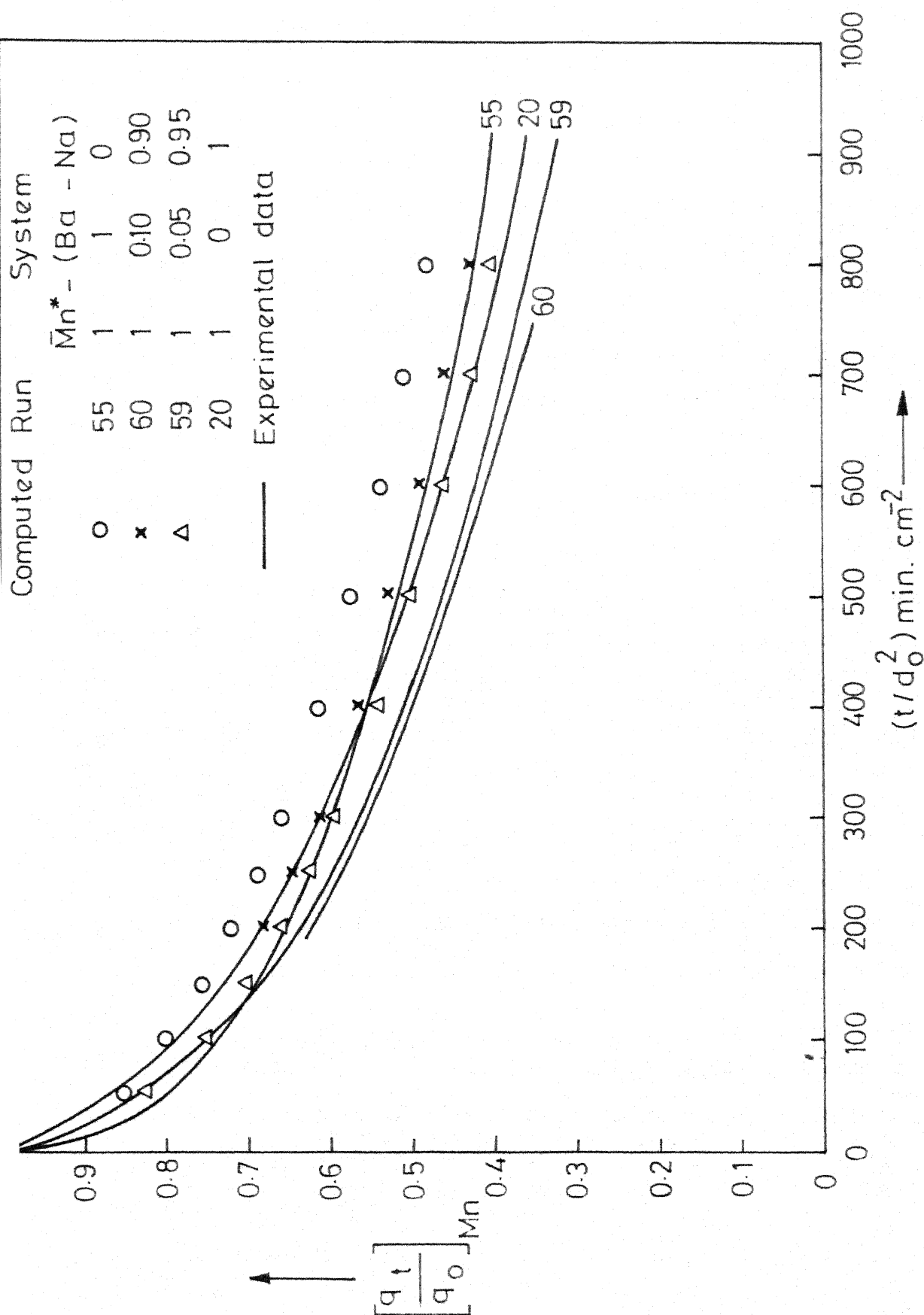


Fig. 18 - Ternary Exchange Rate Data for the System $\bar{Mn}^* - (Cs - Na) -$
Dowex 50W-X8.

Fig.19 - Ternary Exchange Rate Data for the System $\bar{Mn}^*(Ba-Na)$ -

Dowex 50W-X8.

below the two binaries is not as significant as in the case of $\bar{\text{Na}}^*-(\text{Ba-Mn})$ system. As regards to the behaviour predicted by the present model for the $\bar{\text{Mn}}^*-(\text{Ba-Na})$ system, one of the computed ternary-rate curves falls below the computed binary envelope and the other ternary curve falls below the envelope for some portion of the exchange. The above behaviour is not predicted if only particle-diffusion control is considered. It should be also recalled that Mn^{2+} ion is more favourable in the resin phase than Na^+ ion. From the experimental results, following conclusion can be made. When Ba^{2+} ion (the most favourable ion) is present in the solution, the ion initially in the resin phase is speeded up and the ternary depletion curves fall below the binary envelope. The behaviour of Ba-Mn-Na system has again been discussed later in this section. In the case of the $\bar{\text{Mn}}^*-(\text{Cs-Na})$ exchange, the ternary rate curves fall within the envelope composed by the binaries $\bar{\text{Mn}}^*-\text{Na}$ and $\bar{\text{Mn}}^*-\text{Cs}$. The present model also predicts the same behaviour and the agreement between the experimental and computed curves for the case of $\bar{\text{Mn}}^*-(\text{Cs-Na})$ is quite satisfactory.

In Figure 20, the depletion curves of the $\bar{\text{Sr}}^*-(\text{Mn-Cs})$ exchange are presented. The ternary curves fall within the binary envelope composed by $\bar{\text{Sr}}^*-\text{Cs}$ and $\bar{\text{Sr}}^*-\text{Mn}$ exchange curves. The present model represents the data adequately. The Sr^{2+} ion is the most favourable ion in the system, and the exchange

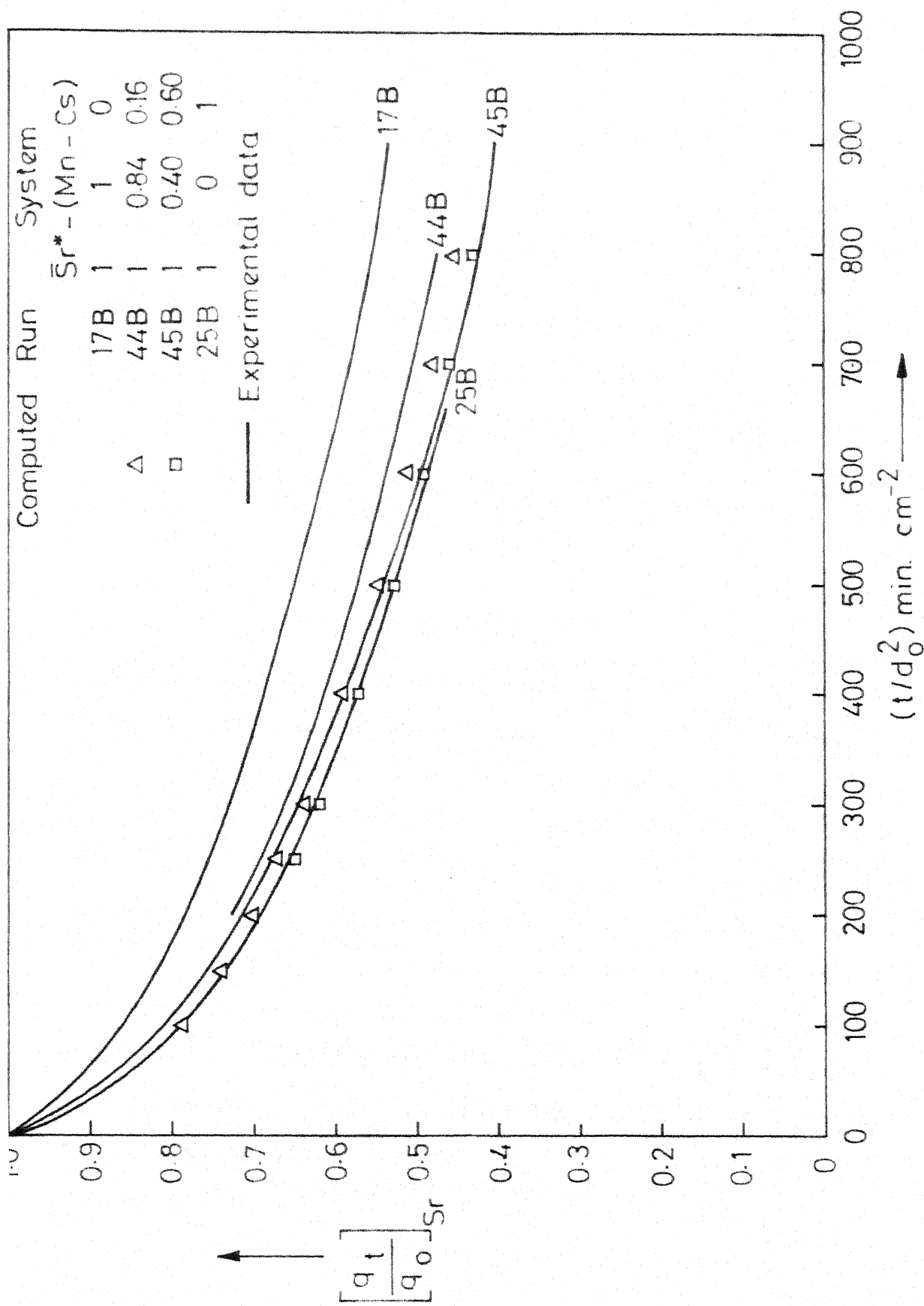


Fig. 20- Ternary Exchange Rate Data for the System: $Sr^*-(Mn-Cs)$ -
Dowex 50W-X8.

is taking place under unfavourable equilibrium conditions. As pointed out earlier, for this unfavourable equilibrium case, an incorporation of film resistance improves considerably the interpretation of the experimental depletion curves. When the film resistance is not considered the computed rate curves fall much below the experimental curves (The ternary exchange data computed without a consideration of film resistance are given in a tabular form in the Appendix E.)

Case ($\bar{A}^*-\bar{B}$)-C: Ternary depletion curves for ($\bar{Na}^*-\bar{Cs}$)-Mn and ($\bar{Na}^*-\bar{Mn}$)-Ba are shown in Figures 21a and 21b. In both the cases, the most favourable ion in the systems is in the bulk fluid-phase. The model interprets the rate data satisfactorily. In the case of ($\bar{Na}^*-\bar{Mn}$)-Ba, the data obtained at two different equivalent fractions of Mn, yielded nearly the same experimental curve whereas the model predicted two different curves. Rate curves for ($\bar{Na}^*-\bar{Ba}$)-Mn and ($\bar{Na}^*-\bar{Mn}$)-Cs exchanges are shown in Figures 21c and 21d. In both the cases, the most favourable ion of the system is the other counterion initially present in the resin phase. Again the model represents the ternary behaviour adequately. The computed curves do not differ whether the film resistance was considered or not. The computed rate data obtained with film diffusion not being considered is presented in the Tables 50 and 56 in the Appendix E. In this case, the more favourable and slower ion (Ba^{2+} or Mn^{2+}) is present

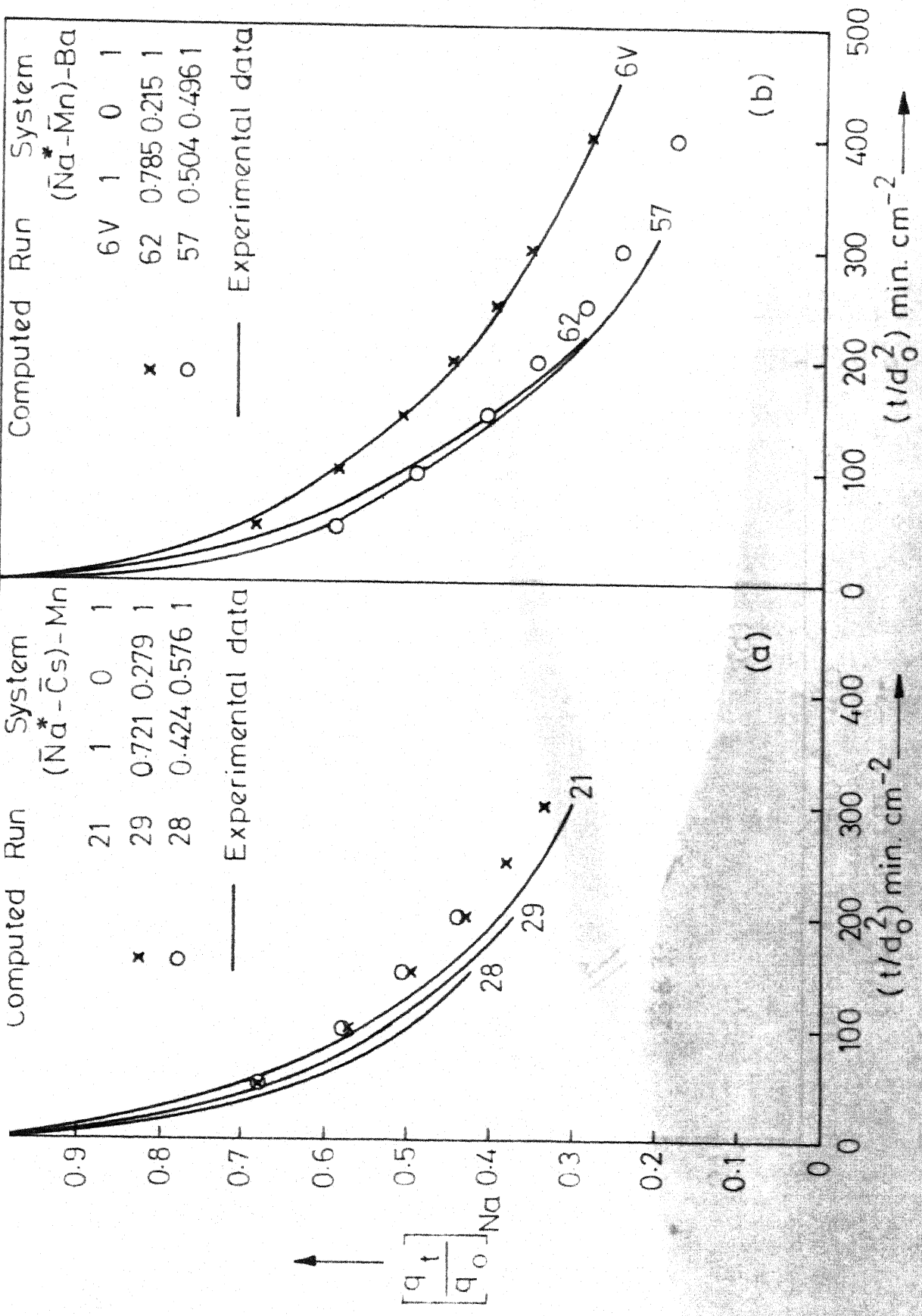


Fig.21 - Ternary Exchange Rate Data for the Systems: (a) $(\bar{Na}^* - \bar{Cs}) - Mn$ - Dowex 50W-X8, (b) $(\bar{Na}^* - \bar{Mn}) - Ba$ - Dowex 50W-X8

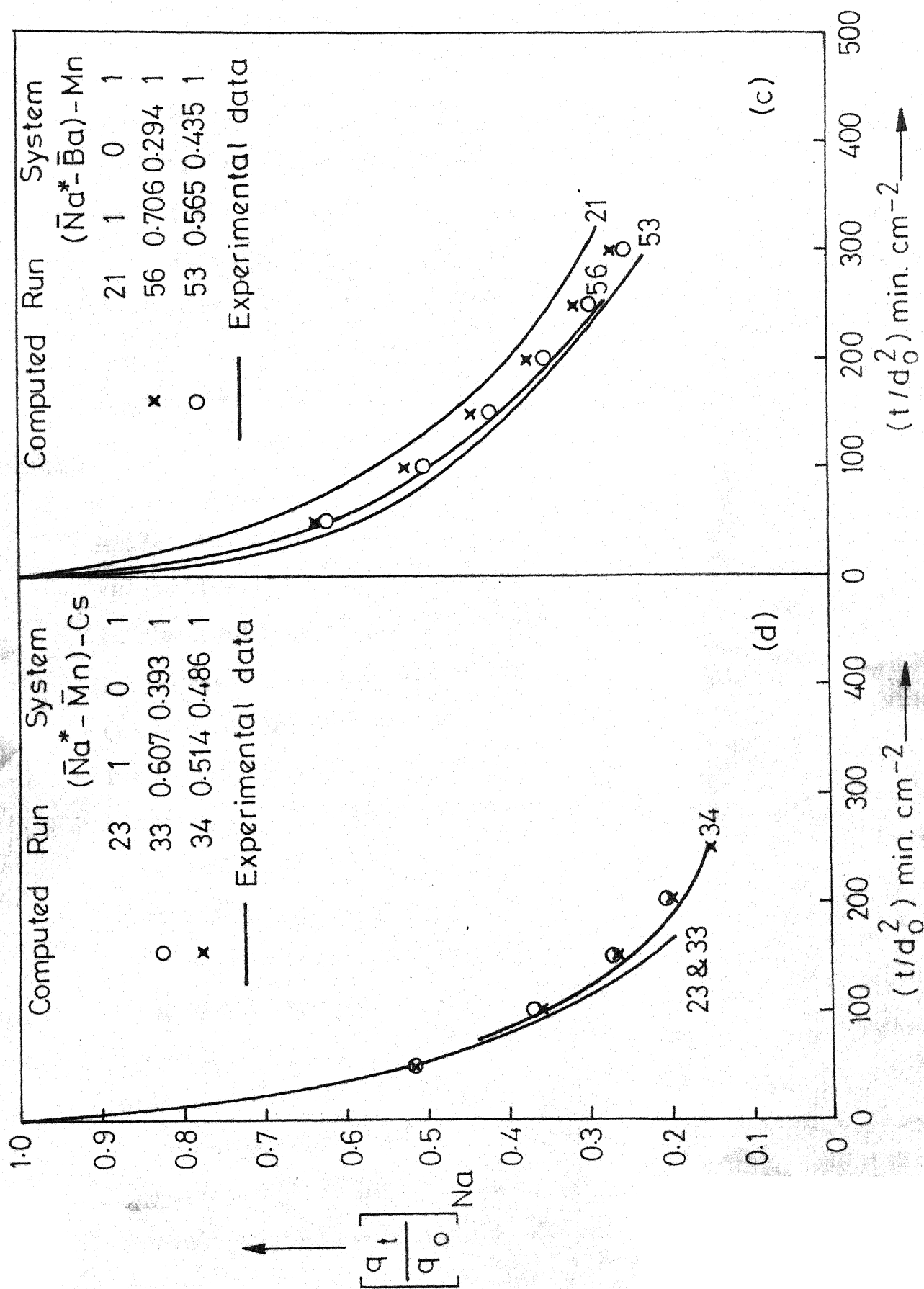


Fig.21- Ternary Exchange Rate Data for the Systems:(c) $(\bar{Na}^* - \bar{Ba}) - Mn$ -
Dowex 50W-X8, (d) $(\bar{Na}^* - \bar{Mn}) - Cs$ - Dowex 50W-X8.

initially in the resin phase, is increasing the depletion rate of the Na^+ ion.

Extensive ternary data were obtained by tagging Mn^{2+} ion in the resin phase. $(\bar{\text{Mn}}^*-\bar{\text{Na}})-\text{Cs}$, $(\bar{\text{Mn}}^*-\bar{\text{Na}})-\text{Ba}$, $(\bar{\text{Mn}}^*-\bar{\text{Cs}})-\text{Na}$, $(\bar{\text{Mn}}^*-\bar{\text{Cs}})-\text{Sr}$, $(\bar{\text{Mn}}^*-\bar{\text{Ba}})-\text{Na}$ and $(\bar{\text{Mn}}^*-\bar{\text{Sr}})-\text{Cs}$ systems were studied, and the ternary exchange curves are shown in Figures 22 to 27 respectively. When Mn^{2+} and Na^+ ions are initially present in the resin, exchanging with either Cs^+ or Ba^{2+} ion, the depletion behaviour of Mn^{2+} ions with respect to Na fraction is similar (Figures 22 and 23). As initial Na ionic fraction in the resin phase is increased, the rate of depletion of Mn is decreased and the depletion curves fall above the binary $(\bar{\text{Mn}}^*-\text{Cs}$ or $\bar{\text{Mn}}^*-\text{Ba})$ except for one case (viz. Run 30, Figure 22). The proposed model also predicted the same trend, but the matching of the curves was not satisfactory. Similarly, in $(\bar{\text{Mn}}^*-\bar{\text{Cs}})-\text{Na}$ and $(\bar{\text{Mn}}^*-\bar{\text{Cs}})-\text{Sr}$ systems, the manganese depletion curves fall above the binaries $(\bar{\text{Mn}}^*-\text{Na})$ or $(\bar{\text{Mn}}^*-\text{Sr})$ as the initial fraction of Cs in the resin phase is increased (Figures 24 and 25). The proposed model also reflected a similar trend, and the correlation of data for the ternary system $(\bar{\text{Mn}}^*-\bar{\text{Cs}})-\text{Na}$ is satisfactory. It is useful to recall that the Mn^{2+} ion is slower and preferred by the resin as compared to Na^+ and Cs^+ ions. When a faster ion is initially present in the resin phase, the depletion rate of the other ion in the resin is decreased and the depletion rate of the

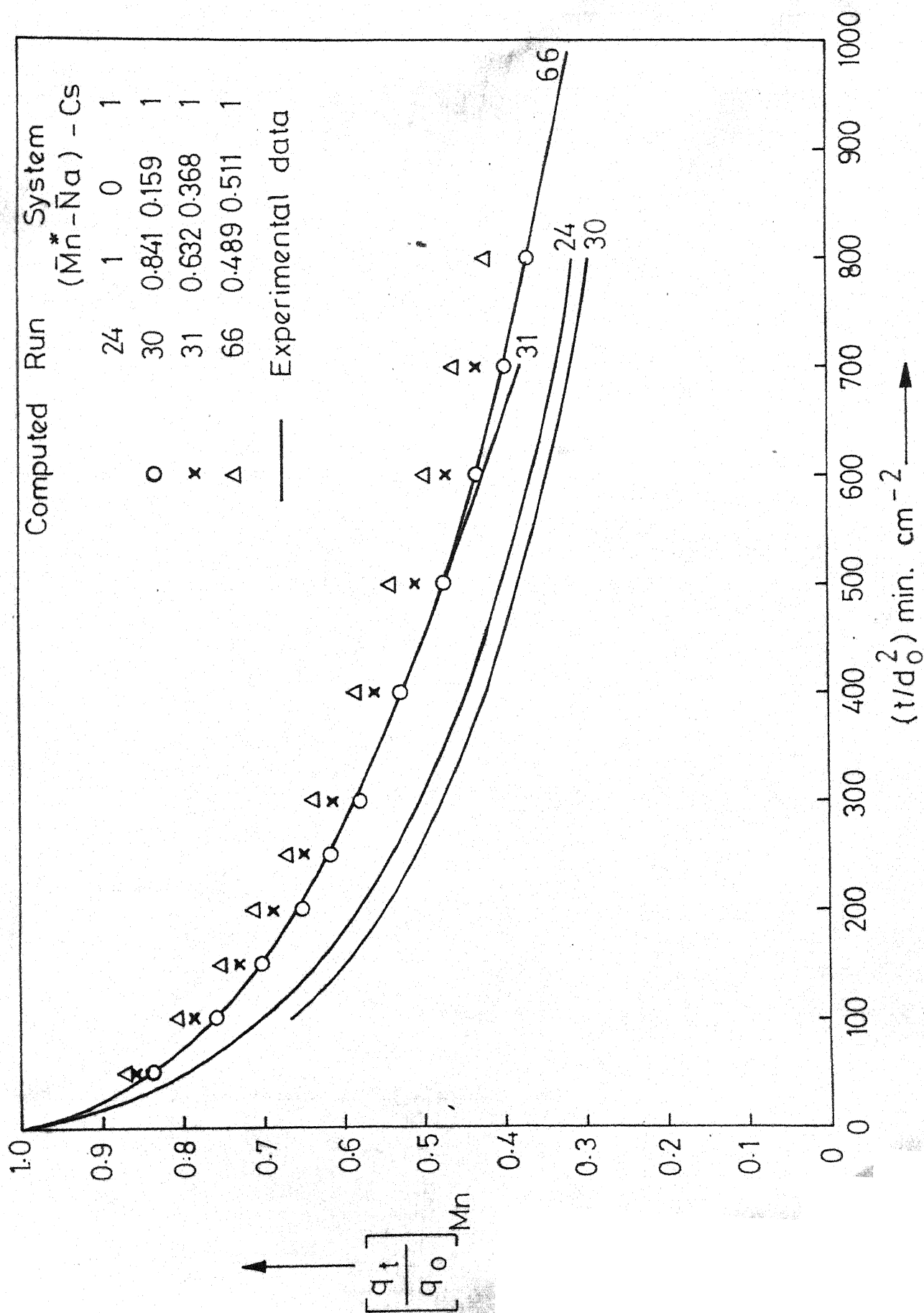


Fig.22 - Ternary Exchange Rate Data for the System: $(\bar{Mn}^* - \bar{Na}) - Cs$ -
 Dowex 50W-X8.

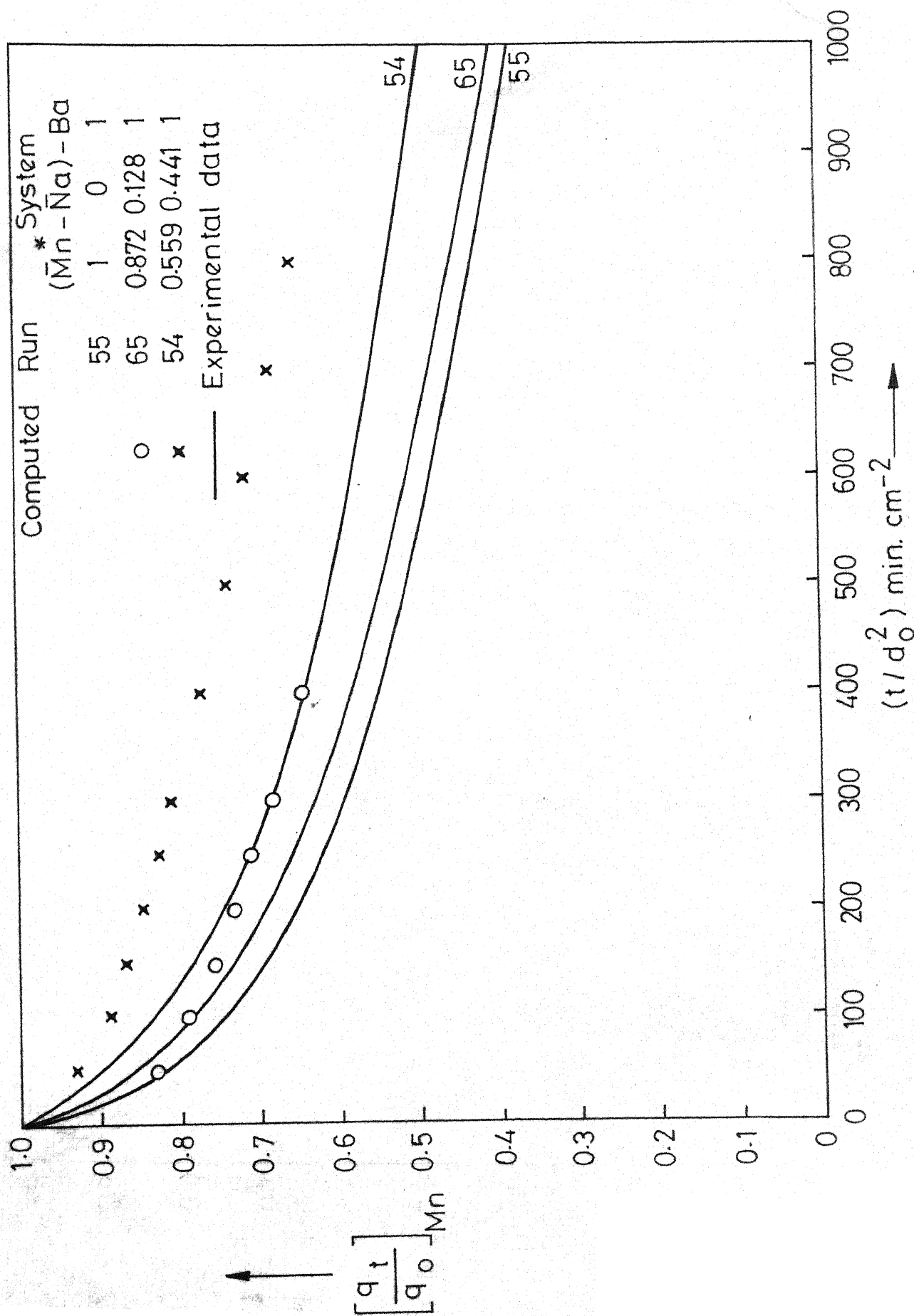


Fig. 23-Ternary Exchange Rate Data for the System: $(\bar{Mn}^* - \bar{Na}) - Ba -$
 Dowex 50W-X8.

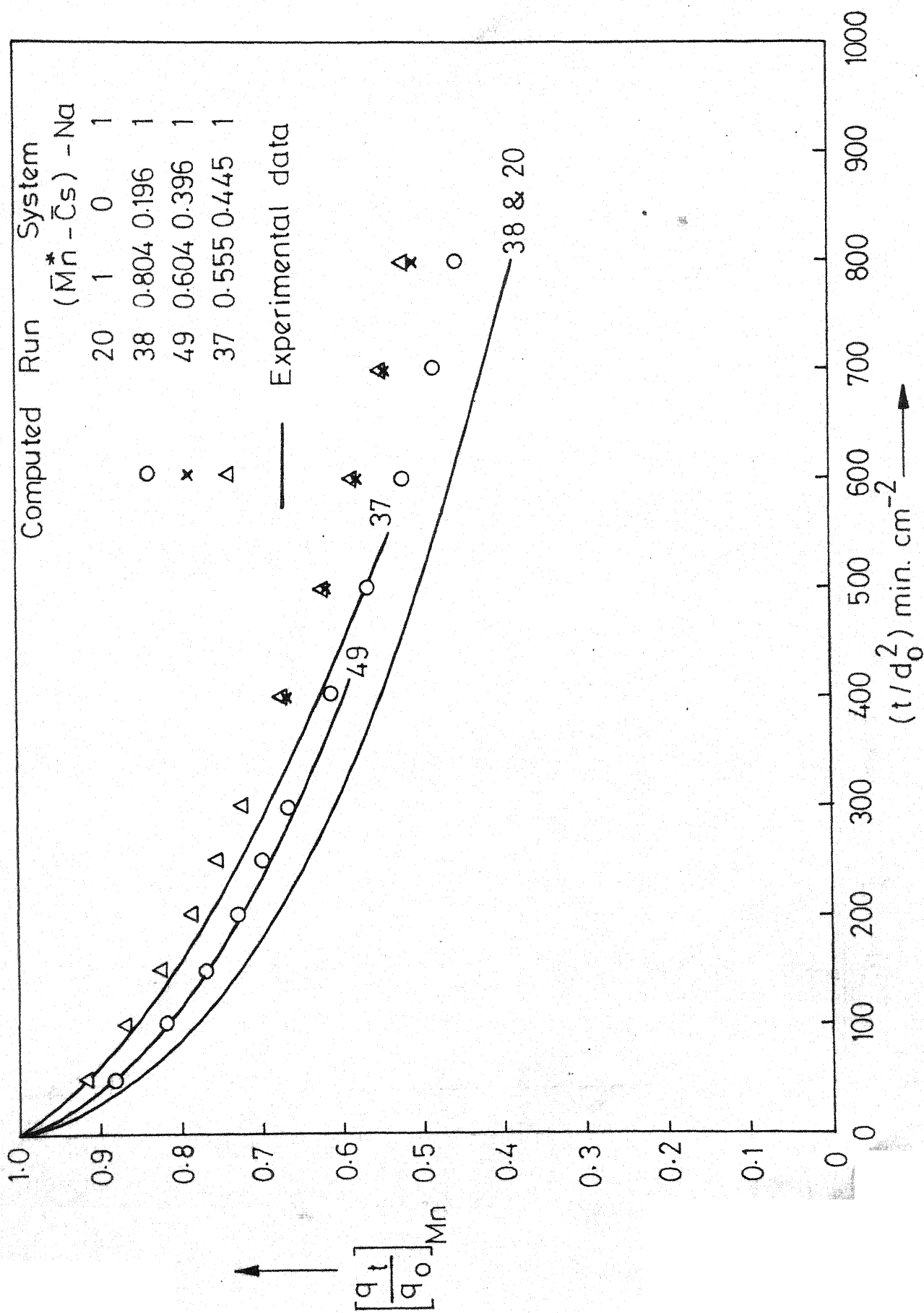


Fig. 24 - Ternary Exchange Rate Data for the System: $(\bar{Mn}^* - \bar{Cs}) - Na$ - Dowex 50W-X8.

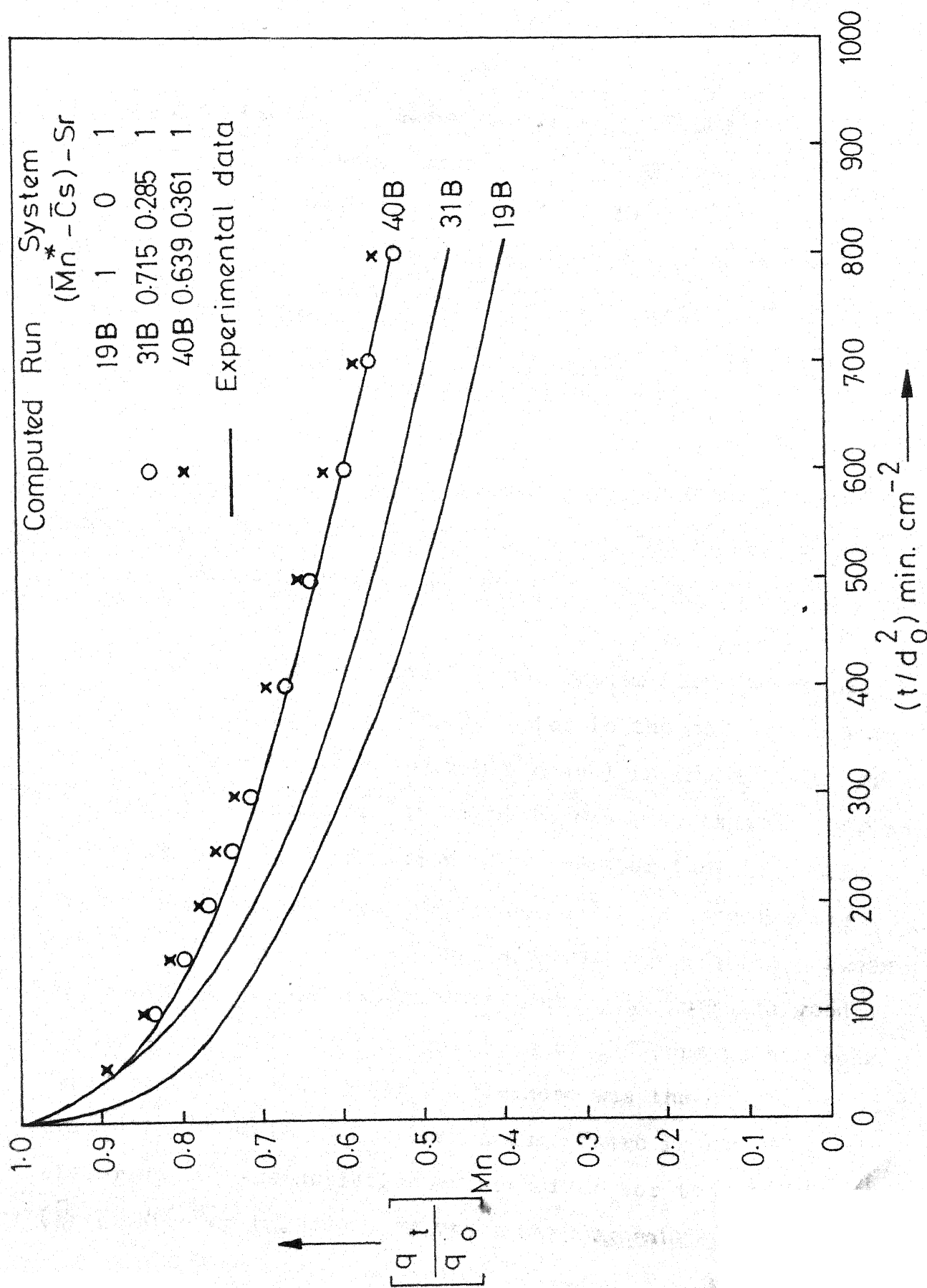


Fig.25-Ternary Exchange Rate Data for the System: $(\bar{Mn}^* - \bar{Cs}) - \text{Sr}$ -

Dowex 50W-X8.

faster ion itself is speeded up. An interesting case is the system ($\bar{\text{Mn}}^*-\bar{\text{Ba}}$)-Na. From the previous results, one would expect the depletion rate of the Mn^{2+} (faster ion) to increase as the Ba fraction is increased. Results presented in Figure 26 confirm the above conclusion. However, depletion of Mn^{2+} ion in the case of the ($\bar{\text{Mn}}^*-\bar{\text{Sr}}$)-Cs system, does not show an appreciable variation from the depletion of manganese in the binary $\bar{\text{Mn}}^*-\text{Cs}$ (See Figure 27). This is because of the fact that the value of resin-phase self diffusivity of Mn^{2+} ions, \bar{D}_{Mn} is nearly equal to that of \bar{D}_{Sr} . The proposed rate model predicts the data adequately.

Ternary exchange data for the system ($\bar{\text{Sr}}^*-\bar{\text{Cs}}$)-Mn are presented in Figure 28. The Sr^{2+} ion is the most favourable and the slowest ion (in the resin phase) in the system. From the previous discussion, it might be expected that an increase in the initial ionic fraction of the faster ion, Cs^+ would decrease the depletion rate of the Sr^{2+} ion. The results confirm the above observation. Also the correlation between the computed and the experimental rate data is quite good. In Figure 29, exchange of Sr^{2+} ions by Cs^+ ions in the bulk fluid phase has been shown. Manganese was the other ion initially present in the resin phase. There is not much of difference in the depletion curves of Sr for the Run 34B ($\bar{\text{Sr}}^*(0.786) \bar{\text{Mn}} (0.214)$) and the binary exchange of $\bar{\text{Sr}}^*-\text{Cs}$,

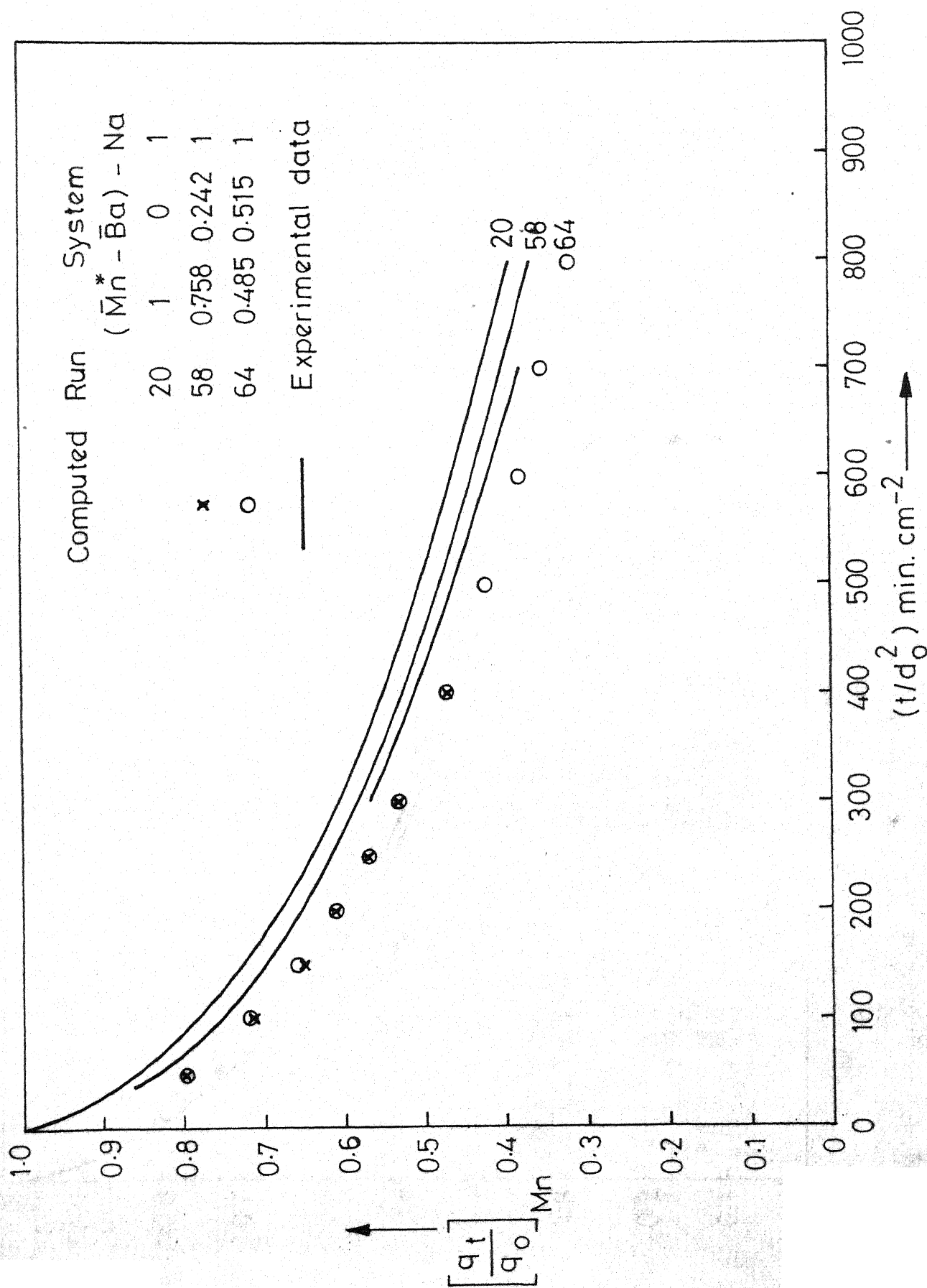


Fig. 26- Ternary Exchange Rate Data for the System: $(\bar{Mn}^* - \bar{Ba}) - Na -$
 Dowex 50W-X8.

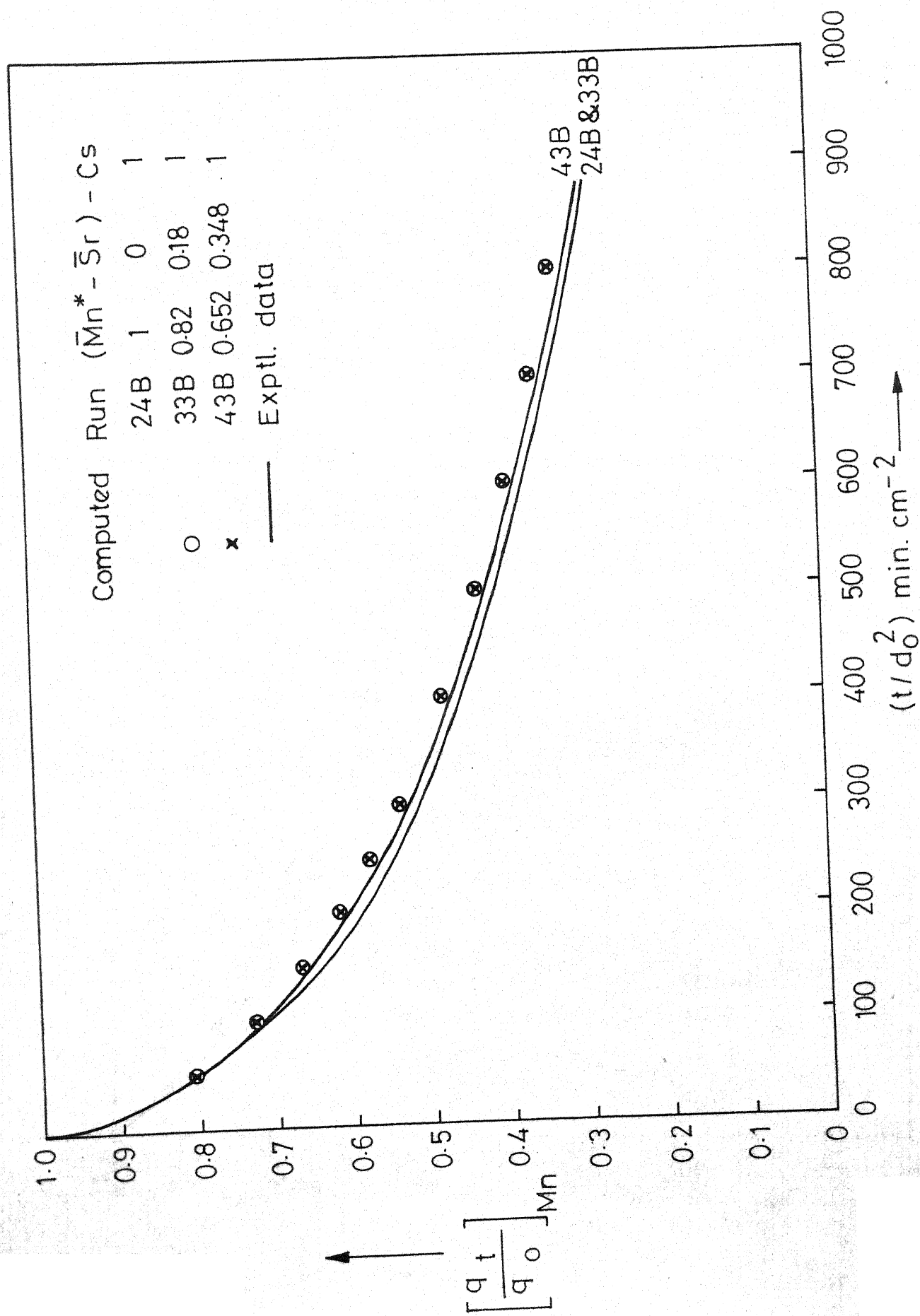


Fig. 27 - Ternary Exchange Rate Data for the System : $(\bar{Mn}^* - \bar{Sr}) - Cs$ -
Dowex 50W-X8.

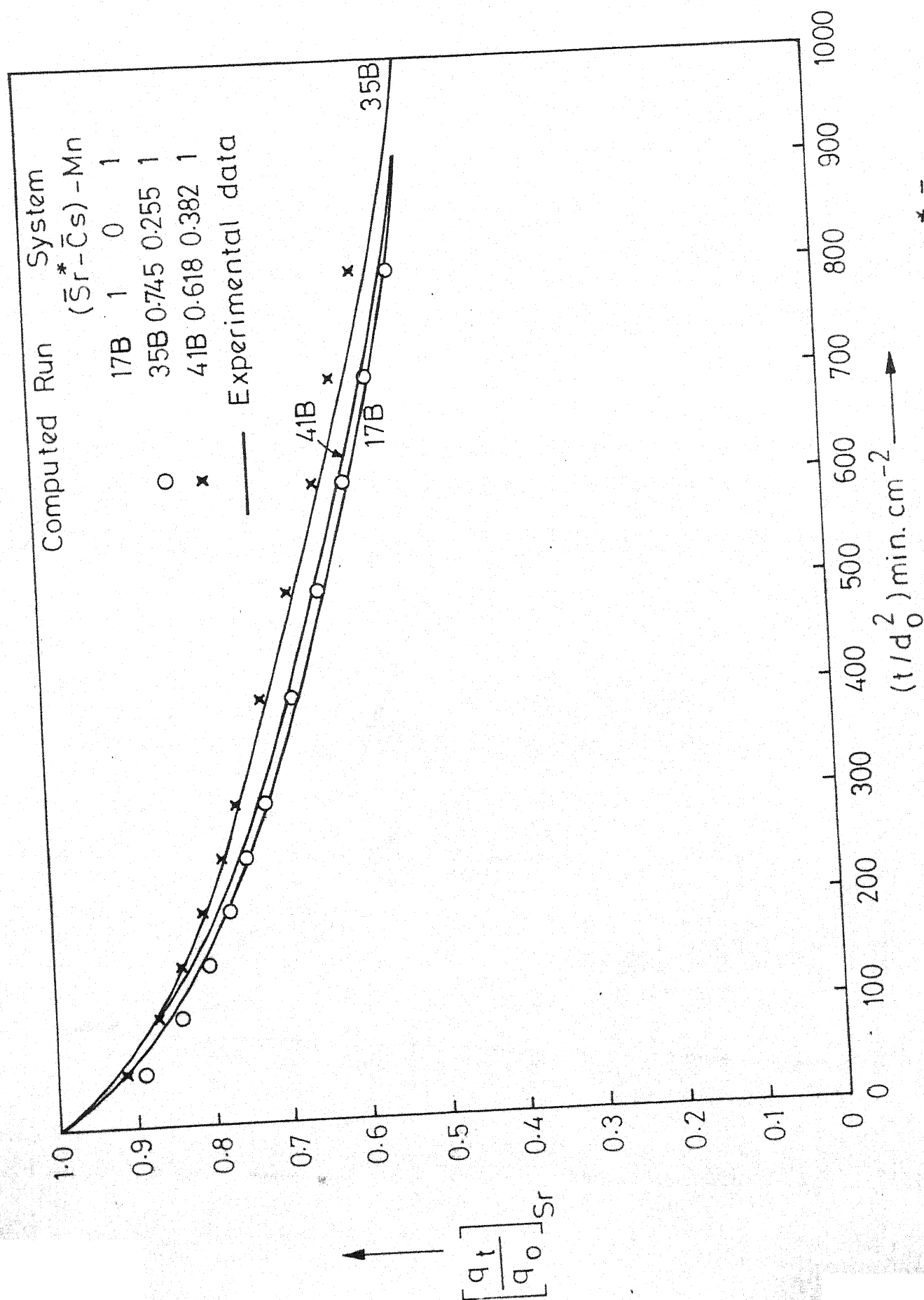


Fig. 28 - Ternary Exchange Rate Data for the System: $(\bar{S}r^* - \bar{C}s) - Mn$ -
 Dowex 50W-X8.

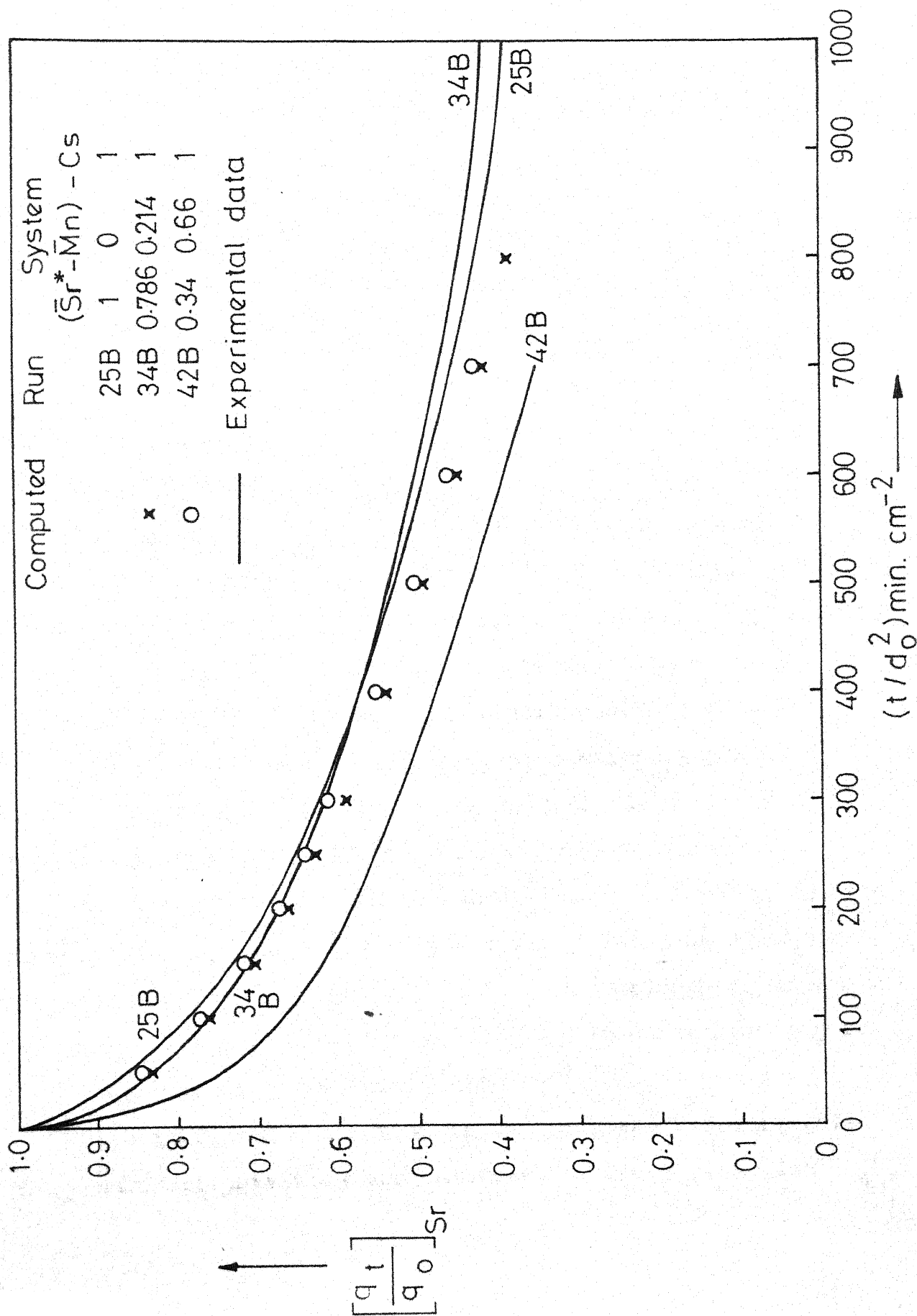


Fig.29- Ternary Exchange Rate Data for the System: $(\bar{Sr}^* - \bar{Mn}) - Cs -$

Dowex 50W-X8.

(Run 25B). However, strontium depletion is relatively faster for an other set of initial values of strontium and manganese fraction (Run 42B). This could not be explained. The computed rate curves do not show much variation.

On the whole, the proposed model correlated the ternary concentration-history curves quite satisfactorily. Even in cases where matching between experimental and computed data was not very good, the model interpreted the trend of the results satisfactorily. One need not expect exact matching between experimental and computed ternary exchange curves because of possible errors in the estimation of parameters used in the computations and also due to experimental errors which were discussed in the Experimental Chapter. For example, in the computations, interfacial ternary equilibrium data were predicted from the component binary equilibrium data. An error of $\pm 12\%$ (based on sample calculation, Appendix D) could be expected in the predicted values. As mentioned earlier in this section, the predicted value of the resin surface composition has considerable effect on the depletion rate of the ions initially in the resin phase. In smoothening the recorded experimental rate data, one could expect an error in the initial part of the curve to be $\pm 1\%$ and a much higher value near the tail end of the curve.

A significant assumption in the proposed model is that ionic self diffusivities are invariant of the resin-phase

composition. This may not be a correct assumption. Earlier work of Soldano and Boyd (S.7) and the recent report of Sharma et al. (S.3) pointed out that ionic self-diffusivities vary in heteroionic systems. This possible variation has not been taken into account in the computations.

A strictly qualitative and limited discussion on this heteroionic effect is presented below. Earlier in this chapter, Sr-Mn binary exchange data have been shown (Figure 14). A significant result of this exchange is that binary rate curves fall outside the two self-exchange curves. Self diffusivities of Mn^{2+} and Sr^{2+} ions in the resin phase are nearly equal to each other. However, Sr^{2+} ion is much more favourable in the resin phase than the Mn^{2+} ion. It has been reported in literature (B.7) that water content of the strontium ionic form of Dowex 50 resins is significantly less than the water content in the manganese ionic form. It has also been reported in literature that resin-phase self-diffusion coefficient of an ion increases with an increase in the water content of the resin (L.1). One can therefore, expect that self-diffusion-coefficient of Sr^{2+} ions in the manganese ionic form of the resin will be larger than its value in the homoionic form of the resin. Therefore, for Mn^{2+} -Sr exchange, Mn^{2+} ions are exchanging with speeded up Sr^{2+} ions. This would result in a faster depletion rate of manganese from the resin phase. Similarly for Sr^{2+} -Mn exchange, the

resin phase mobility of Mn^{2+} ions would be less than that in the homoionic form thus resulting in slowing down of strontium depletion rate.

In Figure 23, depletion curves of manganese in the $(\bar{\text{Mn}}^* - \bar{\text{Na}}) - \text{Ba}$ system are considerably lower than the computed curves. For the Wofatit KS resin (a sulphonated resin of phenolic type), manganese and sodium forms of the resin were reported to have very small variations in swelling (D.4). Moisture content of the barium form of Dowex 50 (4X, 8X, 16X) resins were reported to be very much less than that in the manganese form (B.7). If the above conclusions are applicable for the resin Dowex 50W-X8, barium self-diffusivity in manganese and/or sodium forms of the resin would be higher because of the higher water content of the resin in that form. The speeded up Ba^{2+} ions could cause higher manganese exchange rates. The experimental curves (Figure 23) show much faster rates of manganese depletion than the computed ones.

In the $(\bar{\text{Mn}}^* - \bar{\text{Ba}}) - \text{Na}$ system, when the resin contains both manganese and barium ions (manganese ion being tagged), the experimental depletion curves of manganese are above the computed values (See Figure 26). Manganese self-diffusivity in the presence of barium could be lower than its own value under homoionic conditions because of the low moisture content of the resin containing initially a mixture of Mn^{2+} and Ba^{2+} ions. If that happens, depletion rate of manganese would be

slower than that predicted. This trend can be seen in Figure 26. However, one could not say what the affect would be if both Ba^{2+} and Na^{+} ions are present along with Mn^{2+} in the resin phase. Also, the water content values mentioned in the discussion above are equilibrium values. One cannot say whether the resin in the heteroionic form is reaching its equilibrium water content during the unsteady-state exchange process. Also it should be noted that a resin bead in different ionic forms may have different values of bead diameters. Diameters of 12 resin beads used in the kinetic studies were determined in sodium, cesium and manganese forms. No regular variation in the values for a bead in different cationic forms was observed. In most cases, they were within 1% of each other. The diameter value for a bead in the tagged cationic form was employed in the computations. The change in the bead diameter during the exchange has not been taken into account in the present model.

A significant development in the present rate model is the incorporation of film resistance to mass transfer. In the film diffusion, the electric field effect was also included.

Though the present model for the ternary exchange rates has been derived from the general principles of irreversible thermodynamics, it could also be derived from the Nernst-Planck equations. However, in the present approach, a clear

understanding of the assumptions and limiting conditions involved in the theoretical developments has become possible. Also, a similar model can be used for a system containing more than three ionic components. As mentioned earlier in the dissertation, for the case of particle-diffusion control the present model reduces to the Nernst-Planck model for binary exchange, and the Ficks-law model for self-exchange. In fact in the present study, the same computer programme developed for the ternary system, was used with appropriate additional conditions in the computations for the binary and self-exchanges.

To sum up, families of binary and ternary rate curves can be computed from a knowledge of limiting ionic conductances in the aqueous phase (available in literature) film thickness, ionic self-diffusion coefficients in the resin phase, and component binary equilibrium data, all of which can be obtained experimentally without much difficulty.

* * *

CHAPTER 6

CONCLUSIONS AND RECOMMENDATIONS

CONCLUSIONS

1. The SPRT method is a convenient and a reliable technique for obtaining ion-exchange ternary equilibrium and kinetic data.

Equilibria

2. The selectivity sequence of the resin Dowex 50W-X8 for the ions under investigation is in the order $Ba > Mn > Cs > Na$.

3. The resin-phase activity coefficient of an ionic species A in a binary pair A-B, defined with the convention $\bar{\gamma}_i = 1$ when the resin is entirely in the homoionic form ($i=A, B$), varies with the ionic fraction of A in the resin phase and the nature of the second ion, B.

4. The ternary equilibrium data can be conveniently presented on a triangular diagram with the resin phase composition given by the regular grid and the solution phase composition along the constant parameter curves.

5. Binary equilibrium data were calculated from ternary experimental data neglecting the presence of the third ion. While the deduced data for the two binary pairs containing the most favourable ion, were fairly close to those experimentally observed, the data for the third binary pair (not

containing the most favoured ion) did not agree well with the actual data. The binary data of the ionic pairs Mn-Na and Mn-Cs calculated from the ternary data for the system Mn-Cs-Na agree well with the corresponding experimental data. However, the deduced data for the pair Cs-Na does not compare well with the experimental data. It is to be recalled that Mn^{2+} ion is the most preferred ion in the above ternary system.

6. The triangle rule failed for the system under study when expressed in terms of component binary equilibrium constants.

7. The ternary equilibrium data can be predicted from the binary data of the two pairs each containing the most preferred ion (the pairs are Mn-Na and Mn-Cs for the present case) by any of the methods given below:

- (i) an empirical method in which the binary equilibrium data are used.
- (ii) a semi-theoretical method which employs data on the rational equilibrium constants for the two ionic pairs and their activity coefficients.

Kinetics

8. Binary depletion curves normally fall within the envelope composed by self-exchange curves of the component ions.

When values of self diffusivities of the two component ions are very close to each other, and if one of the ions is substantially more preferred than the other, the binary curves may even fall outside the self-exchange curves.

Sr-Mn is such a binary pair.

9. For exchange of the type $\bar{A}^*-(B-C)$ in a ternary system A-B-C, in general the ternary rate curves fall within the envelope composed by the two binaries \bar{A}^*-B and \bar{A}^*-C . Ternary depletion curves for a case of the type $(\bar{A}^*-\bar{B})-C$, fall below the binary curve \bar{A}^*-C , if B is a slower ion (compared to A in the resin phase). If B is a faster ion, the curves fall above the binary \bar{A}^*-C . In other words, among the two ions initially present in the resin phase the exchange rate of the faster ion is speeded up and that of the slower ion is slowed down.

10. The model proposed in the present study describes particle-diffusion controlled ion-exchange kinetic data adequately for both binary and ternary systems. In the present model, film-diffusion resistance to mass transfer under the experimental conditions is also considered. Particularly for unfavourable exchange, a consideration of film-diffusion resistance to mass transfer is necessary to predict the rate of mass transfer for the so called particle-diffusion controlled ion-exchange kinetics.

11. The computed results show that for a favourable equilibrium exchange, the resin-surface composition is very

close to an equilibrium value with respect to the composition in the bulk fluid phase. For an unfavourable exchange, the resin surface is far from saturation with the incoming ions for a considerable extent of exchange.

12. Families of binary and ternary rate curves can be predicted (readily for the single particle case and with some modifications for the batch system also) with relatively small amount of information, which is either readily accessible or can be obtained with ease from a simple experiment, such as resin-phase self-diffusion coefficients of the component ions, film thickness, limiting ionic conductances and the binary ionic distribution of the component pairs. If information regarding film thickness at other hydrodynamic condition is also available in addition to the data above, the computer programme incorporating the proposed model can be used to predict ternary ion-exchange rate data for cases where both film diffusion and particle diffusion are equally important to mass transfer.

RECOMMENDATIONS FOR FURTHER WORK

1. The ternary equilibrium study carried out during the present investigation is by no means an exhaustive one. Much more work on similar lines is very much desirable.

2. A systematic study to investigate the variation of the self-diffusion coefficients in a heteroionic system is

very much needed. This would definitely help in improving the proposed model.

3. Although some work regarding the prediction of resin-phase ionic self diffusivities from the respective aqueous phase values has been reported in literature, a comprehensive study is still worthwhile in the above area.

4. The model can easily be extended to systems containing four or more number of components.

5. For the prediction of a breakthrough curve in a deep bed ion-exchange system, a comprehensive computer programme can be developed in which the material balance equation, equilibrium relationship and the proposed rate model are incorporated and solved simultaneously with appropriate initial and boundary conditions by means of a high speed computer. To save computer time, development of generalized relationships for fractional attainment of equilibrium (of the type obtained by Helfferich and coworkers (H.6, P.4) for binary systems) as a function of time and diffusivity ratios as parameters would be desirable.

* * *

BIBLIOGRAPHY

- A. 1 Argersinger, Jr., W.J., A.W. Davidson, and O.D. Bonner, Trans. Kans. Acad. Sci., 53, 404 (1950); Chem. Abstr., 45, 422g(1951); J. Am.Chem.Soc., 74, 1044 (1952).
- B. 1 Bajpai, R.K., M.Tech. Thesis, Indian Institute of Technology, Kanpur (India), 1972.
- B. 2 Bajpai, R.K., A.K. Gupta, and M.Gopala Rao, J.Phys. Chem. 77 (1973) (to be published).- published p.1288
- B. 3 Barrer, R.M., R.F. Bartholomew, and L.V.C. Rees, J.Phys. Chem.Solids,24, 309 (1963); R.M. Barrer and L.V.C. Rees, J. Phys. Chem. Solids, 25, 1035 (1964).
- B. 4 Barrer, R.M., and J.D.Falconer, Proc. Roy.Soc.(London), A236, 227 (1956).
- B. 5 Bauman, W.G., and J.Eichorn, J. Am.Chem.Soc., 69, 2830 (1947).
- B. 6 Bodashkova, I.F., A.M. Petrov, I.A. Karushnov, and Chernorukov "Kinetics of Ion Exchange of Sorption of Trace Amounts of Yttrium from the Solutions of Macro-Amounts of Some Elements" in Metody Poluch. Anal. Veschestov Osoboi Chist., Tr. Vres. Konf" p. 190, G.G. Devyatykh (ed.) Nauka, Moscow, USSR, 1968; Chem. Abstr., 75, 122553b (1971).
- B. 7 Bonner, O.D. and L.L.Smith, J. Phys. Chem., 61, 326(1957); O.D. Bonner, C.F. Jumper, and O.C. Rogers, Ibid, 62, 250 (1958).
- B. 8 Boyd, G.E., A.W. Adamson, and L.S. Myers, J. Am.Chem. Soc., 69, 2836 (1947).
- B. 9 Boyd, G.E., and B.A.Soldano, J.Am.Chem.Soc., 75, 6091 (1953).
- C. 1 Clazie, R.N., Ph.D. Thesis, Univ. of California, Berkeley, 1967.
- C. 2 Cloete, F.L.D., C.R.Frost, and M. Streat, "Fractional Separation by Continuous Ion Exchange" in "Ion Exchange in Process Industries" p. 182, Society of Chemical Industry, London, 1970.

- D.1 Davies, C.W., and G.D. Yeoman, Trans. Faraday Soc., 49, 968, 975 (1953).
- D.2 Davydov, A.T., R.B. Radushinskaya, Kolloid Zh., 28, 824 (1966); Chem. Abstr., 66, 59192e (1967).
- D.3 Diamond, R.M., and D.C. Whitney, "Resin Selectivity in Dilute to Concentrated Aqueous Solutions" in "Ion-Exchange, A series of Advances, Vol.1", p. 277, J.A. Marinsky (ed.), Marcel Dekker, Inc., New York, 1966.
- D.4 Djurfeldt, R., and O. Samuelson, Acta Chem. Scand., 11, 1209 (1957).
- D.5 Dranoff, J.S. and L. Lapidus, Ind. Eng. Chem. 49, 1297 (1957).
- D.6 Dranoff, J.S., and L. Lapidus, Ind. Eng. Chem., 50, 1648 (1958); 53, 71 (1961).
- E.1 Ekedahl, E., E. Hogfeldt, and L.G. Sillen, Acta. Chem. Scand., 4, 556, 829, 1471 (1950).
- E.2 Ewing, G.W., "Radioactivity as an Analytical Tool" in "Instrumental Methods of Chemical Analysis", p. 354, McGraw Hill Book Co., New York, Third Edition.
- F.1 Fricke, G.H., Ph.D. Thesis, Clarkson College of Tech., 1971; Diss. Abstr. Int., 31B, 6533 (1971).
- G.1 Gaines, Jr., G.C. and H.C. Thomas, J. Chem. Phys., 21, 714 (1953).
- G.2 Glaski, F.A., and J.S. Dranoff, A.I.Ch.E. Journal, 9, 426 (1963).
- G.3 Gopala Rao, M., Ph.D. Thesis, Univ. of Washington, (Seattle), 1962.
- G.4 Gopala Rao, M., and M.M. David, A.I.Ch.E. Journal, 10, 213 (1964).
- G.5 Gorshkov, V.I., and L.V. Kustova, Russ. J. Phys. Chem., 44, 142, 143 (1970).
- H.1 Harned, H.S., and B.B. Owen, "Physical Chemistry of Electrolyte Solutions", Reinhold Publishing Corporation, New York, Third Edition.

- H.2 Helfferich, F., "Ion Exchange", McGraw Hill Book Co., 1962, (a) Chapter 5, p. 95, (b) p. 177, (c) Chapter 6, p. 250, (d) p. 255, (e) p. 260, (f) p. 264, (g) p. 286, (h) p. 288.
- H.3 Helfferich, F., J. Phys. Chem., 66, 39 (1962).
- H.4 Helfferich, F., J. Phys. Chem., 67, 1157 (1963).
- H.5 Helfferich, F., "Ion-Exchange Kinetics" in "Ion Exchange, A series of Advances, Vol. 1" p. 65, J.A. Marinsky (ed.), Marcel Dekker, Inc., New York, 1966.
- H.6 Helfferich, F., and M.S. Plesset, J. Chem. Phys., 28, 418 (1958).
- H.7 Hering, B., and H. Bliss, A.I.Ch.E. Journal, 9, 495 (1963).
- H.8 Hogfeldt, E., Ark. Kemi, 26 (2829-30), 325 (1966)(Eng.); Chem. Abstr. 67, 260 34x (1967).
- H.9 Huang, T.C., H.S. Weng, and T.T. Tseng, J. Inorg. Nucl. Chem., 31, 1831 (1969).
- J.1 Jangg, G., Oster. Chemiker-Ztg. 59, 331 (1958); Chem. Abstr., 53, 15700d (1959).
- J.2 Jasz, A., and T. Lengyel, Acta Chim. Acad. Sci. Hung., 27, 247 (1961) (Engl); A Jasz, T. Lengyel and G. Schay, Ibid, 253; A Jasz, and T. Lengyel, Ibid, 33, 395 (1962); Chem. Abstr., 56, 13580e, 13580h, (1962); T. Lengyel and A. Jasz, Acta Chim Acad. Sci. Hung. , 34, 19 (1962); Chem. Abstr., 57, 6221g-h (1963).
- K.1 Kataoka, T., M. Sato, K. Ueyama, Kogyo Kagaku Zasshi, 74, 1052 (1971) (Jap.).
- K.2 Kekre, S.Y., Department of Chemical Engineering, IIT-Kanpur, Private Communication, 1969.
- K.3 Kunitaro, K., T. Yasushi, and T. Ukihiko, Kagaku Kogaku, 32, 716 (1968) (Jap.); Chem. Abstr., 69 88358f (1968).
- K.4 Kuo, J.C. and M.M. David, A.I.Ch.E. Journal, 9, 365 (1963).

- L.1 Lagos, A.E., and J.A. Kitchner, Trans. Faraday Soc., 56, 1245 (1960).
- L.2 Lewis, G.N., and M. Randall, "Principle of Constant Ionic Strength" in "Thermodynamics and the Free Energy of Chemical Substances" p. 374, McGraw Hill Book Co., Inc., New York, 1923.
- L.3 Lupa, A.J., Ph.D. Thesis, Northwestern University, 1967.
- M.1 McHardy, W.J., P. Mears, and J.F. Thain, J. Electrochem. Soc., 116, 920 (1969).
- M.2 Mears, P., and J.F. Thain, 72, 2789 (1968).
- M.3 Meyer, Walter, Ph.D. Thesis, Oregon State University, 1964.
- M.4 Morig, C.R. and M. Gopala Rao, Chem. Eng. Sci., 20, 889 (1965).
- P.1 Parsons, R. (ed.) "Handbook of Electrochemical Constants" Butterworths Scientific Publications, London, 1959.
- P.2 Perry, J.H. (ed). "Chemical Engineers' Handbook", McGraw Hill Book Co., Fourth Edition, 16-29.
- P.3 Pieroni, L.J., and J.S. Dranoff, A.I.Ch.E. Journal, 9, 42 (1963).
- P.4 Plesset, M.S., F. Helfferich, and J.N. Franklin, J. Chem. Phys., 29, 1064 (1958).
- R.1 Reddy, M.M., Ph.D. Thesis, State Univ. of New York at Buffalo, 1970; Diss. Abstr. Int., 31B, 5295 (1971); Reddy, M.M. and J.A. Marinsky, "Ion-Exchange Selectivity Coefficients in the Exchange of Calcium, Strontium, Cobalt, Nickel, Zinc and Cadmium Ions with Hydrogen Ions in variously crosslinked, Polystyrene Sulfonate Cation Exchangers at 25°C" in "Permselective Membranes" p. 135, C.E. Rogers (ed.) Marcel Dekker, Inc., New York, 1971.
- R.2 Reichenberg, D., "Ion-Exchange Selectivity" in "Ion Exchange A Series of Advances, Vol. 1" p. 227, J.A. Marinsky (ed.), Marcel Dekker, Inc., New York, 1966.

- S.1 Schlogl, R., and F. Helfferich, J. Chem. Phys., 26, 5 (1957).
- S.2 Schubert, J., Annual Rev. Phys. Chem., 5, 413 (1954).
- S.3 Sharma, H.D., R.E. Jervis, and L.W. McMillen, J. Phys. Chem., 74, 969 (1970).
- S.4 Small, Hamish, J. Am.Chem.Soc., 90, 2217 (1968).
- S.5 Smith, S.E., Eng. Bull. Purdue Univ., Eng. Ext., Series, 132, (Pt.2), 932 (1968).
- S.6 Smith, T.G., and J.S.Dranoff; I. and E.C. Fundamentals, 3, 195 (1964).
- S.7 Soldano, B.A., and G.E. Boyd, J.Am.Chem. Soc., 75, 6107 (1953).
- S.8 Soldatov, V.S. and V.A. Bychkova, Russ. J. Phys. Chem., 44, 1297 (1970).
- S.9 Soldatov, V.S., and O.F. Kharevich, Dokl.Akad., Nauk., Beloruss, SSR, 12, 140 (1968); Chem.Abstr. 69, 70080z (1968).
- S.10 Spiegler, K.S., and C.D. Coryell, J. Phys. Chem., 57, 687 (1953).
- S.11 Subbarao, H.C., and M.M. David, A.I.Ch.E. Journal, 3, 187 (1957).
- T.1 Talasek, V., J.Eliasek; Collect. Czech. Chem. Comm., 36, 77 (1971).
- T.2 Tan, K.S., and I.H. Spinner, Can. J. Chem. Eng., 49, 252 (1971).
- T.3 Tetenbaum, M., and H.P. Gregor; J. Phys. Chem., 58, 1156 (1954).
- T.4 Thibodeaux, L.J., Ph.D. Thesis, Louisiana State Univ. and Agricultural and Mechanical College, 1968; Diss. Abstr., 29B, 1655 (1968).
- T.5 Thomas, H.C., J.Am. Chem. Soc., 66, 1664 (1944).

- T.6 Tracerlab " 132 MA Manual Scaler" Operation Manual, Massachusetts, U.S.A.
- T.7 Tracerlab "231 Universal Ratemeter", Operation Manual, Massachusetts, U.S.A.
- T.8 Tracerlab, "Universal Spectrometer Model 401A" Operation Manual, Massachusetts, U.S.A.
- T.9 Turner, J.C.R., H.R. Church, A.S.W. Johnson, and C.B. Snowden, Chem. Eng. Sci., 21, 317 (1966).
- T.10 Turner, J.C.R., and C.B. Snowden, Chem. Eng. Sci., 23, 221 (1968).
- V.1 Vasishth, R.C., and M.M. David, A.I.Ch.E. Journal, 5, 391 (1959).
- V.2 Vermeulen, T., Ind. Eng. Chem., 45, 1664 (1953).
- V.3 Viswanathan, S., M.Tech. Thesis, Indian Institute of Technology, Kanpur (India), 1968.
- V.4 Viswanathan, S., D.P. Rao, S.Y. Kekre and M. Gopala Rao, "Ternary Ionic Diffusion in Ion-Exchange Resins" in "Ion Exchange in Process Industries," p. 281, Society of Chemical Industry, London, 1970.

APPENDIX A

EXCHANGE CHARACTERISTICS OF ^{137}Cs

In Figure 11, self exchange of Cs^+ ions has been presented along with the self exchanges of Ba^{2+} , Sr^{2+} , Mn^{2+} and Na^+ ions. The depletion curve of Cs^+ ions is unlike those of the other ionic species. No constant value of self-diffusion coefficient of Cs^+ ions in the resin phase \bar{D}_{Cs} , could be obtained by interpreting the data with the Fick's law model. Its numerical value increased as the depletion of cesium isotope progressed.

In Figure 30, a consolidated plot of the exchanges of Cs^+ ions initially in the resin phase with Sr^{2+} , Mn^{2+} and Na^+ ions individually in the solution phase has been presented. Again the depletion curves are not much different from the self-exchange curve of Cs^+ ions. In the same figure has been shown a rate curve of the $\bar{\text{Cs}}^* - \text{Na}$ binary exchange obtained with 1N solution of sodium chloride. In this case, depletion of Cs^+ ions is much faster as compared to that with 0.1N NaCl solution or 0.1N CsCl solution.

It is worthwhile to note the preference by the resin-phase is in the order $\text{Sr}^{2+} > \text{Mn}^{2+} > \text{Cs}^+ > \text{Na}^+$, and magnitudes of self-diffusion coefficients in the aqueous phase of the above four ions are $D_{\text{Mn}} = 70.8 \times 10^{-7} \text{ cm}^2/\text{sec}$, $D_{\text{Sr}} = 78.7 \text{ cm}^2/\text{sec}$, $D_{\text{Cs}} = 205.0 \times 10^{-7} \text{ cm}^2/\text{sec}$ and $D_{\text{Na}} = 133.0 \times 10^{-7} \text{ cm}^2/\text{sec}$.

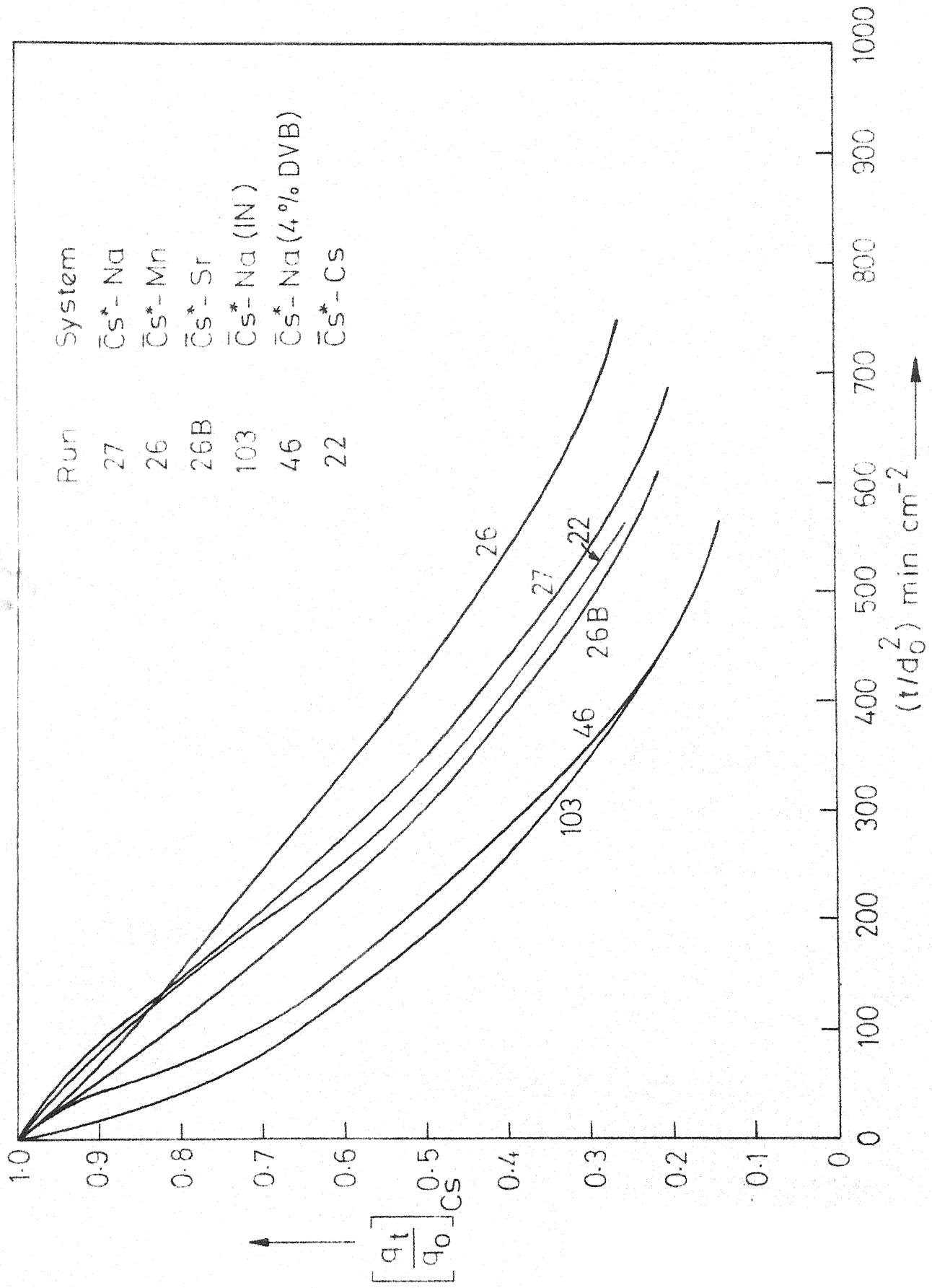


Fig.30-Self and Binary Exchange Curves with Cs in the Resin.

It is also noteworthy that all the ions except Cs^+ gave particle-diffusion controlled curves with solutions of 0.1N total anion concentration and at a superficial fluid velocity of about 25 cm/sec. That the exchange curves were particle-diffusion controlled was established by the velocity effect and particle size effect in the present study (self exchange of Na^+ ions, Table 33) and interruption tests by other research workers (G.3, K.4, M.4) under similar experimental conditions. Helfferich's criterion (H.2(d)) for particle-diffusion control when applied to ions in the present system also gave positive result for particle-diffusion control. Yet, when the bead was tagged with ^{137}Cs and exchanged with other ions, the exchange characteristics were totally different from the data on particle-diffusion control, and Fick's law model, Nernst-Planck model and the proposed model failed to interpret the respective exchange curves.

The author of this dissertation figured that particle-diffusion controlled self exchange curve could perhaps be obtained by using 1N solution of cesium chloride at the same high fluid velocity.

Cs^+ and Na^+ both are ions of alkali metals. The ion-exchange characteristics of Na^+ and Cs^+ ions are quite similar. There is only a slight preference of resin phase for Cs^+ ions over Na^+ ions. Both have the resin-phase

self-diffusivities of the same order of magnitude (B.9). In the present study, the kinetic behaviour of $\bar{\text{Na}}^*\text{-Na}$ (0.1N chloride) system is similar to that of $\bar{\text{Na}}^*\text{-Cs}$ (0.1N chloride) (See Figures 11 and 15). Similarly, $\bar{\text{Mn}}^*\text{-Na}$ and $\bar{\text{Mn}}^*\text{-Cs}$ exchanges show similar rate behaviour (see Figure 18). However, cesium chloride is much more expensive and hardly available in India. In view of this, the author employed 1N NaCl solution (instead of 1N CsCl solution) in the exchange study with cesium tagged bead.

It was quite likely that film resistance was one of the controlling steps for the depletion of cesium ions from the tagged bead with 0.1N chloride solutions of sodium and cesium. The partial control of film resistance is also likely for the exchanges of $\bar{\text{Cs}}^*\text{-Mn}$ and $\bar{\text{Cs}}^*\text{-Sr}$. Sr^{2+} ion is much more preferred by the resin as compared to Mn^{2+} ions, although \bar{D}_{Sr} is slightly less than \bar{D}_{Mn} , the depletion rate of cesium ions in the case of $\bar{\text{Cs}}^*\text{-Sr}$ is faster than in the case of $\bar{\text{Cs}}^*\text{-Mn}$. Film resistance could be of less importance with $\bar{\text{Cs}}^*\text{-Sr}$ exchange than with $\bar{\text{Cs}}^*\text{-Mn}$.

If one assumes that film-diffusion control is eliminated by employing 1N sodium chloride solution, one could use the exchange rate data for calculating \bar{D}_{Cs} with the help of Nernst-Planck model. However, one should note that pore solution effect would be present with 1N solutions. Experimental value of the self-diffusion coefficient of Na^+ ions, \bar{D}_{Na} and various

assumed values of \bar{D}_{Cs} were tried in the Nernst-Planck model to predict the experimental curve \bar{Cs}^*-Na (1N) . The correlation was poor and computed curves were intersecting with the experimental curve. Moreover, these values (of \bar{D}_{Cs}) were much lower than the estimated value obtained from \bar{Na}^*-Cs exchange. It indicated that the resin-phase resistance was not the only controlling step, and some other phenomenon was also taking place.

In Figure 30, a self-exchange kinetic run of cesium obtained with a resin bead of Dowex 50W-X4 and solution of 0.1N anion concentration is also shown (Run 46). Although the exchange rate was faster than that observed with Dowex 50W-X8, it was slower than Na^+ self exchange and also than \bar{Na}^*-Cs binary exchange rate (both with Dowex 50W-X8) and it again confirmed anomalous behaviour observed with cesium tagged beads.

It may also be mentioned that depletion history of Cs^+ ions from a cesium tagged bead in a ternary system (whether only Cs^+ ions were initially present in the resin-phase, exchanging with a mixture of two cationic species in the bulk-fluid phase or whether two ions were initially present in the resin phase, exchanging with the third ion in the solution phase) was not different from cesium self-exchange. Bajpai(B.1) also observed a similar behaviour with cesium tagged beads in the ternary system Sr-Mn-Cs-Dowex 50W-X8. Ternary data obtained

with the system Mn-Cs-Na-Dowex 50W-X8 are presented in a tabular form at the end of this section.

As mentioned earlier, it was also observed during capacity determinations that the capacity of a resin bead in cesium form was 2 to 18 percent less than that in sodium form. Also in the initial stages of the experimental work on equilibrium studies, an equilibrated bead, tagged with ^{137}Cs before equilibration, could not be regenerated easily with 0.1N cesium chloride solution. Afterwards a few ml of 1N cesium chloride solution was used for regeneration purposes.

The author could procure only one batch of ^{137}Cs isotope. Its chemical purity could not be checked. A sample of the ^{137}Cs isotope was tested for the characteristic radioactive gamma-emission of ^{137}Cs and the result was positive.

A possible explanation of the behaviour observed with ^{137}Cs tagged beads could be that the radioactive solution containing ^{137}Cs was contaminated with some non-gamma-emitting impurity which could have formed some complex with the resin matrix. Because of the complex formation some of the exchange sites could have been blocked. This can explain the lower value of capacity of a resin bead in the cesium form. Secondly, blocking of sites could render the passage of exchanging ions more tortuous. This could cause slower rate of exchange than expected.

TABLE 13: SELF EXCHANGE OF Cs⁺ IONS

DOWEX 50W-X8		DOWEX 50W-X4	
Run No. 22	Bead: Cs-8	Run No. 46	Bead: Cs-14
Bead diameter = 0.1025 cm		Bead diameter = 0.1025 cm	
Experimental		Experimental	
$\frac{t}{d_o^2} \left(\frac{\text{min}}{\text{cm}^2} \right)$	$\frac{q_t}{q_o}$	$\frac{t}{d_o^2} \left(\frac{\text{min}}{\text{cm}^2} \right)$	$\frac{q_t}{q_o}$
22.2	0.961	9.0	0.970
44.4	0.938	18.0	0.940
66.6	0.905	27.0	0.905
88.8	0.877	36.0	0.880
111.0	0.848	45.0	0.850
133.0	0.815	67.5	0.790
155.0	0.782	90.0	0.745
178.0	0.749	112.5	0.695
200.0	0.702	135.0	0.650
222.0	0.664	157.5	0.600
266.0	0.578	180.0	0.560
311.0	0.512	202.5	0.520
355.0	0.460	225.0	0.480
400.0	0.407	270.0	0.420
444.0	0.365	315.0	0.360
555.0	0.261	360.0	0.300
		405.0	0.245
		450.0	0.200
		495.0	0.160
		540.0	0.140
		585.0	0.120

TABLE 14: BINARY EXCHANGE RATE DATA :
Cs*-Na SYSTEM

Run No. 27 Bead: Cs-8
Bead diameter: 0.1025 cm
(0.1N NaCl Solution)

A
Experimental

$\frac{t}{d_o^2} \left(\frac{\text{min}}{\text{cm}^2} \right)$	$\frac{q_t}{q_o}$
28.5	1.000
57.0	0.944
85.5	0.904
114.0	0.852
142.5	0.812
171.0	0.766
200.0	0.720
228.0	0.680
257.0	0.634
285.0	0.594
342.0	0.520
400.0	0.446
456.0	0.337
514.0	0.326
570.0	0.274
627.0	0.229
684.0	0.200

Run No. 103 Bead: Cs-1A
Bead diameter: 0.1030 cm
(1.0N NaCl Solution)

B
Experimental

$\frac{t}{d_o^2} \left(\frac{\text{min}}{\text{cm}^2} \right)$	$\frac{q_t}{q_o}$
28.2	0.822
56.4	0.753
84.6	0.684
112.8	0.626
141.0	0.576
169.2	0.525
197.4	0.487
225.5	0.443
253.8	0.412
282.0	0.367
338.4	0.310
394.8	0.253
451.2	0.215
507.6	0.187
564.0	0.139

TABLE 15: BINARY EXCHANGE RATE DATA:
Cs-Mn SYSTEM

Run No. 26 Bead: Cs-7
Bead diameter: 0.0950cm

Experimental

$\frac{t}{d_o^2} (\frac{\text{min}}{\text{cm}^2})$	$\frac{q_t}{q_o}$
34.0	0.950
68.0	0.900
102.0	0.865
136.0	0.833
170.0	0.787
204.0	0.745
238.0	0.716
272.0	0.674
306.0	0.639
340.0	0.603
408.0	0.532
476.0	0.461
544.0	0.390
612.0	0.348
680.0	0.305
748.0	0.262
816.0	0.227

TABLE 16: BINARY EXCHANGE RATE DATA:
 \bar{C}^*
 Cs-Sr SYSTEM

Run No. 26B

Bead: Cs/A7

Bead diameter: 0.1040cm

Experimental

$\frac{t}{d_o^2} \left(\frac{\text{min}}{\text{cm}^2} \right)$	$\frac{q_t}{q_o}$
55.4	0.896
110.8	0.800
166.2	0.704
221.6	0.610
277.0	0.530
332.4	0.465
387.8	0.400
443.2	0.341
498.6	0.294
554.0	0.247
609.4	0.212
664.8	0.171
720.2	0.135

TERNARY EXCHANGE RATE DATA: $\bar{C}s^*$ -(Mn-Na) SYSTEM

TABLE 17

Run No. 44 Bead: Cs-1A
 Bead diameter: 0.1030cm
 $\bar{C}s^*$ -(Mn-Na): \bar{i}^* -(0.30-0.70)
 Experimental

$\frac{t}{d_o^2} \left(\frac{\text{min}}{\text{cm}^2} \right)$	$\frac{q_t}{q_o}$
20.9	0.971
41.8	0.950
62.7	0.922
83.6	0.891
104.5	0.850
125.4	0.809
146.3	0.772
167.2	0.741
188.1	0.704
209.0	0.672
250.8	0.609
293.0	0.545
334.0	0.500
418.0	0.414
523.0	0.318
627.0	0.246
690.0	0.177
836.0	0.127

TABLE 18

Run No. 45 Bead: Cs-8
 Bead diameter: 0.1025 cm
 $\bar{C}s^*$ -(Mn-Na): \bar{i}^* -(0.10-0.90)
 Experimental

$\frac{t}{\text{cm}^2} \left(\frac{\text{min}}{\text{cm}^2} \right)$	$\frac{q_t}{q_o}$
20.4	0.949
44.8	0.914
67.2	0.880
89.6	0.846
112.0	0.817
134.4	0.783
157.0	0.748
179.0	0.720
202.0	0.686
224.0	0.651
269.0	0.589
314.0	0.531
358.0	0.474
448.0	0.361
560.0	0.257
672.0	0.200
783.0	0.154

TERNARY EXCHANGE RATE DATA: ($\bar{C}s^*-\bar{N}a$)-Mn SYSTEM

TABLE 19

Run No. 40 Bead: Cs-8
 Bead diameter: 0.1025 cm
 ($\bar{C}s^*-\bar{N}a$)-Mn: (0.418*-0.582)-1.0

Experimental

$\frac{t}{d_o^2}(\frac{\text{min}}{\text{cm}^2})$	$\frac{q_t}{q_o}$
22.4	0.961
44.8	0.938
67.2	0.914
89.6	0.880
112.0	0.835
134.4	0.817
157.0	0.780
179.0	0.781
202.0	0.712
224.0	0.674
269.0	0.607
314.0	0.550
358.0	0.497
448.0	0.397
560.0	0.301
672.0	0.234
784.0	0.187
896.0	0.139

TABLE 20

Run No. 41 Bead: Cs-7B
 Bead diameter: 0.100 cm.
 ($\bar{C}s^*-\bar{N}a$)-Mn: (0.709*-0.291)-1.0

Experimental

$\frac{t}{d_o^2}(\frac{\text{min}}{\text{cm}^2})$	$\frac{q_t}{q_o}$
22.2	0.916
44.4	0.886
66.6	0.861
88.8	0.832
111.0	0.808
133.0	0.768
155.5	0.734
178.0	0.710
200.0	0.690
222.0	0.660
267.0	0.601
311.0	0.542
356.0	0.488
444.0	0.384
555.0	0.294
666.0	0.217
777.0	0.148
888.0	0.118
1000.0	0.896

TERNARY EXCHANGE RATE DATA: ($\bar{Cs}^*-\bar{Mn}$)-Na SYSTEM

TABLE 21

Run No. 32 Bead: Cs-8
 Bead diameter: 0.1025 cm
 ($\bar{Cs}^*-\bar{Mn}$)-Na: ($\overline{0.71}^*-\overline{0.329}$)-1.0

Experimental

$\frac{t}{d_o^2} \left(\frac{\text{min}}{\text{cm}^2} \right)$	$\frac{q_t}{q_o}$
28.6	0.990
57.2	0.975
85.8	0.935
114.4	0.877
143.0	0.807
171.5	0.756
200.0	0.705
229.0	0.654
257.0	0.615
286.0	0.576
343.0	0.500
400.0	0.436
457.0	0.384
514.0	0.327
572.0	0.282
628.0	0.231
686.0	0.205
743.0	0.180
800.0	0.154

TABLE 22

Run No. 39 Bead: Cs-7B
 Bead diameter: 0.1000 cm
 ($\bar{Cs}^*-\bar{Mn}$)-Na: ($\overline{0.273}^*-\overline{0.727}$)-1.0

Experimental

$\frac{t}{d_o^2} \left(\frac{\text{min}}{\text{cm}^2} \right)$	$\frac{q_t}{q_o}$
330.0	0.949
60.0	0.907
90.0	0.856
120.0	0.798
150.0	0.744
180.0	0.705
210.0	0.664
240.0	0.621
270.0	0.580
300.0	0.546
360.0	0.479
420.0	0.411
480.0	0.345
540.0	0.286
600.0	0.252
660.0	0.202
720.0	0.168
780.0	0.157
840.0	0.134

APPENDIX B

THEORY

SIMPLIFIED EXPRESSIONS FOR IONIC FLUXES

Referring to the developments of Equations 13 to 15 in the Theory Chapter, the expression for ionic flux in the resin phase can be simplified further for each of self, binary and ternary exchanges if the effect of variation of resin-phase activity coefficients is neglected.

$$\text{Assume } \frac{d \ln \bar{\gamma}_i}{d \ln C_i} = 0 \quad i = 1, 2, 3$$

Self Exchange:

$$Z_k = Z_j, \bar{D}_k = \bar{D}_j, C_3 = 0$$

From Equations 14 to 15

$$\begin{aligned} \bar{D}_{kj} &= \frac{\bar{D}_k C_k Z_k Z_j (\bar{D}_3 - \bar{D}_j)}{\sum_{i=1}^2 C_i Z_i^2 \bar{D}_i} \\ &= \frac{C_k (\bar{D}_3 - \bar{D}_k)}{(C_1 + C_2)} \end{aligned}$$

$$\bar{D}_{kk} = \bar{D}_k \left(1 - \frac{C_k (\bar{D}_k - \bar{D}_3) Z_k^2}{\sum_{i=1}^2 C_i Z_i^2 \bar{D}_i} \right)$$

$$= \bar{D}_k \left(1 - \frac{C_k (\bar{D}_k - \bar{D}_3)}{\bar{D}_k (C_1 + C_2)} \right)$$

$$C_1 + C_2 = C = \text{Constant}$$

$$\nabla C_1 = - \nabla C_2$$

$$\begin{aligned}
\therefore J_1 &= -\bar{D}_{11} \nabla C_1 - \bar{D}_{12} \nabla C_2 \\
&= -(\bar{D}_{11} - \bar{D}_{12}) \nabla C_1 \\
&= -(\bar{D}_1 (1 - \frac{C_1(\bar{D}_1 - \bar{D}_3)}{\bar{D}_1 \times C}) - \frac{C_1(\bar{D}_3 - \bar{D}_1)}{C}) \nabla C_1 \\
&= -(\bar{D}_1 - \frac{C_1(\bar{D}_1 - \bar{D}_3)}{C} - \frac{C_1(\bar{D}_3 - \bar{D}_1)}{C}) \nabla C_1 \\
J_1 &= -\bar{D}_1 \nabla C_1 \quad (\text{Fick's law Model})
\end{aligned}$$

Binary Exchange

$$C_3 = 0$$

From Equations 14 and 15

$$\bar{D}_{kk} = \bar{D}_k \left(1 - \frac{z_k^2 C_k (\bar{D}_k - \bar{D}_3)}{\sum_{i=1}^2 C_i z_i^2 \bar{D}_i} \right)$$

$$\bar{D}_{kj} = \frac{\bar{D}_k C_k z_k z_j (\bar{D}_3 - \bar{D}_j)}{\sum_{i=1}^2 C_i z_i^2 \bar{D}_i}$$

$$J_1 = -\bar{D}_1 \left(1 - \frac{z_1^2 C_1 (\bar{D}_1 - \bar{D}_3)}{(C_1 z_1^2 \bar{D}_1 + C_2 z_2^2 \bar{D}_2)} \right) \nabla C_1$$

$$- \frac{\bar{D}_1 C_1 z_1 z_2 (\bar{D}_3 - \bar{D}_2)}{C_1 z_1^2 \bar{D}_1 + C_2 z_2^2 \bar{D}_2} \times \nabla C_2$$

$$C_1 z_1 + C_2 z_2 = C = \text{Constant}; \therefore \nabla C_2 = -\frac{z_1}{z_2} \nabla C_1$$

Substituting for ∇C_2 in the above equation

$$J_1 = - \frac{\bar{D}_1 (C_1 Z_1^2 \bar{D}_1 + C_2 Z_2^2 \bar{D}_2 - Z_1^2 C_1 \bar{D}_1 + Z_1^2 C_1 \bar{D}_3 - C_1 Z_1^2 \bar{D}_3 + C_1 Z_1^2 \bar{D}_2)}{(C_1 Z_1^2 \bar{D}_1 + C_2 Z_2^2 \bar{D}_2)} \times \nabla C_1$$

$$J_1 = - \frac{\bar{D}_1 \bar{D}_2 (C_1 Z_1^2 + C_2 Z_2^2)}{C_1 Z_1^2 \bar{D}_1 + C_2 Z_2^2 \bar{D}_2} \times \nabla C_1$$

This equation is same as obtained from a set of Nernst-Planck equations.

Ternary Exchange

From Equation 13b, one gets

$$J_1 = - \bar{D}_{11} \nabla C_1 - \bar{D}_{12} \nabla C_2$$

$$J_2 = - \bar{D}_{21} \nabla C_1 - \bar{D}_{22} \nabla C_2$$

$$\text{where } \bar{D}_{kk} = \bar{D}_k \left(1 - \frac{Z_k^2 C_k (\bar{D}_k - \bar{D}_3)}{\sum_{i=1}^3 C_i Z_i^2 \bar{D}_i} \right)$$

$$\bar{D}_{kj} = \frac{\bar{D}_k C_k Z_k Z_j (\bar{D}_3 - \bar{D}_j)}{\sum_{i=1}^3 C_i Z_i^2 \bar{D}_i} \quad k \neq j$$

$$\therefore J_1 = - \bar{D}_1 \left(1 - \frac{Z_1^2 C_1 (\bar{D}_1 - \bar{D}_3)}{\sum_{i=1}^3 C_i Z_i^2 \bar{D}_i} \right) \nabla C_1 - \frac{\bar{D}_1 C_1 Z_1 Z_2 (\bar{D}_3 - \bar{D}_2)}{\sum_{i=1}^3 C_i Z_i^2 \bar{D}_i} \times \nabla C_2$$

Interchanging the suffixes 1 and 2, an expression for J_2 can also be written

From Nernst-Planck equations

$$J_1 = - \bar{D}_1 \left(\frac{\partial C_1}{\partial r} + \frac{C_1 Z_1 F}{RT} \frac{\partial \bar{\phi}}{\partial r} \right)$$

$$J_2 = - \bar{D}_2 \left(\frac{\partial C_2}{\partial r} + \frac{C_2 Z_2 F}{RT} \frac{\partial \bar{\phi}}{\partial r} \right)$$

$$J_3 = - \bar{D}_3 \left(\frac{\partial C_3}{\partial r} + \frac{C_3 Z_3 F}{RT} \frac{\partial \bar{\phi}}{\partial r} \right)$$

$$C_1 Z_1 + C_2 Z_2 + C_3 Z_3 = C = \text{Constant}$$

$$\therefore C_3 = \frac{1}{Z_3} (C - C_1 Z_1 - C_2 Z_2)$$

$$\nabla C_3 = - \frac{1}{Z_3} (Z_1 \nabla C_1 + Z_2 \nabla C_2)$$

Substituting for C_3 and ∇C_3 in the expression $\sum_{i=1}^3 Z_i J_i = 0$

$$\begin{aligned} -\bar{D}_1 Z_1 \left(\frac{\partial C_1}{\partial r} \right) - (\bar{D}_1 C_1 Z_1^2 + \bar{D}_2 C_2 Z_2^2 + \bar{D}_3 C_3 Z_3^2) \frac{F}{RT} \frac{\partial \bar{\phi}}{\partial r} \\ - \bar{D}_2 Z_2 \left(\frac{\partial C_2}{\partial r} \right) + \bar{D}_3 Z_3 \left(\frac{1}{Z_3} (Z_1 \frac{\partial C_1}{\partial r} + Z_2 \frac{\partial C_2}{\partial r}) \right) = 0 \end{aligned}$$

$$\therefore \frac{F}{RT} \frac{\partial \bar{\phi}}{\partial r} = - \frac{(\bar{D}_1 - \bar{D}_3) Z_1 \nabla C_1 - (\bar{D}_2 - \bar{D}_3) Z_2 \nabla C_2}{\sum_{i=1}^3 C_i Z_i^2 \bar{D}_i}$$

Substituting for $\frac{F}{RT} \frac{\partial \bar{\phi}}{\partial r}$ in the expressions for J_1 and J_2

$$J_1 = - \bar{D}_1 \left(1 - \frac{C_1 Z_1^2 (\bar{D}_1 - \bar{D}_3)}{\sum_{i=1}^3 C_i Z_i^2 \bar{D}_i} \right) \nabla C_1$$

$$+ \frac{\bar{D}_1 c_1 z_1 z_2 (\bar{D}_2 - \bar{D}_3)}{\sum_{i=1}^3 c_i z_i^2 \bar{D}_i} \times \nabla c_2$$

$$\text{and } J_2 = - \frac{\bar{D}_2 c_2 z_2 z_1 (\bar{D}_1 - \bar{D}_3)}{\sum_{i=1}^3 c_i z_i^2 \bar{D}_i} \times \nabla c_1 - \bar{D}_2 \left(1 - \frac{c_2 z_2^2 (\bar{D}_2 - \bar{D}_3)}{\sum_{i=1}^3 c_i z_i^2 \bar{D}_i} \right) \nabla c_2$$

The expressions are same as obtained above after simplifying Equations 13 to 15.

COMPUTER PROGRAMMES

Kinetic Studies

General Difference Equations: Resin-Phase

$$\frac{\partial \bar{C}_i}{\partial t} = \frac{1}{r^2} \frac{\partial}{\partial r} \left(r^2 (\bar{D}_{ii} \nabla \bar{C}_i + \bar{D}_{ij} \frac{z_i}{z_j} \nabla \bar{C}_j) \right)$$

$$i, j = 1, 2 \quad i \neq j$$

$$\frac{\partial \bar{C}_i}{\partial t} = \frac{\bar{C}_i \Big|_{r+\Delta r}^t - \bar{C}_i \Big|_r^t}{\Delta t}$$

$$\nabla \bar{C}_i = \frac{\partial \bar{C}_i}{\partial r} = \frac{\bar{C}_i \Big|_{r+\Delta r}^t - \bar{C}_i \Big|_r^t}{\Delta r}$$

$$\bar{D}_{ij} = \bar{D}_{ij} \left(\frac{\bar{C}_i \Big|_{r+\Delta r}^t + \bar{C}_i \Big|_r^t}{2}, \frac{\bar{C}_j \Big|_{r+\Delta r}^t + \bar{C}_j \Big|_r^t}{2} \right)$$

$$i, j = 1, 2$$

The length of the radius was divided into ten equal parts;

the mid points of various parts were assigned numbers 1 (nearest to the centre) to 10 (nearest to the surface).

The surface was marked point no. 11.

$$\left. \frac{\partial \bar{C}_i}{\partial r} \right|_{r=r_0}^t = \frac{\bar{C}_i|_{11}^t - \bar{C}_i|_{10}^t}{\frac{\Delta r}{2}}$$

$J_{i,R}$ = Flux of species i at the resin surface

$$J_{i,R} = J_{i,R} \left(\frac{\bar{C}_i|_{11}^t + \bar{C}_i|_{10}^t}{2}, \frac{\bar{C}_j|_{11}^t + \bar{C}_j|_{10}^t}{2}, \right.$$

$$\left. \frac{2}{\Delta r} (\bar{C}_i|_{11}^t - \bar{C}_i|_{10}^t), \frac{2}{\Delta R} \times (\bar{C}_j|_{11}^t - \bar{C}_j|_{10}^t) \right)$$

Film-Phase

$$J_{i,f} = J_{i,f} \left(\frac{C_{1,\text{soln}} + C_{1,\text{interface}}}{2}, \frac{C_{2,\text{soln}} + C_{2,\text{interface}}}{2}, \right. \\ \left. \frac{C_{3,\text{soln}} + C_{3,\text{interface}}}{2}, \frac{\Delta C_1}{\delta}, \frac{\Delta C_2}{\delta}, \frac{\Delta C_3}{\delta} \right)$$

At interface

$$J_{i,f} = J_{i,R}$$

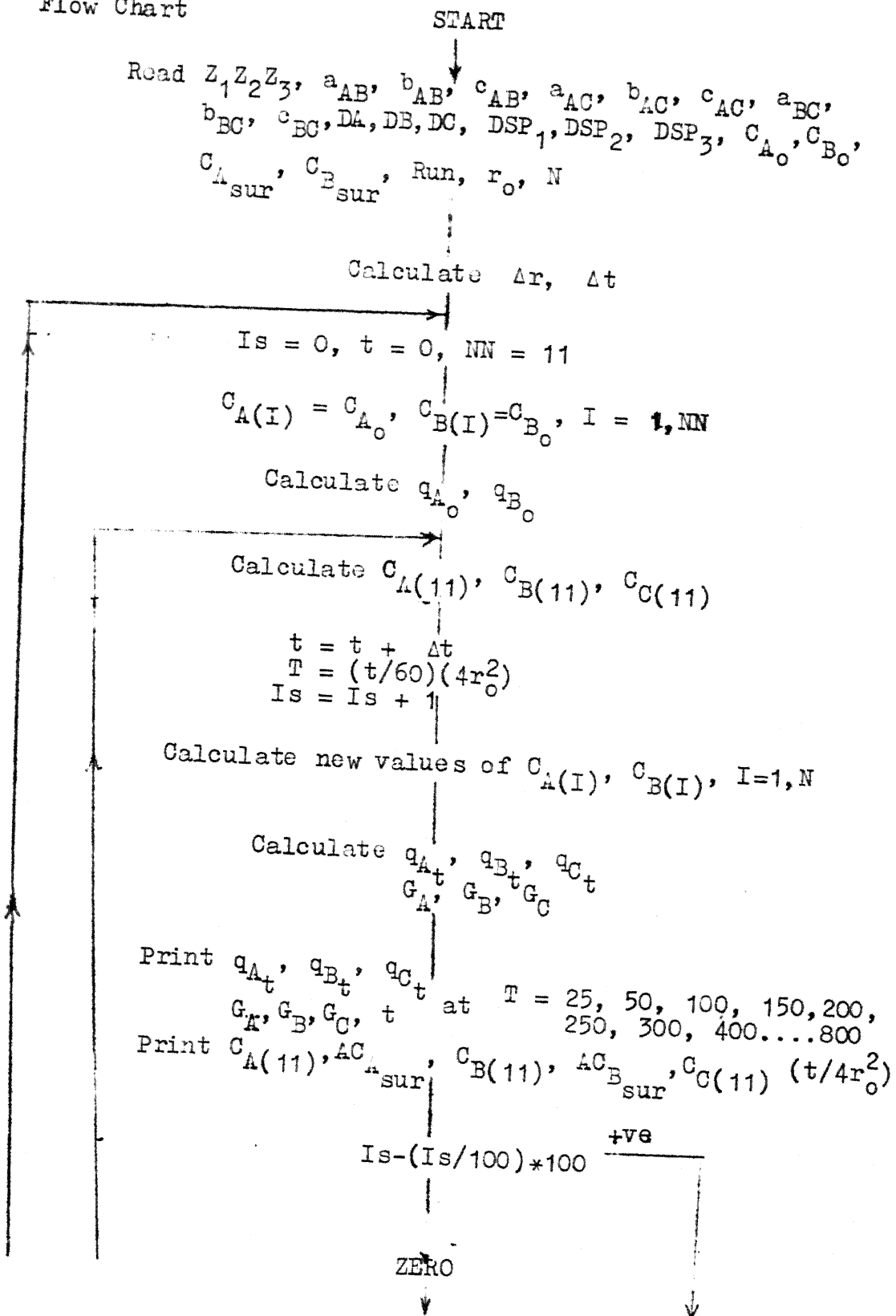
$$\bar{C}_i(11) = y_{i,R} = \lambda_i y_{i,f}$$

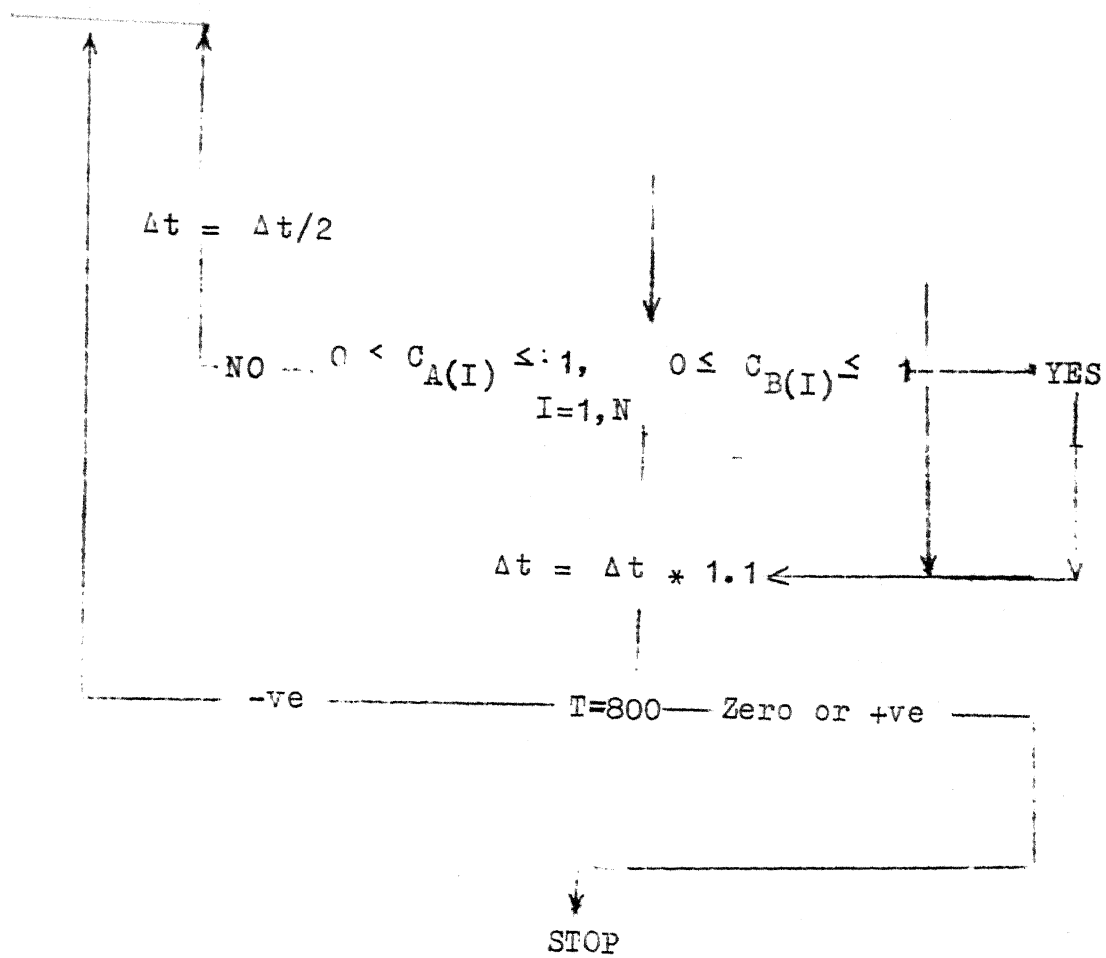
Various terms have been defined at appropriate places in the text of the thesis and also in the Nomenclature.

Nomenclature for the Flow Chart of the Computer Programme:

a_{ij}, b_{ij}, c_{ij}	Empirical constants for the pair, i, j ; $i, j = 1, 2, 3 \quad i \neq j$
DA	Diffusion coefficient of species A in aqueous phase
DSP _i	Diffusion coefficient of species i in the resin phase
C_{i_0}	Resin-phase initial equivalent fraction of species i
$C_{i_{sur}}$	Solution-phase equivalent fraction of species i
N	Number of parts into which the length of the radius is divided = 10
Is	Number of time increments
$C_{i(I)}$	Equivalent fraction of species i at the radial position I
G_i	q_{i_t}/q_{i_0}
AC _{i_{sur}}	Resin surface equivalent fraction of species i

Flow Chart





```

$II-FTC MAIN      NO DECK
C      FILM DIFFUSION ALSO CONSIDERED
C      A MOS3 FAVORABLE AND C LEAST
C      SPFI=FRACTION OF I IN SOLN/FRACTION OF I IN RESIN
C      SPFIJ=SPFI W.O.R.T. J
C      SPFI EVALUATED FROM SPFIJ AND SPFIK
C      CNSTAI,CNSTBI,CNSTCI RELATE TO THE THREE CONSTANTS OF SECOND
C      DEGREE POLYNOMIAL FOR SPECIES A AND I
C      CNSTA,CNSTB,CNSTC THREE CONSTANTS OF POLYNOMIAL RELATING
C      SPFB AND SPFC IN THE ABSENCE OF A
C      CISUR=SOLN PHASE FRACTION OF I
C      CIFM=CONCN OF I IN FILM=(CONCN IN SOLN(CISN)+CONCN AT SURFACE(ACISUR))/2
C      DI=DIFFUSIVITY OF I IN SOLN AT INF DILN
C      SPFIJ1=VALUE OF SPFIJ FOR YIJ ZERO TO YIJLIM
C      YIJLIM=LIMITING VALUE OF YIJ BELOW WHICH LINEARIZATION OF EQUILIBRIUM
C      ISOTHERM HAS BEEN ASSUMED
C      YBLIM AND SPFB1 FOR PAIR B - C
C      A=SR,B=MN,C=CS
C      DIMENSION CC(12)
C      DIMENSION RW(10)
C      DIMENSION CA(100),CB(100),YA(100),YB(100)
C      DIMENSION RRA(2,100),RRB(2,100),CON(3)
C      DIMENSION DS(3),DTER(3,3),Z(3)
C      DIMENSION D1D3R(4)
C      DIMENSION D2D3R(5)
C      DIMENSION VLNCA(2),VLNCB(2)
C      DIMENSION DSP(3),DSPP(3)
C      DIMENSION YC(13)
C      COMMON DS,Z,CNOT,GRADA,GRADB,FLUXA,FLUXB,DSP,AKAC,AKCA,DSPP
C      COMMON CASN,CBSN,CCSN,ACASUR,ACBSUR,ACCSUR,YA,YB,YC
C      COMMON SPFA,SPFB,SPFC,KLM
C      COMMON DA,DB,DC,CAFM,CBFM,CCFM,AAA,BBB,CCC,FLM
C      COMMON BL6,F1FLM,F2FLM,F3FLM,F4FLM,F5FLM,F6FLM
C      COMMON BL7,F1R,F2R,F3R,F4R
1001 FORMAT(3F7.2)
1002 FORMAT(3E16.6)
1003 FORMAT(4F8.4,I4,F7.4)
1004 FORMAT(F7.3)
1005 FORMAT(2E11.4,3F7.3)
1006 FORMAT(F7.4)
1007 FORMAT(6X,*FILM THICKNESS=*,E10.3)
1008 FORMAT(6F7.4)
1009 FORMAT(6E12.5)
1010 FORMAT(3F7.3)
1011 FORMAT(3E11.4)
1012 FORMAT(6X,*CNSTAB=*,F7.3,1X,*CNSTB=*,F7.3,1X,*CNSTC=*,F7.3)
1013 FORMAT(6X,*CNSTAC=*,F7.3,1X,*CNSTBC=*,F7.3,1X,*CNSTCC=*,F7.3)
1014 FORMAT(6X,*CNSTA=*,F7.3,1X,*CNSTB=*,F7.3,1X,*CNSTC=*,F7.3)
1015 FORMAT(6X,*DA=*,E11.4,1X,*DB=*,E11.4,1X,*DC=*,E11.4)
1016 FORMAT(1X,*SPFAB1=*,F7.4,1X,*YABLIM=*,F7.4,1X,*SPFAC1=*,F7.4,1X,
1017 1*YACLIM=*,F7.4,1X,*SPFB1=*,F7.4,1X,*YBLIM=*,F7.4)

```

```

1023 FORMAT(1X,12F6.3)
106 FORMAT( 6X,*RUN=*,I4)
107 FORMAT(I4,F6.2)
101 FORMAT(/ 5X,12HINITIAL DATA,15X,1HA,15X,1HB,15X,1HC/
1 10X,18HSELF DIFFUSIVITIES,2X,3E16.8/ 10X,14HCHARGE NUMBERS ,6X,
2 F6.2,10X,F6.2, 10X, F6.2/ 10X, 14HRESIN CAPASITY, 2X,E16.8/
3 10X,20HRESIN PARTICLE SIZE=,2X,E16.7/10X,
4 34HLENGTH DIVISIONS ALONG THE RADIUS =,15/10X,6HCANOT=,E17.8/
5 10X,6HCBNOT=,E17.8/10X,6HCASUR=,E17.8,6HCBUR=,E17.8)
102 FORMAT(12X,5HQ(BA),7X,5HG(BA),9X,5HQ(MN),7X,5HG(MN),
1 9X,5HQ(NA),7X,5HG(NA),9X,6HT(SEC),7X,10HTM(DMNLES))
103 FORMAT(1X,I4,3X,F11.7,1X,E11.7,3X,F11.7,1X,F11.7,3X,F11.7,1X,
1 F11.7,3X,E14.7,1X,E14.7,3X,I4)
10627 FORMAT(F5.2,3F5.1)
10628 FORMAT(F5.2,4F5.2)
104 FORMAT(1H1)
105 FORMAT(1H1)
FLM=0.000354
CNOT=1.0
KLM=10
DO 777 JARI=1,2
READ 1001,(Z(I),I=1,3)
READ1009,CNSTAB,CNSTBB,CNSTCB
READ1009,CNSTAC,CNSTBC,CNSTCC
READ1009,CNSTA,CNSTB,CNSTC
READ1010,DA,DB,DC
READ1002,(DSP(I),I=1,3)
READ1007,SPFAB1,YABLM,SPFAC1,YACLIM,SPFB1,YBLIM
4567 DO777IARI=1,KLM
READ 1003 , CANOT,CBNOT,CASUR,CBSUR,IRUN,RNOT
CASN=CASUR*0.1
CBSN=CBSUR*0.1
6789 N=10
1 PI=4.*ATAN(1.0)
11 AK=N
12 DR=RNOT/AK
DT=0.050*DR**2/DSP(3)
14 NN=N+1
8 IS=0
9 IP=0
15 DO 17 I=1,N
16 CA(I)=CANOT
CB(I)=CBNOT
17 CC(I)=1.-CA(I)-CB(I)
CA(NN)=CA(N)
CB(NN)=CB(N)
CC(11)=1.-CA(11)-CB(11)
20 PRINT101,(DSP(I),I=1,3),(Z(I),I=1,3),CNOT,RNOT,N,CANOT,CBNOT,

```

```

1  CASUR,CBSUR
  PRINT106,IRUN
  PRINT1061,FLM
  PRINT1011,CNSTAB,CNSTBB,CNSTCB
  PRINT1012,CNST,C,CNSTBC,CNSTCC
  PRINT1013,CNSTA,CNSTB,CNSTC
  PRINT1014,DA,DB,DC
  PRINT1015,SPFAB1,YABLIM,SPFAC1,YACLIM,SPFB1,YBLIM
201 PRINT 102
  21 TSEC=0.0
211 PRP=25.
  22 NM=N-1
  24 QANOT=(4./3.)*PI*(RNOT**3)*CNOT*CANOT
  25 QBNOT=(4./3.)*PI*(RNOT**3)*CNOT*CBNOT
  27 CONTINUE
    CC(11)=1.-CA(11)-CB(11)
  32 DO 34 IOL=1,NN
  33 YA(IOL)=CA(IOL)
    YB(IOL)=CB(IOL)
  34 YC(IOL)=1.-YA(IOL)-YB(IOL)
C  GENERAL PROGRAM FOR TERNARY INCORPORATING FILM RESISTANCE
  IF (YA(11)) 4112,4112,3405
  3405 YAB=YA(11)/(YA(11)+YB(11))
    YAC=YA(11)/(YA(11)+YC(11))
  4011 IF (YAB-YABLIM) 4012,4012,4014
  4012 SPFAB=SPFAB1
    GO TO 4015
  4014 SPFAB=1./(CNSTAB-CNSTBB*YAB+CNSTCB*YAB**2)
  4015 IF (YAB-1.) 4104,4106,4106
  4104 SPFBA=(1.-YAB*SPFAB/(1.-YAB))
    GO TO 4107
  4106 SPFBA=1.
  4107 IF (YAC-YACLIM) 5101,5101,5103
  5101 SPFAC=SPFAC1
    GO TO 5104
  5103 SPFAC=1./(CNSTAC-CNSTBC*YAC+CNSTCC*YAC**2)
  5104 IF (YAC-1.) 4108,4110,4110
  4108 SPFCA=(1.-YAC*SPFAC/(1.-YAC))
    GO TO 5111
  4110 SPFCA=1.
  5111 IF (YB(11)) 5112,5112,4111
  5112 ACBSUR=0.
    GO TO 5113
  4111 ACBSUR=SPFAC*YAC*0.1*(1.-YAB*SPFAB)/(YAB*SPFAB*(1.-YAC*SPFAC)+
    1 SPFAC*YAC)
  5113 ACASUR=SPFAC*YAC*(0.1-ACBSUR)
    ACCSUR=0.1-ACASUR-ACBSUR
    GO TO 4121
  4112 SPFA=1.
    ACASUR=0.
    IF (YB(11)-YBLIM) 5002,5002,5004
  5002 SPFB=2PFB1

```

```

GO TO 4114
5004 SPFB=1./((CNSTA-CNSTB*YB(11)+CNSTC*YB(11)**2)
ACBSUR=YB(11)*SPFB*0.1
4114 IF (YB(11)-1.) 4115,4117,4117
4115 SPFC=(1.-YB(11)*SPFB/(1.-YB(11)))
ACASUR=0.0
ACBSUR=YB(11)*SPFB*0.1
ACCSUR=0.1-ACASUR-ACBSUR
GO TO 4121
4117 SPFC=1.
4121 DS(1)=DSP(1)
DS(2)=DSP(2)
DS(3)=DSP(3)
4124 IF (ACASUR) 4125,4125,4127
4125 SPFA=1.0
GO TO 4128
4127 SPFA=ACASUR/(0.1*YA(11))
4128 IF (ACBSUR) 4129,4129,4131
4129 SPFB=1.
GO TO 4133
4131 SPFB=ACBSUR/(0.1*YB(11))
ACCSUR=0.1-ACASUR-ACBSUR
4133 IF (ACCSUR) 4134,4134,4138
4136 IF (YC(11)) 4134,4134,4138
4134 SPFC=1.
GO TO 4137
4138 SPFC=ACCSUR/(0.1*YC(11))
IF (SPFA) 4139,4139,4141
4139 PRINT1016
SPFA=1.
4141 IF (SPFB) 4142,4142,4144
4142 PRINT1017
SPFB=1.0
4144 IF (SPFC) 4145,4145,4137
4145 PRINT1018
SPFC=1.0
4137 CONTINUE
CALL DIFLM(ACASUR,ACBSUR,1,CCSUR)
GRADA=(CA(11)-CA(10))*2./DR
GRADB=(CB(11)-CB(10))*2./DR
CALL DIFCOE((CA(11)+CA(10))/2.,(CB(11)+CB(10))/2.)
AONE=F3FLM*SPFC/SPFA-F1FLM-F1R*2./((DR*0.1*SPFA)
TWO=F3FLM*SPFC/SPFB-F2FLM-F2R*2./((DR*0.1*SPFB)
THREE=-F1R*2.*YA(10)/DR-F2R*2.*YB(10)/DR-F1FLM*CASN-F2FLM*CBSN-
1 F3FLM*CCSN+F3FLM*SPAC*0.1
FOUR=F6FLM*SPFC/SPFA-F4FLM-F3R*2./((DR*0.1*SPFA)
FIVE=F6FLM*SPFC/SPFB-F5FLM-F4R*2./((DR*0.1*SPFB)
SIX=-F3R*2.*YA(10)/DR-F4R*2.*YB(10)/DR-F4FLM*CASN-F5FLM*CBSN-
1 F6FLM*CCSN+F6FLM*SPFC*0.1
ACBSUR=(SIX-THREE*FOUR/AONE)/(FIVE-FOUR*TWO/AONE)
ACASUR=(THREE-TWO*ACBSUR)/AONE
ACCSUR=0.1-ACASUR-ACBSUR
CA(11)=ACASUR/(0.1*SPFA)

```

```

28 IZERO=0
29 IS=IS+1
30 TSEC=TSEC+DT
301 TAW=TSEC*DSP(3)/((2.*RNOT)**2)
31 TMCM2=TSEC/(60.0*((2.*RNOT)**2))
311 TSCM2=TMCM2*60.
35 IZERO=IZERO+1
   I=N
3801 GRADA=2.*(CA(NN)-CA(N))/DR
3901 GRADB=2.*(CB(NN)-CB(N))/DR
   CALL DIFLM((SPFA*0.1*CA(11)),(SPFB*0.1*CB(11)),(SPFC*0.1*CC(11)))
40 FOUTA=FLUXA
41 FOUTB=FLUXB
42 DO 53 J=1,NM
43 I=I-1
44 GRADA=(CA(I+1)-CA(I))/DR
45 GRADB=(CB(I+1)-CB(I))/DR
   CALL DIFCOE((CA(I+1)+CA(I))/2.0,(CB(I+1)+CB(I))/2.0)
77 FINA=FLUXA
47 FINB=FLUXB
48 XS=I
49 RRA(IZERO,I+1)=((XS+1.0)**2*FOUTA-XS**2*FINA)*(DT/DR)/(((2.*XS+1.0)
1 /2.0)**2)
50 RRB(IZERO,I+1)=((XS+1.0)**2*FOUTB-XS**2*FINB)*(DT/DR)/(((2.*XS+1.0)
1 /2.0)**2)
51 FOUTA=FINA
52 FOUTB=FINB
53 CONTINUE
54 RRA(IZERO,1)=FOUTA*DT*3.0/DR
55 RRB(IZERO,1)=FOUTB*DT*3.0/DR
   CB(11)=ACBSUR/(0.1*SPFB)
   CC(11)=1.-CA(11)-CB(11)
56 IF(IZERO-1)57,57,61
57 DO 59 IOL=1,N
58 CA(IOL)=YA(IOL)+RRA(IZERO,IOL)
59 CB(IOL)=YB(IOL)+RRB(IZERO,IOL)
60 GO TO 35
61 DO 63 IOL=1,N
62 CA(IOL)=YA(IOL)+(RPA(1,IOL)+RRA(2,IOL))/2.0
63 CB(IOL)=YB(IOL)+(RPB(1,IOL)+RRB(2,IOL))/2.0
66 QA=0
67 QB=0
68 DO 72 L=2,N,2
69 COL=(L-1)**2
70 COM=L**2
71 QA=QA+2.*COL*(CA(L-1)+CA(L))+COM*(CA(L)+CA(L+1))
72 QB=QB+2.*COL*(CB(L-1)+CB(L))+COM*(CB(L)+CB(L+1))
73 QA=(QA-COM*(CA(N)+CA(NN))*0.5)*(DR/RNOT)**3
74 QB=(QB-COM*(CB(N)+CB(NN))*0.5)*(DR/RNOT)**3
75 QC=1.-QA-QB
753 IF(CANOT) 756,756,754

```

```

754 GA=QA/CANOT
755 GO TO 757
757 GA=QA
757 IF(CBNOT)760,760,758
758 GB=QB/CBNOT
759 GO TO 761
760 GB=QB
761 IF(1.-CANOT-CBNOT)764,764,762
762 GC=QC/(1.-CANOT-CBNOT)
7633 GO TO 376
764 GC=QC
376 IF (IS-(IS/100)*100)77,77,8613
77 DO 82 IOL=1,N
78 IF(CA(IOL)-1.)79,79,85
79 IF(CB(IOL)-1.)80,80,85
80 IF(CA(IOL))85,81,81
81 IF(CB(IOL))85,82,82
82 CONTINUE
83 DT=DT*1.1
843 GO TO 8613
85 DT=DT/2.0
86 GO TO 14
8613 IF (TMCM2-RRP) 9321,8621,8621
88621 PRINT103,IP,QA,GA,QB,GB,QC,GC,TSEC,TAW,IP
PRINT1008,ACASUR,CA(11),ACBSUR,CB(11),ACCSUR,TSCM2
863 IF(RRP-50.)864,866,868
864 RRP=RRP+25.0
865 GO TO 870
866 RRP=RRP+50.0
867 GO TO 870
868 IF(RRP-300.)866,869,869
869 RRP=RRP+100.0
870 IP=IP+1
9321 IF(TMCM2-800.) 27,933,933
933 CONTINUE
IARJ=IARI/2
IF(IARI-2*IARJ) 961,961,777
961 PRINT 104
9623 CONTINUE
888 CONTINUE
777 CONTINUE
999 CONTINUE
99 STOP
END
$IFFTC SUB NODECK
SUBROUTINE DIFCOE(AA,BB)
COMMONDS,Z,CNOT,GRADA,GRADB,FLUXA,FLUXB,DSp,AKAC,AKCA,DSpp
COMMON CASN,CBSN,CCSN,ACASUR,ACBSUR,ACCSUR,YA,YB,YC
COMMON SPFA,SPFB,SPFC,KLM
COMMON DA,DB,DC,CAFM,CBFM,CCFM,AAA,BBB,CCC,FLM
COMMON BL6,F1FLM,F2FLM,F3FLM,F4FLM,F5FLM,F6FLM
COMMON BL7,F1R,F2R,F3R,F4R
DIMENSION DS(3),DTER(3,3),Z(3)

```

```

DIMENSION DSP(3),DSPP(3)
DIMENSION YA(100),YB(100),YC(13)
DIMENSION CON(3)
1 CON(1)=AA
2 CON(2)=BB
CON(3)=CNOT-AA-BB
DS(1)=DSP(1)
DS(2)=DSP(2)
DS(3)=DSP(3)
D=DS(1)*Z(1)*CON(1)+DS(2)*Z(2)*CON(2)+DS(3)*Z(3)*CON(3)
F1=(DS(1)-DS(1)*CON(1)*Z(1)*(DS(1)-DS(3))/D)
F2=(DS(2)*CON(1)*(DS(2)-DS(3))/D)
F2=-F2*Z(1)
F3=(DS(2)*CON(2)*(DS(1)-DS(3))/D)
F3=-F3*Z(2)
F4=(DS(2)-DS(2)*CON(2)*Z(2)*(DS(2)-DS(3))/D)
9 FLUXA=F1*GRADA,F2*GRADB
10 FLUXB=F3*GRADA,F4*GRADB
F1R=F1
F2R=F2
F3R=F3
F4R=F4
RETURN
END
IFTC SUB1 NODECK
SUBROUTINE DIFLM(ABNDRY,BBNDRY,CBNDRY)
COMMONS,Z,CNOT,GRADA,GRADB,FLUXA,FLUXB,DSP,AKAC,AKCA,DSPP
COMMON CASN,CBSN,CCSN,ACASUR,ACBSUR,ACCSUR,YA,YB,YC
COMMON SPFA,SPFB,SPFC,KLM
COMMON DA,DB,DC,CAFM,CBFM,CCFM,AAA,BBB,CCC,FLM
COMMON BL6,F1FLM,F2FLM,F3FLM,F4FLM,F5FLM,F6FLM
COMMON BL7,F1R,F2R,F3R,F4R
DIMENSION YA(100),YB(100),YC(13),Z(3)
DIMENSION DS(3),DSP(3),DSPP(3)
ACCSUR=CBNDRY
ACBSUR=BBNDRY
ACASUR=ABNDRY
SBSN=CBSN
CCSN=0.1-CASN-CBSN
CAFM=(CASN+ACASUR)/2.
CBFM=(CBSN+ACBSUR)/2.
CCFM=(CCSN+ACCSUR)/2.
GRDFMA=(CASN-SPFA*YA(11)*.1)/FLM
GRDFMB=(SBSN-SPFB*YB(11)*.1)/FLM
GRDFMC=(CCSN-SPFC*YC(11)*0.1)/FLM
F1=DA*DB*CBFM*Z(2)+DA*DC*CCFM*Z(3)
F2=-DA*CAFM*Z(1)*Z(2)*DB/Z(2)
F3=-DA*CAFM*Z(1)*DC
F4=-DB*CBFM*Z(2)*Z(1)*DA/Z(1)
F5=DB*DA*CAFM*Z(1)+DB*DC*CCFM*Z(3)
F6=-DB*CBFM*Z(2)*Z(3)*DC/Z(3)
FLUXA=F1*GRDFMA+F2*GRDFMB+F3*GRDFMC
FLUXB=F4*GRDFMA+F5*GRDFMB+F6*GRDFMC

```

```
SUM=DA*CAFM*Z(1)+DB*CBFM*Z(2)+DC*CCFM*Z(3)
FLUXA=FLUXA/(SUM*2.003)
FLUXB=FLUXB/(SUM*2.003)
F1FLM=F1/(SUM*2.003*FLM)
F2FLM=F2/(SUM*2.003*FLM)
F3FLM=F3/(SUM*2.003*FLM)
F4FLM=F4/(SUM*2.003*FLM)
F5FLM=F5/(SUM*2.003*FLM)
F6FLM=F6/(SUM*2.003*FLM)
RETURN
END
```

ENTRY

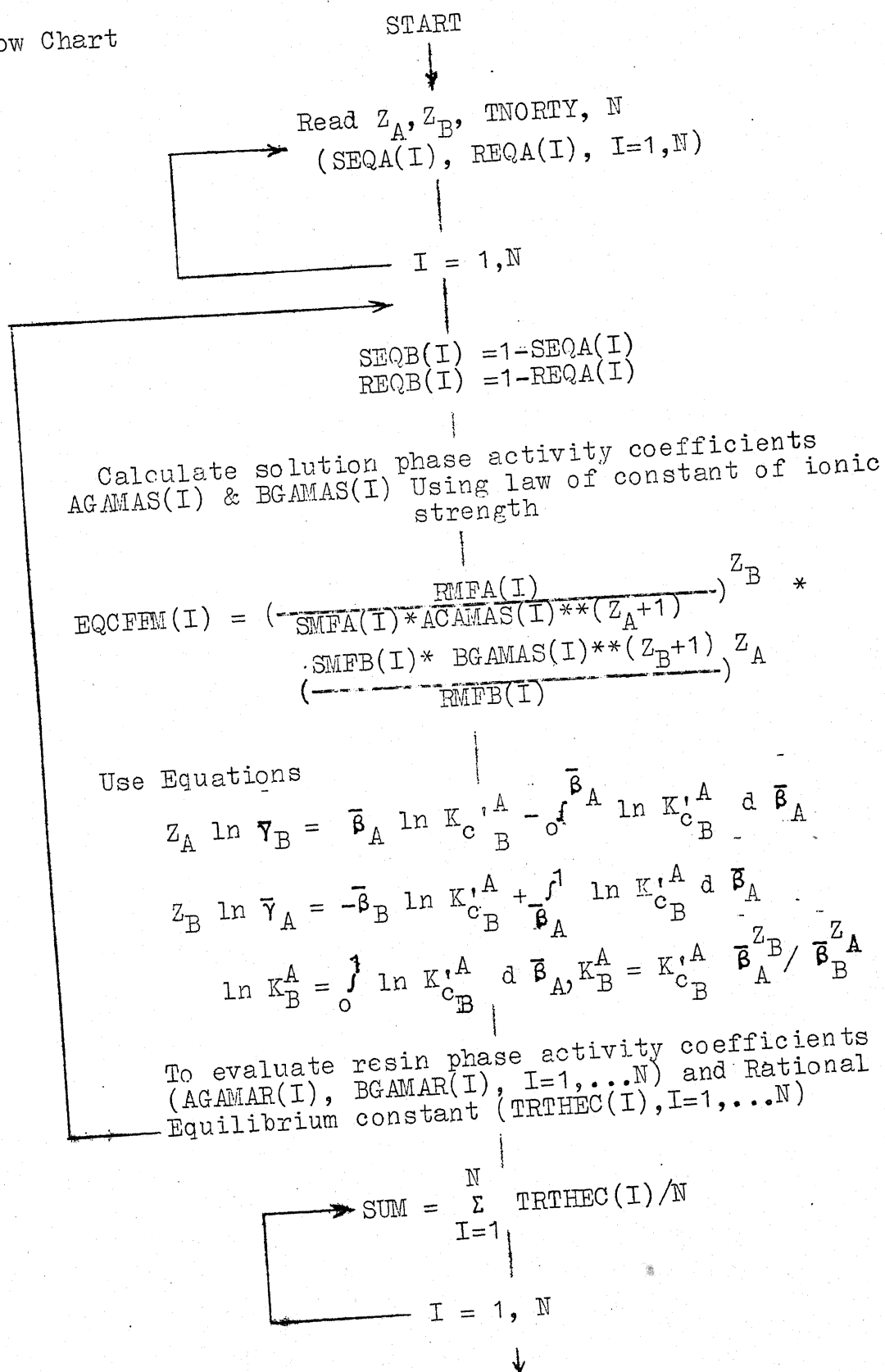
Equilibrium Studies

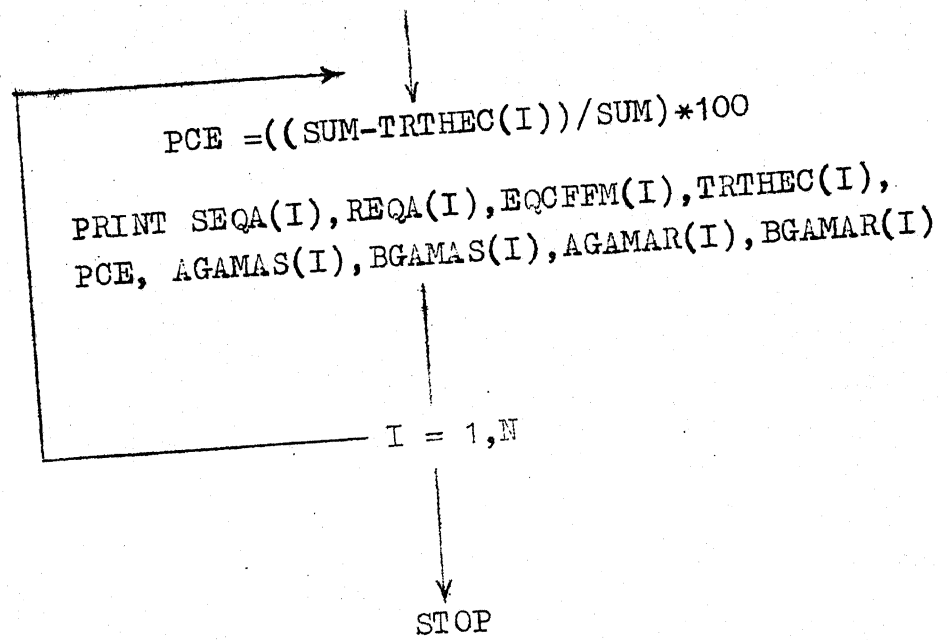
Calculation of Resin-Phase Activity Coefficients

Nomenclature

TNORTY	Total normality
N	Number of experimental points
SEQA	Solution-phase equivalent fraction of A
REQA	Resin-phase equivalent fraction of A
EQCFEM	Modified selectivity coefficient
AGAMAS	Solution-phase activity coefficient of chloride of A
BGAMAS	Solution-phase activity coefficient of chloride of B
SMFA	Solution-phase mole fraction of species A
SMFB	Solution-phase mole fraction of species B
AGAMAR	Resin-phase activity coefficient of species A
BGAMAR	Resin-phase activity coefficient of species B
TRTHEC	Rational equilibrium constant
PCE	Percent error

Flow Chart





\$IBFTC MAIN

```

C      SEQA,SEQB      EQUIVALENT FRACTIONS IN SOLUTION PHASE
C      REQA,REQB      RESIN PHASE EQUIVALENT FRACTIONS
C      SMFA,SMFB      SOLUTION PHASE MOLE FRACTIONS
C      RMFA,RMFB      RESIN PHASE MOLE FRACTIONS
C      SMLTY,GAMAS     LITERATURE VALUES OF MOLALITY AND ACTIVITY
C      COEFFICIENTS IN SOLUTION PHASE
C      AGAMAS,BGAMAS   SOLUTION PHASE (MIXTURE) ACTIVITY COEFFICIENTS
C      AGAMAR,BGAMAR   RESIN PHASE ACTIVITY COEFFICIENTS
C      EQCFFM          MODIFIED SELECTIVITY COEFFICIENTS
C      TRTHEC          TRUE THERMODYNAMIC EQUILIBRIUM CONSTANT
      DIMENSION AB1(10,7),AB2(10,7),AB4(10,7),AB5(10,7),ABSUM(10)
      DIMENSION SEQA(20),REQA(20),GAMASA(20),GAMASB(20),SMLTYA(20),
1 SMLTYB(20),B1(20),B2(20),SEQB(20),REQB(20),SMFA(20),SMFB(20),
1 RMFA(20),RMFB(20),AGAMAS(20),BGAMAS(20),EQCFFM(20),EQCFML(20),
1 B3(20),BGAMRL(20),AGAMRL(20),AGAMAR(20),BGAMAR(20),TRTHEC(20)
      DIMENSION B4(20),B5(20)
      DIMENSION SGRMEK(20),C3(20)
      DIMENSION AZ(10),AFZ(10)
1000 FORMAT(3F7.3,I3)
1001 FORMAT(10F7.4)
1002 FORMAT(10F7.4)
1003 FORMAT(13X,*SMLTYA*, 14X,*GAMASA*,8X,*GAMASA(CAL.)*,17X,*ERR*,17X,
1 *PCE*,15X,*ERSQS*)
1004 FORMAT(13X,*SMLTYB*, 14X,*GAMASB*,8X,*GAMASB(CAL.)*,17X,*ERR*,17X,
1 *PCE*,15X,*ERSQS*)
1005 FORMAT(15X,*REQA*,14X,*EQCFML*,8X,*EQCFML(CAL.)*,17X,*ERR*=17X,
1 *PCE*,15X,*ERSQS*)
1006 FORMAT(14X,*REQA*,14X,*SEQA*,12X,*SGRMEK*,12X,*AGAMRL*,12X,*BGAMRL
1 *,12X,*AGAMAR*,12X,*BGAMAR*)
1007 FORMAT( 4X,7(E14.7,4X))
1008 FORMAT(5X,5(E14.7,10X))
1009 FORMAT(15X,*SEQA*,20X,*REQA*,18X,*EQCFFM*,18X,*TRTHEC*,18X,*PCE*)
1010 FORMAT(73X,*AVG=*,E14.7)
1011 FORMAT( 12X,*SEQA*,12X,*REQA*,12X,*SMFA*,12X,*RMFA*,10X,
1 *AGAMAS*,10X,*BGAMAS*,10X,*AGAMAR*,10X,*BGAMAR*)
1012 FORMAT(8F16.7)
1013 FORMAT(/////////////////)
1014 FORMAT(1H1)
1015 FORMAT(10X,*BA-MN*,20X,*A=BA AND B=MN*)
1016 FORMAT(10X,*BA - CU *,20X,* A=BA AND B=CU. *)
1017 FORMAT(10X,* CU - NA *,20X,* A=CU AND B=NA. *)
1018 FORMAT(15X,*SEQA*,14X,*AGAMAR*,8X,*AGAMAR(CAL.)*,17X,*ERR*,
1 17X,*PCE*,15X,*ERSQS*)

```

```

1019 FORMAT(15X,*SEQB*,14X,*BGAMAR*,8X,*BGAMAR(CAL.)*,17X,*ERR*,
1 17X,*PCE*,15X,*ERSQS*)
1021 FORMAT(10X,*BA,MN*,20X,*A=BA AND B=MN*)
1022 FORMAT(10X,*MN-CS*,20X,*A=MN AND B=CS *)
1023 FORMAT(10X,*CS-NA*,20X,*A=CS AND B=NA *)
DO 41 III=1,2
DO 30 IARI=1,3
PRINT 1014
IF(III.EQ.2) GO TO 1
IF(IARI.EQ.1) PRINT 1015
IF(IARI.EQ.2) PRINT 1016
IF(IARI.EQ.3) PRINT 1017
GO TO 2
1 IF(IARI.EQ.1) PRINT 1021
IF(IARI.EQ.2) PRINT 1022
IF(IARI.EQ.3) PRINT 1023
2 CONTINUE
M=8
M1=8
L=5
L1=5
READ 1000,ZA,ZB,TNORTY,N
READ 1001,(SEQA(I),I=1,N)
READ 1001,(REQA(I),I=1,N)
READ 1002,(GAMASA(I),I=1,M)
READ 1002,(GAMASB(I),I=1,M1)
READ 1002,(SMLTYA(I),I=1,M)
READ 1002,(SMLTYB(I),I=1,M1)
MN=1
AZ(1)=0.
AFZ(1)=1.
998 GO TO 999
996 PRINT 1013
PRINT 1003
CALL INTRAP(B1,GAMASA,SMLTYA,M,L,AZ,MN,AFZ)
PRINT 1013
PRINT 1004
CALL INTRAP(B2,GAMASB,SMLTYB,M1,L,AZ,MN,AFZ)
DO 10 I=1,N
SEQB(I)=1.-SEQA(I)
REQB(I)=1.-REQA(I)
EVALUATE SOLUTION PHASE ACTIVITY COEFFICIENTS BY RULE OF
CONSTANT IONIC STRENGTH
SMFA(I)=(SEQA(I)/ZA)/(SEQA(I)/ZA+SEQB(I)/ZB)
SMFB(I)=1.-SMFA(I)
RMFA(I)=(REQA(I)/ZA)/(REQA(I)/ZA+REQB(I)/ZB)
RMFB(I)=1.-RMFA(I)
AMOLTY=SEQA(I)*TNORTY/ZA
BMOLTY=SEQB(I)*TNORTY/ZB
AMOLY=(ZA*(ZA+1.)*AMOLTY+ZB*(ZB+1.)*BMOLTY)/(ZA*(ZA+1.))
BMOLY=(ZA*(ZA+1.)*AMOLTY+ZB*(ZB+1.)*BMOLTY)/(ZB*(ZB+1.))
AGAMAS(I)=B1(1)

```

```

DO 11 J=2,L
AGAMAS(I)=AGAMAS(I)+B1(J)*AMOLY**(J-1)
BGAMAS(I)=BGAMAS(I)+B2(J)*BMOLY**(J-1)
11 CONTINUE
999 DO 997 IJK=1,M
AGAMAS(IJK)=GAMASA(IJK)
9 7 BGAMAS(IJK)=GAMASB(IJK)
C CALCULATION OF MODIFIED EQUILIBRIUM COEFFICIENTS
EQCFFM(I)=(RMFA(I)**ZB/RMIB(I)**ZA)*(SMFB(I)*BGAMAS(I)**(ZB+1.))**
1ZA/(SMFA(I)*AGAMAS(I)**(ZA+1.))**ZB
IF(EQCFFM(I).LE.0.0) EQCFFM(I)=1.0E-20
EQCFML(I)=ALOG(EQCFFM(I))
10 CONTINUE
GO TO 34
35 CONTINUE
AZ(1)=0.
AZ(2)=1.
AFZ(1)=0.
AFZ(2)=1.
CALL INTRAP(C3,REQA,SEQA,N,L,AZ,MN,AFZ)
DO 32 I=1,N
SGRMEK(I)=C3(2)
DO 33 J=3,L
AJ=J-1
33 SGRMEK(I)=SGRMEK(I)+AJ*C3(J)*SEQA(I)**(J-2)
SGRMEK(I)=SGRMEK(I)*EQCFM(I)
32 CONTINUE
34 CONTINUE
PRINT 1013
PRINT 1005
MN=0
CALL INTRAP(B3,EQCFML,REQA,N,L,AZ,MN,AFZ)
C CALCULATION OF RESIN PHASE ACTIVITY COEFFICIENTS AND TRUE
DO 21 I=1,N
BGAMRL(I)=REQA(I)*EQCFML(I)
DO 22 J=1,L1
AJ=J
22 BGAMRL(I)=BGAMRL(I)-B3(J)*REQA(I)**J/AJ
BGAMRL(I)=BGAMRL(I)/ZA
AGAMRL(I)=-REQB(I)*EQCFML(I)
DO 23 J=1,L1
AJ=J
23 AGAMRL(I)=AGAMRL(I)+B3(J)*(1.-REQA(I)**J)/AJ
AGAMRL(I)=AGAMRL(I)/ZB
AGAMAR(I)=EXP(AGAMRL(I))
BGAMAR(I)=EXP(BGAMRL(I))
C THERMODYNAMIC EQUILIBRIUM CONSTANT
TRTHEC(I)=EQCFFM(I)*AGAMAR(I)**ZB/BGAMAR(I)**ZA
21 CONTINUE
PRINT 1018
MN=0
AZ(1)=1.

```

```

AFZ(1)=1.
CALL INTRAP(B4,AGAMAR,SEQA,N,L,AZ,MN,AFZ)
PRINT 1019
CALL INTRAP(B5,BGAMAR,SEQB,N,L,AZ,MN,AFZ)
DO 31 I=1,L
  AB1(I,IARI)=B1(I)
  AB2(I,IARI)=B2(I)
  AB4(I,IARI)=B4(I)
  AB5(I,IARI)=B5(I)
31 CONTINUE
PRINT 1013
PRINT 1006
DO 24 I=1,N
  PRINT 1007,REQA(I),SEQA(I),EQCFML(I),AGAMRL(I),BGAMRL(I),AGAMARUI
  1,BGAMAR(I)
24 CONTINUE
PRINT 1013
PRINT 1011
DO 27 I=1,N
  PRINT 1012,SEQA(I),REQA(I),SMFA(I),RMFA(I),AGAMAS(I),BGAMAS(I),
  1AGAMAR(I),BGAMAR(I)
27 CONTINUE
SUM=0.
DO 25 I=1,N
  SUM=SUM+TRTHEC(I)
25 CONTINUE
AN=N
SUM=SUM/AN
PRINT 1013
PRINT 1009
DO 26 I=1,N
  ERR=SUM-TRTHEC(I)
  PCE=ERR/SUM*10.
  PRINT 1008,SEQA(I),REQA(I),EQCFFM(I),TRTHEC(I),PCE
26 CONTINUE
PRINT 1010,SUM
30 CONTINUE
41 CONTINUE
STOP
END
$1-LFTC SUB 1
SUBROUTINE INTRAP(BI,ALPH,BETA,N,L,Z,M,FZ)
DIMENSION Y(20),ALPH(20),F(10,20),BETA(20),A(10,10),B(10,1),BI(10)
DIMENSION Z(10),FZ(10)
DIMENSION Y1(20),FF(10,20)
120 FORMAT(5X,6(E14.7,6X))
100 FORMAT(1X,130(1H-))
DO 1 J=1,N
  Y(J)=ALPH(J)
  Y1(J)=Y(J)
  F(1,J)=1.
  DO 2 K=2,L
    F(K,J)=BETA(J)**(K-1)

```

```

DO 3 I=1,L
3 FF(I,J)=F(I,J)
  IF(M.EQ.0) GO TO 7
  DO 81 K=1,M
  Y(J)=Y(J)-FZ(K)
81 F(1,J)=F(1,J)-1.
  DO 82 I=2,L
  DO 82 K=1,M
82 F(I,J)=F(I,J)-Z(K)**(I-1)
7 CONTINUE
1 CONTINUE
  DO 51 I=1,L
  DO 51 K=1,I
  A(K,I)=0.
  DO 61 J=1,N
  A(K,I)=A(K,I)+F(I,J)*F(K,J)
61 CONTINUE
  A(I,K)=A(K,I)
51 CONTINUE
  DO 70 K=1,L
  B(K,1)=0.
  DO 70 J=1,N
  B(K,1)=B(K,1)+Y(J)*F(K,J)
70 CONTINUE
  CALL MATINV(A,B,L,L,1,1)
  PRINT 100
  PRINT ,B(1,1)
  IF(M.EQ.0) GO TO 4
  DO 5 K=2,L
5 B(1,1)=FZ(1)-B(K,1)*Z(1)**(K-1)
4 CONTINUE
  PRINT 120,(B(I,1),I=1,L)
  PRINT 100
  ERSQS=0.
  DO 80 J=1,N
  RCAL=0.
  DO 79 K=1,L
  BI(K)=B(K,1)
79 RCAL=RCAL+B(K,1)*FF(K,J)
  ERR=RCAL-Y1(J)
  IF(Y1(J)) 10, 20, 10
10 PCE=ERR/Y1(J)*100.
  GO TO 15
20 PCE=0.
15 CONTINUE
  ERSQS=ERR*ERR+ERSQS
  PRINT 120,BETA(J),Y1(J),RCAL,EPR,PCE,ERSQS
80 CONTINUE
  RETURN

```

```

      END
$IEFTC SUB 1
      SUBROUTINE MATINV(A,B,NN,N,MM,M)
      DIMENSION A(10,10),B(10,1),IPIVOT(20),PIVOT(20),INDEX(20,2)
      EQUIVALENCE(IROW,JPOW),(ICOLUM,JCOLUM),(AMAX,T,SWAP)
10  DETERM=1.
15  DO 20 J=1,N
20  IPIVOT(J)=0
30  DO 550 I=1,N
C    SEARCH FOR PIVOT ELEMENT
40  AMAX=0.
45  DO 105 J=1,N
50  IF(IPIVOT(J)-1) 60,105,60
60  DO 100 K=1,N
70  IF(IPIVOT(K)-1) 80,100,740
80  IF(ABS(AMAX)-ABS(A(J,K))) 85,100,100
85  IROW=J
90  ICOLUM=K
   5 AMAX=A(J,K)
100 CONTINUE
105 CONTINUE
110 IPIVOT(ICOLUM)=IPIVOT(ICOLUM)+1
C    INTERCHANGE ROWS TO PUT PIVOT ELEMENT ON DIAGONAL
130 IF(IROW-ICOLUM) 140,260,140
140 DETERM=-DETERM
150 DO 200 L=1,N
160 SWAP=A(IROW,L)
170 A(IROW,L)=A(ICOLUM,L)
200 A(ICOLUM,L)=SWAP
205 IF(M) 260,260,210
210 DO 250 L=1,M
220 SWAP=B(IROW,L)
230 B(IROW,L)=B(ICOLUM,L)
250 B(ICOLUM,L)=SWAP
260 INDEX(I,1)=IROW
270 INDEX(I,2)=ICOLUM
310 PIVOT(I)=A(ICOLUM,ICOLUM)
320 DETERM=DETERM*PIVOT(I)
330 A(ICOLUM,ICOLUM)=1.
340 DO 350 L=1,N
350 A(ICOLUM,L)=A(ICOLUM,L)/PIVOT(I)
355 IF(M) 380,380,360
360 DO 370 L=1,M
370 B(ICOLUM,L)=B(ICOLUM,L)/PIVOT(I)
C    REDUCE NON PIVOT ROWS
380 DO 550 L1=1,N
390 IF(L1-ICOLUM) 400,550,400
400 T=A(L1,ICOLUM)
420 A(L1,ICOLUM)=0.
430 DO 450 L=1,N

```

```
450 A(L1,L)=A(L1,L)-A(ICOLUM,L)*T
455 IF(M) 550,550,460
460 DO 500 L=1,M
500 B(L1,L)=B(L1,L)-B(ICOLUM,L)*T
550 CONTINUE
C   INTERCHANGE COLUMNS
600 DO 710 I=1,N
610 L=N+1-I
620 IF(INDEX(L,1)-INDEX(L,2)) 630,710,630
630 JROW=INDEX(L,1)
640 JCOLUM=INDEX(L,2)
650 DO 705 K=1,N
660 SWAP=A(K,JROW)
670 A(K,JROW)=A(K,JCOLUM)
700 A(K,JCOLUM)=SWAP
705 CONTINUE
710 CONTINUE
750 CONTINUE
740 RETURN
    END
$ENTRY
```

Prediction of Ternary Data with the Help of Binary Equilibrium Constants and Activity Coefficient Data

To reduce the number of iterations and save the computer time, a simplified procedure was adopted which requires binary ionic distribution data in addition to the knowledge of binary equilibrium constants and activity coefficient data. The procedure is as follows:

- (i) For any two pairs, say A-B and A-C, calculate

$$\beta_A \Big|_{AB}, \quad \beta_A \Big|_{AC}, \quad \beta_B \Big|_{AB}, \quad \beta_C \Big|_{AC}$$

$$\beta_A \Big|_{AB} = \frac{\beta_A}{\beta_A + \beta_B}, \quad \beta_B \Big|_{AB} = 1 - \beta_A \Big|_{AB}$$

$$\beta_A \Big|_{AC} = \frac{\beta_A}{\beta_A + \beta_C}, \quad \beta_C \Big|_{AC} = 1 - \beta_A \Big|_{AC}$$

- (ii) From the binary distribution data, find $\bar{\beta}_A \Big|_{AB}$ corresponding to $\beta_A \Big|_{AB}$ and $\bar{\beta}_A \Big|_{AC}$ corresponding to $\beta_A \Big|_{AC}$

- (iii) Find $\bar{\gamma}_A \Big|_{AB}, \quad \bar{\gamma}_A \Big|_{AC}, \quad \bar{\gamma}_B \Big|_{AB}, \quad \bar{\gamma}_B \Big|_{BC}, \quad \bar{\gamma}_C \Big|_{AC}$
and $\bar{\gamma}_C \Big|_{BC}$

Calculate $\bar{\beta}_A, \bar{\beta}_B$ and $\bar{\beta}_C$ from equations

$$\frac{\bar{\beta}_A}{\bar{\beta}_A + \bar{\beta}_B} = \bar{\beta}_A \Big|_{AB}, \quad \frac{\bar{\beta}_A}{\bar{\beta}_A + \bar{\beta}_C} = \bar{\beta}_A \Big|_{AC}$$

and $\bar{\beta}_A + \bar{\beta}_B + \bar{\beta}_C = 1$

(iv) Calculate $\bar{\gamma}_A$, $\bar{\gamma}_B$, $\bar{\gamma}_C$ from the equation

$$\bar{\gamma}_A = \frac{\bar{\beta}_B}{\bar{\beta}_B + \bar{\beta}_C} \times \bar{\gamma}_A|_{AB} + \frac{\bar{\beta}_C}{\bar{\beta}_B + \bar{\beta}_C} \times \bar{\gamma}_A|_{AC}$$

$$\bar{\gamma}_B = \frac{\bar{\beta}_C}{\bar{\beta}_A + \bar{\beta}_C} \times \bar{\gamma}_B|_{AC} + \frac{\bar{\beta}_A}{\bar{\beta}_A + \bar{\beta}_C} \times \bar{\gamma}_B|_{AB}$$

$$\bar{\gamma}_C = \frac{\bar{\beta}_A}{\bar{\beta}_A + \bar{\beta}_B} \times \bar{\gamma}_C|_{AC} + \frac{\bar{\beta}_B}{\bar{\beta}_B + \bar{\beta}_C} \times \bar{\gamma}_C|_{BC}$$

(v) Plug in these values of $\bar{\gamma}_A$, $\bar{\gamma}_B$ and $\bar{\gamma}_C$ in the following equations

$$\left(\frac{\bar{x}_A}{x_A}\right)^{Z_B} \left(\frac{x_B}{\bar{x}_B}\right)^{Z_A} \times \left(\frac{\gamma_B}{\bar{\gamma}_B}\right)^{Z_A} \left(\frac{\bar{\gamma}_A}{\gamma_A}\right)^{Z_B} = K_B^A$$

$$\left(\frac{\bar{x}_A}{x_A}\right)^{Z_C} \left(\frac{x_C}{\bar{x}_C}\right)^{Z_A} \times \left(\frac{\bar{\gamma}_A}{\gamma_A}\right)^{Z_C} \left(\frac{\gamma_C}{\bar{\gamma}_C}\right)^{Z_A} = K_C^A$$

$$\bar{x}_A + \bar{x}_B + \bar{x}_C = 1$$

to calculate \bar{x}_A , \bar{x}_B , \bar{x}_C .

(vi) Repeat similar calculations while considering the ionic pairs A-B and B-C, and B-C and A-C.

\$IFTC MAIN

```

C      N=TOTAL NUMBER OF EXPERIMENTAL POINTS
C      ABSUM(1)=RATIONAL EQUILIBRIUM CONSTANT FOR THE PAIR 1
C      PAIR 1 =2-3 IONS,PAIR 2 =1-3 IONS,PAIR 3 =1-2 IONS
C      TNMLTY=TOTAL NORMALITY
C      SEQFT(I,1)=SOLN.PHASE EQVT.FRACTION OF SPECIES 1 AT ITH EXPTL PT.
C      REQFT(I,1)=RESINPHASE EQVT.FRACTION OF SPECIES 1 AT ITH EXPTL PT.
C      SMFT(I,1)=SOLN.PHASE MOLE FRACTION OF SPECIES 1 AT ITH EXPTL PT
C      RMFT(I,1)=RESINPHASE MOLE FRACTION OF SPECIES 1 AT ITH EXPTL PT
C      AB(K,1)=KTH EMPIRICAL CONSTANT IN THE FOURTH ORDER POLYNOMIAL
C      RELATING SOLN. PHASE ACT.COEFF. OF CHLORIDE OF SPECIES 1 IN AQUEOUS
C      PHASE WITH MOLALITY IN THE SOLUTION
C      BA(1,K,2)=KTH EMPIRICAL CONSTANT IN THE POLYNOMIAL RELATING RESIN
C      PHASE ACT.COEFF. OF SPECIES 2 IN THE PAIR 1
C      SGAMA(I,1)=SOLN. PHASE ACT.COEFF. OF SPECIES 1 AT ITH EXPTL.PT.
C      GR1=RESIN PHASE ACT.COEFF.OF SPECIES J1 IN THE PAIR J
C      GR2=RESIN PHASE ACT.COEFF.OF SPECIES J2 IN THE PAIR J
C      RGAMA(I,1)=RESIN PHASE ACT.COEFF.OF SPECIES 1 AT ITH EXPTL.PT.
C      IN THE TERNARY MIXTURE
C      E12,E13,E23 RESIN PHASE EQVT.FRACTION OF SPECIES 1 AT ITH EXPTL.
C      PT.CALCULATED WITH THE HELP OF PAIRS 1-2,1-3AND 2-3 RESPECTIVELY
C      F19,F13,F23 RESIN PHASE EQVT.FRACTIONS OF SPECIES 2
C      G12,G13,G23 RESIN PHASE EQVT.FRACTIONS OF SPECIES 3
C      REQCAL(I,1)=CALCULATED MEAN VALUE OF RESIN PHASE ACT.COEFF. OF SPECIES 1 AT ITH EXPTL. POINT
C      DIMENSION AB1(8,1),AB2(8,2),AB4(8,3),AB5(8,3),Z(3),SEQFT(19,3)
C      DIMENSION REQFT(19,3),AB(8,3),BA(3,8,3),SMFT(19,3),RMFT(19,3),
C      1AAM(3),SGAMA(19,3),ABSUM(3),RGAMA(19,3),REQCAL(19,3)
C      DIMENSION ABETA(20),BBETA(20),AGA(20),BGA(20),RI(10),SI(10)
3000 FORMAT(5E14.7)
3001 FORMAT(10F7.4)
3041 FORMAT(10F7.4)
3099 FORMAT(I2)
4000 FORMAT(10F7.4)
4001 FORMAT(10F7.5)
4002 FORMAT(1X,3F14.7,44X,3F14.7)
4003 FORMAT(40X,*1,2*,1X,3F14.7)
4004 FORMAT(40X,*2,3*,1X,3F14.7)
4005 FORMAT(40X,*1,3*,1X,3F14.7)
4006 FORMAT(/1X,130(1H-))//////)
4007 FORMAT(1X,3F14.7,1X,3F14.7,1X,3F14.7)
4008 FORMAT(6X,* SOLUTION PHASE EQUIVALENT FRACTIONS*,10X,* RESIN PHASE
1 EQUIVALENT FRACTION*,8X,* SOLUTION PHASE MASS FRACTION*)
4009 FORMAT(6X,* RESIN PHASE EQUIVALENT FRACTIONS*,3X,* CALCULATED
1 FRACTION TAKING A PAIR AT A TIME*,3X,* AVG CAL. RESIN EQUI.FR.*)
4010 FORMAT(3E14.7)
4019 FORMAT(1X,* SOLUTION PHASE ACTIVITY COEFF. *,54X,* RESIN PHASE
1 ACTIVITY COEFF.*)
4020 FORMAT(1H1)

```

```

ACTIVITY COEFF. TAKEN IN TO ACCOUNT          *//)
ACTIVITY COEFF NOT TAKEN IN TO ACCOUNT        *//)
4021 FORMAT(//*
4022 FORMAT(//*
88001 FORMAT(5X, 40H*****SYSTEM--- SR-MN-CS---*****)
88002 FORMAT(5X, 40H*****SYSTEM--- BA-CU-NA---*****)
88003 FORMAT(5X, 80(1H*))
88004 FORMAT(//*)
88006 FORMAT(5X, 40H*****SYSTEM--- MN-CS-NA---*****)
IPQR=3
PRINT 4020
PRINT 8003
PRINT 8003
PRINT 8004
IF(IPQR.EQ.1) PRINT 8001
IF(IPQR.EQ.2) PRINT 8002
IF(IPQR.EQ.3) PRINT 8006
PRINT 8004
PRINT 8003
PRINT 8003
READ 3099,N
L=6
LI=15
READ 3000,(AB1(K,1),K=1,L)
READ 3000,(AB2(K,1),K=1,L)
READ 3000,(AB2(K,2),K=1,L)
READ 3000,(ABSUM(I),I=1,3)
IF(IPQR.EQ.2) GO TO 455
READ 3000,(AB4(K,1),K=1,L)
READ 3000,(AB5(K,1),K=1,L)
READ 3000,(AB4(K,2),K=1,L)
READ 3000,(AB5(K,2),K=1,L)
READ 3000,(AB4(K,3),K=1,L)
READ 3000,(AB5(K,3),K=1,L)
GO TO 1
455 CONTINUE
DO 189 IJ=1,3
IF(IJ.EQ.3) LI=10
READ 3001,(ABETA(I),I=1,LI)
READ 3001,(AGA(I),I=1,LI)
READ 3001,(BGA(I),I=1,LI)
DO 188 I=1,LI
188 BBETA(I)=1.-ABETA(I)
CALL INTRAP(RI,AGA,ABETA,LI,L)
CALL INTRAP(SI,BGA,BBETA,LI,L)
DO 187 K=1,L
AB4(K,IJ)=RI(K)
AB5(K,IJ)=SI(K)
187 CONTINUE
189 CONTINUE
1 CONTINUE
READ 4000,TNMLTY,(Z(J),J=1,3)
READ 4001,(SEQFT(I,1),I=1,N)

```

```

READ 4001,(SEQFT(I,2),I=1,N)
READ 4001,(REQFT(I,1),I=1,N)
READ 4001,(REQFT(I,2),I=1,N)
DO 401 K=1,L
  AB(K,1)=AB1(K,1)
  AB(K,2)=AB2(K,1)
  AB(K,3)=AB2(K,2)
  BA(1,K,2)=AB4(K,3)
  BA(1,K,3)=AB4(K,1)
  BA(2,K,3)=AB4(K,2)
  BA(2,K,1)=AB5(K,3)
  BA(3,K,1)=AB5(K,1)
  BA(3,K,2)=AB5(K,2)
401 CONTINUE
DO 402 I=1,N
DO 451 IABC=1,2
  SEQFT(I,3)=1.-SEQFT(I,1)-SEQFT(I,2)
  REQFT(I,3)=1.-REQFT(I,1)-REQFT(I,2)
  AM=TNM-TY
  S=0.
  R=0.
DO 403 J=1,3
  S=S+SEQFT(I,J)/Z(J)
  R=R+REQFT(I,J)/Z(J)
  AM=AM+SEQFT(I,J)*TNMLTY*Z(J)
403 CONTINUE
DO 404 J=1,3
  SMFT(I,J)=SEQFT(I,J)/Z(J)/S
  RMFT(I,J)=REQFT(I,J)/Z(J)/R
  AAM(J)=AM/(Z(J)*(Z(J)+1.))
  SGAMA(I,J)=AB(I,J)
DO 405 K=2,L
  SGAMA(I,J)=SGAMA(I,J)+AB(K,J)*AAM(J)**(K-1)
405 CONTINUE
404 CONTINUE
DO 406 J=1,3
  J1=J+1
  J2=J+2
  IF(J1.GT.3) J1=J1-3
  IF(J2.GT.3) J2=J2-3
  AI=SEQFT(I,J)/(SEQFT(I,J)+SEQFT(I,J1))
  BI=SEQFT(I,J)/(SEQFT(I,J)+SEQFT(I,J2))
  X=1.0E-06
  GR1=BA(J,1,J1)
  IF(AI.LT.X) GO TO 1089
DO 407 K=2,L
407 GR1=GR1+BA(J,K,J1)*AI**(K-1)
1089 CONTINUE
  GR2=BA(J,1,J2)
  IF(BI.LT.X) GO TO 1090
DO 408 K=2,L
408 GR2=GR2+BA(J,K,J2)*BI**(K-1)

```

```

1090 CONTINUE
  C1=SEQFT(I,J1)/(SEQFT(I,J1)+SEQFT(I,J2))
  RGAMA(I,J)=GR1*C1+(1.-C1)*GR2
406 CONTINUE
  IF(IAB+.EQ.2) GO TO 452
  PRINT 4021
  A=ABSUM(1)*SMFT(I,1)/SMFT(I,3)**2*SGAMA(I,1)**3/SGAMA(I,3)**4*
  1RGAMA(I,3)**2/RGAMA(I,1)
  B=ABSUM(2)*SMFT(I,1)/SMFT(I,2)**2*SGAMA(I,1)**3/SGAMA(I,2)**4*
  1RGAMA(I,2)**2/RGAMA(I,1)
  C=ABSUM(3)*SMFT(I,2)/SMFT(I,3)*SGAMA(I,2)**2/SGAMA(I,3)**2*
  1RGAMA(I,3)/RGAMA(I,2)
  GO TO 453
452 CONTINUE
  PRINT 4022
  A=ABSUM(1)*SMFT(I,1)/SMFT(I,3)**2
  B=ABSUM(2)*SMFT(I,1)/SMFT(I,2)**2
  C=ABSUM(3)*SMFT(I,2)/SMFT(I,3)
453 CONTINUE
  G12=(-(SQRT(A/B)+1.))+SQRT((SQRT(A/B)+1.))**2+4.*A)/2./A
  F12=G12*SQRT(A/B)
  E12=A*G12**2
  G23=(-(C+1.))+SQRT((C+1.))**2+4.*B*C**2)/(2.*B*C**2)
  F23=C*G23
  E23=B*F23**2
  G13=(-(C+1.))+SQRT((C+1.))**2+4.*A)/(2.*A)
  F13=C*G13
  E13=A*G13**2
  EE=E12*Z(1)+F12*Z(2)+G12*Z(3)
  FF=E23*Z(1)+F23*Z(2)+G23*Z(3)
  GG=E13*Z(1)+F13*Z(2)+G13*Z(3)
  E12=E12*Z(1)/EE
  F12=F12*Z(2)/EE
  G12=G12*Z(3)/EE
  E23=E23*Z(1)/FF
  F23=F23*Z(2)/FF
  G23=G23*Z(3)/FF
  E13=E13*Z(1)/GG
  F13=F13*Z(2)/GG
  G13=G13*Z(3)/GG
  REQCAL(I,1)=(E12+E13+E23)/3.
  REQCAL(I,2)=(F12+F13+F23)/3.0

```

```

REQCAL(I,3)=(G12+G13+G23)/3.0
PRINT 4009
PRINT 4002,(REQFT(I,J),J=1,3),(REQCAL(I,J),J=1,3)
PRINT 4003,E12,F12,G12
PRINT 4004,E23,F23,G23
PRINT 4005,E13,F13,G13
451 CONTINUE
PRINT 4006
402 CONTINUE
PRINT 4008
DO 409 I=1,N
PRINT 4007,(SEQFT(I,J),J=1,3),(REQFT(I,J),J=1,3),(SMFT(I,J),J=1,3)
409 CONTINUE
PRINT 4019
DO 410 I=1,N
PRINT 4002,(SGAMA(I,J),J=1,3),(RGAMA(I,J),J=1,3)
410 CONTINUE
454 CONTINUE
STOP
END
$IBFTC SUB
SUBROUTINE INTRAP(BI,G,E,NSN,L)
DIMENSION BI(1)
DIMENSION G(20),E(20),A(6,6),B(6,1)
DIMENSION BMN(6,1),BSR(6,1)
DIMENSION F(6,20),Y(20)
DIMENSION DS(3),Z(3),DSP(3),DSPP(3)
N=NSN
100 FORMAT(1X,130(1H-))
120 FORMAT(2X,5(E14.7,10X))
130 FORMAT(10X,*Y( ) *,20X,*RCAL*,20X,*ERR *,20X,*PCE *,20X,*ERSQS*)
DO 69 J=1,N
Y(J)=G(J)
F(1,J)=1.
F(2,J)=E(J)
F(3,J)=F(2,J)**2
F(4,J)=F(3,J)*F(2,J)
F(5,J)=F(4,J)*F(2,J)
69 F(6,J)=F(5,J)*F(2,J)
121 FORMAT(2X,5(E14.7,10X))
DO 51 I=1,L
DO 51 K=1,I
A(K,I)=0.
DO 61 J=1,N
A(K,I)=A(K,I)+F(I,J)*F(K,J)
61 CONTINUE
A(I,K)=A(K,I)
51 CONTINUE
DO 70 K=1,L

```

```

      B(K,1)=0.
      DO 70 J=1,N
      B(K,1)=B(K,1)+Y(J)*F(K,J)
70  CONTINUE
      CALL MATINV(A,B,L,L,1,1)
      PRINT 100
      PRINT 120,(B(I,1),I=1,L)
      PRINT 100
      ERSQS=0.
      PRINT 130
      DO 80 J=1,N
      RCAL=0.
      DO 79 K=1,L
79  RCAL=RCAL+B(K,1)*F(K,J)
      ERR=RCAL-Y(J)
      IF(Y(J).EQ.0.) GO TO 82
      PCE=ERR/Y(J)*100.
      GO TO 83
82  PCE=0.
83  CONTINUE
      ERSQS=ERSQS+ERR*ERR
      PRINT 121,Y(J),RCAL,ERR,PCE,ERSQS
80  CONTINUE
      PRINT 100
      DO 81 K=1,L
81  BI(K)=B(K,1)
      RETURN
      END
$IBFTC MATINV
      SUBROUTINE MATINV(A,B,NN,N,MM,M)
      DIMENSION DS(3),Z(3),DSP(3),DSPP(3)
      DIMENSION BMN(6,1),BSR(6,1)
      DIMENSION A(10,10),B(10,1),IPIVOT(20),PIVOT(20),INDEX(20,2)
      EQUIVALENCE (IROW,JROW),(ICOLUMN,JCOLUMN),(AMAX,T,SWAP)
10  DETERM=1.
15  DO 20 J=1,N
20  IPIVOT(J)=0.
30  DO 550 I=1,N
C  SEARCH FOR THE PIVOT ELEMENT.
40  AMAX=0.
45  DO 105 J=1,N
50  IF(IPIVOT(J)-1) 60,105,60
60  DO 100 K=1,N
70  IF(IPIVOT(K)-1) 80,100,740
80  IF(ABS(AMAX)-ABS(A(J,K))) 85,100,100
85  IROW=J
90  ICOLUMN=K
95  AMAX=A(J,K)
100 CONTINUE
105 CONTINUE
110 IPIVOT(ICOLUMN)=IPIVOT(ICOLUMN)+1

```

C INTERCHANGE THE ROWS TO PUT PIVOT ELEMENT ON DIAGONAL.

130 IF(IROW-ICOLUM) 140,260,140

140 DETERM8-DETERM

150 DO 200 L=1,N

160 SWAP=A(IROW,L)

170 A(IROW,L)=A(ICOLUM,L)

200 A(ICOLUM,L)=SWAP

205 IF(M) 260,260,210

210 DO 250 L=1,M

230 B(IROW,L)=B(ICOLUM,L)

250 B(ICOLUM,L)=SWAP

260 INDEX(I,1)=IROW

270 INDEX(I,2)=ICOLUM

310 PIVOT(I)=A(ICOLUM,ICOLUM)

320 DETERM=DETERM*PIVOT(I)

C DEVIDE THE PIVOT ROW BY THE PIVOT ELEMENT.

330 A(ICOLUM,ICOLUM)=1.

340 DO 350 L=1,N

350 A(ICOLUM,L)=A(ICOLUM,L)/PIVOT(I)

355 IF(M) 380,380,360

360 DO 370 L=1,M

370 B(ICOLUM,L)=B(ICOLUM,L)/PIVOT(I)

C REDUCE NON-PIVOT ROWS.

380 DO 550 L1=1,N

390 IF(L1-ICOLUM) 400,550,400

400 T=A(L1,ICOLUM)

420 A(L1,ICOLUM)=0.

430 DO 450 L=1,N

450 A(L1,L)=A(L1,L)-A(ICOLUM,L)*T

455 IF(M) 550,550,460

460 DO 500 L=1,M

500 B(L1,L)=B(L1,L)-B(ICOLUM,L)*T

C INTERCHANGE COLUMNS.

550 CONTINUE

600 DO 710 I=1,N

610 L=N+1-I

620 IF(INDEX(L,1)-INDEX(L,2)) 630,710,630

630 JROW=INDEX(L,1)

640 JCOLUM=INDEX(L,2)

650 DO 705 K=1,N

660 SWAP=A(K,JROW)

670 A(K,JROW)=A(K,JCOLUM)

700 A(K,JCOLUM)=SWAP

705 CONTINUE

710 CONTINUE

750 CONTINUE

740 RETURN

END

*ENTRY

APPENDIX C

EXPERIMENTAL

SAMPLE OBSERVATIONS AND CALCULATIONS - EQUILIBRIUM STUDIES

TABLE 23: CAPACITY MEASUREMENTS

Count Rate Measurements

Bead: 32D/9 - Diameter in Na^+ ionic form = 0.118 cm

Capacity measurements in manganese form: Scaler settings:

Gain : 10

Discriminator : 40

High voltage knob. : 395

(Log book - 2 p. 286)

Tagged bead from isotope (^{54}Mn) solution

	Time* min.	Counts for S. S.	Counts for Bead
Bead (D, 5W, D, 5W, D) ¹	1		166432 166003
S. S.	5	67602	
Bead (5W, D)	1		163536 163506
S. S.	5	65760	
Bead (5W, D)	1		157718 157756
S. S.	5	63949	
Bead (5W, D)	1		157817 157697
Washing completed			

*Time for counts measurements; 1
5W-washed the bead 5 times
S. S. Standard source
D-Dried the bead with tissue paper

Table 23 (contd)

216

	Time min.	Counts for S.S.	Counts for Bead
S. S.	5	63773	
Bead in the vial**	1		160520
	3		478500
	30		4777475
S. S.	5	64489	
Added to it 1 ml of 0.1013 N $MnCl_2$ solution (Log book-2 p.289)			
S. S.	5	66261	
Bead +solution	1		156301
	10		1557021
S. S.	5	65722	
The equilibrated bead was washed thoroughly (as shown earlier).			
S. S.	5	65559	
Vial** (Back ground)	1		185
	60		11577
S. S.	5	65210	
Bead in vial** + 1 ml of double distilled water)			
	1		3008
	60		178115
S. S.	5	63272	

Calculations

S. S. counts	Tagged Bead	Equilibrated bead + solution	Vial**
(before)	63773	66261	65559
(after)	64489	65722	63210
(Total)	<u>128262</u>	<u>131983</u>	<u>128769</u>

**Proper vial (thoroughly cleaned)

S.S. Counts	Equilibrated bead
(before)	63270
(after)	<u>63272</u>
(Total)	126542

With respect to (equilibrated bead + solution) counts:

$$\begin{aligned} \text{Ratio of counts} &= \frac{178145 \times \frac{131983}{126542} - 11577 \times \frac{131983}{128769}}{1557021 \times 6 - 178145 \times \frac{131983}{126542}} \\ &= 1.90 \times 10^{-2} \end{aligned}$$

Capacity of the bead = $1.90 \times 10^{-2} \times 0.1013 = 1.925$ micro-equivalents

With respect to tagged bead counts:

$$\begin{aligned} \text{Ratio of counts} &= \frac{178145 \times \frac{128262}{126542} - 11577 \times \frac{128262}{128769}}{4777475 \times 2 - 178145 \times \frac{128262}{126464}} \\ &= 1.805 \times 10^{-2} \end{aligned}$$

Capacity of the bead = $1.805 \times 10^{-2} \times 0.1013 = 1.83$ micro-equivalents

Bead transferred to ^{54}Mn isotope solution

Capacity measurements (Second Time):

Capacity of bead with respect to (equilibrated bead + solution) counts = 1.894 micro equivalents

Capacity of bead with respect to (tagged bead) counts = 1.790 microequivalents

Mean Values of Capacity:

With respect to (equilibrated bead + solution) counts = 1.910 micro equivalents

With respect to (tagged bead) counts = 1.810 micro equivalents

Binary Equilibrium Measurements

Equilibrating solution - nominal composition:

80% Na^+ , 20% Mn^{2+}

10 ml of 0.1013N MnCl_2 solution + 40 ml of 0.1137N NaCl solution

= 50 ml of 0.1112 N equilibrating solution

1 ml of this solution was used for equilibration (micro-equivalents of cations in one ml of solution = 111.2)

Resin-phase manganese ionic equivalents percent --

$$= \bar{\beta}_{\text{Mn}} = 81.1$$

Solution-phase manganese ionic equivalents percent

$$= \beta_{\text{Mn}} = 18.2$$

Tagged bead used: 20B/11

Solution-phase manganese ionic equivalents percent after equilibration

$$= 18.55$$

Resin-phase sodium ionic equivalents percent = 22.65

Solution-phase ionic equivalents percent of sodium = 81.8

Tagged bead used: 34C/10

Solution-phase sodium ionic equivalents percent after equilibration = 83.0

Resin-phase normalized fractions:

$$\begin{aligned}\text{Sum total of individual ionic fractions} &= 0.811 + 0.2265 \\ &= 1.0375\end{aligned}$$

$$\text{Normalized manganese fraction} = \frac{0.811}{1.0375} = 0.782$$

$$\text{Normalized sodium fraction} = \frac{0.2265}{1.0375} = 0.218$$

Ternary Equilibrium Measurements

Equilibrating solution no.: 32

$$\text{Solution-phase equivalents percent (nominal)} = \begin{matrix} \beta_{\text{Mn}} & \beta_{\text{Cs}} & \beta_{\text{Na}} \\ 5 & 35 & 60 \end{matrix}$$

60 ml of 0.1027 N NaCl + 35 ml of 0.0998 N CsCl + 5 ml of 0.0998 N MnCl₂

= 100 ml of 0.1016 N equilibrating solution

1 ml each of this solution was used for equilibration:

Ion	β_{Na}	β_{Cs}	β_{Mn}
Equivalents fraction %	60.70	34.40	4.90

Resin-Phase Sodium Ionic Fraction:

Tagged bead used: 34C/10

$$\begin{aligned}\text{Equivalents percent of sodium in resin-phase} &= 22.4 \\ \text{Equivalents percent of Na}^+ \text{ in solution (after equilibration)} &= 62.2\end{aligned}$$

Resin-Phase Cesium Ionic Fraction:

Tagged bead used: 20B/11

$$\begin{aligned}\text{Equivalents percent of Cesium in resin-phase} &= 37.6 \\ \text{Equivalents percent of Cs}^+ \text{ in solution (after equilibration)} &= 35.3\end{aligned}$$

Resin-phase Manganese Ionic Fraction:

Tagged bead used = 32D/9

Equivalents percent of manganese in resin phase: 50.00

Equivalents percent of Mn^{2+} in solution (after equilibration)
= 5.82

Sum total of resin phase individual ionic fractions

$$= 0.224 + 0.376 + 0.500 = 1.100$$

$$\text{Normalized sodium ionic fraction} = \frac{0.224}{1.1} = 0.204$$

$$\text{Normalized cesium ionic fraction} = \frac{0.376}{1.1} = 0.342$$

$$\text{Normalized manganese ionic fraction} = \frac{0.50}{1.1} = 0.454$$

TABLE 24: BINARY EQUILIBRIUM DATA: EXPERIMENTAL RESIN-PHASE COMPOSITION
(NON-NORMALIZED)

Equilibrating Solution		Experimental Resin-Phase				
Equivalents %		Equivalents %				
β_{Mn}	β_{Cs}	β_{Na}	β_{Mn}	β_{Cs}	β_{Na}	$\beta_{Mn} + \beta_{Cs} + \beta_{Na}$
-	19.5	80.5	-	34.3	67.3	101.60
-	29.9	70.1	-	42.3	60.0	102.30
-	37.4	62.6	-	47.4	52.7	100.1
-	59.3	40.7	-	73.6	31.1	104.7
-	79.9	20.1	-	82.6	14.3	97.4
9.9	-	90.1	64.4	-	36.5	100.9
18.2	-	81.8	81.1	-	22.65	103.75
29.7	-	70.3	83.8	-	17.7	101.5
39.7	-	60.3	85.5	-	13.7	99.2
59.7	-	40.3	95.7	-	4.9	100.6
9.94	90.06	-	48.6	48.2	-	96.8
19.89	80.11	-	59.6	43.2	-	103.1
40.00	60.00	-	67.0	39.1	-	106.1
60.00	40.00	-	81.0	22.6	-	103.6

TABLE 25: TERNARY EQUILIBRIUM DATA - EXPERIMENTAL RESIN-PHASE COMPOSITION
(NON-NORMALIZED)

Nominal Solution Phase			Experimental Resin-Phase			$\bar{\beta}_{\text{Mn}} + \bar{\beta}_{\text{Cs}^+} \bar{\beta}_{\text{Na}}$
Equivalents%			Equivalents%			
β_{Mn}	β_{Cs}	β_{Na}	$\bar{\beta}_{\text{Mn}}$	$\bar{\beta}_{\text{Cs}}$	$\bar{\beta}_{\text{Na}}$	
5.0	15.0	80.0	54.3	20.3	34.8	109.4
5.0	35.0	60.0	50.0	37.6	22.4	110.0
5.0	60.0	35.0	49.8	47.6	11.9	109.3
10.0	10.0	80.0	62.4	16.7	27.2	106.3
10.0	20.0	70.0	60.8	26.6	23.4	110.8
10.0	30.0	60.0	61.3	30.8	18.2	110.3
10.0	60.0	30.0	58.5	41.4	11.2	111.1
10.0	70.0	20.0	55.6	48.2	5.5	109.3
10.0	80.0	10.0	54.5	49.6	2.8	106.8
20.0	10.0	70.0	69.4	12.2	17.2	98.8
20.0	40.0	40.0	68.3	30.7	8.3	107.2
20.0	70.0	10.0	59.0	45.1	1.7	105.8
30.0	10.0	60.0	80.0	12.7	13.1	105.8
30.0	60.0	10.0	72.2	32.6	1.8	106.6
40.0	20.0	40.0	82.2	16.0	6.4	104.6
40.0	40.0	20.0	82.0	28.2	3.0	113.2
60.0	20.0	20.0	84.0	15.1	2.8	101.9

22

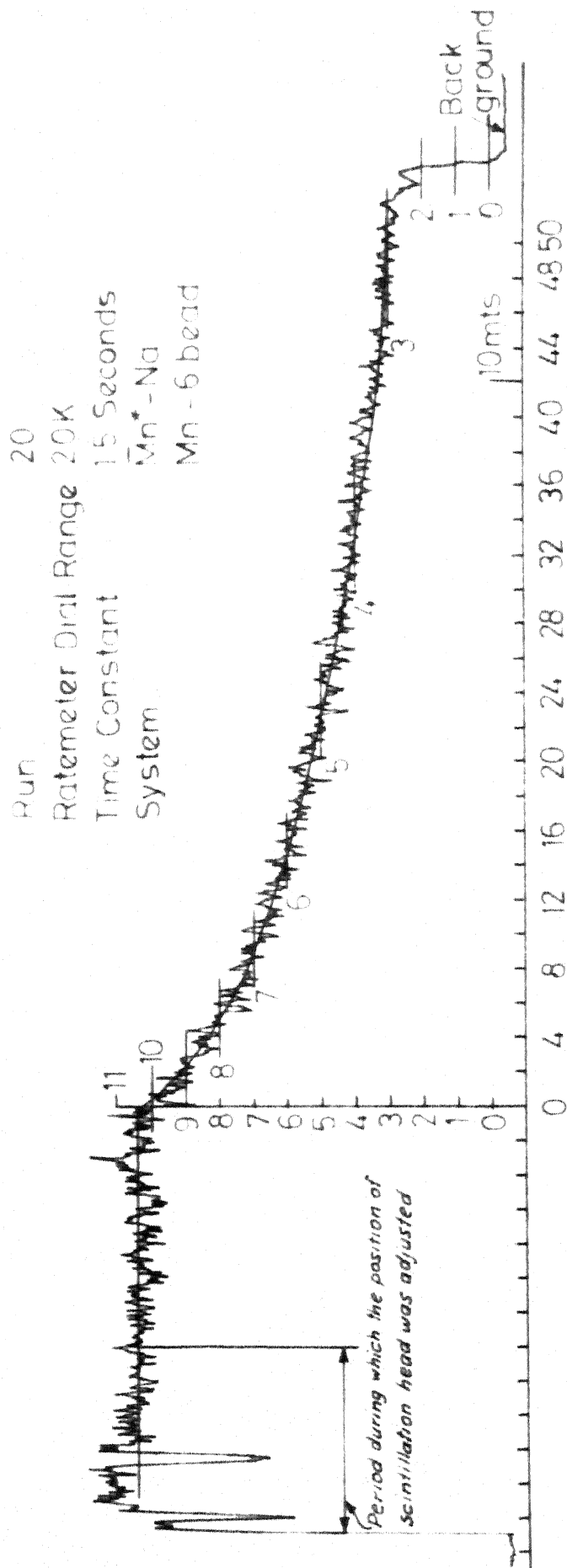


TABLE 26: EXPERIMENTAL KINETIC RUN

Run No. 20 $\overline{\text{Mn}}^* - \text{Na}(\text{C.1 NaCl Solution})$
 Bead: Mn-6 Bead diameter(d_0): 0.1020 cm
 Ratemeter dial setting: 20K
 Back Ground Signal: -0.5
 Speed of the recorder chart: 42 divisions in 10 minutes

No.	Time (Chart Scale)	Signal	Actual Signal	$\frac{q_t}{q_0}$	$\frac{t}{d_0^2} (\frac{\text{min}}{\text{cm}^2})$
0	0	10.40	10.90	1.000	0
1	1	9.65	10.15	0.931	22.9
2	2	9.10	9.60	0.880	45.8
3	3	8.65	9.15	0.840	68.7
4	4	8.30	8.80	0.807	91.6
5	5	7.95	8.45	0.775	114.5
6	6	7.60	8.10	0.743	137.5
7	7	7.35	7.85	0.720	161.0
8	8	7.15	7.65	0.701	184.0
9	9	6.95	7.45	0.684	206.0
10	10	6.70	7.20	0.660	229.0
11	12	6.40	6.90	0.632	275.0
12	14	6.10	6.60	0.606	320.0
13	16	5.80	6.30	0.679	356.0
14	18	5.50	6.00	0.550	412.0
15	20	5.25	5.75	0.527	458.0
16	25	4.65	5.15	0.472	572.0
17	30	4.20	4.70	0.431	688.0
18	35	3.75	4.25	0.390	801.0
19	40	3.40	3.90	0.358	916.0
20	45	3.15	3.65	0.335	1030.0

Entries in fifth column ($= q_t/q_0$) were obtained by taking the ratio of the signal at any time to the signal at time $t=0$.

APPENDIX D

ION-EXCHANGE EQUILIBRIA: DATA CORRELATION

TABLE 27: RATIONAL EQUILIBRIUM CONSTANT

Ba - Mn - Dowex 50W - X8 SYSTEM

A = Ba

B = Mn

Assumption: Activity coefficients of the chloride solutions
at 0.1N strength are same as those of 0.05
molality

$$\gamma_{\text{Ba Cl}_2} = 0.559$$

$$\gamma_{\text{Mn Cl}_2} = 0.52$$

No.	β_A	$\bar{\beta}_A$	$\sqrt{\bar{K}'_{c_B} \frac{A}{B}}$	$\bar{\gamma}_A$	$\bar{\gamma}_B$	K_B^A
1.	0.015	0.1	10.90	0.719	1.110	49.9
2.	0.030	0.2	9.10	0.763	0.990	49.2
3.	0.050	0.3	8.50	0.798	0.967	49.2
4.	0.075	0.4	7.90	0.839	0.945	49.2
5.	0.110	0.5	7.25	0.883	0.912	49.2
6.	0.165	0.6	6.19	0.947	0.832	49.9
7.	0.260	0.7	5.37	0.961	0.735	49.2
8.	0.400	0.8	4.85	1.020	0.707	49.4
9.	0.580	0.9	5.15	1.020	0.741	49.6

TABLE 28: ION-EXCHANGE EQUILIBRIA: Ba-Na-DOWEX
50W-X8 SYSTEM (K.2)

A = Ba

B = Na

No.	Solution-phase Equivalents%		Resin-phase Equivalents%	
	β_A	β_B	$\bar{\beta}_A$	$\bar{\beta}_B$
1.	0.95	99.05	15.10	84.90
2.	4.75	95.25	39.50	60.50
3.	9.55	90.45	90.90	9.10
4.	48.80	51.20	99.20	0.80

TABLE 29: EMPIRICAL CONSTANTS FOR VARIOUS PAIRS
OF IONS

$$\lambda_A = \frac{\bar{\beta}_A}{\beta_A} = a + b \bar{\beta}_A + c \bar{\beta}_A^2$$

Ionic Pair		Constants		
A	B	a	b	c
Cs	Na	1.741	-1.115	0.374
Mn	Na	32.200	-52.000	20.800
Mn	Cs	13.550	-23.400	10.850
Sr	Cs	29.700	-60.200	31.500
Sr	Mn	2.918	-2.253	0.335
Ba	Na	50.000	-49.000	0.000
Ba	Mn	10.720	-15.050	5.330

CORRELATION OF BINARY AND TERNARY EQUILIBRIUM DATA

Deduction of Binary Data from Ternary Data

Experimental Data:

Solution-Phase Composition			Resin-phase Composition		
\bar{B}_{Mn}	\bar{C}_{Cs}	\bar{C}_{Na}	\bar{B}_{Mn}	\bar{B}_{Cs}	\bar{B}_{Na}
0.20	0.40	0.40	0.635	0.286	0.079

Neglecting the Presence of Na^+ Ions

Mn-Cs pair

$$\bar{B}_{Mn} = \frac{0.20}{0.20+0.40} = 0.333$$

$$\bar{B}_{Mn} = \frac{0.635}{0.635+0.286} = \frac{0.635}{0.921} = 0.69$$

Neglecting the Presence of Cs^+ Ions

Mn - Na pair

$$\bar{B}_{Mn} = \frac{0.2}{0.2+0.4} = 0.333$$

$$\bar{B}_{Mn} = \frac{0.635}{0.635+0.079} = \frac{0.635}{0.714} = 0.89$$

Neglecting the Presence of Mn^{2+} Ions

Cs-Na pair

$$\bar{B}_{Cs} = \frac{0.4}{0.8} = 0.5$$

$$\bar{B}_{Cs} = \frac{0.286}{0.286+0.079} = \frac{0.286}{0.365} = 0.783$$

Deduced Data:

Ionic Pair		Solution-Phase Equivalent Fr.	Resin-Phase Equivalent Fr.	
A	B	β_A	Deduced	Experimental
Mn	Cs	0.333	0.690	0.650
Mn	Na	0.333	0.890	0.855
Cs	Na	0.500	0.783	0.605

Prediction of Ternary Data From Binary Data

Ternary Solution-Phase Composition:

	β_{Mn}	β_{Cs}	β_{Na}
	0.20	0.40	0.40
1. Empirical Method		From Binary Experimental Plots	
$\beta_{Mn} Mn-Cs$	0.333	$\beta_{Mn} Mn-Cs$	= 0.650
$\beta_{Mn} Mn-Na$	0.333	$\beta_{Mn} Mn-Na$	= 0.875
$\beta_{Cs} Cs-Na$	0.500	$\beta_{Cs} Cs-Na$	= 0.605

(i) From the pairs Mn-Cs and Mn-Na

$$\frac{\beta_{Mn}}{\beta_{Mn} + \beta_{Cs}} = 0.65, \quad \frac{\beta_{Mn}}{\beta_{Mn} + \beta_{Na}} = 0.875$$

$$\beta_{Mn} + \beta_{Cs} + \beta_{Na} = 1.0$$

Solving for β_{Mn} , β_{Cs} , β_{Na} ,

$$\beta_{Mn} = 0.595, \quad \beta_{Cs} = 0.32, \quad \beta_{Na} = 0.085$$

(ii) From the pairs Mn-Na and Cs-Na

$$\frac{\bar{\beta}_{\text{Mn}}}{\bar{\beta}_{\text{Mn}} + \bar{\beta}_{\text{Na}}} = 0.875$$

$$\frac{\bar{\beta}_{\text{Cs}}}{\bar{\beta}_{\text{Cs}} + \bar{\beta}_{\text{Na}}} = 0.605$$

$$\bar{\beta}_{\text{Mn}} + \bar{\beta}_{\text{Cs}} + \bar{\beta}_{\text{Na}} = 1.0$$

Solving for $\bar{\beta}_{\text{Mn}}$, $\bar{\beta}_{\text{Cs}}$, $\bar{\beta}_{\text{Na}}$

$$\bar{\beta}_{\text{Mn}} = 0.735, \quad \bar{\beta}_{\text{Cs}} = 0.160, \quad \bar{\beta}_{\text{Na}} = 0.105$$

(iii) From the data for the pairs Mn-Cs and Cs-Na

$$\frac{\bar{\beta}_{\text{Mn}}}{\bar{\beta}_{\text{Mn}} + \bar{\beta}_{\text{Cs}}} = 0.65$$

$$\frac{\bar{\beta}_{\text{Cs}}}{\bar{\beta}_{\text{Cs}} + \bar{\beta}_{\text{Na}}} = 0.605$$

$$\bar{\beta}_{\text{Mn}} + \bar{\beta}_{\text{Cs}} + \bar{\beta}_{\text{Na}} = 1.0$$

Solving for $\bar{\beta}_{\text{Mn}}$, $\bar{\beta}_{\text{Cs}}$, $\bar{\beta}_{\text{Na}}$

$$\bar{\beta}_{\text{Mn}} = 0.53, \quad \bar{\beta}_{\text{Cs}} = 0.285, \quad \bar{\beta}_{\text{Na}} = 0.185$$

Comparison of the predicted data:

$$\bar{\beta}_{\text{Mn}} = 0.20, \quad \bar{\beta}_{\text{Cs}} = 0.40, \quad \bar{\beta}_{\text{Na}} = 0.40$$

Experimental		Predicted		
		Pairs Mn-Cs Mn-Na	Pairs Mn-Na Cs-Na	Pairs Mn-Cs Cs-Na
$\bar{\beta}_{\text{Mn}}$	0.635	0.595	0.735	0.530
$\bar{\beta}_{\text{Cs}}$	0.286	0.320	0.160	0.285
$\bar{\beta}_{\text{Na}}$	0.079	0.085	0.105	0.185

It is evident from the above results that ternary data are predicted the best when each of the two pairs contains the ion most preferred by the resin-phase. Incidentally the above calculations also indicate that the calculated value of the resin-phase fraction of the common ion in the two pairs also approaches the correct value (obtained from the experimental data). But to get such calculated values, it would necessitate the knowledge of the ionic distribution for the three pairs (instead of that for only two pairs in the most favoured ion approach).

TABLE 30: SOLUTION-PHASE ACTIVITY COEFFICIENTS IN
TERNARY MIXTURES (EMPLOYED IN EXPERIMENTAL
STUDIES)

No.	x_{MnCl_2}	x_{CsCl}	x_{NaCl}	γ_{MnCl_2}	γ_{CsCl}	γ_{NaCl}
1	0.05	0.15	0.80	0.6716	0.749	0.778
2	0.05	0.35	0.60	0.671	0.749	0.778
3	0.05	0.60	0.35	0.671	0.749	0.778
4	0.10	0.10	0.80	0.666	0.744	0.777
5	0.10	0.20	0.70	0.666	0.744	0.777
6	0.10	0.30	0.60	0.666	0.744	0.777
7	0.10	0.60	0.30	0.666	0.744	0.777
8	0.10	0.70	0.20	0.666	0.744	0.777
9	0.10	0.80	0.10	0.666	0.744	0.777
10	0.20	0.10	0.70	0.657	0.734	0.774
11	0.20	0.40	0.40	0.657	0.734	0.774
12	0.20	0.70	0.10	0.657	0.734	0.774
13	0.30	0.10	0.60	0.649	0.722	0.772
14	0.30	0.60	0.10	0.649	0.722	0.772
15	0.40	0.20	0.40	0.640	0.710	0.769
16	0.60	0.20	0.20	0.626	0.680	0.764

APPENDIX E

ION-EXCHANGE KINETICS

Nernst-Einstein Equation

$$D_i = \frac{RT l_{oi}}{Z_i F^2} \quad (G.3)*$$

where

D_i = Ionic diffusivity in the aqueous phase (extremely dilute solutions) cm^2/sec .

l_{oi} = Limiting ionic conductance of species i,
 $\text{cm}^2, \text{ohm}^{-1} \text{ equivalent}^{-1}$

F = Faraday constant coulombs/equivalent

R = Gas-law constant joules $\text{gm.mole}^{-1} \text{ } ^\circ\text{K}^{-1}$

T = Temperature $^\circ\text{K}$

$l_{\text{Na}} = 50.10 \text{ cm}^2 \text{ ohm} \quad (P.1)$

$$D_{\text{Na}} = \frac{8.3144 \times 298 \times 50.10}{(96,500)^2 \times 1} = 133 \times 10^{-7} \text{ cm}^2/\text{sec}$$

Calculation of Film Thickness:

$$1 - \frac{q_t}{q_o} = 1 - \exp \left(- \frac{3Z_i D_i C_i t}{r_o \delta C_o} \right) \quad (45)$$

or

$$\frac{q_t}{q_o} = \exp \left(- \frac{3Z_i D_i C_i t}{r_o \delta C_o} \right)$$

*Limiting ionic conductances and ionic diffusivities in infinitely dilute solutions both available from Parsons' handbook (P.1), were correlated by Gopala Rao (G.3) by the above correlation.

Taking log of both sides

$$\log \frac{q_t}{q_0} = - \frac{1}{2.303} \times \frac{3 Z_i D_i C_i t}{r_0 \delta C_0}$$

From a plot of $\log \frac{q_t}{q_0}$ vs $t(\text{sec})$, a straight line was obtained passing through origin, (Run 108).

$$\text{Slope of the plot} = - \frac{0.25}{280}$$

$$\therefore \frac{3}{2.303} \times \frac{Z_i D_i C_i}{r_0 \delta C_0} = \frac{0.25}{280} \quad \delta = \frac{3 \times 280}{0.25 \times 2.303} \times \frac{Z_i D_i C_i}{r_0 C_0}$$

Bead diameter = 0.1065 cm (Na-3)

Bead capacity = 1.265 microequivalents

$$\begin{aligned} \text{Ionic concentration in the resin-phase} &= \frac{6 \times 1.265}{\pi \times (0.1065)^3} = 2003 \text{ micro equivalent/ml} \\ &= 2.003 \text{ milliequivalent/ml} \end{aligned}$$

Substituting for D_{Na} , C_0 , r_0 and C_{Na}

$$\delta = 3.54 \times 10^{-4} \text{ cm.}$$

TABLE 31: LIMITING IONIC CONDUCTANCES AND DIFFUSIVITIES OF IONS EMPLOYED IN THE PRESENT STUDY

$$D_i = \frac{RT}{F^2} \frac{l_{0i}}{Z_i} = 2.66 \times 10^{-7} \frac{l_{0i}}{Z_i} \text{ cm}^2/\text{sec}$$

Ion i	l_{0i}	$D_i \text{ cm}^2/\text{sec}$
Na ⁺	50.10	133.0×10^{-7}
Cs ⁺	77.30	205.0×10^{-7}
Mn ²⁺	53.50	70.8×10^{-7}
Sr ²⁺	59.40	78.7×10^{-7}
Ba ²⁺	63.60	84.4×10^{-7}

Helfferich's Criterion for Film/Particle-Diffusion Control(H.2

$$\frac{C_o \bar{D}_i \delta}{Z_i C_i \bar{D}_i r_o} (5 + 2 \alpha_B^A) \ll 1 \quad \text{Particle-diffusion control}$$

$$\frac{C_o \bar{D}_i \delta}{Z_i C_i \bar{D}_i r_o} (5 + 2 \alpha_B^A) \gg 1 \quad \text{Film-diffusion control}$$

α_B^A = Separation factor, unity for isotopic exchange**

For Run 108 (sodium self exchange employing 0.001938N solution)

$$\frac{2.003 \times 20.5 \times 10^{-7} \times 3.54 \times 10^{-4} \times 2}{0.001938 \times 133 \times 10^{-7} \times 0.1065} \times 7 = 7.4 \gg 1$$

Na⁺ ionic self exchange - Run 17 (Bead: Na-1A, d_o = 0.1025 cm)

$$\frac{2.003 \times 20.5 \times 10^{-7} \times 3.54 \times 10^{-4} \times 2 \times 7}{0.1 \times 133 \times 10^{-7} \times 0.1025} = 0.149 \ll 1$$

Mn²⁺ ionic self exchange - Run 25 (Bead: Mn-6 d_o = 0.1020 cm)

$$\frac{2.003 \times 2.22 \times 10^{-7} \times 3.54 \times 10^{-4} \times 2 \times 7}{0.1 \times 70.8 \times 10^{-7} \times 0.1020} = 0.0306 \ll 1$$

Therefore sodium and manganese self exchanges obtained with 0.1N chloride solutions are particle-diffusion controlled.

**

$$\alpha_B^A = \frac{\bar{B}_A}{B_A} \frac{B_B}{\bar{B}_B}$$

Assuming that value of film thickness obtained in the studies by Viswanathan (V.3) and Bajpai (B.1) is same as obtained in the present investigation.

Ba²⁺ ionic self exchange - Run 1V

$$\frac{2.003 \times 1.16 \times 10^{-7} \times 3.54 \times 10^{-4} \times 2 \times 7}{0.1 \times 84.4 \times 10^{-7} \times 0.0865} = 0.0156 \ll 1$$

Sr²⁺ ionic self exchange - Run 13B

$$\frac{2.003 \times 1.95 \times 10^{-7} \times 3.54 \times 10^{-4} \times 2 \times 7}{0.1 \times 78.7 \times 10^{-7} \times 0.0980} = 0.0250 \ll 1$$

Therefore, both barium and strontium self exchanges with 0.1N chloride solutions are particle-diffusion controlled.

TABLE 32: COMPUTED FILM-DIFFUSION CONTROLLED
EXCHANGE RATE DATA: Mn*-Na SYSTEM

Case 1: $C_{Cl,f}$ ** is not constant, and is obtained from solving Nernst-Planck equations for ionic fluxes for Na^+ , Mn^{2+} and Cl^- ions in the film phase simultaneously by finite difference technique.

Case 2: $C_{Cl,f}$ = Anion concentration in the bulk
= 0.1N

Assumed film thickness = 0.0007 cm,
Assumed bead diameter = 0.1000 cm

t(sec)	$C_{Cl,f}$ not constant		$C_{Cl,f} = 0.1N$
	$C_{Cl,f}$	q_t/q_o	q_t/q_o
0.1	0.1000	1.0000	1.0000
0.2	0.1312	1.0000	1.0000
0.3	0.1302	0.9957	0.9957
0.4	0.1264	0.9908	0.9914
0.5	0.1244	0.9863	0.9873
1.0	0.1194	0.9678	0.9701
5.0	0.1093	0.8902	0.8931
10.0	0.1063	0.8369	0.8394
20.0	0.1041	0.7687	0.7706
40.0	0.1026	0.6839	0.6852
60.0	0.1019	0.6264	0.6274
80.0	0.1015	0.5821	0.5829
100.0	0.1013	0.5458	0.5469
150.0	0.1009	0.4759	0.4765
200.0	0.1007	0.4239	0.4243
250.0	0.1006	0.3824	0.3823

** $C_{Cl,f}$ = Anion (chloride) concentration in the film-phase at interface.

Sample calculations for predicting solution-phase composition at the interface from the resin surface composition

Experimental Values

Solution-Phase			Resin-Phase		
β_{Mn}	β_{Cs}	β_{Na}	$\bar{\beta}_{Mn}$	$\bar{\beta}_{Cs}$	$\bar{\beta}_{Na}$
0.100	0.304	0.596	0.555	0.279	0.166

Ionic Pair				
A	B	a	b	c
Mn	Cs	13.55	-23.40	10.85
Mn	Na	32.20	-52.00	20.80

$$\frac{\bar{\beta}_{Mn}}{\bar{\beta}_{Mn} + \bar{\beta}_{Cs}} = \frac{0.555}{0.555 + 0.279} = 0.665$$

$$\bar{\beta}_{Mn} |_{Mn-Cs} = 13.55 - 23.40 \times 0.665 + 10.85 \times 0.665^2 = 2.8$$

$$\therefore \frac{\beta_{Mn}}{\beta_{Mn} + \beta_{Cs}} = \frac{0.665}{2.8} = 0.238 \quad (A)$$

$$\frac{\beta_{Mn}}{\beta_{Mn} + \beta_{Na}} = \frac{0.555}{0.555 + 0.166} = 0.77$$

$$\bar{\beta}_{Mn} |_{Mn-Na} = 32.20 - 52.00 \times 0.77 + 20.80 \times 0.77^2 = 4.5$$

$$\frac{\beta_{Mn}}{\beta_{Mn} + \beta_{Na}} = \frac{0.77}{4.5} = 0.171 \quad (B)$$

$$\beta_{Mn} + \beta_{Cs} + \beta_{Na} = 1.0 \quad (C)$$

Solving for β_{Mn} , β_{Cs} , β_{Na} from Equations A, B and C.

$$\begin{array}{lll} \beta_{Mn} = 0.110, & \beta_{Cs} = 0.355 & \beta_{Na} = 0.535 \\ 0.10 & 0.304 & 0.595 \quad (\text{experimental values}) \end{array}$$

ION-EXCHANGE RATE DATA (SELF EXCHANGE)

TABLE 33: SELF EXCHANGE OF SODIUM IONS (0.1NaCl SOLUTION)

Run No. 16

Bead: Na-3

Bead diameter: 0.1065cm

Experimental	
$\frac{t}{d_o^2} (\frac{\text{min}}{\text{cm}^2})$	$\frac{q_t}{q_o}$
4.17	0.932
8.34	0.884
12.50	0.845
16.70	0.800
20.80	0.761
25.00	0.730
29.20	0.703
33.40	0.677
37.60	0.651
41.70	0.626
50.00	0.587
58.50	0.555
66.80	0.528
75.10	0.490
83.40	0.458
104.00	0.406
125.00	0.361
146.00	0.328
167.00	0.303

Table 33 (continued)

Run No. 17

Bead: Na-1A

Bead diameter: 0.1025 cm

Experimental		Computed(Fick's law Modal)		Proposed Model
$\frac{t}{d_o^2}(\frac{\text{min}}{\text{cm}^2})$	$\frac{q_t}{q_o}$	$\frac{t}{d_o^2}(\frac{\text{min}}{\text{cm}^2})$	$\frac{q_t}{q_o}$	$\frac{q_t}{q_o}$
4.5	0.929	25.3	0.656	0.686
9.0	0.868	50.5	0.538	0.568
13.5	0.819	101.2	0.395	0.422
18.0	0.778	150.0	0.300	0.324
22.5	0.748	200.0	0.232	0.253
27.0	0.718	250.0	0.180	0.219
31.5	0.688	300.5	0.141	0.157
36.0	0.668	401.0	0.086	0.098
40.5	0.638	501.0	0.053	0.061
45.0	0.613	601.0	0.032	0.039
54.0	0.572	701.0	0.020	0.024
63.0	0.537	800.0	0.012	0.015
72.0	0.497			
81.0	0.467			
90.0	0.447			
113.0	0.397			
135.0	0.337			
158.0	0.286			
180.0	0.271			

TABLE 34: SELF EXCHANGE OF SODIUM IONS
(0.001938N NaCl SOLUTION)

Run No. 108

Bead: Na-3

Bead diameter: 0.1065 cm

Experimental	
$\frac{t}{d_o} \left(\frac{\text{sec}}{\text{cm}} \right)$	$\frac{q_t}{q_o}$
16.9	0.957
33.9	0.915
50.8	0.880
67.8	0.837
84.7	0.800
102.0	0.770
119.0	0.740
136.0	0.711
153.0	0.680
170.0	0.657
204.0	0.614
238.0	0.584
271.0	0.536
305.0	0.492
339.0	0.452
424.0	0.362
508.0	0.295
593.0	0.241
678.0	0.205
762.0	0.169
847.0	0.145

TABLE 35: SELF EXCHANGE OF MANGANESE IONS

Run No.25

Bead: Mn-6

Bead diameter: 0.1020 cm

Experimental		Computed (Fick's law Model)	
$\frac{t}{d_o^2} (\frac{\text{min}}{\text{cm}^2})$	$\frac{q_t}{q_o}$	$\frac{t}{d_o^2} (\frac{\text{min}}{\text{cm}^2})$	$\frac{q_t}{q_o}$
28.2	0.882	28.2	0.852
56.4	0.816	56.3	0.812
84.6	0.764	103.0	0.759
113.0	0.740	150.0	0.717
141.0	0.716	206.0	0.674
169.0	0.693	254.0	0.644
197.0	0.653	301.0	0.617
226.0	0.638	403.0	0.566
254.0	0.630	506.0	0.523
282.0	0.636	600.0	0.489
403.0	0.575	705.0	0.456
460.0	0.551	806.0	0.426
575.0	0.504		
634.0	0.481		
690.0	0.465		
740.0	0.441		

TABLE 36: SELF-EXCHANGE OF BARIUM IONS

Run No. 1V

Bead diameter: 0.0865 cm

Experimental	
$\frac{t}{d_o^2} \left(\frac{\text{min}}{\text{cm}^2} \right)$	$\frac{q_t}{q_o}$
66.7	0.882
133.5	0.824
267.0	0.733
401.0	0.667
534.0	0.623
668.0	0.588
801.0	0.560
935.0	0.530
1070.0	0.510
1201.0	0.486
1335.0	0.466

TABLE 37: SELF-EXCHANGE OF STRONTIUM IONS

Run No. 13E

Bead: Sr/A18

Bead diameter: 0.0980 cm

Experimental	
$\frac{t}{d_o^2} \left(\frac{\text{min}}{\text{cm}^2} \right)$	$\frac{q_t}{q_o}$
30.0	0.910
60.0	0.860
120.0	0.790
180.0	0.735
240.0	0.695
300.0	0.660
420.0	0.600
540.0	0.548
660.0	0.504
780.0	0.462
900.0	0.430

BINARY EXCHANGE

TABLE 38: BINARY EXCHANGE RATE DATA: $\text{Na}^+ - \text{Mn}^{2+}$ SYSTEM

Run No. 21

Bead: Na-1A,

Bead diameter: 0.1025 cm

Experimental			Computed			
$\frac{t}{d_o^2} \left(\frac{\text{min}}{\text{cm}^2} \right)$	$\frac{q_t}{q_o}$	$\frac{t}{d_o^2}$	N.P. Model q_t/q_o	With act. coeff. variation q_t/q_o	Proposed Model $\frac{q_t}{q_o}$	$y_{\text{Na}, R}$
4.5	0.961	25.6	0.783	0.809	0.755	6.04×10^{-3}
9.1	0.924	50.6	0.696	0.739	0.674	3.15×10^{-3}
13.6	0.885	100.0	0.512	0.627	0.567	2.39×10^{-3}
18.2	0.856	150.0	0.498	0.555	0.487	1.82×10^{-3}
22.7	0.826	200.0	0.432	0.496	0.423	1.48×10^{-3}
27.2	0.798	250.0	0.377	0.444	0.371	1.24×10^{-3}
31.7	0.779	300.0	0.331	0.398	0.326	1.07×10^{-3}
36.3	0.755	400.0	0.256	0.324	0.252	0.82×10^{-3}
40.8	0.740	500.0	0.198	0.265	0.195	0.64×10^{-3}
45.4	0.721	600.0	0.151	0.216	0.149	0.52×10^{-3}
68.0	0.644	700.0	0.114	0.176	0.112	0.41×10^{-3}
90.7	0.586	800.0	0.084	0.142	0.083	0.33×10^{-3}
114.0	0.529					
136.0	0.481					
159.0	0.448					
182.0	0.418					
205.0	0.385					
237.0	0.356					
272.0	0.322					
318.0	0.279					

TABLE 39: BINARY EXCHANGE RATE DATA: \bar{Mn}^* -Na SYSTEM

Run No. 20

Bead: Mn-6

Bead diameter: 0.1020cm

Experimental			Computed			
$\frac{t}{d_o^2} (\frac{\text{min}}{\text{cm}^2})$	$\frac{q_t}{q_o}$	$\frac{t}{d_o^2} (\frac{\text{min}}{\text{cm}^2})$	N.P. Model q_t/q_o	With act. coeff. variation q_t/q_o	Proposed Model q_t/q_o	$y_{Mn,R}$
22.9	0.931	25.3	0.810	0.817	0.891	0.546
45.8	0.880	50.6	0.751	0.768	0.847	0.494
68.7	0.840	100.0	0.669	0.699	0.781	0.430
91.6	0.807	150.0	0.609	0.645	0.729	0.387
115.0	0.775	200.0	0.561	0.602	0.686	0.355
138.0	0.743	251.0	0.521	0.565	0.644	0.329
161.0	0.720	301.0	0.487	0.533	0.616	0.307
184.0	0.701	401.0	0.430	0.479	0.560	0.272
206.0	0.684	500.0	0.384	0.434	0.513	0.244
229.0	0.660	601.0	0.396	0.397	0.473	0.221
275.0	0.632	701.0	0.314	0.365	0.438	0.201
320.0	0.606	800.0	0.286	0.337	0.407	0.184
356.0	0.579					
413.0	0.550					
458.0	0.527					
572.0	0.472					
688.0	0.431					
801.0	0.390					
916.0	0.358					
1030.0	0.335					

TABLE 40: BINARY EXCHANGE RATE DATA: $\bar{\text{Na}}^*$ -Ba SYSTEM

Run No. 6V

Bead diameter: 0.0942 cm

Experimental			Computed		
$\frac{t}{d_o^2} (\frac{\text{min}}{\text{cm}^2})$	$\frac{q_t}{q_o}$	$\frac{t}{d_o^2} (\frac{\text{min}}{\text{cm}^2})$	N.P. Model q_t/q_o	Proposed Model	
				q_t/q_o	$y_{\text{Na}, R}$
22.5	0.802	25.5	0.818	0.711	0.354×10^{-3}
45.0	0.731	51.0	0.741	0.674	0.484×10^{-3}
67.5	0.663	101.0	0.652	0.600	0.447×10^{-3}
90.0	0.616	151.0	0.584	0.535	0.374×10^{-3}
112.8	0.570	201.0	0.527	0.482	0.312×10^{-3}
169.0	0.485	251.0	0.479	0.438	0.271×10^{-3}
225.5	0.430	300.0	0.439	0.397	0.239×10^{-3}
282.0	0.372	400.0	0.369	0.330	0.192×10^{-3}
338.0	0.333	500.0	0.312	0.274	0.158×10^{-3}
450.0	0.255	601.0	0.264	0.228	0.133×10^{-3}
675.0	0.170	701.0	0.224	0.189	0.114×10^{-3}
		801.0	0.189	0.156	0.097×10^{-3}

TABLE. 41: BINARY EXCHANGE RATE DATA: $\bar{\text{Ba}}^*$ -Na SYSTEM

Run No.5V

Bead diameter: 0.1090cm

Experimental		Computed			
$\frac{t}{d_o^2} (\frac{\text{min}}{\text{cm}^2})$	$\frac{q_t}{q_o}$	$\frac{t}{d_o^2} (\frac{\text{min}}{\text{cm}^2})$	N.P. Model	Proposed Model	
				q_t/q_o	$y_{\text{Ba}, R}$
42.0	0.901	25.5	0.866	0.911	0.598
84.0	0.834	51.0	0.816	0.881	0.555
126.0	0.799	101.0	0.742	0.831	0.492
168.0	0.765	151.0	0.695	0.791	0.447
210.0	0.732	201.0	0.656	0.756	0.413
252.0	0.709	251.0	0.622	0.726	0.384
336.0	0.667	300.0	0.593	0.699	0.360
420.0	0.630	400.0	0.543	0.652	0.320
525.0	0.550	501.0	0.501	0.611	0.290
700.0	0.525	601.0	0.466	0.575	0.265
		701.0	0.435	0.544	0.243
		801.0	0.408	0.516	0.225

TABLE 42: BINARY EXCHANGE RATE DATA: $\bar{\text{Na}}^*$ -Cs SYSTEM

Run No. 23

Bead: Na-2

Bead diameter: 0.1070cm

Experimental		Computed (N.P. Model)	
$\frac{t}{d_o^2} (\frac{\text{min}}{\text{cm}^2})$	$\frac{q_t}{q_o}$	$\frac{t}{d_o^2} (\frac{\text{min}}{\text{cm}^2})$	$\frac{q_t}{q_o}$
4.17	0.896	25.2	0.636
8.34	0.840	50.5	0.514
12.50	0.787	100.0	0.369
16.70	0.748	150.0	0.274
20.90	0.712	200.0	0.208
25.00	0.679	250.0	0.159
29.20	0.644	300.0	0.123
33.40	0.621	400.0	0.074
37.50	0.598	500.0	0.045
41.70	0.574	600.0	0.027
58.40	0.506	800.0	0.010
66.70	0.471		
75.10	0.439		
83.40	0.408		
91.70	0.379		
108.00	0.333		
125.10	0.287		
146.00	0.236		
167.00	0.218		
188.00	0.195		
209.00	0.184		

TABLE 43: BINARY EXCHANGE RATE DATA: \bar{Mn}^* -Sr SYSTEM

Run No. 19B

Bead: Mn/B13

Bead diameter: 0.1190cm

Experimental		Computed			
$\frac{t}{d_o^2} \left(\frac{\text{min}}{\text{cm}^2} \right)$	$\frac{q_t}{q_o}$	Proposed Model		N.P. Model	
$\frac{t}{d_o^2} \left(\frac{\text{min}}{\text{cm}^2} \right)$	$\frac{q_t}{q_o}$	$\frac{t}{d_o^2} \left(\frac{\text{min}}{\text{cm}^2} \right)$	$\frac{q_t}{q_o}$	$\frac{t}{d_o^2} \left(\frac{\text{min}}{\text{cm}^2} \right)$	$\frac{q_t}{q_o}$
50.4	0.814	25.4	0.870	32.1	0.849
100.8	0.738	50.8	0.832	53.5	0.820
151.2	0.691	105.0	0.773	107.0	0.761
201.6	0.651	152.0	0.727	161.0	0.715
302.4	0.590	201.0	0.684	202.0	0.684
403.2	0.545	250.0	0.657	250.0	0.650
504.0	0.507	300.0	0.628	301.0	0.620
604.8	0.463	400.0	0.579	406.0	0.574
806.4	0.396	500.0	0.537	501.0	0.534
1008.0	0.343	600.0	0.501	608.0	0.496
		700.0	0.469	705.0	0.465
		800.0	0.440	800.0	0.438

TABLE 44: BINARY EXCHANGE RATE DATA: $\text{Sr}^*\text{-Mn}$ SYSTEM

Run No. 16B

Bead: Sr/Al6

Bead diameter: 0.1065cm

Experimental	
$\frac{t}{d_o^2} \left(\frac{\text{min}}{\text{cm}^2} \right)$	$\frac{q_t}{q_o}$
42.0	0.932
84.0	0.870
126.0	0.835
168.0	0.806
210.0	0.777
294.0	0.728
378.0	0.694
462.0	0.664
546.0	0.638
630.0	0.617
840.0	0.561
1092.0	0.488

TABLE 44 (Contd)

Run No. 17B

Bead: Sr/A18

Bead diameter: 0.0980 cm

Experimental		Computed			
$\frac{t}{d_o^2} \left(\frac{\text{min}}{\text{cm}^2} \right)$	$\frac{q_t}{q_o}$	N.P. Model		Proposed Model	
		$\frac{t}{d_o^2} \left(\frac{\text{min}}{\text{cm}^2} \right)$	$\frac{q_t}{q_o}$	$\frac{t}{d_o^2} \left(\frac{\text{min}}{\text{cm}^2} \right)$	$\frac{q_t}{q_o}$
49.7	0.917	32.4	0.846	25.4	0.896
99.4	0.860	53.5	0.821	50.7	0.862
149.0	0.813	107.0	0.764	100.7	0.808
199.0	0.778	161.0	0.719	150.0	0.764
249.0	0.748	207.0	0.688	200.5	0.727
348.0	0.701	256.0	0.655	250.0	0.696
447.0	0.661	301.0	0.625	300.0	0.668
547.0	0.626	406.0	0.580	400.5	0.619
746.0	0.552	501.0	0.541	500.0	0.579
894.0	0.522	608.0	0.504	600.5	0.543
1093.0	0.473	705.0	0.474	700.0	0.511
		800.0	0.447	800.0	0.483

Note: Computed results for Runs 16B and 17B are almost identical (in terms of t/d_o^2 vs q_t/q_o)

TABLE 45: BINARY EXCHANGE RATE DATA: \bar{Mn}^* -Cs SYSTEM

Run No. 24

Bead: Mn-5

Bead diameter: 0.1005 cm

Experimental		Computed (Proposed Model)	
$\frac{t}{d_o^2} \left(\frac{\text{min}}{\text{cm}^2} \right)$	$\frac{q_t}{q_o}$	$\frac{t}{d_o^2} \left(\frac{\text{min}}{\text{cm}^2} \right)$	$\frac{q_t}{q_o}$
29.7	0.855	25.6	0.867
59.4	0.782	50.6	0.812
89.1	0.727	100.6	0.733
119.0	0.685	150.0	0.674
149.0	0.632	200.0	0.626
178.0	0.606	250.0	0.585
208.0	0.576	300.0	0.550
238.0	0.552	400.0	0.491
267.0	0.528	500.0	0.443
297.0	0.509	600.0	0.403
357.0	0.467	700.0	0.368
416.0	0.430	800.0	0.338
475.0	0.406		
535.0	0.382		
594.0	0.364		
654.0	0.358		
713.0	0.323		
772.0	0.321		

TABLE 46: BINARY EXCHANGE RATE DATA: $\bar{\text{Sr}}^*\text{-Cs}$ SYSTEM

Run No.25B

Bead: Sr/B13

Bead diameter:0.1160cm

Experimental		Computed (Proposed Model)	
$\frac{t}{d_o^2}(\frac{\text{min}}{\text{cm}^2})$	$\frac{q_t}{q_o}$	$\frac{t}{d_o^2}(\frac{\text{min}}{\text{cm}^2})$	$\frac{q_t}{q_o}$
44.6	0.881	25.6	0.875
89.2	0.805	50.6	0.826
156.0	0.723	101.0	0.755
201.0	0.685	150.0	0.702
268.0	0.648	200.0	0.657
357.0	0.591	250.0	0.620
446.0	0.541	300.0	0.587
535.0	0.490	400.0	0.531
624.0	0.454	500.0	0.486
714.0	0.439	600.0	0.446
803.0	0.423	700.0	0.413
892.0	0.410	800.0	0.383
981.0	0.391		

TABLE 47: BINARY EXCHANGE RATE DATA: \bar{Mn}^* -Ba SYSTEM

Run No. 55

Bead: Mn-6

Bead diameter: 0.1020cm

Experimental		Computed (Proposed Model)	
$\frac{t}{d_o^2} (\frac{\text{min}}{\text{cm}^2})$	$\frac{q_t}{q_o}$	$\frac{t}{d_o^2} (\frac{\text{min}}{\text{cm}^2})$	$\frac{q_t}{q_o}$
22.3	0.856	25.4	0.886
45.6	0.807	50.8	0.854
68.4	0.771	100.6	0.799
91.2	0.746	150.0	0.756
114.0	0.726	201.0	0.720
137.0	0.705	250.0	0.690
169.6	0.684	300.5	0.663
182.4	0.669	401.0	0.617
205.2	0.654	500.0	0.577
228.0	0.634	600.0	0.543
273.6	0.613	700.0	0.502
339.6	0.584	800.0	0.484
364.8	0.573		
410.4	0.553		
456.0	0.532		
570.0	0.492		
684.0	0.452		
798.0	0.421		
912.0	0.400		

TERNARY EXCHANGE

TABLE 48: TERNARY EXCHANGE RATE DATA:

 \bar{Na}^* -(Mn-Cs) SYSTEMA

Run No. 35

Bead: Na-3

Bead diameter: 0.1065 cm

 \bar{Na}^* -(Mn-Cs): \bar{i}^* -(0.4 - 0.6)

Experimental		Computed (Proposed Model)	
$\frac{t}{d_o^2} \left(\frac{\text{min}}{\text{cm}^2} \right)$	$\frac{q_t}{q_o}$	$\frac{t}{d_o^2} \left(\frac{\text{min}}{\text{cm}^2} \right)$	$\frac{q_t}{q_o}$
5.3	0.902	25.4	0.698
10.7	0.838	50.8	0.592
16.0	0.786	101.0	0.461
21.4	0.740	151.0	0.372
26.7	0.701	201.0	0.305
32.0	0.662	251.0	0.254
37.4	0.636	301.0	0.212
42.7	0.610	401.0	0.149
53.4	0.571	501.0	0.107
64.1	0.532	601.0	0.076
74.8	0.506	701.0	0.055
85.4	0.481	800.0	0.039
106.8	0.429		
133.7	0.377		
160.0	0.338		
187.0	0.286		
214.0	0.247		
240.0	0.220		
267.5	0.208		

Table 48 (contd)

B

Run No.36

Bead: Na-1A

Bead diameter: 0.1025 cm

 $\bar{N}_a^*-(\text{Mn-Cs}): \bar{q}^*-(0.833 - 0.167)$

Experimental		Computed (Proposed Model)	
$\frac{t}{d_o^2}(\frac{\text{min}}{\text{cm}^2})$	$\frac{q_t}{q_o}$	$\frac{t}{d_o^2}(\frac{\text{min}}{\text{cm}^2})$	$\frac{q_t}{q_o}$
5.7	0.935	25.2	0.734
11.4	0.887	50.8	0.644
17.1	0.824	101.0	0.524
22.8	0.807	151.0	0.445
28.5	0.775	201.0	0.380
34.2	0.744	251.0	0.328
39.9	0.720	301.0	0.283
45.6	0.696	401.0	0.214
57.0	0.648	501.0	0.169
68.4	0.616	601.0	0.122
79.8	0.568	701.0	0.091
91.2	0.520	800.0	0.067
114.0	0.456		
147.0	0.408		
171.0	0.376		
200.0	0.336		
228.0	0.312		
286.0	0.264		
342.0	0.200		
400.0	0.160		

TABLE 49: TERNARY EXCHANGE RATE DATA:
($\bar{Na}^* - \bar{Cs}$)-Mn SYSTEM

A

Run No.28

Bead: Na-3

Bead diameter= 0.1065 cm

($\bar{Na}^* - \bar{Cs}$)-Mn: (0.424* - 0.576) - 1.0

Experimental		Computed (Proposed Model)	
$\frac{t}{d_o^2} (\frac{\text{min}}{\text{cm}^2})$	$\frac{q_t}{q_o}$	$\frac{t}{d_o^2} (\frac{\text{min}}{\text{cm}^2})$	$\frac{q_t}{q_o}$
5.3	0.910	25.2	0.752
10.6	0.849	50.4	0.680
15.9	0.795	99.8	0.580
21.2	0.758	149.2	0.504
26.5	0.727	199.5	0.443
31.8	0.696	248.0	0.393
37.0	0.681		
42.3	0.659		
47.7	0.644		
53.0	0.629		
64.0	0.606		
74.2	0.576		
84.7	0.545		
95.3	0.523		
106.0	0.500		
132.3	0.444		
159.0	0.417		
185.0	0.394		
212.0	0.356		
265.0	0.288		
318.0	0.258		
370.0	0.212		

Table 49(contd)

B

Run No.29

Bead: Na-4A

Bead diameter: 0.1000 cm

 $(\bar{N}_a^* - \bar{C}_s) - Mn: (0.721^* - .279) - 1.0$

Experimental		Computed (Proposed Model)	
$\frac{t}{d_o^2} (\frac{\text{min}}{\text{cm}^2})$	$\frac{q_t}{q_o}$	$\frac{t}{d_o^2} (\frac{\text{min}}{\text{cm}^2})$	$\frac{q_t}{q_o}$
6.0	0.911	25.4	0.756
12.0	0.850	50.8	0.678
18.0	0.812	100.6	0.574
24.0	0.774	150.8	0.496
36.0	0.712	201.1	0.434
48.0	0.675	250.3	0.382
60.0	0.637	300.7	0.337
72.0	0.606	401.3	0.264
84.0	0.575	501.4	0.205
96.0	0.550	601.0	0.158
108.0	0.525	701.0	0.120
120.0	0.500	800.0	0.088
150.0	0.438		
180.0	0.387		
210.0	0.356		
240.0	0.325		
300.0	0.256		
360.0	0.225		
420.0	0.188		

TABLE 50: TERNARY EXCHANGE RATE DATA:
($\bar{\text{Na}}^*-\bar{\text{Mn}}$)-Cs SYSTEM

A

Run No.33

Bead: Na-2

Bead diameter: 0.1070 cm

($\bar{\text{Na}}^*-\bar{\text{Mn}}$)-Cs: (0.607* - 0.393) - 1.0

Experimental		Computed (N.P. Model)	
$\frac{t}{d_o^2}(\frac{\text{min}}{\text{cm}^2})$	$\frac{q_t}{q_o}$	$\frac{t}{d_o^2}(\frac{\text{min}}{\text{cm}^2})$	$\frac{q_t}{q_o}$
5.2	0.888	25.3	0.619
10.4	0.815	50.6	0.495
15.7	0.753	100.0	0.347
20.9	0.692	150.0	0.253
26.1	0.650	200.0	0.187
31.3	0.612	250.0	0.140
36.5	0.576	300.0	0.105
41.8	0.551	400.0	0.060
47.0	0.527	500.0	0.034
52.2	0.503	600.0	0.020
62.6	0.460	700.0	0.011
73.1	0.429	800.0	0.007
83.5	0.392		
94.0	0.362		
104.4	0.331		
114.8	0.313		
125.3	0.276		
135.7	0.252		
146.2	0.227		
167.5	0.196		

Table 50A (contd)

Computed (Proposed Model)	
$\frac{t}{d_o^2} \left(\frac{\text{min}}{\text{cm}^2} \right)$	$\frac{q_t}{q_o}$
25.4	0.636
50.9	0.516
100.4	0.368
151.0	0.273
201.5	0.205
250.5	0.156
301.0	0.119
400.0	0.070
502.0	0.041
602.0	0.024
701.0	0.015
801.0	0.009

Table 50 (contd)

B

Run No. 34

Bead: Na-4A

Bead diameter: 0.1000 cm

 $(\bar{M}_w^* - \bar{M}_n) - Cs: (0.514^* - 0.486) = 1.0$

Experimental		Computed			
$\frac{t}{d_o^2} \left(\frac{\text{min}}{\text{cm}^2} \right)$	q_t/q_o	N.P. Model		Proposed Model	
		$\frac{t}{d_o^2} \left(\frac{\text{min}}{\text{cm}^2} \right)$	q_t/q_o	$\frac{t}{d_o^2} \left(\frac{\text{min}}{\text{cm}^2} \right)$	q_t/q_o
5.0	0.888	25.3	0.614	25.4	0.632
12.0	0.809	50.6	0.489	50.8	0.512
18.0	0.749	100.0	0.340	100.6	0.364
24.0	0.696	150.0	0.246	150.8	0.268
30.0	0.650	200.0	0.018	201.0	0.200
36.0	0.610	250.0	0.134	250.3	0.152
42.0	0.584	300.0	0.100	300.7	0.115
48.0	0.544	400.0	0.056	401.3	0.066
54.0	0.518			501.4	0.039
60.0	0.497			601.0	0.023
72.0	0.457			701.0	0.013
84.0	0.417			800.0	0.008
96.0	0.378				
108.0	0.338				
120.0	0.311				
150.0	0.245				
180.0	0.206				
210.0	0.172				
240.0	0.159				

TABLE 51: TERNARY EXCHANGE RATE DATA:
Mn⁺-(Cs-Na) SYSTEM

A

Run No.43

Bead: Mn-6

Bead diameter: 0.1020 cm

Mn⁺-(Cs-Na): $\bar{1}^*$ - (0.1 - 0.9)

Experimental		Computed (Proposed Model)	
$\frac{t}{d_o^2}(\frac{\text{min}}{\text{cm}^2})$	q_t/q_o	$\frac{t}{d_o^2}(\frac{\text{min}}{\text{cm}^2})$	q_t/q_o
22.6	0.914	25.4	0.881
45.2	0.856	50.8	0.833
67.7	0.808	100.6	0.763
90.3	0.770	151.0	0.709
113.0	0.738	201.0	0.664
136.0	0.711	250.5	0.626
158.0	0.685	301.0	0.593
180.7	0.657	401.0	0.536
203.0	0.636	501.0	0.489
226.0	0.621	600.0	0.449
271.0	0.588	700.0	0.415
316.0	0.562	800.0	0.385
361.0	0.535		
406.0	0.513		
452.0	0.492		
565.0	0.428		
678.0	0.385		
790.0	0.347		
903.0	0.310		
1050.0	0.278		
1130.0	0.251		

Table 51 (contd)

B

Run No. 70

Bead: Mn-5B

Bead diameter: 0.0980 cm

 \bar{M}^*
Mn-(Cs-Na): $\bar{M}^*(0.4 - 0.6)$

Experimental		Computed (Proposed Model)	
$\frac{t}{d_o^2} \left(\frac{\text{min}}{\text{cm}^2} \right)$	q_t/q_o	$\frac{t}{d_o^2} \left(\frac{\text{min}}{\text{cm}^2} \right)$	q_t/q_o
24.7	0.909	25.4	0.871
49.3	0.836	50.8	0.819
74.0	0.789	100.7	0.749
98.6	0.745	151.0	0.689
123.2	0.712	201.0	0.644
147.7	0.678	250.5	0.604
172.5	0.654	300.7	0.570
197.0	0.617	401.0	0.512
222.0	0.605	502.0	0.465
246.5	0.586	601.0	0.425
296.0	0.555	701.0	0.391
345.0	0.519	800.0	0.361
394.0	0.494		
444.0	0.469		
494.0	0.444		
615.0	0.389		
738.0	0.352		
834.0	0.335		

TABLE 52: TERNARY EXCHANGE RATE DATA:
 $(\bar{Mn}^* - \bar{Na}) - Cs$ SYSTEM

A

Run No. 30

Bead: Mn-5

Bead diameter: 0.1005 cm

$(\bar{Mn}^* - \bar{Na}) - Cs : (0.841^* - 0.159) - 1.0$

Experimental		Computed (Proposed Model)	
$\frac{t}{d_o^2} (\frac{\text{min}}{\text{cm}^2})$	q_t/q_o	$\frac{t}{d_o^2} (\frac{\text{min}}{\text{cm}^2})$	q_t/q_o
29.7	0.842	25.4	0.890
59.3	0.757	50.8	0.836
89.0	0.691	100.7	0.761
119.0	0.645	151.0	0.704
150.0	0.605	201.0	0.651
178.0	0.579	250.5	0.617
208.0	0.552	300.7	0.582
237.0	0.526	401.0	0.523
267.0	0.507	502.0	0.475
300.0	0.487	601.0	0.434
356.0	0.454	701.0	0.399
415.0	0.421	800.0	0.368
475.0	0.395		
534.0	0.375		
593.0	0.355		
653.0	0.229		
712.0	0.316		
771.0	0.303		
831.0	0.290		
890.0	0.276		
1190.0	0.204		

Table 52 (contd)

B

Run No. 31

Bead: Mn-6

Bead diameter: 0.1020 cm

 $(\bar{M}_n^* - \bar{M}_n) - Cs: (0.632^* - 0.368) - 1.0$

Experimental		Computed (Proposed Model)	
$\frac{t}{d_o^2} \left(\frac{\text{min}}{\text{cm}^2} \right)$	q_t/q_o	$\frac{t}{d_o^2} \left(\frac{\text{min}}{\text{cm}^2} \right)$	q_t/q_o
29.0	0.903	25.4	0.907
57.7	0.843	50.8	0.859
86.5	0.795	100.6	0.789
115.0	0.744	151.0	0.734
144.0	0.722	201.0	0.689
173.0	0.686	250.5	0.652
201.7	0.662	300.5	0.617
230.7	0.638	401.0	0.560
259.3	0.614	501.0	0.512
290.0	0.602	600.0	0.471
346.0	0.566	700.0	0.435
403.0	0.530	800.0	0.403
461.0	0.494		
577.0	0.434		
703.0	0.385		
865.0	0.349		
1010.0	0.313		
1150.0	0.273		
1300.0	0.253		

Table 52 (contd)

C

Run No.66

Bead: Mn-5B

Bead diameter:0.0980 cm

$$(\bar{M}^* - \bar{N}_a) - C_3: (0.489^* - 0.511) - 1.0$$

Experimental		Computed (Proposed Model)	
$\frac{t}{d_o^2} (\frac{\text{min}}{\text{cm}^2})$	q_t/q_o	$\frac{t}{d_o^2} (\frac{\text{min}}{\text{cm}^2})$	q_t/q_o
24.7	0.900	25.4	0.918
49.4	0.854	50.9	0.874
74.1	0.802	100.6	0.808
98.8	0.770	151.0	0.756
123.5	0.731	201.0	0.712
148.0	0.703	250.5	0.676
173.0	0.680	301.0	0.642
197.0	0.646	401.0	0.586
222.0	0.637	501.0	0.538
247.0	0.618	602.0	0.497
290.0	0.590	700.0	0.462
346.0	0.552	800.0	0.430
394.0	0.524		
444.0	0.505		
494.0	0.486		
600.0	0.439		
739.0	0.401		
865.0	0.354		
986.0	0.321		
1020.0	0.288		
1230.0	0.254		
1358.0	0.241		
1475.0	0.220		

TABLE 53: TERNARY EXCHANGE RATE DATA:
 $(\bar{Mn}^* - \bar{Cs}) - Na$ SYSTEM

A

Run No. 38

Bead: Mn-6

Bead diameter: 0.1020 cm

$(\bar{Mn}^* - \bar{Cs}) - Na: (0.804^* - 0.196) - 1.0$

Experimental		Computed (Proposed Model)	
$\frac{t}{d_o^2} \left(\frac{\text{min}}{\text{cm}^2} \right)$	q_t/q_o	$\frac{t}{d_o^2} \left(\frac{\text{min}}{\text{cm}^2} \right)$	q_t/q_o
23.8	0.901	25.4	0.920
57.7	0.844	50.8	0.881
86.5	0.799	100.6	0.823
115.0	0.760	151.0	0.775
144.0	0.733	201.0	0.735
173.0	0.707	251.0	0.701
202.0	0.681	301.0	0.669
231.0	0.661	401.0	0.613
260.0	0.643	501.0	0.566
288.0	0.616	600.0	0.525
346.0	0.590	700.0	0.489
403.0	0.552	800.0	0.457
461.0	0.526		
519.0	0.500		
578.0	0.474		
703.0	0.409		
865.0	0.357		
1008.0	0.312		
1153.0	0.279		
1442.0	0.227		

Table 53 (contd)

B

Run No. 37

Bead: Mn-5

Bead diameter: 0.1005 cm

 $(\bar{M}_n^* - \bar{C}_s) - Na: (0.555^* - 0.445) - 1.0$

Experimental		Computed (Proposed Model)	
$\frac{t}{d_o^2} \left(\frac{\text{min}}{\text{cm}^2} \right)$	q_t/q_o	$\frac{t}{d_o^2} \left(\frac{\text{min}}{\text{cm}^2} \right)$	q_t/q_o
29.7	0.950	25.4	0.943
58.7	0.905	50.8	0.913
89.0	0.874	100.7	0.864
119.0	0.841	157.0	0.823
148.5	0.817	201.0	0.787
177.0	0.785	251.0	0.756
208.0	0.766	301.0	0.726
238.0	0.741	401.0	0.674
267.0	0.722	502.0	0.629
297.0	0.696	601.0	0.589
357.0	0.652	701.0	0.552
416.0	0.614	800.0	0.519
475.0	0.576		
434.0	0.538		
594.0	0.507		
742.0	0.443		
891.0	0.386		
1040.0	0.342		
1190.0	0.298		
1333.0	0.266		
1485.0	0.253		

Table 53 (contd)

C

Run No. 49

Bead: Mn-54

Bead diameter: 0.0950 cm

$$(\bar{M}_n^* - \bar{C}_s) - N_a: (0.604^* - 0.396) - 1.0$$

Experimental		Computed (Proposed Model)	
$\frac{t}{d_o^2} (\frac{\text{min}}{\text{cm}^2})$	q_t/q_o	$\frac{t}{d_o^2} (\frac{\text{min}}{\text{cm}^2})$	q_t/q_o
26.1	0.930	25.4	0.942
52.2	0.890	50.8	0.910
78.3	0.855	100.7	0.860
104.5	0.820	151.0	0.818
130.5	0.790	201.0	0.782
157.0	0.765	250.5	0.750
183.0	0.745	300.5	0.721
209.0	0.725	401.0	0.668
234.0	0.705	501.0	0.623
261.0	0.680	601.0	0.583
313.0	0.650	700.0	0.597
366.0	0.620	800.0	0.514
417.0	0.590		
926.0	0.390		
979.0	0.370		
1035.0	0.350		
1085.0	0.330		
1190.0	0.320		
1328.0	0.290		
1450.0	0.265		
1580.0	0.250		

TABLE 54: TERNARY EXCHANGE RATE DATA:
 \bar{Na}^* -(Ba-Mn) SYSTEM

A

Run No.63

Bead: Na-3

Bead diameter:0.1065 cm

\bar{Na}^* -(Ba-Mn): $\bar{1}^*$ -(0.1 - 0.9)

Experimental		Computed (Proposed Model)	
$\frac{t}{d_o^2}(\frac{\text{min}}{\text{cm}^2})$	q_t/q_o	$\frac{t}{d_o^2}(\frac{\text{min}}{\text{cm}^2})$	q_t/q_o
8.4	0.870	25.4	0.670
16.8	0.791	50.9	0.554
25.2	0.734	100.7	0.412
33.5	0.687	151.0	0.319
41.9	0.649	201.0	0.251
50.3	0.622	250.0	0.201
58.7	0.590	301.0	0.161
67.1	0.564	401.0	0.105
75.3	0.539	500.0	0.069
84.0	0.519	601.0	0.046
105.0	0.467	701.0	0.031
126.0	0.428	800.0	0.021
145.0	0.383		
167.0	0.338		
190.0	0.318		
210.0	0.292		
231.0	0.286		
252.0	0.260		

Table 54A(Contd)

Computed (N.P. Model)	
$\frac{t}{d_o^2} \left(\frac{\text{min}}{\text{cm}^2} \right)$	q_t/q_o
25.3	0.801
50.6	0.717
101.0	0.606
150.0	0.524
200.0	0.459
250.0	0.405
300.0	0.358
400.0	0.283
500.0	0.224
600.0	0.176
700.0	0.136
800.0	0.104

Table 54 (contd)

B

Run No. 67

Bead: Na-2

Bead diameter: 0.1070 cm

 $\bar{N}a^*-(Ba-Mn): \bar{I}^*-(0.4 - 0.6)$

Experimental		Computed			
$\frac{t}{d_o^2}(\frac{\text{min}}{\text{cm}^2})$	q_t/q_o	N.P. Model	q_t/q_o	Proposed Model	
		$\frac{t}{d_o^2}(\frac{\text{min}}{\text{cm}^2})$		$\frac{t}{d_o^2}(\frac{\text{min}}{\text{cm}^2})$	q_t/q_o
8.3	0.884	25.3	0.818	25.4	0.698
16.6	0.801	50.6	0.740	50.8	0.592
24.9	0.743	100.0	0.635	100.8	0.461
33.6	0.694	150.0	0.556	151.0	0.372
41.6	0.660	200.0	0.493	201.0	0.305
49.8	0.637	250.0	0.440	250.5	0.254
58.0	0.607	300.0	0.394	300.1	0.212
66.7	0.587	400.0	0.319	401.5	0.149
75.0	0.569	500.0	0.259	502.0	0.107
83.2	0.549	600.0	0.209	602.0	0.076
104.0	0.500	700.0	0.168	700.0	0.055
125.0	0.456	800.0	0.134	801.0	0.039
145.3	0.427				
166.3	0.394				
187.0	0.364				
208.0	0.340				
229.0	0.326				
250.0	0.306				
271.0	0.292				
292.0	0.286				

TABLE 55: TERNARY EXCHANGE RATE DATA:
($\bar{\text{Na}}^*\text{-}\bar{\text{Mn}}$)-Ba SYSTEM

A

Run No.57

Bead: Na-4A

Bead diameter:0.1000 cm

($\bar{\text{Na}}^*\text{-}\bar{\text{Mn}}$)-Ba: (0.504^{*} - 0.496)-1

Experimental		Computed (Proposed Model)	
$\frac{t}{d_o^2}(\frac{\text{min}}{\text{cm}^2})$	q_t/q_o	$\frac{t}{d_o^2}(\frac{\text{min}}{\text{cm}^2})$	q_t/q_o
9.6	0.877	25.0	0.655
19.1	0.770	50.5	0.591
28.7	0.709	100.0	0.487
38.2	0.658	150.0	0.409
46.7	0.612	200.0	0.346
57.3	0.591	250.0	0.293
66.7	0.571	300.5	0.249
74.4	0.551	400.0	0.178
85.7	0.531	500.0	0.125
95.5	0.505	600.0	0.085
119.0	0.459	700.0	0.056
143.0	0.413	800.0	0.036
167.0	0.378		
191.0	0.342		
216.0	0.296		
238.0	0.270		
262.0	0.240		
286.0	0.220		
310.0	0.199		

Table 55 (contd)

B

Run No.62

Bead: Na-4A

Bead diameter:0.1000 cm

 $(\bar{N}a^* - \bar{M}n) - Ba: (0.785^* - 0.215) - 1.0$

Experimental		Computed (Proposed Model)	
$\frac{t}{d_o^2} (\frac{\text{min}}{\text{cm}^2})$	q_t / q_o	$\frac{t}{d_o^2} (\frac{\text{min}}{\text{cm}^2})$	q_t / q_o
9.55	0.870	25.0	0.763
19.1	0.794	50.5	0.690
28.7	0.742	100.0	0.591
38.2	0.697	150.0	0.515
46.7	0.654	200.0	0.454
57.3	0.615	250.0	0.403
66.7	0.584	300.5	0.359
76.4	0.564	400.0	0.286
85.7	0.545	500.0	0.227
95.5	0.525	600.0	0.180
119.0	0.474	700.0	0.141
143.0	0.423	800.0	0.109
167.0	0.372		
191.0	0.327		
216.0	0.302		
238.0	0.276		
262.0	0.250		
286.0	0.225		
310.0	0.205		
330.0	0.180		

TABLE 56: ION-EXCHANGE RATE DATA:

($\bar{\text{Na}}^* - \bar{\text{Ba}}$)-Mn SYSTEMA

Run No. 53

Bead: Na-3

Bead diameter: 0.1065 cm

($\bar{\text{Na}}^* - \bar{\text{Ba}}$)-Mn : (0.565* - 0.435) - 1.0

Experimental		Computed			
		N.P. Model		Proposed Model	
$\frac{t}{d_o^2} (\frac{\text{min}}{\text{cm}^2})$	q_t/q_o	$\frac{t}{d_o^2} (\frac{\text{min}}{\text{cm}^2})$	q_t/q_o	$\frac{t}{d_o^2} (\frac{\text{min}}{\text{cm}^2})$	q_t/q_o
8.3	0.851	25.4	0.710	25.0	0.745
16.7	0.761	50.4	0.624	50.5	0.652
25.0	0.701	100.7	0.503	100.0	0.529
33.3	0.649	151.0	0.417	150.0	0.443
41.7	0.612	201.5	0.349	200.0	0.375
50.0	0.582	250.0	0.294	250.0	0.320
58.4	0.560	301.0	0.249	300.5	0.274
66.6	0.537	401.0	0.176	400.0	0.201
75.0	0.522	501.0	0.123	500.0	0.147
83.4	0.507	601.0	0.083	600.0	0.104
104.0	0.470	700.0	0.053	700.0	0.073
125.0	0.433	800.0	0.032	800.0	0.049
146.0	0.410				
167.0	0.388				
187.0	0.358				
208.0	0.338				
250.0	0.276				
292.0	0.224				

Table 56 (cont.)

B

Run No. 56

Bead: Na-3

Bead diameter: 0.1065 cm

 $(\bar{N}a^* - \bar{B}a) - Mn: (0.706^* - 0.294) - 1.0$

Experimental		Computed			
$\frac{t}{d_o^2} \left(\frac{\text{min}}{\text{cm}^2} \right)$	q_t/q_o	N.P. Model		Proposed Model	
		$\frac{t}{d_o^2} \left(\frac{\text{min}}{\text{cm}^2} \right)$	q_t/q_o	$\frac{t}{d_o^2} \left(\frac{\text{min}}{\text{cm}^2} \right)$	q_t/q_o
6.4	0.861	25.4	0.725	25.0	0.759
16.8	0.786	50.9	0.642	50.5	0.668
25.2	0.729	100.7	0.523	100.0	0.549
33.6	0.689	150.0	0.439	150.0	0.463
42.0	0.660	201.5	0.372	200.0	0.396
50.4	0.626	250.0	0.317	250.0	0.342
58.8	0.591	301.0	0.271	300.5	0.296
67.2	0.569	401.0	0.197	400.0	0.222
75.6	0.546	501.0	0.142	500.0	0.166
84.0	0.517	601.0	0.099	600.0	0.122
202.0	0.339	700.0	0.067	700.0	0.087
210.0	0.328	800.0	0.043	800.0	0.061
213.0	0.316				
227.0	0.304				
235.0	0.293				
243.0	0.282				
252.0	0.270				
273.0	0.247				
294.0	0.224				

TABLE 57: TERNARY EXCHANGE RATE DATA:
 \bar{Mn}^* -(Ba-Na) SYSTEM

A

Run No. 59

Bead: Mn-5A

Bead diameter: 0.0950cm

 \bar{Mn}^* -(Ba-Na): \bar{r}^* - (0.050 - 0.950)

Experimental		Computed			
$\frac{t}{d_o^2} (\frac{\text{min}}{\text{cm}^2})$	q_t/q_o	N.P. Model	Proposed Model		
		$\frac{t}{d_o^2} (\frac{\text{min}}{\text{cm}^2})$	q_t/q_o	$\frac{t}{d_o^2} (\frac{\text{min}}{\text{cm}^2})$	q_t/q_o
26.0	0.894	25.4	0.823	25.6	0.870
52.0	0.835	51.8	0.772	50.8	0.825
78.0	0.781	100.6	0.698	100.7	0.758
104.0	0.745	151.0	0.643	151.0	0.705
130.0	0.712	201.0	0.599	201.0	0.662
156.0	0.681	250.0	0.561	250.5	0.626
182.0	0.655	300.5	0.529	300.5	0.595
203.0	0.628	401.0	0.476	401.5	0.542
234.0	0.601	500.0	0.432	502.0	0.499
260.0	0.591	600.0	0.396	601.5	0.463
312.0	0.553	700.0	0.365	700.5	0.431
364.0	0.532	800.0	0.338	800.0	0.404
416.0	0.506				
463.0	0.479				
520.0	0.458				
650.0	0.405				
780.0	0.357				
910.0	0.315				

Table 57 (contd)

B

Run No. 60

Bead: Mn-6

Bead diameter: 0.1020 cm

 \bar{M}_n^* -(Ba-Na): \bar{I}^* - (0.1 - 0.9)

Experimental		Computed			
$\frac{t}{d_o^2} \left(\frac{\text{min}}{\text{cm}^2} \right)$	q_t/q_o	R.P. Model		Proposed Model	
		$\frac{t}{d_o^2} \left(\frac{\text{min}}{\text{cm}^2} \right)$	q_t/q_o	$\frac{t}{d_o^2} \left(\frac{\text{min}}{\text{cm}^2} \right)$	q_t/q_o
21.1	0.897	25.4	0.874	25.0	0.851
47.2	0.840	51.8	0.833	50.5	0.814
63.3	0.793	100.6	0.771	100.0	0.757
84.4	0.752	151.0	0.721	150.0	0.711
105.5	0.726	201.0	0.681	200.0	0.674
126.6	0.700	250.0	0.647	250.0	0.641
147.7	0.679	305.0	0.617	300.5	0.613
168.8	0.658	401.0	0.567	400.0	0.565
190.0	0.638	500.0	0.526	500.0	0.526
201.0	0.622	600.0	0.491	600.0	0.491
253.0	0.586	700.0	0.460	700.0	0.461
295.0	0.554	800.0	0.433	800.0	0.434
338.0	0.534				
380.0	0.508				
422.0	0.487				
530.0	0.445				
633.0	0.403				
737.0	0.356				
844.0	0.340				
950.0	0.309				

TABLE 58: TERNARY EXCHANGE RATE DATA:
($\bar{Mn}^* - \bar{Ba}$)-Na SYSTEM

A

Run No. 58

Bead: Mn-6

Bead diameter: 0.1020 cm

($\bar{Mn}^* - \bar{Ba}$)-Na: (0.758^{*} - 0.242) -1.0

Experimental		Computed (Proposed Model)	
$\frac{t}{d_o^2} \left(\frac{\text{min}}{\text{cm}^2} \right)$	q_t/q_o	$\frac{t}{d_o^2} \left(\frac{\text{min}}{\text{cm}^2} \right)$	q_t/q_o
22.6	0.900	25.4	0.855
45.2	0.850	51.3	0.799
67.8	0.800	100.6	0.717
90.3	0.765	151.0	0.656
113.0	0.735	201.0	0.606
134.0	0.715	250.0	0.564
158.3	0.695	301.0	0.528
182.3	0.670	401.0	0.468
203.3	0.650		
226.0	0.630		
271.0	0.605		
317.0	0.570		
362.0	0.535		
407.0	0.510		
450.0	0.485		
498.0	0.460		
543.0	0.440		
590.0	0.415		
633.0	0.405		
678.0	0.390		
760.0	0.365		

Table 58 (contd)

B

Run No. 64

Bead: Mn-5A

Bead diameter: 0.0950 cm

 $(\bar{M}_n^* - \bar{B}_a) - Na: (0.485^* - 0.515) - 1.0$

Experimental		Computed (Proposed Model)	
$\frac{t}{d_o^2} (\frac{\text{min}}{\text{cm}^2})$	q_t/q_o	$\frac{t}{d_o^2} (\frac{\text{min}}{\text{cm}^2})$	q_t/q_o
26.1	0.897	25.6	0.850
52.2	0.840	50.8	0.797
78.2	0.787	101.0	0.721
104.0	0.747	151.0	0.661
130.0	0.716	201.0	0.612
156.0	0.690	251.0	0.572
182.0	0.664	301.0	0.536
209.0	0.639	402.0	0.475
234.0	0.619	502.0	0.426
261.0	0.592	602.0	0.385
313.0	0.572	701.0	0.350
365.0	0.546	800.0	0.319
417.0	0.520		
469.2	0.490		
530.0	0.469		
652.0	0.418		
772.0	0.366		
892.0	0.330		

TABLE 59: TERNARY EXCHANGE RATE DATA:
 $(\bar{\text{Mn}}^* - \bar{\text{Na}}) - \text{Ba}$ SYSTEM

A

Run No. 65

Bead: Mn-6

Bead diameter: 0.1020

$(\bar{\text{Mn}}^* - \bar{\text{Na}}) - \text{Ba}: (0.872^* - 0.128) - 1.0$

Experimental		Computed (Proposed Model)	
$\frac{t}{d_o^2} \left(\frac{\text{min}}{\text{cm}^2} \right)$	q_t/q_o	$\frac{t}{d_o^2} \left(\frac{\text{min}}{\text{cm}^2} \right)$	q_t/q_o
22.7	0.906	25.4	0.868
45.3	0.857	51.8	0.832
68.0	0.819	100.6	0.795
90.7	0.789	151.0	0.763
113.0	0.760	201.0	0.735
136.0	0.740	250.0	0.710
159.0	0.720	300.5	0.687
181.0	0.701	401.0	0.645
204.0	0.681		
227.0	0.671		
272.0	0.642		
317.0	0.622		
363.0	0.603		
408.0	0.583		
453.0	0.563		
567.0	0.526		
680.0	0.495		
793.0	0.456		
910.0	0.427		
1020.0	0.397		

Table 59 (contd)

B

Run No. 54

Bead: Mn-5A

Bead diameter: 0.0950 cm

 $(\overline{Mn-Na})^*-Ba: (0.\overline{559}^* - 0.\overline{441}) - 1.0$

Experimental		Computed (Proposed Model)	
$\frac{t}{d_o^2} (\frac{min}{cm^2})$	q_t/q_o	$\frac{t}{d_o^2} (\frac{min}{xm^2})$	q_t/q_o
26.1	0.945	25.8	0.943
52.2	0.902	51.2	0.928
78.3	0.868	101.0	0.897
104.0	0.834	150.0	0.871
130.0	0.800	200.0	0.848
156.0	0.780	250.0	0.827
183.0	0.759	300.0	0.809
209.0	0.738	400.0	0.774
235.0	0.717	500.0	0.743
261.0	0.704	600.0	0.713
313.0	0.683	700.0	0.684
365.0	0.662	800.0	0.658
417.0	0.649		
469.0	0.620		
522.0	0.607		
651.0	0.565		
770.0	0.538		
1045.0	0.482		

TABLE 60: TERNARY EXCHANGE RATE DATA:
 $(\bar{Mn}^* - \bar{Cs})$ -Sr SYSTEM

A

Run No. 31B

Bead: Mn/A16

Bead diameter: 0.1090cm

$(\bar{Mn}^* - \bar{Cs})$ -Sr: $(0.715^* - 0.285) - 1.0$

Experimental		Computed (Proposed Model)	
$\frac{t}{d_o^2} (\frac{\text{min}}{\text{cm}^2})$	q_t/q_o	$\frac{t}{d_o^2} (\frac{\text{min}}{\text{cm}^2})$	q_t/q_o
50.4	0.867	25.5	0.906
100.8	0.804	50.9	0.878
151.0	0.752	101.0	0.832
202.0	0.715	167.0	0.795
302.0	0.652	202.0	0.762
403.0	0.595	251.0	0.738
504.0	0.555	301.0	0.713
605.0	0.527	402.0	0.668
706.0	0.490	502.0	0.629
806.0	0.459	601.0	0.593
907.0	0.425	700.0	0.560
1008.0	0.392	800.0	0.529

B

Run No. 40B

Bead: Mn/A16

Bead diameter: 0.1090 cm

 $(\bar{M}_n^* - \bar{C}_s) - \text{Sr}: (0.639^* - 0.361) - 1.0$

Experimental		Computed (Proposed Model)	
$\frac{t}{d_o^2} \left(\frac{\text{min}}{\text{cm}^2} \right)$	q_t/q_o	$\frac{t}{d_o^2} \left(\frac{\text{min}}{\text{cm}^2} \right)$	q_t/q_o
50.4	0.875	25.4	0.914
100.8	0.818	50.9	0.888
151.2	0.785	100.8	0.845
202.0	0.761	151.0	0.811
302.0	0.721	202.0	0.782
403.0	0.681	251.0	0.756
504.0	0.640	302.0	0.733
605.0	0.602	402.0	0.690
706.0	0.558	502.0	0.652
806.0	0.509	601.0	0.618
907.0	0.480	700.0	0.585
1008.0	0.450	800.0	0.554

TABLE 61: TERNARY EXCHANGE RATE DATA:
($\bar{\text{Mn}}^* - \bar{\text{Sr}}$)-Cs SYSTEM

A

Run No. 33B

Bead: Mn/A-18 Bead diameter: 0.1010 cm

($\bar{\text{Mn}}^* - \bar{\text{Sr}}$)-Cs: (0.820* - 0.180), -1.0

Experimental		Computed (Proposed Model)	
$\frac{t}{d_0^2} \left(\frac{\text{min}}{\text{cm}^2} \right)$	q_t/q_0	$\frac{t}{d_0^2} \left(\frac{\text{min}}{\text{cm}^2} \right)$	q_t/q_0
29.4	0.866	25.4	0.858
58.8	0.793	50.9	0.804
88.2	0.733	101.0	0.726
118.0	0.768	151.0	0.666
147.0	0.645	201.0	0.618
176.0	0.613	253.0	0.577
206.0	0.585	301.0	0.542
235.0	0.560	401.0	0.482
265.0	0.536	501.0	0.434
294.0	0.520	602.0	0.394
353.0	0.483	701.0	0.359
412.0	0.453	800.0	0.330
471.0	0.420		
529.0	0.397		
588.0	0.373		
735.0	0.326		
882.0	0.288		

Table 61 (contd)

B

Run No. 43B

Bead: Mn/A18

Bead diameter: 0.1010 cm

 $(\bar{M}_n^* - \bar{S}_r) - C_s: (0.652^* - 0.348) - 1.0$

Experimental		Computed (Proposed Model)	
$\frac{t}{d_o^2} (\frac{\text{min}}{\text{cm}^2})$	q_t/q_o	$\frac{t}{d_o^2} (\frac{\text{min}}{\text{cm}^2})$	q_t/q_o
29.4	0.846	25.4	0.853
58.8	0.782	50.9	0.799
88.2	0.731	101.0	0.722
118.0	0.692	151.0	0.662
147.0	0.660	201.0	0.614
177.0	0.628	256.0	0.574
206.0	0.603	301.0	0.539
235.0	0.577	401.0	0.480
265.0	0.541	501.0	0.432
294.0	0.532	601.0	0.392
353.0	0.494	701.0	0.358
412.0	0.462	800.0	0.328
470.0	0.423		
529.0	0.397		
588.0	0.378		
735.0	0.323		
882.0	0.308		

TABLE 62: TERNARY EXCHANGE RATE DATA:

 $\bar{S}r^{*}-(Mn-Cs)$ SYSTEMA

Run No. 44B

Bead: Sr/B13

Bead diameter: 0.1190 cm

 $\bar{S}r^{*}-(Mn-Cs): \bar{I}^{*}-(0.840 - 0.160)$

Experimental		Computed			
$\frac{t}{d_o^2} (\frac{\text{min}}{\text{cm}^2})$	q_t/q_o	N.P. Model		Proposed Model	
		$\frac{t}{d_o^2} (\frac{\text{min}}{\text{cm}^2})$	q_t/q_o	$\frac{t}{d_o^2} (\frac{\text{min}}{\text{cm}^2})$	q_t/q_o
50.2	0.866	50.8	0.790	25.4	0.873
100.3	0.804	101.0	0.715	50.8	0.836
150.5	0.758	151.0	0.665	100.7	0.780
200.6	0.724	201.0	0.625	151.0	0.734
301.0	0.668	251.0	0.590	201.0	0.697
401.3	0.619	301.0	0.560	250.5	0.666
502.0	0.569	401.0	0.510	301.0	0.637
602.0	0.536	501.0	0.472	401.5	0.588
803.0	0.479	601.0	0.430	502.0	0.548
1003.0	0.408	701.0	0.401	601.0	0.512
		800.0	0.370	700.0	0.481
				800.0	0.453

Table 62 (contd)

B

Run No. 45B

Bead: Sr/A19

Bead diameter: 0.1040 cm

 $\bar{S}r^*-(Mn-Cs): \bar{I}^*-(0.400 - 0.600)$

Experimental		Computed (Proposed Model)	
$\frac{t}{d_o^2}(\frac{min}{cm^2})$	q_t/q_o	$\frac{t}{d_o^2}(\frac{min}{cm^2})$	q_t/q_o
44.0	0.874	25.4	0.875
88.0	0.791	50.8	0.834
154.0	0.714	100.7	0.773
198.0	0.672	151.0	0.725
264.0	0.626	201.5	0.685
352.0	0.573	251.0	0.652
440.0	0.524	301.0	0.624
572.0	0.466	402.0	0.572
660.0	0.427	501.0	0.531
792.0	0.384	602.0	0.500
880.0	0.364	701.0	0.465
		801.0	0.437

Note: The computed data for Nernst-Planck Model were not available for the Run No. 45B.

TABLE 63: TERNARY EXCHANGE RATE DATA:
 $(\bar{\text{Sr}}^*-\bar{\text{Mn}})-\text{Cs}$ SYSTEM

A

Run No. 34B

Bead: Sr/B13

Bead diameter: 0.1160 cm

$(\bar{\text{Sr}}^*-\bar{\text{Mn}})-\text{Cs}: (0.786^*-0.214)-1.0$

Experimental		Computed (Proposed Model)	
$\frac{t}{d_o^2} \left(\frac{\text{min}}{\text{cm}^2} \right)$	q_t/q_o	$\frac{t}{d_o^2} \left(\frac{\text{min}}{\text{cm}^2} \right)$	q_t/q_o
44.6	0.844	25.4	0.859
69.2	0.772	50.8	0.817
156.1	0.701	100.7	0.751
200.7	0.669	150.8	0.699
267.6	0.630	201.5	0.656
312.2	0.610	250.2	0.619
401.4	0.569	301.0	0.587
490.0	0.535	401.5	0.532
579.0	0.506	501.0	0.486
669.0	0.475	601.5	0.448
802.0	0.441	701.0	0.415
892.0	0.426	801.0	0.385
981.0	0.416		

Table 63 (contd)

B

Run No. 42B

Bead: Sr/B13

Bead diameter: 0.1160 cm

 $(\bar{S}r^* - \bar{M}n) - Cs: (0.340^* - 0.660) - 1.0$

Experimental		Computed (Proposed Model)	
$\frac{t}{d_o^2} (\frac{\text{min}}{\text{cm}^2})$	q_t/q_o	$\frac{t}{d_o^2} (\frac{\text{min}}{\text{cm}^2})$	q_t/q_o
44.6	0.831	25.4	0.894
89.2	0.690	50.8	0.844
156.0	0.611	101.0	0.774
201.0	0.577	151.0	0.720
268.0	0.540	201.5	0.676
312.0	0.579	251.0	0.638
401.0	0.481	301.0	0.605
491.0	0.438	401.5	0.548
580.0	0.399	501.0	0.502
669.0	0.360	602.0	0.463
		701.0	0.428
		801.0	0.398

TABLE 64: TERNARY EXCHANGE RATE DATA:
 $(\bar{S}r^* - \bar{C}s) - Mn$ SYSTEM

A

Run No. 35B

Bead: Sr/A19

Bead diameter: 0.1040 cm

$(\bar{S}r^* - \bar{C}s) - Mn: (0.745^* - 0.255) - 1.0$

Experimental		Computed (Proposed Model)	
$\frac{t}{d_o^2} \left(\frac{\text{min}}{\text{cm}^2} \right)$	q_t/q_o	$\frac{t}{d_o^2} \left(\frac{\text{min}}{\text{cm}^2} \right)$	q_t/q_o
55.5	0.913	25.4	0.907
111.0	0.860	50.8	0.882
166.5	0.820	100.7	0.839
222.0	0.791	151.0	0.803
333.0	0.749	202.0	0.772
444.0	0.699	251.0	0.745
555.0	0.657	301.0	0.720
666.0	0.608	402.0	0.676
777.0	0.569	501.0	0.637
888.0	0.540	602.0	0.601
999.0	0.510	701.0	0.569
1110.0	0.478	801.0	0.539
1221.0	0.439		
1332.0	0.415		

Table 64 (contd)

B

Run No. 41B

Bead: Sr/A19

Bead diameter: 0.1040 cm

 $(\bar{S}r^* - \bar{C}s) - Mn: (0.618^* - 0.382) - 1.0$

Experimental		Computed (Proposed Model)	
$\frac{t}{d_o^2} (\frac{min}{cm^2})$	q_t/q_o	$\frac{t}{d_o^2} (\frac{min}{cm^2})$	q_t/q_o
55.5	0.916	25.4	0.928
111.0	0.867	50.8	0.905
167.0	0.821	101.0	0.866
222.0	0.783	151.0	0.833
333.0	0.724	202.0	0.804
444.0	0.659	251.0	0.779
555.0	0.629	301.0	0.758
666.0	0.793	402.0	0.714
777.0	0.557	501.0	0.677
888.0	0.522	602.0	0.643
999.0	0.488	701.0	0.611
1110.0	0.463	801.0	0.581
1221.0	0.414		
1332.0	0.379		